FIELD PERFORMANCE EVALUATION OF MULTIPLE FIBER-REINFORCED POLYMER BRIDGE DECK SYSTEMS OVER EXISTING GIRDERS - Phase I

FINAL REPORT

Roberto Lopez-Anido[1], Issam Harik[2], Piyush Dutta [3],

and

Bahram Shahrooz [4]

[1] University of Maine, Orono, ME
[2] University of Kentucky, Lexington, KY
[3] Cold Regions Research & Engineering Laboratory, ERDC, Hanover, NH
[4] University of Cincinnati, Cincinnati, OH

June 7, 2001

Prepared in cooperation with the Ohio Department of Transportation and the U.S. Department of Transportation, Federal Highway Administration

1. Report No.	2. Government Accession No.	3. Recipient's Catalog No.
FHWA/HWY-2001/10		

4. Title and SubtitleL	5. Report Date
Field Performance Evaluation of Multiple Fiber-Reinforced Polymer Deck Systems Over Existing Girders	June, 2001
	6. Performing Organization Code
	8. Performing Organization Report No.

7. Author(s)	10. Work Unit No. (TRAIS)
Bahram Shahrooz	

9. Performing Organization Name and Address	11. Contract or Grant No.
University of Cininnati Department of Civil and Environmental Engineering PO Box 210071 Cincinnati, OH 45221-0071	State Job No. 14708 (0)
	13. Type of Report and Period Covered Final Report
12. Sponsoring Agency Name and Address Ohio Department of Transportation 1980 W Broad Street Columbus, OH 43223	14. Sponsoring Agency Code

15. Supplementary Notes

16. Abstract

The research work presented in this report is focused on the experimental evaluation of fiber reinforced polymer (FRP) deck systems, which have been used on two side-by-side bridges on Route 49 in Dayton, Ohio (MOT-49-10). The long spans of the bridges allowed evaluation of FRP deck systems from four FRP deck manufacturers under similar loading and environmental conditions. The first phase of the project, reported herein, focused on the performance criteria and extensive laboratory testing. The objectives of Phase I of the project were to: (1) Assess the performance criteria developed by Ohio DOT for FRP deck systems; (2) Evaluate the mechanical properties of the FRP deck materials; (3) Evaluate the bending and shear stiffness of the FRP deck panels; (4) Evaluate the ultimate strength response of the FRP deck panels; (5) Evaluate the fatigue response of the FRP deck panels on steel girders at high and low temperature; and (6) Evaluate the environmental durability of the FRP deck materials.

The fabricators provided FRP material coupons representative of the deck systems. The coupons were laminates with the same type of multi-axial reinforcement, fiber content and resin system that were used for the deck panels. The following properties were measured: tensile strength and tensile modulus in the longitudinal and transverse directions and interlaminar shear strength in the longitudinal direction. The materials were found to be consistent in their properties and the coefficients of variation are relatively small.

Environmental durability tests were performed, and the results were analyzed based on the criteria of the HITEC panel on FRP composite bridge decks. The HITEC evaluation criteria establish minimum levels of retained properties after exposure to the accelerated environmental exposure conditions covered in this report. The HITEC panel's minimum levels of retained material properties after 36 months of accelerated aging are as follows: 85% retention of the average as-received test values and 75% retention of each individual as-received test value. The environmental exposure and durability study served to discriminate the FRP materials that satisfied the durability requirements.

Deflection limits of FRP panels were determined, and based on the deflection of conventional reinforced-concrete decks subjected to a simulated AASHTO HS25-44 design load with an impact factor of 30%, the results were analyzed. The deflection of the conventional reinforced-concrete deck was obtained from analysis following the standard AASHTO procedure for design. The deflection limits were applied in the static tests of FRP panels for three different simply supported spans and one continuous span. Strain limits in the FRP panels subjected to AASHTO HS25-44 design load with an impact factor of 30% were based on 20% of ultimate strains computed from tensile tests. These strain limits measured in the material coupon tests were correlated with the strains measured in the static tests of the FRP panels. The static and failure test of panels served to characterize stiffness coefficients and establish a safety factor.

Fatigue performance at extreme temperatures was evaluated for the FRP decks supplied by the four manufacturers stated before. A fifth deck, made of reinforced concrete as per a conventional design of the Ohio Department of Transportation, was also subjected to the same series of fatigue tests as those of the FRP decks to provide the reference benchmark data. This report includes results of each deck for the first one million load cycles at 49°C (120°F) and the second one million cycles at –30°C (–22°F). The extremely high- and low-temperature fatigue cycling served to assess the performance of the FRP panels, the panel-to-panel joint and the specific connections to the steel girders proposed by the fabricators for this study.

17. Key Words	18. Distribution Statement
Bridge, Bride Deck, Composite, Durability, Fatigue Test, Fiber Reinforced Polymer, High Temperature, Low Temperature, Material Testing, Panels, Steel Stringer	No Restrictions. This document is available to the public through the National Technical Information Service, Springfield, Virginia 22161

19. Security Classif. (of this report)	20. Security Classif. (of this page)	21. No. of Pages	22. Price
Unclassified	Unclassified		

FIELD PERFORMANCE EVALUATION OF MULTIPLE FIBER-REINFORCED POLYMER BRIDGE DECK SYSTEMS OVER EXISTING GIRDERS - Phase I

FINAL REPORT

Roberto Lopez-Anido[1], Issam Harik[2], Piyush Dutta [3],

and

Bahram Shahrooz [4]

[1] University of Maine, Orono, ME
[2] University of Kentucky, Lexington, KY
[3] Cold Regions Research & Engineering Laboratory, ERDC, Hanover, NH
[4] University of Cincinnati, Cincinnati, OH

June 7, 2001

Prepared in cooperation with the Ohio Department of Transportation and the U.S. Department of Transportation, Federal Highway Administration

The contents of this report reflect the views of the authors, who are responsible for the facts and the accuracy of the data presented herein. The contents do not necessarily reflect the official views or policies of the Ohio Department of Transportation of the Federal Highway Administration. This report does not constitute a standard, specification or regulation.

PREFACE

This report was prepared by Roberto Lopez-Anido (University of Maine), Issam Harik (University of Kentucky), Piyush Dutta (U.S. Army ERDC-CRREL), and Bahram Shahrooz (University of Cincinnati). Funding was provided by the Federal Highway Administration and the Ohio Department of Transportation under Ohio State job number 14708(0) and Contract number 8991. The project title was "Field Performance Evaluation of Multiple Fiber-Reinforced Polymer Bridge Deck Systems Over Existing Girders."

The authors thank Stephen Morton and Brad Fagrell from the Ohio Department of Transportation, who served as Project Technical Monitors.

T LE OF CONTENTS

FIELD PERFO CE EVALUATION OF MULTIPLE FIBER-REINFORCED POLYMER BRIDGE DECK SYSTEMS OVER EXISTING GIRDERS - Phase I

EXECUTIVE SUMMARY

Roberto Lopez-Anido[1], Issam Harik[2], Piyush Dutta [3]

and

Bahram Shahrooz [4]

[1] University of Maine, Orono, ME
[2] University of Kentucky, Lexington, KY
[3] Cold Regions Research & Engineering Laboratory, ERDC, Hanover, NH
[4] University of Cincinnati, Cincinnati, OH

Introduction

In recent years, fiber-reinforced polymer (FRP) deck systems have emerged as a viable alternative to conventional systems, namely reinforced-concrete slabs. The use of such systems to replace existing, deteriorated bridge deck systems offers both economic benefits and improved performance. The economic advantages are possible for a number of reasons: since such composite systems are lighter, considerable savings are realized by reduced transportation costs (several deck systems can be transported on one truck); erection costs will be less as relatively light cranes can be used to install the decks; and construction time is reduced, which eliminates long traffic delays. Due to the high resistance of FRP deck systems to environmental effects and corrosion attack, the long-term performance is also expected to be improved significantly, leading to lower maintenance and longer service life. In addition to economic advantages, FRP deck systems offer structural advantages as well. For example, higher live loads can be

resisted by supporting steel stringers, as the dead load applied by the FRP deck system is about one fifth of a conventional reinforced-concrete deck.

The research work presented in this report is focused on the experimental evaluation of FRP deck systems, which have been used on two side-by-side bridges on Route 49 in Dayton, Ohio. The pair is called First Salem Bridge (Bridge No. MO-49-10) and spans the Great Miami River. The bridges consist of built-up steel stringers with five spans of 130, 137, 145, 137, and 130 ft. The long spans of the bridges allow evaluation of FRP deck systems from four FRP deck manufacturers under similar loading and environmental conditions.

The study plan was organized in two phases. Phase I of the project focused on the performance criteria and extensive laboratory testing. Phase II of the proposed research includes continuing laboratory testing of fatigue and environmental durability response, as well as field testing and monitoring of the bridges. This report summarizes the work conducted in the Phase I.

A team composed of four organizations performed the research work. The University of Maine performed the material characterization and durability studies, the University of Kentucky evaluated the panel stiffness and ultimate strength responses, and the U..S. Army Engineer Research and Development Center, Cold Regions Research and Engineering Laboratory evaluated the fatigue response at high and low temperatures. The University of Cincinnati provided the overall direction and control of the projects of the above organizations.

Objectives

The objectives of Phase I of the project are to:

1. Assess the performance criteria developed by Ohio DOT for FRP deck systems;
2. Evaluate the mechanical properties of the FRP deck materials;
3. Evaluate the bending and shear stiffness of the FRP deck panels;
4. Evaluate the ultimate strength response of the FRP deck panels;
5. Evaluate the fatigue response of the FRP deck panels on steel girders at high and low temperature; and
6. Evaluate the environmental durability of the FRP deck materials.

Scope of the Work

To achieve the objectives of this study, the following tasks were performed:

I – Environmental Exposure Characterization of FRP Materials

II – Static and Failure Tests of FRP Deck Panels

III – Fatigue Evaluation of FRP Bridge Decks at Extreme Temperature Conditions.

FRP Deck systems

Two structural types of FRP bridge decks were studied: a) all FRP decks and b) hybrid FRP-concrete decks. Decks of the first structural type, all FRP, behave as orthotropic plates. These decks are constructed using the concept of sandwich construction or the concept of interlocking components. Decks of the second structural type, hybrid FRP-concrete, behave as a reinforced-concrete slab. In this design the FRP material serves as stay-in-place formwork and tension reinforcement. Therefore, the

design of this type of decks is similar to the design of traditional reinforced-concrete decks.

Four FRP bridge deck manufacturers provided test materials for this study:

1. All FRP deck based on interlocking components provided by Creative Pultrusions, Inc. (CPI);
2. Hybrid FRP-concrete deck provided by DFI Pultruded Composites/Composite Deck Solutions (DFI);
3. All FRP deck based on sandwich construction deck provided by Hardcore Composites (HCC); and
4. All FRP deck based on sandwich construction deck provided by Infrastructure Composites International, LLC, (ICI).

Experimental Work

Mechanical Properties

FRP material coupons representative of the deck systems were provided by the fabricators. The coupons were laminates with the same type of multi-axial reinforcement, fiber content and resin system that were used for the deck panels. The following properties were measured: tensile strength and tensile modulus in the longitudinal and transverse directions and interlaminar shear strength in the longitudinal direction.

Static and Failure Tests

Deflection limits of FRP panels were determined, and based on the deflection of conventional reinforced-concrete decks subjected to a simulated AASHTO HS25-44 design load with an impact factor of 30%, the results were analyzed. The deflection of

the conventional reinforced-concrete deck was obtained from analysis following the standard AASHTO procedure for design. The deflection limits were applied in the static tests of FRP panels for three different simply supported spans and one continuous span. Strain limits in the FRP panels subjected to AASHTO HS25-44 design load with an impact factor of 30% were based on 20% of ultimate strains computed from tensile tests. These strain limits measured in the material coupon tests were correlated with the strains measured in the static tests of the FRP panels.

Environmental Durability

Environmental durability tests were performed, and the results were analyzed based on the criteria of the HITEC panel on FRP composite bridge decks. The HITEC evaluation criteria establish minimum levels of retained properties after exposure to the accelerated environmental exposure conditions covered in this report. The HITEC panel's minimum levels of retained material properties after 36 months of accelerated aging are as follows: 85% retention of the average as-received test values and 75% retention of each individual as-received test value.

Fatigue at Extreme Temperatures

Fatigue performance at extreme temperatures was evaluated for the FRP decks supplied by the four manufacturers stated before. A fifth deck, made of reinforced concrete as per a conventional design of the Ohio Department of Transportation, was also subjected to the same series of fatigue tests as those of the FRP decks to provide the

reference benchmark data. This report includes results of each deck for the first one million load cycles at 49°C (120°F) and the second one million cycles at –30°C (–22°F).

Conclusions

The results of the experimental investigations of the four FRP decks selected by ODOT for the First Salem Bridge in Dayton, Ohio, are given in this report in three subsequent sections. The coupon level materials testing of each deck material type have shown that the materials are consistent in their properties and the coefficients of variation are relatively small. The environmental exposure and durability study served to discriminate the FRP materials that satisfied the durability requirements. The static and failure test of panels served to characterize stiffness coefficients and establish a safety factor. The extremely high- and low-temperature fatigue cycling served to assess the performance of the FRP panels, the panel-to-panel joint and the specific connections to the steel girders proposed by the fabricators for this study.

FIELD PERFORMANCE EVALUATION OF MULTIPLE FIBER REINFORCED POLYMER BRIDGE DECK SYSTEMS OVER EXISTING GIRDERS – Phase I

SECTION I

ENVIRONMENTAL EXPOSURE CHARACTERIZATION OF FRP MATERIALS

Roberto Lopez-Anido[1] and Keith Wood[2]

Abstract

Fiber reinforced polymer (FRP) bridge deck systems are an alternative to traditional reinforced concrete decks. FRP deck systems do not corrode as do traditional reinforced concrete decks. The use of FRP bridge decks will decrease the dead load on existing bridges and allow the load capacity of the bridges to be increased. However, for bridge decks to be made of FRP materials, design codes must be established. Most state and federal departments of transportation are reluctant to design systems for infrastructure without design codes and proof that the system will work as designed. This work investigated the effects of traditional bridge deck environments on FRP bridge deck systems to develop factors for these environments that can be used in the design of bridge decks made of FRP materials.

This work was part of a multi-university research program to evaluate and install multiple FRP bridge deck systems. The Ohio Department of Transportation (ODOT) recently installed multiple FRP bridge deck systems on two side-by-side five-span continuous bridges on Route 49 in Dayton, Ohio. The long spans of the bridges allow comparison of FRP deck systems from four manufactures under similar loading and environmental conditions. For this reason, Ohio DOT proposed a performance

[1] Assistant Professor, Department of Civil and Environmental Engineering, Advanced Engineered Wood Composites Center, University of Maine, Orono, ME.

[2] Bridge Engineer, Maine Department of Transportation, Augusta, ME (formerly graduate student at the University of Maine).

evaluation program. This program includes: 1) static and failure evaluation of FRP deck panels, 2) accelerated aging of FRP deck material that is representative of harsh environmental conditions, and 3) fatigue testing of FRP deck-steel beam systems under extreme temperatures. The accelerated environmental aging and durability evaluation was conducted at the Advanced Engineered Wood Composites Center (AEWC) at the University of Maine. The goal of the study presented in this section is to characterize the effects of environmental exposure on the mechanical properties of fiber-reinforced polymer (FRP) composite materials used in bridge decks systems. This work had three main objectives:

1. Develop an environmental exposure test protocol and mechanical property indicators to characterize the durability of FRP materials used for bridge deck construction.
2. Characterize the effects of environmental exposure on the mechanical properties of FRP materials through statistical analysis, mechanics modeling and degradation kinetics.
3. Propose material capacity reduction factors ("knock-down factors") to account for the reduction in mechanical properties as a function of environmental exposure.

Table of Contents

SECTION I
ENVIRONMENTAL EXPOSURE CHARACTERIZATION OF FRP MATERIALS

List of Tables

List of Figures

I.1 Materials

Two structural types of FRP bridge decks were studied: a) all FRP decks, and b) hybrid FRP-concrete decks. Decks of the first structural type, all FRP, behave as orthotropic plates. These decks are constructed using the concept of sandwich construction or the concept of interlocking components. Therefore, the design of this type of deck is similar to the design of orthotropic decks. Decks of the second structural type, hybrid FRP-concrete, behave as a reinforced-concrete slab. In this design the FRP material serves as stay-in-place formwork and tension reinforcement. Therefore, the design of this type of decks is similar to the design of traditional reinforced-concrete decks. Four FRP bridge deck manufacturers provided test materials for this study:

1. All FRP deck based on interlocking components provided by Creative Pultrusions, Inc. (CPI);
2. Hybrid FRP-concrete deck provided by DFI Pultruded Composites/Composite Deck Solutions (DFI);
3. All FRP deck based on sandwich construction deck provided by Hardcore Composites (HCC); and
4. All FRP deck based on sandwich construction deck provided by Infrastructure Composites International, LLC, (ICI).

The following sections describe the different deck systems and how the samples for this project were obtained. The sample plates came from the manufacturers with the exposed edges sealed with the manufacture's choice of resin system. The samples provided by the manufacturers were specified to be from the same fabrication bath. For

example, the pultruded plates were cut from a single pultrusion run. The lay-up plates were cut from a large molded plate.

Each manufacturer was asked to provide 33 longitudinal sample plates with dimensions of 152.4 × 304.8 mm (6 × 12 in.). Each manufacturer provided three plates precut to conduct tension tests of the as-received material (five longitudinal tension coupons were cut from each plate). In addition, the manufacturers provided other specific samples. DFI provided an additional three sample plates precut for transverse tension coupons and five epoxy-coated (DFI-E) longitudinal sample plates. HCC provided 33 additional transverse sample plates of which three were precut for transverse tension samples. ICI provided two sets of samples, ICI-B and ICI-C. ICI-B had the actual deck reinforcement fabric (stitched) and ICI-C had an alternative reinforcement fabric (knitted). Table I.1.1 summarizes the types and numbers of plates supplied by each manufacturer.

Table I.1.1 Samples Provided by Individual Manufacturers

	Longitudinal Sample Plates	Transverse Sample Plates
CPI	33	0
DFI	33	3
DFI-E	5	0
HCC	33	33
ICI-B	33	0
ICI-C	33	0

I.1.1 Material Systems

I.1.1.1 Resin Matrix

The resin matrix for each manufacturer was a vinyl ester, a polyester, or a mix of the two systems. The basic properties of vinyl ester and polyester resins are summarized

herein. The base materials for a vinyl ester matrix are an epoxy resin and an unsaturated carboxylic acid, usually methacrylic acid or acrylic acid (Mallick, 1993). Typically, for commercial resins, DGEBA epoxy and methacrylic acid are synthesized together to form vinyl ester resin. Points of unstaturation in the vinyl ester molecule occur where there are carbon–carbon double bonds. These bonds only occur at the ends of the vinyl ester molecule, so cross-linking can only occur at these points. Cured vinyl ester resins are more flexible and have higher fracture toughness than polyester resins due to the fewer cross-links. The vinyl ester molecule also contains hydroxyl (OH) groups that allow for the formation of hydrogen bonds with similar groups located on the surface of the glass fibers. These bonds result in excellent wet-out of the glass fibers, which produces a good bond between the fibers and the resin matrix. The base material of a polyester matrix is an unsaturated polyester such as maleic anhydride, which contains multiple carbon–carbon double bonds. A step polymerization process of the unsaturated polyester with a glycol forms the polyester resin. In a polyester resin molecule, the unsaturated double bonds occur within the molecule. The cross-linking of the molecules occurs via the step polymerization process. Consequently the properties of the polyester resins are highly dependent on the density of the cross-linking. As the cross-link density of the polyester resin increases, the modulus of elasticity, glass transition temperature, and thermal stability of the system are improved, but reductions occur in the strain to failure and impact energy.

I.1.1.2 Fiber Reinforcement

The type of E-glass reinforcement used for each type of material sample plates varied greatly depending on the fabricator. The variations in fiber architecture lead to

very different fiber volume fractions in the common reinforcing directions. All of the stitched fabric reinforcement used by the different FRP deck systems was supplied by Brunswick Technologies, Inc. (BTI). An alternative knitted fabric reinforcement supplied by Collins Craft Composites (CCC) was considered for one FRP deck system.

I.1.1.3 Fabrication Process

The fabrication processes used by the manufacturers are also different and are summarized in Table I.1.2. The differences in the fabrication processes result in variations in the thickness of the specimens.

Table I.1.2 Fabrication Process for the Deck Systems

Specimen	Fabrication Process
CPI	Pultrusion
DFI	Pultrusion
HCC	VARTM
ICI	Contact molding hand lay-up

I.1.2 FRP Material Fabricated by Pultrusion for Bridge Decks (CPI)

I.1.2.1 Bridge Deck System

The pultruded deck samples are representative of the top and bottom faces of the deck system. This FRP deck system used pultruded interlocking sections that act as beams to transfer the loads to the girders. The deck sections are composed of hexagon and double-trapezoid profiles, which are bonded together with a high-strength adhesive to form prefabricated panels. The two sections that make up the deck are shown in Figure I.1.1. The panels are shipped to the site and are field bonded with the same high-strength

adhesive. The samples for this project are of the same lay-up configuration as the flange of the double trapezoid section, since this is the face that is directly exposed to the weather.

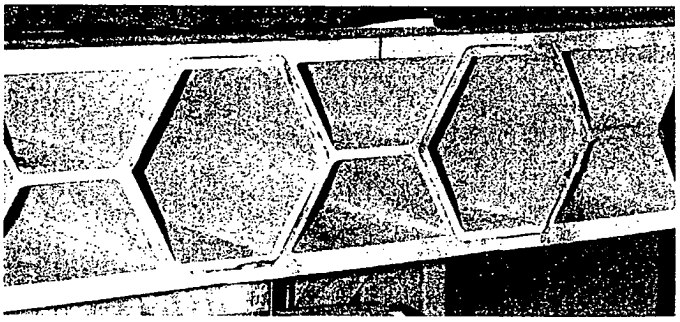

Figure I.1.1 Cut-Away of CPI Deck Sections

I.1.2.2 Materials and Fabrication

The polymer matrix used was vinyl ester resin from Reichhold (Atlac 580-05). The pultruded material was reinforced with a combination of rovings and a multi-axial stitched fabric, as shown in Table I.1.3.

Table I.1.3 E-Glass Reinforcement for Pultruded Material (CPI)

Fabrication Method	Rovings 0°	Fabric Orientation	Stitched Fabric	Fabric Designation	Fabric Supplier
Pultrusion	X	90 / ± 45	x	TH4000/ THX1501	BTI

The total volume percentage of fiber reinforcement ranges was 49.2%, as shown in Table I.1.4. The percentage of the fibers in the longitudinal direction was 18.9%. In the transverse direction, the fiber volume fraction was 10.7%. In the biased directions (±45°) the fiber content was 16%. The mat layers were 3.6% by volume.

Table I.1.4 Fiber Volume Content of Pultruded Material (CPI)

Fabrication Method	Volume Fraction					
	0 (%)	90 (%)	-45 (%)	45 (%)	Mat (%)	Total (%)
Pultrusion	18.9	10.7	8.0	8.0	3.6	49.2

The sample plates fabricated by the pultrusion process have consistent thickness dimensions as shown in Table I.1.5.

Table I.1.5 Thickness of Tensile Specimens for Pultruded Material (CPI)

Fabrication Method	Average Thickness (mm)	Standard Deviation (mm)	COV (%)
Pultrusion	9.881	0.0178	0.18

I.1.3 FRP Material Fabricated by Pultrusion for Reinforcing Concrete Bridge Decks (DFI)

I.1.3.1 Bridge Deck System

The FRP pultruded panels act as a cast-in-place form and tension reinforcement for a concrete bridge deck. A cross section of the composite deck panel is shown in Figure I.1.2, and a cut-away of an actual deck is show in Figure I.1.3. The prefabricated sections span between the bridge girders on the bottom side of the deck. The samples for this project are of a similar lay-up representing the thinnest part of the bottom face of the deck.

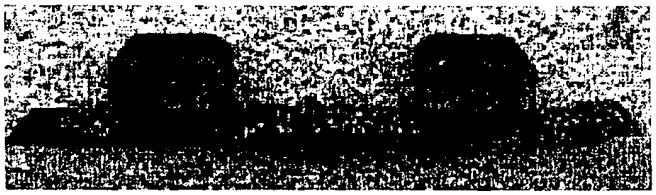

Figure I.1.2 Cross Section of DFI Pultruded FRP Deck Panel

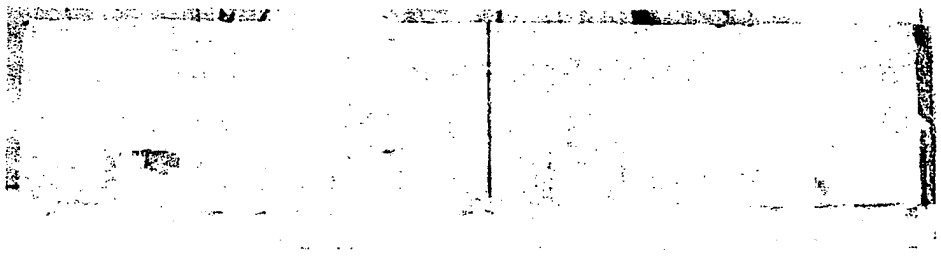

Figure I.1.3 DFI Pultruded Section with Cast Concrete to Form Deck Section

I.1.3.2 Materials and Fabrication

The polymer matrix used was a vinyl ester (Hetron 922 HV) and isophthalic polyester (Aropol 7030) blend from Ashland Chemicals. The pultruded material was reinforced with a combination of rovings and a multi-axial stitched fabric, as shown in Table I.1.6.

Table I.1.6 E-Glass Reinforcement for Pultruded Material (DFI)

Fabrication Method	Rovings 0°	Fabric Orientation	Stitched Fabric	Fabric Designation	Fabric Supplier
Pultrusion	x	± 45	x	XM2408	BTI

The total volume percentage of fiber reinforcement was 60.6%, as shown in Table I.1.7. The percentage of the fibers in the longitudinal direction was 50.3%. In the transverse direction, there were no fibers. In the biased directions (±45°) the fiber content was 8%. The mat layers were 2.3% by volume.

Table I.1.7 Fiber Volume Content of Pultruded Material (DFI)

Fabrication Method	Volume Fraction					
	0 (%)	90 (%)	-45 (%)	45 (%)	Mat (%)	Total (%)
Pultrusion	50.3	0	4.0	4.0	2.3	60.6

The sample plates fabricated by the pultrusion process had consistent thickness dimensions, as shown in Table I.1.8.

Table I.1.8 Thickness of Tensile Specimens for Pultruded Material (DFI)

Fabrication Method	Average Thickness (mm)	Standard Deviation (mm)	COV (%)
Pultrusion	8.001	0.0084	0.11

The fabricator supplied additional pultruded sample plates that were completely coated on all sides with an epoxy resin. These samples were used to evaluate if the epoxy coating decreased the rate of environmental attack in the alkali environment that may develop in hybrid FRP-concrete decks.

I.1.4 FRP Material Fabricated by VARTM for Bridge Decks (HCC)

I.1.4.1 Bridge Deck System

The VARTM FRP deck system uses an integral cell core, which is encased with layers of E-glass fabrics to form the faces of the deck. The core and the faces are then placed in a mold and injected with resin using the vacuum-assisted resin transfer molding process (VARTM). The integral cells are wrapped with an E-glass fabric before they are placed in the mold and after the VARTM process. They act as bi-directional webs for the deck. Figure I.1.4 depicts the parts of the HCC deck system, and a cross section of the deck system is show in Figure I.1.5.

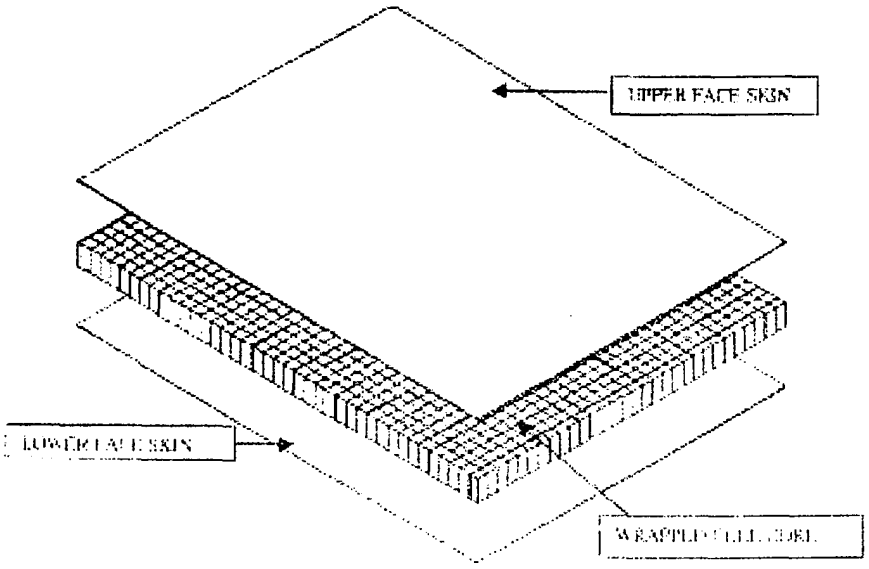

Figure I.1.4 HCC Deck System Schematic (Hardcore Composites, 1998)

The samples for this project are from the top and bottom faces of the deck system. They were fabricated by the VARTM process and are composed of the same resin and E-glass fabric. However, they are not as thick as the actual faces of the deck. The samples are roughly 6.6 mm (0.26 in.), whereas the actual faces of the deck vary from 11.0 mm (0.432 in.) to 18.3 mm (0.720 in.). The samples for this project have four layers of E-glass fabric, whereas the actual bridge decks have between six and ten layers of fabric, depending upon the spacing of the girders.

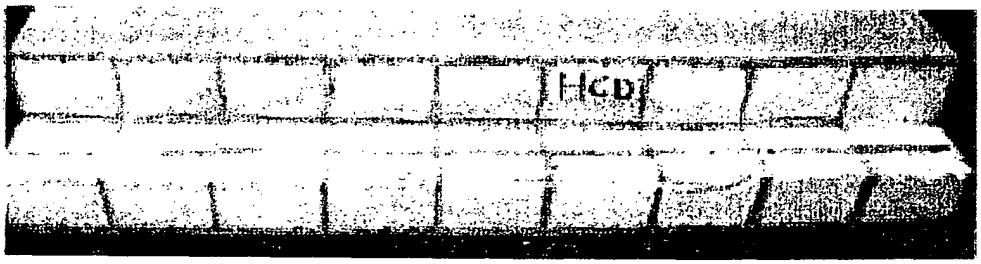

Figure I.1.5 Cross Section of the HCC Deck

I.1.4.2 Materials and Fabrication

The polymer matrix used was vinyl ester resin from Dow (Derakane 411). The VARTM material was reinforced with multi-axial stitched fabric, as shown in Table I.1.9. The total volume percentage of fiber reinforcement was in the range of 55.6%, as shown in Table I.1.10. The percentage of the fibers in the longitudinal direction was 20%. In the transverse direction, the fiber volume fraction was 12.2%. In the biased directions (±45°) the fiber content was 18.4%. The mat layers were 5.1% by volume.

Table I.1.9 E-Glass Reinforcement for VARTM Material (HCC)

Fabrication Method	Rovings 0°	Fabric Orientation	Stitched Fabric	Fabric Designation	Fabric Supplier
VARTM		0 / 90 / ± 45	x	QM6408	BTI

Table I.1.10 Fiber Volume Content of VARTM Material (HCC)

Fabrication Method	Volume Fraction					
	0 (%)	90 (%)	-45 (%)	45 (%)	Mat (%)	Total (%)
VARTM	20.0	12.2	9.2	9.2	5.1	55.6

The sample plates fabricated by the VARTM process have relatively high variations in thickness compared to other fabrication processes. For this fabrication process the tool side of the specimens is smooth while the vacuum bag side exhibits waviness, as shown in Table I.1.11.

Table I.1.11 Thickness of Tensile Specimens for VARTM Material (HCC)

Fabrication Method	Average Thickness (mm)	Standard Deviation (mm)	COV (%)
VARTM	6.934	0.1786	2.57

I.1.5 FRP Material Fabricated by Contact Molding Hand Lay-Up for Bridge Decks (ICI)

I.1.5.1 Bridge Deck System

This FRP deck system consists of a low-density honeycomb core sandwiched between two contact-molded hand lay-up FRP face sheets. A cut-away of a typical deck is shown in Figure I.1.6, and a cross section of the actual deck system is show in Figure I.1.7.

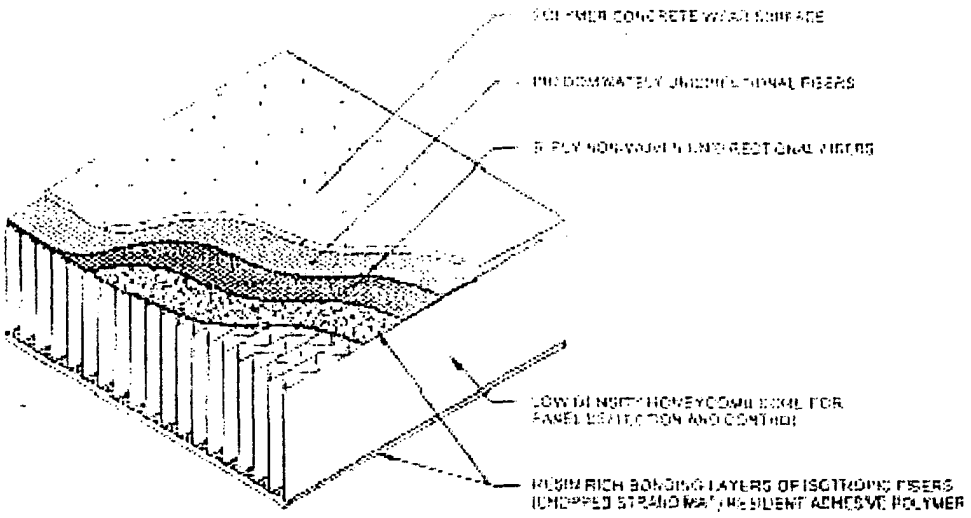

Figure I.1.6 ICI Deck System (Nagy and Kunz, 1998)

The panels are 1.8 m (6 ft) to 2.4 m (8 ft) wide and can be as long as 14.6 m (48 ft). The thickness of the core and face skin is adjusted to make the system work for the different girder spacings. The samples for this project are hand lay-up samples with the same fiber reinforcement and resin system as the top and bottom faces of the actual deck panels.

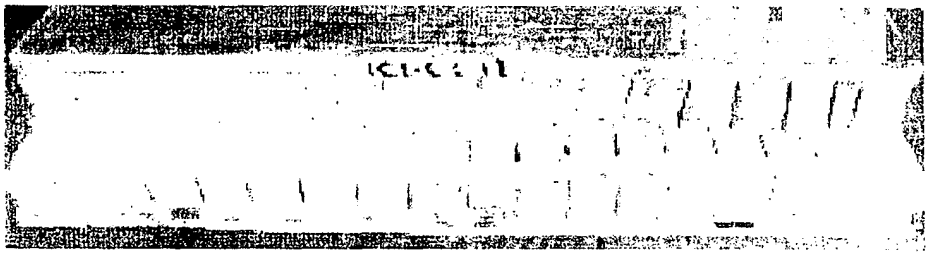

Figure I.1.7 Cross Section of the ICI Deck System

I.1.5.2 Materials and Fabrication

The polymer matrix used was isophthalic/terephthalic polyester from AOC (Vibrin F457-BRP-25). The only difference between the isophthalic and terephthalic polyesters is the locations of the two COOH groups on the benzene ring. The two groups are oriented in a linear arrangement on the benzene ring for the isophthalic polyester and in a non-linear fashion for the terephthalic polyester. The compaction molding hand lay-up material sample plates were reinforced with bi-axial fabrics, which were supplied by two different fabric manufacturers, as shown in Table I.1.12.

Table I.1.12 E-Glass Reinforcement for Hand Lay-Up Material (ICI)

Fabrication Method	Rovings 0°	Fabric Orientation	Stitched Fabric	Knitted Fabric	Fabric Designation	Fabric Supplier
Hand lay-up		0 / 90	x		CM4810	BTI
Hand lay-up		0 / 90		x	A1118	CCC

The total volume percentages of fiber reinforcement ranges are 34.2% and 25.7% for the stitched and knitted reinforcement, respectively, as shown in Table I.1.13. The percentages of the fibers in the longitudinal direction are 14.4% and 12.9%, respectively. In the transverse direction, the fiber volume fraction is the same as in the longitudinal direction (balanced design). In the biased directions (±45°), there is no fiber reinforcement. The mat layers are 5.4% and 0% by volume, respectively.

Table I.1.13 Fiber Volume Content of Hand Lay-Up Material (ICI)

Fabric Reinforcement	Volume Fraction					
	0 (%)	90 (%)	-45 (%)	45 (%)	Mat (%)	Total (%)
Stitched (B)	14.4	14.4	0	0	5.4	34.2
Knitted (C)	12.9	12.9	0	0	0	25.7

The specimens fabricated by contact molding hand lay-up exhibited moderate thickness variability compared to other fabrication processes, as shown in Table I.1.14.

Table I.1.14 Thickness of Tensile Specimens for Hand Lay-Up Material (ICI)

Fabric Reinforcement	Average Thickness (mm)	Standard Deviation (mm)	COV (%)
Stitched (B)	8.788	0.148	1.68
Knitted (C)	8.763	0.189	2.14

It is worth noting that the fabricator provided the hand lay-up samples with an alternative reinforcement fabric that was knitted and was evaluated for specific environmental exposures to determine the effect of the type of reinforcement.

I.2 Test Methods

The test program adopted for this project followed the basic approach of using mechanical test indicators to evaluate retained properties after environmental conditioning. First, baseline values were established, followed by accelerated environmental aging of the materials and mechanical testing of the aged materials. The aged material properties were compared to the baseline values to determine the effects of the environmental conditioning. The data provided by the tests were used to determine the degradation mechanisms, which occur within each individual deck system.

I.2.1 Environmental Exposure

Traditional concrete bridge decks in service today encounter a variety of environmental conditions every day. Table I.2.1 summarizes the most common environments for bridge decks and the corresponding durability test for each environment. The following sections discuss the test methods for each exposure treatment.

Table I.2.1 Traditional Bridge Deck Environments

Actual Environmental Exposure in the Field during the Life of the Bridge Deck (50 years)	Environmental Durability Test
Accumulation of surface water due to the deck profile and drainage conditions	Water Resistance
Use of de-icing chemicals and marine environments	Salt water resistance
Casting a reinforced concrete slab on a FRP material	Alkali resistance
Freeze-thaw cycles combined with the presence of water	Freeze-thaw resistance
Synergistic natural weathering	Exterior exposure resistance
Exterior weathering due to UV exposure and rain	UV and spray resistance

I.2.1.1 Control

Two sets of control samples were established for this project. The first set of control samples consisted of the as-received coupons from the manufacturers. The second consisted of the unexposed coupons cut from sample plates after 18 months of storage at room temperature with uncontrolled humidity. These coupons were referred to as the control coupons aged in air. The second set of control coupons were conditioned at a room temperature of 23°C ± 3°C (73 ± 5°F) and relative humidity of (50 ± 5%) for seven days prior to testing.

I.2.1.2 Immersion

Sample plates from each manufacturer as shown in Table I.2.2 were conditioned for 1,000, 3,000, and 10,000 hours in water, salt water, and alkali solutions at room temperature. The reagent water for this test was Type IV reagent water in accordance with ASTM D1193, "Standard Specification for Reagent Water." The substitute ocean water was in accordance with ASTM D1141, "Standard Specification for Substitute Ocean Water." The test protocols for each of the immersion conditions are given in Wood and Lopez-Anido (2000).

Table I.2.2 Sample Plate Distribution for Immersion Tests

	Water (hours)			Salt Water (hours)			Alkali (hours)		
	1,000	3,000	10,000	1,000	3,000	10,000	1,000	3,000	10,000
CPI	2	2	2	2	2	2	0	0	0
DFI	2	2	2	2	2	2	1	1	1
DFI-E	0	0	0	0	0	0	1	1	1
HCC-L	2	2	2	2	2	2	0	0	0
HCC-T	1	1	1	1	1	1	0	0	0
ICI-B	2	2	2	2	2	2	0	0	0
ICI-C	2	2	2	2	2	2	0	0	0

Only sample plates from DFI were subjected to the alkali condition since they come into direct contact with concrete in the actual bridge deck system. The alkali solution for this test was a standard solution of $CaCO_3$ with a pH of 9.5. To maintain the pH of the solution at 9.5, drops of 0.1-M sodium hydroxide (NaOH) were added to the solution periodically and stirred thoroughly.

The immersion treatments were conducted in high-density polyethylene (HDPE) containers. The sample plates from each manufacturer were immersed in separate tanks for each solution so as not to mix resin systems. The HDPE containers had a capacity of 20 L (5.3 gal.), with dimensions of 30.5 × 45.7 × 22.9 cm (12 × 18 × 9 in.). The containers were covered with lids to minimize the effects of evaporation and spillage during handling. The sample plates were weighed prior to immersion and were placed vertically in the containers on HDPE blocks that were grooved to support the samples. Figure I.2.1 shows the HDPE containers with the sample plates for the water immersion treatment.

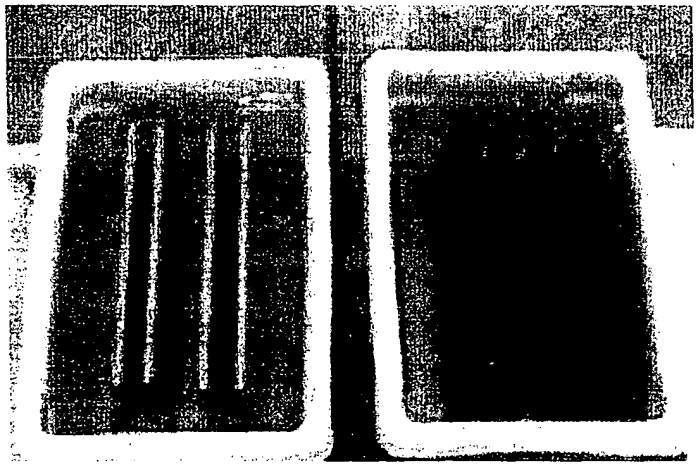

Figure I.2.1 Water Immersion Baths

The sample plates were removed periodically to determine the mass change of the samples as a function of time. In this process the samples were removed from the containers, dried with lint-free rags, weighed, and returned to the containers as soon as possible. After the samples were aged for the predetermined periods, they were removed from the containers, dried with lint-free rags, and weighed. The sample plates were stored in sealed plastic bags at room temperature until they were tested in tension and short beam shear, except for when they were cut and tabbed.

I.2.1.3 Freeze-Thaw Resistance

Sample plates from each manufacturer as shown in Table I.2.3 were subjected to 20, 40, and 60 cycles of freezing and thawing. This test followed the procedure for freeze-thaw cycling for ICBO AC 125.

Table I.2.3 Sample Plate Distribution for the Freeze-Thaw Condition

	Freeze-Thaw Condition		
	20 Cycles	40 Cycles	60 Cycles
CPI	2	2	2
DFI	2	2	2
DFI-E	0	0	0
HCC-L	2	2	2
HCC-T	1	1	1
ICI-B	2	2	2
ICI-C	2	2	2

The test setup consisted of separate HDPE containers filled with Type I distilled water, equipped with submersible 250-W heaters, and 4-L/min circulator pumps, and a chest freezer. The heaters and the circulator pumps were set to maintain a 38°C (100°F) temperature immersion bath, and the freezer was set to −18°C (0°F). The sample plates from each manufacture were immersed in separate tanks so as not to mix resin systems. Figure I.2.2 and Figure I.2.3 show the water baths used to conduct the freeze-thaw

cycling treatments for each manufacturer. The sample plates were placed vertically in the containers and were supported by HDPE blocks that were grooved to support the samples. The same type of HDPE blocks were used to support the sample plates in the freezer.

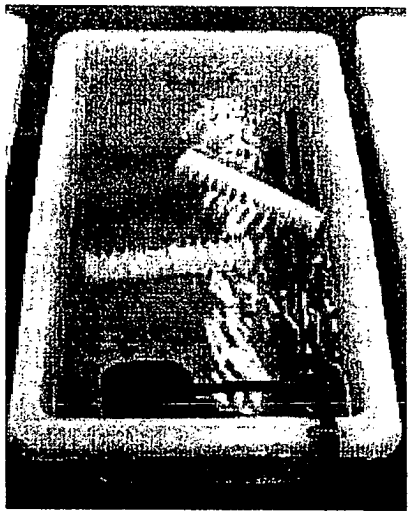

Figure I.2.2 Hot Water Bath for the Thawing Cycle of the Freeze-Thaw Treatments

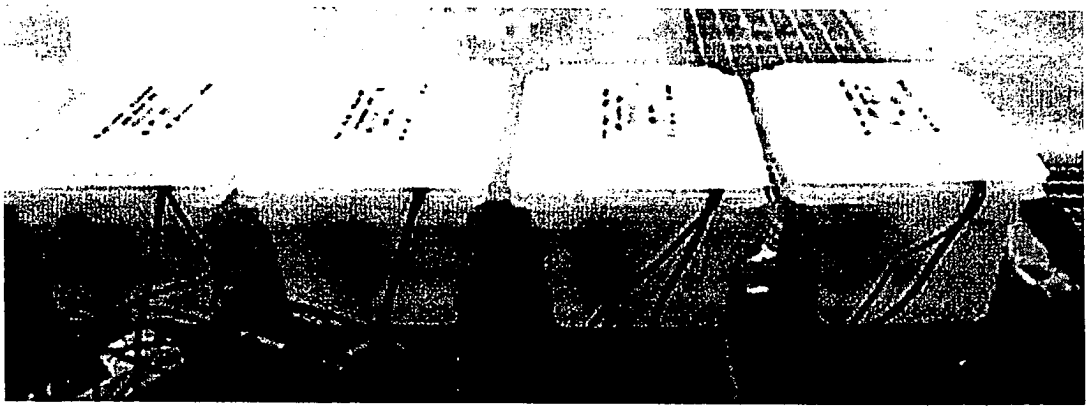

Figure I.2.3 Hot Water Baths for Freeze-Thaw Treatments

The sample plates were conditioned for 21 days in a water bath prior to freeze-thaw cycling. Each freeze-thaw cycle consisted of 12 hours of freeze in the freezer

followed by 12 hours of immersion in the water bath. Each time the samples were removed from the water bath and placed in the freezer, they were dried with a lint-free rag to remove the surface water. The sample plates were weighed prior to immersion, after the 21-day conditioning period, and after every 20 cycles of freezing and thawing to determine mass change. After the samples were subjected to the required number of freeze-thaw cycles, they were removed from the containers and dried with lint-free rags. The sample plates were stored in sealed plastic bags at room temperature until they were tested in tension and short beam shear, except for when they were cut and tabbed.

I.2.1.4 Weathering

I.2.1.4.1 UV and Water Spray Resistance

Sample plates for each manufacturer as shown in Table I.2.4 were subjected to a QUV weathering machine for 1000 and 2000 cycles of normalized weathering. The weatherometer chamber for this test was in accordance with ASTM G 53. UVA 340 bulbs with an irradiance level of 0.55 $W/m^2/nm$ to match the effects of normal sunlight were used as the UV light source. Figure I.2.4 shows the QUV machine used to conduct the UV and water spray treatments.

Table I.2.4 UV and Spray Test Matrix

	QUV Weathering (cycles)	
	1000	2000
CPI	2	2
DFI	2	2
DFI-E	0	0
HCC-L	2	2
HCC-T	1	1
ICI-B	2	2
ICI-C	0	0

The exposure cycle from ASTM G 23 was used for this test since it is more severe than the cycle specified in ASTM G 53. The samples were flipped and rotated every 500 hours to ensure even exposure over the face of each sample and on either face of the sample. A cycle consisted of 102 minutes of light, followed by 18 minutes of spray and light. Distilled water was supplied to machine from a 190-L (50-gal.) tank, which was refilled every 200 hours. The water in the tank was recycled through the machine for this time period, and the filter for the water supply was changed every time the water tank was refilled. The UV sensors were calibrated every 400 hours.

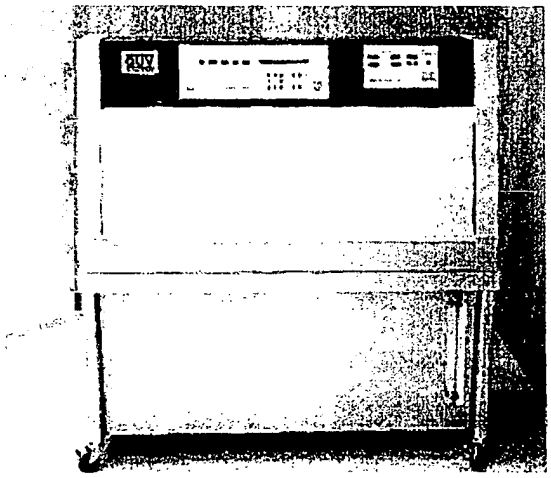

Figure I.2.4 QUV Weathering Machine for UV and Water Spray Treatments

I.2.1.4.2 Exterior Exposure Resistance

To compare the effects of standardized weathering tests to normal weathering conditions, samples were weathered in an exterior climate. Two sample plates for the first exposure time and one for the second exposure time as shown in Table I.2.5 were subjected to the following treatment. The sample plates were weathered facing south at 45° to the ground on the roof of Boardman Hall. Figure I.2.5 shows the weathering rack

the sample plates were mounted on for the exterior exposure treatments. The samples were flipped over once a month to ensure even exposure on both faces. The samples exposed for two years were part of the work for this project but were not considered part of this study.

Table I.2.5 Exterior Exposure Test Matrix

	Exterior Weathering (years)	
	1	2
CPI	2	1
DFI	2	1
DFI-E		
HCC-L	1	1
HCC-T	1	
ICI-B	2	1
ICI-C		

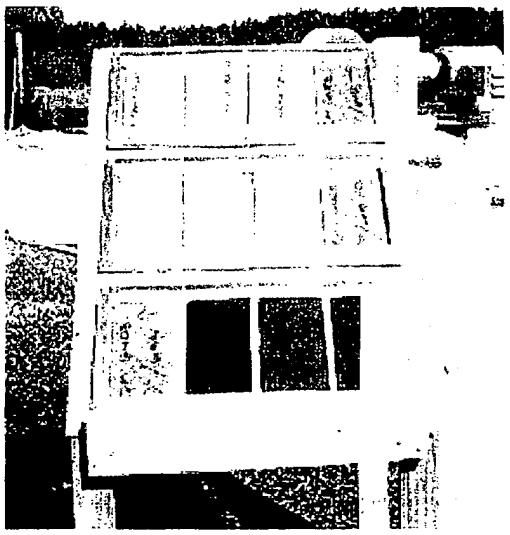

Figure I.2.5 Weathering Rack for the Exterior Exposure Tests

I.2.1.5 Environmental Test Matrix

To summarize, the four decks systems were subjected to the test matrix given in Table I.2.6. The sample plate distribution for each company and each test is summarized in Table I.2.7. Sample plates were identified according to the following parameters:

manufacturer and fabric, environmental aging condition, and sample number. The sample plate designation was formed by a dash separating each of the three parameters. Table I.2.8 shows the categories under each parameter and their reference.

Table I.2.6 Environmental Durability Test Matrix

Environmental Durability Test	Test Conditions	Test Duration
Water Resistance	Immersion in reagent water at 23°C	1000, 3000, and 10,000 hours
Salt Water Resistance	Immersion in salt water at 23°C	1000, 3000, and 10,000 hours
Alkali Resistance	Immersion in calcium carbonate with pH of 9.5 at 23°C (pultruded materials from DFI only)	1000, 3000, and 10,000 hours
Freeze-Thaw Resistance	Water immersion at 38°C followed by consecutive cycles of 12 hours of freeze at –18°C and 12 hours of water immersion at 38°C	21 days conditioning followed by 20, 40, and 60 cycles of FT
Exterior Exposure Resistance	Natural environmental conditions	1 year
QUV Resistance	Cycles of 1hour and 42 minutes of light followed by 18 minutes of spray and light	1000 and 2000 cycles

Table I.2.7 Summary of Sample Plate Immersion for Environmental Aging

Aging Test	Control		Water Immersion			Salt Water Immersion			Alkali Immersion			Freeze-Thaw Cycling			UV and Spray		Exterior Aging	
Test Duration	0 year	1.5 years	1,000 hours	3,000 hours	10,000 hours	1,000 hours	3,000 hours	10,000 hours	1,000 hours	3,000 hours	10,000 hours	20 cycles	40 cycles	60 cycles	1,000 cycles	2,000 cycles	1 year	2 years
CPI	1	2	2	2	2	2	2	2	0	0	0	2	2	2	2	2	2	1
DFI	0	2	2	2	2	2	2	2	1	1	1	2	2	2	2	2	2	1
DFI-E	0	0	0	0	0	0	0	0	1	1	1	0	0	0	0	0	0	0
HCC-L	0	2	2	2	2	2	2	2	0	0	0	2	2	2	2	2	1	1
HCC-T	0	1	1	1	1	1	1	1	0	0	0	1	1	1	1	1	1	0
ICI-B	0	2	2	2	2	2	2	2	0	0	0	2	2	2	2	2	2	1
ICI-C	0	2	2	2	2	2	2	2	0	0	0	2	2	2	0	0	0	0

Table I.2.8 Sample Plate Identification System

Manufacturer and Fabric	
Designation	**Reference**
CPI	Creative Pultrusions, Inc
DFI	DFI Pultruded Composites/ Composite Deck Solutions
DFI-E*	DFI Pultruded Composites Epoxy Coated
HCL/HCT	Hardcore Composites
ICB	Infrastructure Composites International, LLC BTI fabric
ICC	Infrastructure Composites International, LLC CoFaB fabric

Environmental Aging Condition	
Designation	**Reference**
A	Calcium Carbonate Immersion
E	Exterior Exposure Condition
FT	Freeze-Thaw Cycling
S	Salt Water Immersion
U	UV and Spray Condition
W	Water Immersion

Sample Number	
Designation	**Reference**
1,2,3...	Number of individual coupon

I.2.2 Evaluation Methods

I.2.2.1 Physical Properties

The physical properties investigated for this project were the density, fiber volume fraction, matrix volume fraction, and void content of the control samples. The appearance and the apparent change in mass of the sample plates were monitored throughout the aging process.

I.2.2.1.1 Appearance

The appearance of each sample was recorded before and after environmental aging. The condition of the resins used to seal the edges of the material, along with any

other changes in the edges of the materials, such as delamination, were noted at that time. Color changes in the surface of the samples, along with any other changes in the surface of the samples such as the presence of exposed fibers, were noted at that time.

I.2.2.1.2 Density

Density tests were conducted to more accurately determine the volume of the specimens used for the burnout tests. Density tests were conducted in accordance with ASTM D 792 Method A, "Standard test Methods for Density and Specific Gravity (Relative Density) of Plastics by Displacement." Ten specimens were cut with a wet saw from control sample plates of each deck system with dimensions of 1.9 cm (0.75 in.) square. The specimens were washed with tap water and were conditioned for two days at a temperature of 26°C ± 1°C (78°F ± 2°F) and humidity 50% ± 20% RH.

The samples were massed in air with a balance accurate to 0.1 mg and immersed in distilled water and massed a second time. The specific gravity of the specimens was determined as

$$Sp \quad gr \quad 23/23^{\circ}C = \frac{a}{a-b} \tag{I-2-1}$$

where a is the apparent mass of the specimen in air, and b is the apparent mass of the specimen total immersed in distilled water. The specific gravity of composite laminates is the ratio of the densities of the composite and water. Thus, the density of the specimens was determined as the product of the specific gravity of the composite and the density of water as shown below:

$$D^{23C} \quad kg/m^3 = Sp \quad gr \quad 23/23^{\circ}C \times 997.6 \tag{I-2-2}$$

I.2.2.1.3 Fiber Volume Fraction

Burnout tests were conducted in accordance with ASTM D 2548, "Standard Test Method for Ignition Loss of Cured Reinforced Resins." Ten specimens from the sample set used for density tests for each deck system were burned in a muffle furnace for one and a half hours at 565°C (1049°F) in such a manner that only the fibers remained after burnout. The samples were placed in aluminum crucibles and weighed prior to testing and following cooling in a desiccator after the burnout tests were conducted. The difference in the two weights is the weight of the resin in the samples, and the weight of the residue constitutes the weight of the fibers.

The fiber volume fraction was determined based upon the data collected from the previous two tests. The fiber weight fraction, W_f, and matrix weight fraction, W_m, were calculated as follows:

$$W_f(\%) = \frac{W_2}{W_1} \times 100 \tag{I-2-3}$$

$$W_m(\%) = \frac{W_1 - W_2}{W_1} \times 100 \tag{I-2-4}$$

where W_1 is the weight of the specimen prior to burnout and W_2 is the weight of the residue after burnout. The fiber volume fraction, V_f, was calculated as

$$V_f(\%) = W_f \times \frac{\rho_e}{\rho_f} \times 100 \tag{I-2-5}$$

where ρ_e is the experimental density of the specimens and ρ_f is the density of the E-glass fibers, which is taken as 2.54 g/cm^3. If the density of the cured solid resin including additives and fillers, ρ_m, is known, then the resin volume fraction can be computed as

$$V_m(\%) = W_m \times \frac{\rho_c}{\rho_m} \times 100 \quad . \tag{I-2-6}$$

Then the void volume fraction, V_v, can be calculated as

$$V_v(\%) = 100 - V_f - V_m \quad . \tag{I-2-7}$$

In this work the actual ρ_m for the matrices and processes considered was not evaluated. Typical densities of solid resins are in the range of 1.12 to 1.40 g/cm^3 (Ashland Chemical 1998, Dow Plastics 1992). It is worth noting that the density of solid resin supplied by the manufacturers is only an approximation and cannot be used to compute an accurate void content. However, the solid density supplied by the manufacturers can be used, as shown in Chapter 5, to estimate the matrix volume fraction in the micromechanics predictions of elastic moduli.

I.2.2.2 Mechanical Properties

The mechanical properties investigated before and after environmental aging were tensile strength in the longitudinal and transverse directions and interlaminar shear strength in the longitudinal direction. The outputs of these tests were tensile strength in the longitudinal and transverse directions, modulus of elasticity in the longitudinal and transverse directions, and interlaminar shear strength in the longitudinal direction. Coupons were identified according to the following parameters: manufacturer and fabric, test performed, environmental aging condition, age of coupon, and coupon number. The coupon designation was formed by a dash separating each of the five parameters. Table I.2.9 shows the categories under each parameter and their reference.

Table I.2.9 Coupon Identification System

Manufacturer and Fabric	
Designation	**Reference**
CPI	Creative Pultrusions, Inc
DFI	DFI Pultruded Composites/
DFI-E	DFI Pultruded Composites/ Epoxy Coated Coupons
HCC	Hardcore Composites
ICI-B	Infrastructure Composites International, LLC BTI fabric
ICI-C	Infrastructure Composites International, LLC CoFaB fabric

Test Performed	
Designation	**Reference**
L	Longitudinal Tensile Test – D3039
T	Transverse Tensile Test – D3039
S	Interlaminar Shear Test – D2344

Environmental Aging Condition	
Designation	**Reference**
A	Calcium Carbonate Immersion
E	Exterior Exposure
FT	Freeze-Thaw Cycling
S	Salt Water Immersion
U	UV and Spray
W	Water Immersion

Age	
Designation	**Reference**
0, 1,000, 3,000, and 10,000	1,000, 3,000 and 10,000 Hours of Immersion
20, 40 and 60	20, 40 and 60 Cycles

Coupon Number	
Designation	**Reference**
1,2,3…	Number of individual coupon

I.2.2.2.1 Coupon Preparation

Test coupons were cut from the sample plates using a wet saw equipped with a diamond-tipped blade. The dimensions of the test coupons are summarized in Table I.2.10. The dimensions of the interlaminar shear coupons were determined according to ASTM Standard D-2344, which calls for a width of 6.35 mm (0.25 in.), a depth equal to the thickness of the coupon and a length equal to seven times the thickness of the coupon. Figure I.2.6 shows how the first sample plate was cut to obtain all the longitudinal tension coupons and the transverse tension coupons from HCC. Figure I.2.7 shows how the first sample plate from DFI was cut for the 25.4- × 1.27-cm tension coupons and the interlaminar shear coupons. Figure I.2.8, Figure I.2.9, and Figure I.2.10 show how the second plates that were immersed were cut for the transverse tension coupons, interlaminar shear coupons, and additional longitudinal tension coupons.

Table I.2.10 Test Coupon Dimensions

Manufacturer	Longitudinal Tensile Tests	Transverse Tensile Tests	Longitudinal Interlaminar Shear Tests
CPI	25.4 × 2.54 cm (10 × 1 in..)	15.3 × 2.54 cm (6 × 1 in.)	6.92 × 0.635 cm (2.724 × 0.25 in.)
DFI	25.4 × 2.54 cm* (10 × 1 in.)* 25.4 × 1.27 cm (10 × 0.5 in.)	15.3 × 2.54 cm (6 × 1 in.)	5.60 × 0.635 cm (2.204 × 0.25 in.)
HCC	25.4 × 2.54 cm (10 × 1 in.)	25.4 × 2.54 cm (10 × 1 in.)	4.84 × 0.635 cm (1.904 × 0.25 in.)
ICI-B	25.4 × 2.54 cm (10 × 1 in.)		6.15 × 0.635 cm (2.422 × 0.25 in.)
ICI-C	25.4 × 2.54 cm (10 × 1 in.)		6.14 × 0.635 cm (2.416 × 0.25 in.)

* The 2.54-cm-wide coupons were used for all 1000 hours of exposure, 20 cycles of freeze-thaw, and the as-received control tests only.

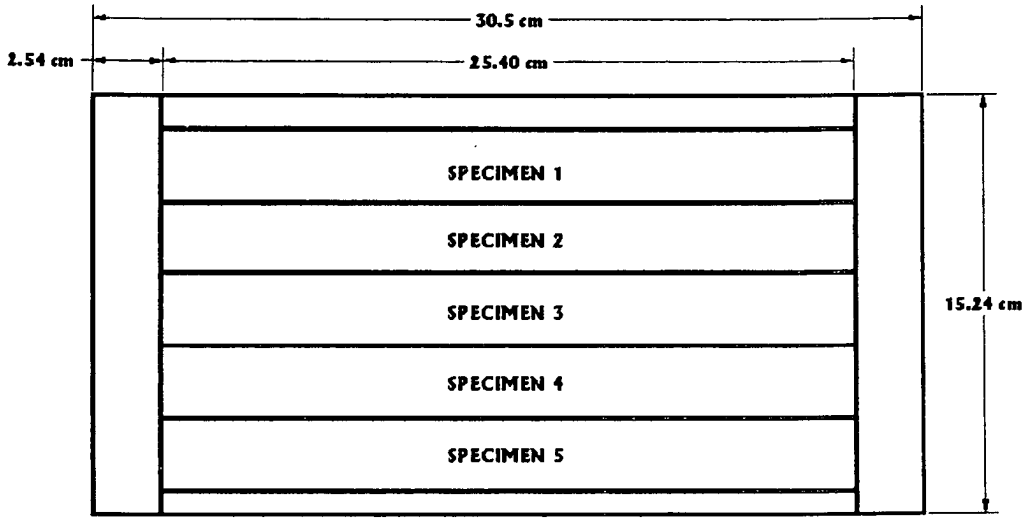

Figure I.2.6 Sample Plate Cutting Configuration for 2.54- × 25.4-cm Tension Coupons

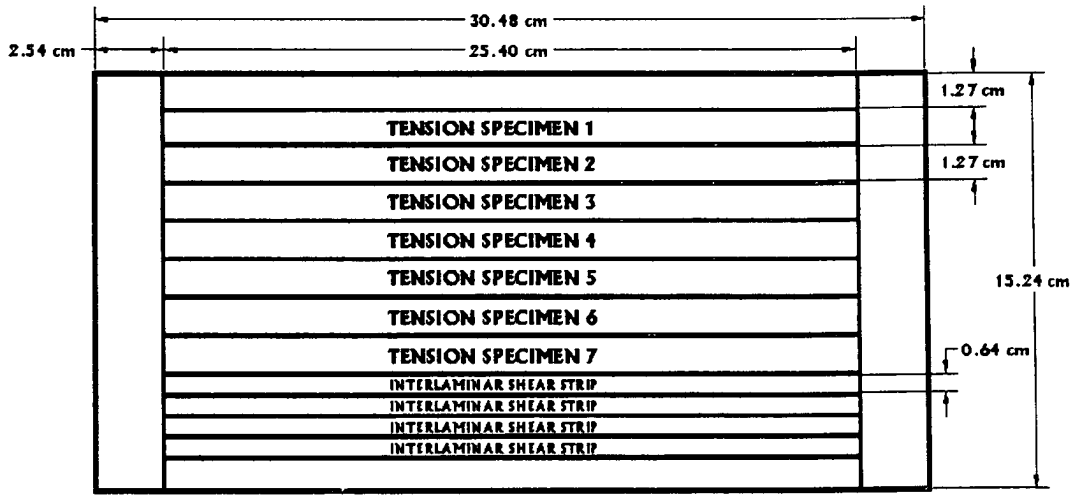

Figure I. 2.7 Sample Plate Cutting Configuration for 1.27- × 25.4-cm Tension Samples and Interlaminar Shear Coupons

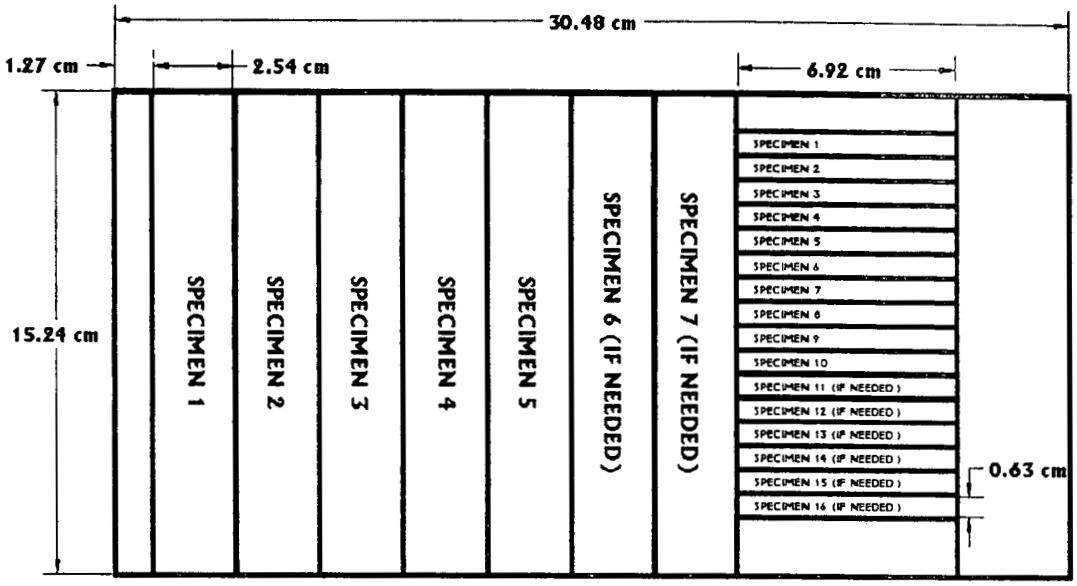

Figure I.2.8 Sample Plate Cutting Configuration for CPI Coupons

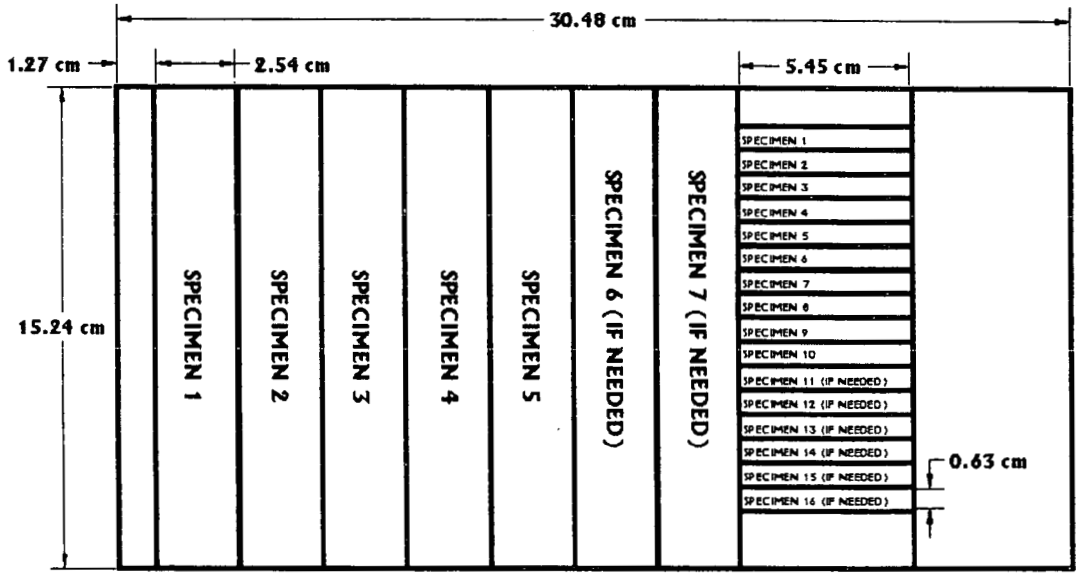

Figure I.2.9 Sample Plate Cutting Configuration for DFI Coupons

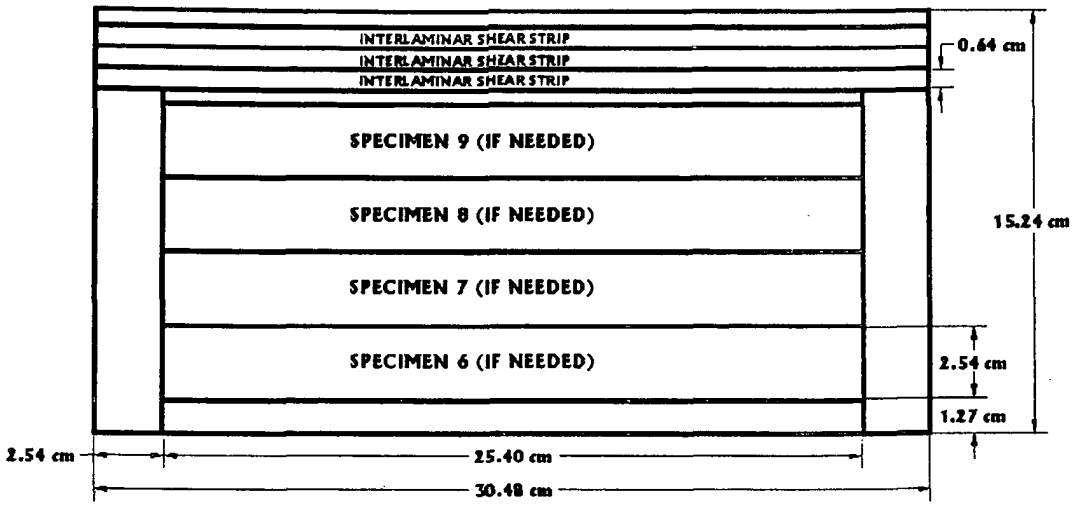

Figure I.2.10 Sample Plate Cutting Configuration for 2nd Plate from HCC, ICI-B, and ICI-C

I.2.2.2.2 Tensile Strength

I.2.2.2.2.1 Control Tests

Static tension tests were conducted in accordance with ASTM D3039-D, "Standard Test Method for Tensile Properties of Polymer Matrix Composite Materials." All the longitudinal control coupons and the transverse coupons from HCC were tested with an MTS 810 Material Testing System at the Advanced Composites Design Laboratory (ACDL) in Crosby Hall at the University of Maine. The MTS 810 is a servo-hydraulic testing machine capable of applying a maximum load of 500 N (112 kip). The MTS was equipped with hydraulic grips with a line pressure of 20.6 MPa (3000 psi), which required the use of aluminum tabs to prevent grip damage and failure during testing. The aluminum tabs were 3.2 × 25.4 × 57.2 mm (1/8 × 1 × 2¼ in.) and were bonded to the coupons with epoxy that was heat cured. Foil strain gages were bonded to the tool side of the coupons, and the P-3500 was connected to the computer's data acquisition system to record strains. A crosshead displacement rate of 1.27 mm/min

(0.05 in./min) was used, and the coupons were loaded up to the first reversal in applied load to determine the initial mode of failure. A description of the failed coupon was recorded in accordance with the criteria established in Table I.2.11.

Table I.2.11 Criteria for Failed Coupon Description of Tension Samples

First Character		Second Character		Third Character	
Failure Type	Code	Failure Area	Code	Failure Location	Code
Angled	A	Inside grip/tab	I	Bottom	B
Edge Delimitation	D	At grip/tab	A	Top	T
Grip/tab	G	<1W from grip/tab	W	Left	L
Lateral	L	Gage	G	Right	R
Multi-mode	M	Multiple areas	M	Middle	M
Long. Splitting	S	Various	V	Various	V
EXplosive	X	Unknown	U	Unknown	U
Other	O				

The transverse control tensile coupons from CPI and DFI were tested using the Instron 4204 Material Testing System in Boardman Hall at the University of Maine. The Instron 4204 is a screw-driven testing machine capable of applying a maximum load of 44.5 N (10 kips). The Instron was equipped with mechanical grips, which did not require the use of tabs to prevent grip damage and failure during testing. The width and thickness of the coupons were measured at four points along the gage line and averaged to determine the area. Strain gages were again bonded to the smooth surface of each coupon to record strains. A crosshead displacement rate of 1.27 mm/min (0.05 in./min) was used, and the coupons were loaded up to failure. A description of the failed coupon was recorded in accordance with the criteria established in Table I.2.11.

The data were collected using a laptop computer and the data collection software LABVIEW. The outputs from the load cell of the Instron testing machine and the P-3500 strain indicator were connected to a data acquisition card and calibrated to use with the

LABVIEW software. The tests were run with the Instron's manual controls while the computer recorded the applied load and strain at 1-s intervals. The data from all the control tests were imported into an Excel spreadsheet for analysis.

I.2.2.2.2.2 Environmentally Aged Tests

All of the environmentally aged and the 10,000 hours of control tensile coupons were tested in one of the two Instron 8800 Series Testing Frames in the Mechanical Testing Laboratory in the Advanced Engineered Wood Composites Center (AEWC) at the University of Maine. The 8801 and the 8803 testing frames are servo-hydraulic and capable of applying a maximum load of 100 kN (22 kips) and 500 kN (112 kips), respectively. During the tests the relative ambient humidity ranged from 40 to 70%, and the temperature ranged from 21 to 30°C (70 to 85°F). The Instron 8800 Series Testing Frames were equipped with hydraulic grips, for which the grip pressure could be regulated. Strain gages or an extensometer was used to measure strains during the tests. A crosshead displacement rate of 1.27 mm/min (0.05 in./min) was used, and the coupons were loaded to failure. The mode of failure was recorded in accordance with the criteria established in Table I.2.11.

Aluminum tabs with dimensions of 3.2 × 25.4 × 57.2 mm (1/8 × 1 × 2¼ in.) were bonded to all of the longitudinal coupons and the transverse coupons from HCC for 1000 hours of immersion in all solutions and 20 cycles of freeze-thaw. The tabs were bonded to the water coupons immersed for 1000 hours with same epoxy used for the control tests, which was heat cured. PLIOGRIP, a polyurethane adhesive from Ashland Chemicals, was used to bond the aluminum tabs to the coupons exposed to freeze-thaw cycling, calcium carbonate, and salt water. For the coupons subjected to 3,000, and 10,000 hours

of immersion, UV and spray, exterior exposure, and 40 and 60 cycles of freeze-thaw, tabs were only bonded to the HCC and ICI-C samples. An appropriate grip pressure was applied to all the none-tabbed coupons during testing to prevent failures due to the grips.

I.2.2.2.2.3 Problems Encountered

An extensometer was used to measure strains for all the coupons subjected to 1000 hours of immersion in water. After reduction of the data, it was determined that the extensometer was faulty, and the data from the longitudinal tension test were thrown out. New test coupons were cut from the remaining sample plates and tested with strain gages.

The coupons from DFI that were exposed to the alkali, water, and salt water conditions for 3000 hours, along with the coupons subjected to 40 and 60 cycles of freeze-thaw, were originally cut with a width 25.4 cm. When these coupons were tested in the 500-kN Instron, either most of the coupons were squashed by the grips or they failed. Therefore, 1.27-cm-wide coupons were cut from the remaining tension coupons for 40 cycles of freeze-thaw, and 1.27-cm-wide coupons were cut from the sample plates intended for the transverse coupons for water and salt water exposures. The tensile coupons for the alkali condition and freeze-thaw condition for 60 cycles were lost. A second epoxy-coated sample plate was immersed for 3000 hours to replace the lost coupons. However, the other coupons could not be replaced due to the lack of sample plates. Finally, the epoxy coating was scraped off of the tab area of the tension samples prior to testing to prevent grip slippage during testing.

I.2.2.2.3 Interlaminar Shear Strength

Static interlaminar shear tests were conducted in accordance with ASTM D2344, "Standard Test Method for Apparent Interlaminar Shear Strength of Parallel Fiber Composites by Short-Beam Method." These tests evaluated the strength of the decking material between the individual layers of E-glass and the resin matrix. The interlaminar shear coupons were tested using the Instron 4204 Material Testing System in Boardman Hall at the University of Maine. The Instron was equipped with a three-point bending fixture conforming to the ASTM standard. The width and thickness of the coupons were measured at three points along the coupon and averaged to determine the coupon dimensions.

The coupons from CPI and DFI were placed in the bending fixture randomly with respect to the tension and compression faces. The coupons from HCC and ICI were placed in the bending fixture with the non-tool side on the tension face and the tool side on the compression face. Preliminary testing showed that this loading configuration resulted in a higher percentage of interlaminar shear failures as compared to those coupons loaded with the non-tool side on the compression face and the tool side on the tension face. During the tests the relative humidity ranged from 35 to 60%, and the temperature ranged from 18 to 30°C (65 to 80°F). A crosshead displacement rate of 1.27 mm/min (0.05 in./min) was used, and the coupons were loaded up to the first failure. The load at the first failure, along with the mode and location of failure, were recorded in accordance with the criteria established in Table I.2.12 and Table I.2.13. The test procedure was repeated until ten coupons of each type failed in an interlaminar manner.

Table I.2.12 Modes of Failure for Interlaminar Shear Tests

Mode of Failure	Code	Description
Interlaminar Shear	1	The formation of a horizontal crack between the individual fiber layers
Tension	2	The formation of a vertical failure on the bottom face of the sample near its midpoint
Compression	3	The appearance of a deformation at the support locations or at the point of load application.
Inclined Shear at Angle	4	The formation an inclined crack/failure at roughly a 45° angle through multiple fabric laminations. Characterized by a band of discoloration in the coupon at a 45° angle starting from the top loading point and moving towards the support at the bottom of the sample.
Unknown/Other	5	None of the modes of failures listed above.

Table I.2.13 Location of Failure for Interlaminar Shear Tests

First Code		Second Code		Third Code	
Horizontal Loc.	Code	Vertical Location	Code	Fabric Location	Code
At the end of coupon	E	Center of coupon	C	Between the fabric and the roving	FR
Center of the coupon	C	Between the bottom and the center	BC	Between two layers of fabric	FF
Between the center and the end of the coupon	CE	Between the top and the center	TC	In an individual layer of fabric	IF
		Between the top and bottom of the coupon	TB	Between the rovings	RR
				In the resin-rich region between the layers of fabric	RRR

I.2.3 Data Analysis

I.2.3.1 Tensile Tests

The data were analyzed to determine the applied stress for each individual data point, and the maximum stress was recorded for each individual test. For the DFI

coupons coated with epoxy and exposed to the alkali solution, the epoxy coating was considered non-structural, and the thickness of the coupon was taken as 8.00 mm (0.315 in.), the average thickness of the control coupons. Stress versus strain was plotted between 1000 and 3000 microstrains, and a trend line was fitted to determine the modulus of elasticity for the longitudinal tension samples. Since the ultimate strain for the DFI materials in the transverse direction was approximately 0.3%, a range of strains from 1000 to 2000 microstrains was used to determine the modulus of elasticity.

I.2.3.2 Data Analysis of Interlaminar Shear Tests

The apparent interlaminar shear strength, S_H, of the coupons was calculated using the following equation, from ASTM D 2344:

$$S_H = \frac{0.75 \cdot P_B}{b \cdot d} \tag{I-2-8}$$

where P_B is the applied breaking load (applied shear, V, is equal to half the breaking load), b is the width of the coupon, and d is the depth of the coupon.

For the DFI coupons coated with epoxy and exposed to the alkali solution, the depth of the coupon was taken as 8.00 mm (0.315 in.), the average thickness of the control coupons. The interlaminar shear strength was taken as the average of the interlaminar shear failures for the coupons from CPI, DFI, and HCC. The interlaminar shear strength for the coupons from ICI was the average of ten tests, since the coupons did not consistently fail in an interlaminar shear manner.

I.2.4 Statistical Analysis

Statistical analysis of the mechanical properties of the individual deck systems after each environmental aging condition was performed using both one-way and two-way analyses of variance (ANOVA) with the SYSTAT software package. A two-way analysis of variance was performed on the results (strength and modulus data) of the immersion treatments to determine the dependency of the results. The analysis of variance determined if the response was a function of time, treatment, or the interaction of the two. One-way analyses of variance were performed on the results (strength and modulus data) for each exposure for each deck to allow for a comparison of the degraded and baseline results. A student's t-distribution was used for all of the statistical analyses.

The model for a one-way ANOVA is represented symbolically as follows:

$$Y_{ij} = \mu_i + Treatment\_Time_j + \varepsilon_{ij} \qquad \text{(I-2-9)}$$

where Y_{ij} is the observed mechanical property for the treatment j in block i, μ_i is the mean mechanical property for block i, $Treatment\_Time_j$ is the effect on the mechanical property for treatment of time j, and ε_{ij} represents the random unit variation within the block. Under this model the differences between the blocks of data do not affect the comparison between the treatment times, and the only factors for the estimate of the difference between the means are the true differences between the means and the random variation between the coupons within the blocks. A pairwise multiple comparison between the treatment periods was done using the Tukey Test method with a confidence level $\alpha = 0.05$.

The model for a two-way ANOVA is represent as follows:

$$Y_{ijk} = \mu_{ijk} + Treatment_i + Time_j + (Treatment \times Time)_{ij} + \varepsilon_{ijk} \quad \text{(I-2-10)}$$

where Y_{ijk} is the actual physical measurement; μ_{ijk} is the mean value of the physical measurement; $Treatment_i$ is either water, salt water, alkali, or control; $Time_j$ is the exposure time in hours (0, 1,000, 3,000, or 10,000); $(Treatment \times Time)_{ij}$ is the effect of interaction between the i^{th} treatment and the j^{th} time; ε_{ijk} is the experimental error associated with y_{ijk}; and k is the k^{th} observation of the ij^{th} treatment. A confidence level of $\alpha = 0.05$ was used to evaluate the results of the two-way ANOVA.

I.3 Experimental Results

This chapter summarizes the experimental results of the environmental exposure test matrix. The chapter is organized into sections for each FRP deck system. The sections for each deck system are divided into subsections for the control, immersion, freeze-thaw, and weathering treatments with the corresponding results for the physical and mechanical tests and indicators.

The results for each FRP deck laminate correspond to tests performed before and after the environmental treatments. Tests to determine the physical properties, density, void content, fiber volume fraction, and matrix volume fraction of the deck laminates were only performed on samples that were not subjected to the environmental treatments. A description of the appearance of the sample plates prior to subjecting them to the environmental treatments was noted and was considered as the control appearance.

To determine the mechanical properties of the FRP deck laminates, tension and interlaminar shear tests were conducted before and after the environmental exposure treatments. The mechanical tests conducted on the coupons that were not subjected to the environmental exposure treatments were considered control. However, there were two sets of control: the as-received coupons tested prior to the environmental exposure and the aged coupons tested after the exposure periods for the environmental treatments were completed. The coupons tested prior to the environmental exposure treatments were considered baseline control, and those tested after the exposure periods were considered aged control. The baseline control results were used as a reference to determine the amount of degradation in the coupons subjected to the environmental exposure treatments. The results of the tension and interlaminar shear tests conducted on the

coupons from the environmental exposure treatments were considered degraded data for the treatment.

I.3.1 FRP Material Fabricated by Pultrusion Used in Bridge Decks (CPI)

I.3.1.1 Control (Unexposed)

This section is a summary of the results from the control tests conducted on the CPI pultruded laminates prior to subjecting them to the environmental exposure treatments and for the aged control samples. Baseline properties were established for appearance, longitudinal and transverse tensile strength, longitudinal and transverse tensile modulus of elasticity, and longitudinal interlaminar shear strength. The results of the ignition loss tests were used for verification of the results from the laminate analysis.

I.3.1.1.1 Appearance

Observations of the appearance of the sample plates were made before and after environmental exposure. The appearance of the pultruded sample plates was a light gray material with all four edges sealed with a clear resin. The sample plates had consistent dimensions. These observations served as a reference for evaluating the environmentally aged samples. The pultruded sample plates were sealed on all four sides with Hetron 197 Isophthalic polyester resin.

I.3.1.1.2 Tensile

The tensile strength of the control coupons (unexposed) was measured at two different times to determine the effects of further curing during the exposure period. Table I.3.1 and Table I.3.2 are summaries of the results of the tension tests for the

baseline control and aged control coupons. A one-way ANOVA was performed on the tension test data (strength and elastic modulus) to determine differences between the baseline control and aged results. The results of the individual tension test and the statistical analysis for the control condition are located in Wood and Lopez-Anido (2000).

Table I.3.1 Ultimate Tensile Strength of Control Coupons for the Pultruded Material

Direction	Time (years)	Sample Size	Ultimate Tensile Strength MPa (ksi)	Residual Strength (%)	COV (%)	Statistical Level
Longitudinal	0	7	294 (42.6)	97.3	3.38	A
	1.5	5	286 (41.5)		2.12	A
Transverse	0	5	150 (21.8)	100	10.17	A
	1.5	7	150 (21.8)		3.61	A

Table I.3.2 Modulus of Elasticity of Control Coupons for the Pultruded Material

Direction	Time (years)	Sample Size	Modulus of Elasticity GPa (msi)	Residual Modulus (%)	COV (%)	Statistical Level
Longitudinal	0	7	22.4 (3.25)	99.1	2.52	A
	1.5	5	22.2 (3.22)		2.82	A
Transverse	0	5	15.9 (2.31)	103	7.47	A
	1.5	7	16.3 (2.36)		5.11	A

The results of the tension tests on the two sets of control samples are not statistically different. Thus, the baseline strength of the material does not change with respect to time. The minor changes in the values from the baseline control to the aged control were within the coefficient of variation of the baseline controls. The coefficients of variation for the transverse tests were higher than the longitudinal tests due to the inherent variability within the material.

The mode of failure of the tension coupons did not change after exposure in air at room temperature. The failure of the longitudinal tension samples was characterized as

an explosive failure across the gauge length and diagonally across the thickness from one end of the sample to the other, as shown in Figure I.3.1. The transverse tension coupons broke in a similar but less explosive manner. The coupons failed diagonally across the thickness from one end of the sample to the other, but the failure through the thickness was less explosive than the longitudinal coupons. Typical failures of the control and aged control coupons are shown in Figure I.3.2.

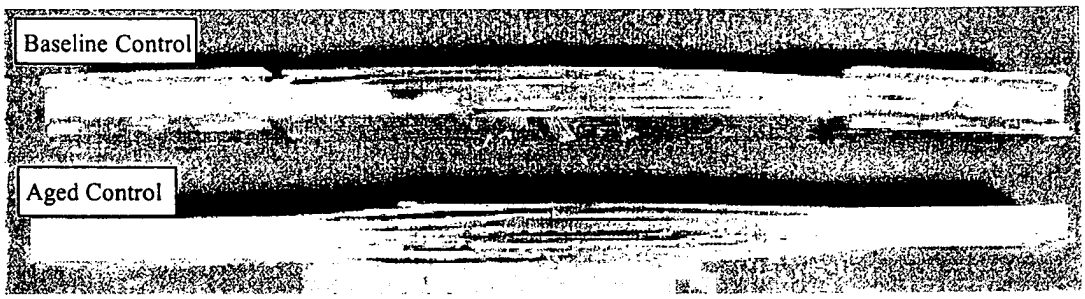

Figure I.3.1 Control Longitudinal Tension Coupons for the Pultruded Material

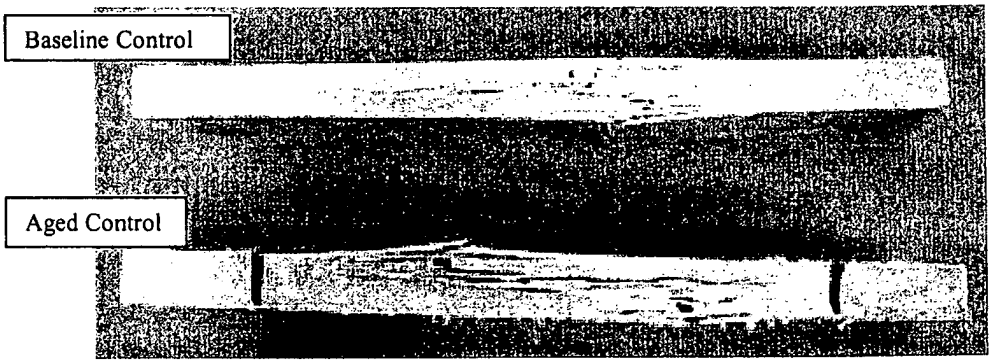

Figure I.3.2 Control Transverse Tension Coupons for the Pultruded Material

I.3.1.1.3 Interlaminar Shear

Interlaminar shear tests were conducted before and after environmental exposure to evaluate the interface between the fibers and the matrix. The results of the interlaminar shear tests of the baseline and aged control coupons are shown in Table I.3.3. A one-way ANOVA was performed on the interlaminar shear test data to

determine differences between the baseline control and aged results. The results of the individual interlaminar shear tests and the statistical analysis of the results are located in Wood and Lopez-Anido (2000).

There was no significant change in the interlaminar shear strength between the baseline control and the aged control sample sets. The interlaminar shear coupons failed in either a roving layer or at the interface between the roving layers and the stitched fabric.

Table I.3.3 Interlaminar Shear Strength of the Control Coupons in the Longitudinal Direction for the Pultruded Material

Time (years)	Sample Size	Interlaminar Shear Strength MPa (ksi)	Residual ILSS (%)	Coefficient of Variation (%)	Statistical Level
0	9	26.8 (3.88)	98.1	4.80	A
1.5	10	26.3 (3.82)		4.16	A

I.3.1.1.4 Ignition Loss

Ignition loss tests (ASTM D 2548) were conducted to verify the fiber volume fraction used in the laminate analysis. Ignition loss tests were conducted on ten specimens, and the average fiber volume fraction was found to be 54.1% with a COV of 1.72%. The results of the individual ignition loss tests are located in Wood and Lopez-Anido (2000).

I.3.1.2 Immersion Treatments

This section summarizes the results of the pultruded samples plates subjected to the environmental exposure treatments of immersion in water and salt water solutions for 1,000, 3,000, and 10,000 hours

I.3.1.2.1 Appearance

The general appearance of the samples after the environmental exposure treatment was characterized by flaking off the sealant resin from the faces and edges of the sample plates. The appearance of the sample plates after environmental exposure in immersion treatments is summarized in Table I.3.4.

Table I.3.4 Appearance of Immersion Samples after Environmental Exposure Treatments

Condition	1,000 Hours	3,000 Hours	10,000 Hours
Water	Resin used to seal edges varied from gray to white	Resin used to seal edges varied from gray to white	Resin used to seal the edges was white and translucent. 25% of the sealant resin flaked off.
Salt water	No visual changes	No visual changes	Resin used to seal edges has flaked of parts of the edges and faces

I.3.1.2.2 Mass Change

Table I.3.5 summarizes the average change in mass of the sample plates after the immersion treatments. The change in mass of the sample plates was similar for each treatment and exposure period. The data from the monitoring of the sample plates during the exposure process are located in Wood and Lopez-Anido (2000).

Table I.3.5 Mass Change of the Pultruded Immersion Plates after Environmental Exposure Treatments of Water and Salt Water

Treatment	Average Mass Change after Environmental Exposure (%)		
	1,000 Hours	3,000 Hours	10,000 Hours
Water	0.04	0.27	0.43
Salt Water	0.16	0.23	0.37

I.3.1.2.3 Tensile Strength

Table I.3.6 and Table I.3.7 are summaries of the results of the tension tests of the coupons from the sample plates for the water and salt water treatments. A one-way analysis of variance was used to compare all possible pairs of the mechanical test results (strength and elastic modulus) for each treatment of a particular exposure, baseline control, and aged control. A two-way analysis of variance was used to determine the dependency (time, treatment, or interaction of time and treatment) of the mechanical response. The results of the individual tensile tests and the statistical analysis for tension coupons are located in Wood and Lopez-Anido (2000).

The coupons cut from the pultruded sample plates for the immersion treatments only showed statistically significant decreases of the longitudinal tensile strength for the water and salt water treatments. The response of this property was a function of the treatments. The largest decreases in longitudinal tensile strength were 10.5% and 6.8% for the water and saltwater conditions, respectively. The modulus of elasticity and the transverse tensile strength were statistically unaffected by the immersion treatments.

The mode of failure of the tension coupons was not affected by the immersion treatments. Typical failures of the tension coupons from the immersion treatments are shown in Figure I.3.3 and Figure I.3.4.

Table I.3.6 Tensile Strength Results for the Tension Coupons Cut from the Pultruded Sample Plates after the Environmental Exposure Treatments of Water and Salt Water

Direction	Treatment	Time (hr)	Sample Size	Ultimate Tensile Strength MPa (ksi)	Retained Strength (%)	COV (%)	Strength Statistic Level	Depend. System Statistic
Long.	Water	1,000	5	273 (39.6)	93.0	3.46	BC	COND. (B)
		3,000	5	277 (40.2)	94.3	2.57	ABC	
		10,000	5	263 (38.1)	89.4	1.39	C	
	Salt Water	1,000	5	277 (40.2)	94.4	4.36	ABC	COND. (B)
		3,000	5	281 (40.8)	95.9	5.45	ABC	
		10,000	5	274 (39.8)	93.5	2.91	BC	
Trans.	Water	1,000	6	134 (19.3)	89.1	15.3	A	NONE
		3,000	6	139 (20.2)	91.8	3.49	A	
		10,000	7	134 (19.5)	89.5	4.53	A	
	Salt Water	1,000	7	147 (21.3)	98.6	13.6	A	
		3,000	5	143 (20.8)	94.4	3.16	A	
		10,000	7	140 (20.3)	93.4	7.25	A	

Table I.3.7 Modulus of Elasticity Results for the Tension Coupons Cut from the Pultruded Sample Plates after the Environmental Exposure Treatments of Water and Salt Water

Direction	Treatment	Time (hrs)	Sample Size	Modulus of Elasticity GPa (msi)	Retained Strength (%)	COV (%)	Modulus Statistic Level	Depend. System
Long.	Water	1,000	0	NDA	-	-	-	NONE
		3,000	5	21.6 (3.14)	96.6	7.64	A	
		10,000	5	21.9 (3.18)	98.0	2.05	A	
	Salt Water	1,000	5	22.8 (3.31)	102	3.64	A	
		3,000	5	22.0 (3.19)	98.1	2.99	A	
		10,000	5	22.5 (3.26)	100	1.17	A	
Trans.	Water	1,000	6	134 (19.3)	89.1	15.3	A	NONE
		3,000	6	139 (20.2)	91.8	3.49	A	
		10,000	7	134 (19.5)	89.5	4.53	A	
	Salt Water	1,000	7	147 (21.3)	98.6	13.6	A	
		3,000	5	143 (20.8)	94.4	3.16	A	
		10,000	7	140 (20.3)	93.4	7.25	A	

NDA* - No Data available

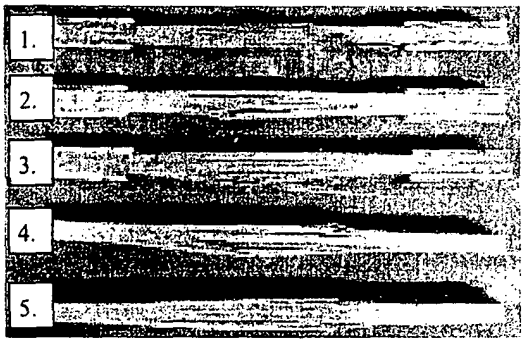

1. Baseline Control, 2. 1,000 Hours, 3. 3,000 Hours, 4. 10,000 Hours 5. Aged Control

(a)

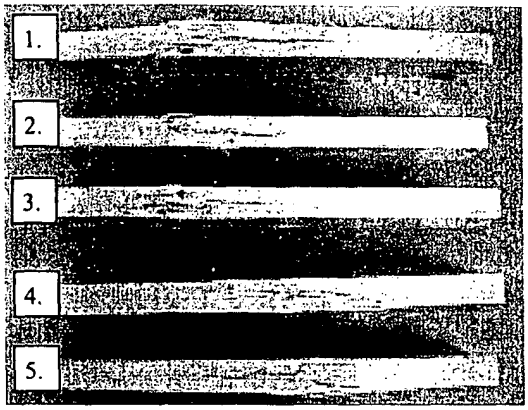

1. Baseline Control, 2. 1,000 Hours, 3. 3,000 Hours, 4. 10,000 Hours 5. Aged Control

(b)

Figure I.3.3 Pultruded Water Immersion Coupons: (a) Longitudinal, (b) Transverse

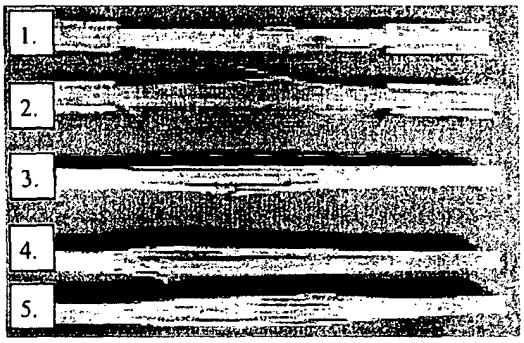

1. Baseline Control, 2. 1,000 Hours, 3. 3,000 Hours, 4. 10,000 Hours 5. Aged Control

(a)

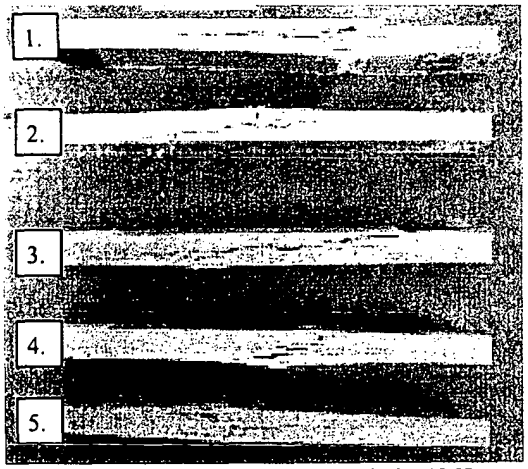

1. Baseline Control, 2. 1,000 Hours, 3. 3,000 Hours, 4. 10,000 Hours 5. Aged Control

(b)

Figure I. 3.4 Pultruded Salt Water Immersion Coupons in the Transverse

I.3.1.2.4 Interlaminar Shear Strength

The results of the interlaminar shear test conducted on the coupons from the sample plates for the immersion treatments are summarized in Table I.3.8. A one-way analysis of variance was used to compare all possible pairs of the interlaminar shear test results for each treatment of a particular exposure, baseline control, and aged control. The

results of the individual interlaminar shear test and the corresponding statistical analysis are located in Wood and Lopez-Anido (2000).

The interlaminar shear response of the laminates to the immersion treatments was a function of the exposure time. The laminates showed an increase of 2–6% in interlaminar shear strength for the first 3,000 hours, followed by decreases of 6.4–8.1% at 10,000 hours. However, the decreases in interlaminar shear strength were not statistically different from the control.

Table I.3.8 Interlaminar Shear Strength for the Longitudinal Coupons Cut from the Pultruded Sample Plates after the Environmental Exposure Treatments of Water and Salt Water Immersion

Treatment	Time (hours)	Sample Size	Interlaminar Shear Strength (MPa) (ksi)	Retained Strength (%)	COV (%)	ILS Strength Statistic Level	Depend. System Statistic
Water	1,000	10	27.3 (3.97)	102	4.56	AB	TIME
	3,000	10	27.2 (3.95)	103	8.54	AB	
	10,000	10	25.0 (3.62)	93.9	5.39	BC	
Salt Water	1,000	10	26.7 (3.87)	101	7.07	A	
	3,000	10	28.3 (4.11)	106	7.98	A	
	10,000	10	26.5 (3.84)	98.9	2.89	A	

I.3.1.3 Freeze-Thaw Cycling Treatment

This section is a summary of the results from the monitoring of the pultruded sample plates during the freeze-thaw treatments and the mechanical test performed on the coupons cut from the plates after the treatments.

I.3.1.3.1 Appearance

The only noticeable change in the appearance of the pultruded freeze-thaw sample plates was the progressive loss of the resin sealing the edges. Table I.3.9 summarizes the change in appearance of the pultruded sample plates after the freeze-thaw treatments.

Table I.3.9 Appearance of CPI Sample Plates after the Freeze-Thaw Cycling Treatments

20 Cycles	40 Cycles	60 Cycles
Resin used to seal the edges turns white and flakes off the samples	More of the resin used to seal the edges flakes off.	Almost all of the resin used to seal the edges flaked off.

I.3.1.3.2 Mass Change

The change in mass of the pultruded sample plates for the freeze-thaw treatments is summarized in Table I.3.10. For the freeze-thaw treatments there was an increase in mass after the 21-day immersion period followed by decreases for 20 and 40 cycles of the treatment. Some of the decrease in mass may be attributed to the loss of the sealant resin. The data from the monitoring of the sample plates during the exposure process are located in Wood and Lopez-Anido (2000).

Table I.3.10 Average Mass Change of Pultruded Samples Plates after the Freeze-Thaw Cycling Treatments

Average Mass Change (%) after Treatment			
Immersion for 21 Days	20 Cycles	40 Cycles	60 Cycles
0.24	0.15	0.11	0.11

I.3.1.3.3 Tensile Strength

Table I.3.11 and Table I.3.12 are summaries of the results of the tension tests of the coupons from the sample plates for the freeze-thaw cycling treatments. A one-way analysis of variance was used to compare all possible pairs of the mechanical test results (strength and elastic modulus) for each freeze-thaw treatment, baseline control, and aged control. The results of the individual tensile tests and the statistical analysis for coupons are located in Wood and Lopez-Anido (2000).

The coupons tested in the longitudinal direction after 20 freeze-thaw cycles showed a statistically significant decrease of 9.8%. However, the tensile strength of the coupons from 40 and 60 cycles of freeze-thaw did not show statistically significant decreases. The transverse tensile strength and the modulus of elasticity in both directions were statistically unaffected by the freeze-thaw cycles.

Table I.3.11 Tensile Strength Results for Coupons Cut from the Pultruded Sample Plates after the Environmental Exposure Treatments of Freeze-Thaw Cycling

Direction	Time (cycles)	Sample Size	Ultimate Tensile Strength MPa (ksi)	Retained Strength (%)	COV (%)	Strength Statistic Level
Longitudinal	20	5	265 (38.4)	90.2	3.89	B
	40	5	281 (40.7)	95.6	2.15	A
	60	5	289 (42.0)	98.6	1.71	A
Transverse	20	7	139 (20.2)	92.6	3.99	A
	40	7	141 (20.4)	93.8	7.73	A
	60	5	146 (21.1)	97.2	3.90	A

Table I.3.12 Modulus of Elasticity Results for the Tension Coupons Cut from the Pultruded Sample Plates after the Environmental Exposure Treatments of Freeze-Thaw Cycling

Direction	Time (cycles)	Sample Size	Modulus of Elasticity GPa (msi)	Retained Strength (%)	COV (%)	Modulus Statistic Level
Longitudinal	20	4	23.2 (3.37)	104	9.10	A
	40	5	22.6 (3.28)	101	7.28	A
	60	5	23.2 (3.36)	103	5.63	A
Transverse	20	7	15.2 (2.21)	95.7	6.04	A
	40	7	16.1 (2.34)	102	4.85	A
	60	5	15.7 (2.28)	99.1	2.32	A

The mode of failure of the tension coupons was unaffected by the freeze-thaw cycling treatments. Typical failures of the tension coupons are shown in Figure I.3.5.

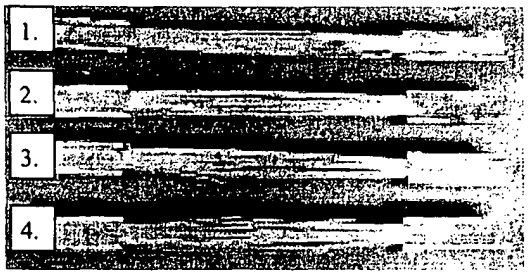

1. Baseline Control, 2. 20 Freeze-Thaw Cycles, 3. 40 Freeze-Thaw Cycles, and 4. 40 Freeze-Thaw Cycles

(a)

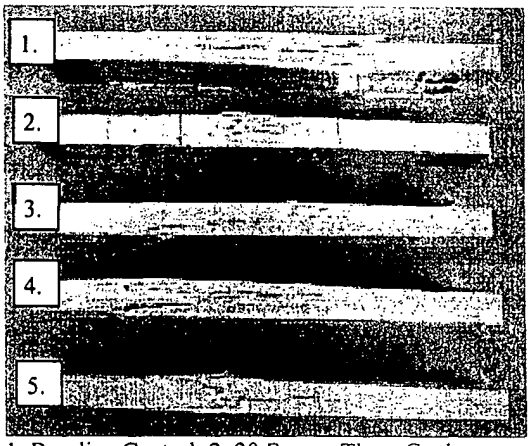

1. Baseline Control, 2. 20 Freeze-Thaw Cycles, 3. 40 Freeze-Thaw Cycles, and 4. 40 Freeze-Thaw Cycles

(b)

Figure I.3.5 Pultruded Freeze-Thaw Cycling Coupons: (a) Longitudinal, (b) Transverse

I.3.1.3.4 Interlaminar Shear Strength

The results of the interlaminar shear strength for the coupons from the sample plates for freeze-thaw treatments are summarized in Table I.3.13. A one-way analysis of variance was used to compare all possible pairs of the interlaminar shear test results for each freeze-thaw treatment, baseline control, and aged control. The results of the individual interlaminar shear test and the corresponding statistical analysis are located in Wood and Lopez-Anido (2000).

The response of the interlaminar shear strength to the freeze-thaw cycles was statistically unaffected by the treatments. The mode of failure of the interlaminar shear coupons did not change with the freeze-thaw cycling treatments.

Table I.3.13 Interlaminar Shear Strength for the Longitudinal Coupons Cut from the Pultruded Sample Plates after the Environmental Exposure Treatments of Freeze-Thaw Cycling

Time (Cycles)	Sample Size	Interlaminar Shear Strength MPa (ksi)	Retained ILS Strength (%)	COV (%)	ILSS Statistic
20	10	25.3 (3.67)	94.5	9.82	A
40	10	27.1 (3.93)	101	10.3	A
60	10	26.3 (3.81)	98.1	7.38	A

I.3.1.4 Weathering

This section is a summary of the results from the monitoring of the pultruded sample plates during the weathering treatments and the mechanical test performed on the coupons cut from the plates after the treatments.

I.3.1.4.1 Appearance

The appearance of the sample plates after one year of exterior exposure was very similar to the UV and water spray. Table I.3.14 is a summary of the appearance of the pultruded sample plates after the UV and water spray and exterior exposure treatments. The edge sealant of the samples subjected to the UV and water spray condition did not change color since the edges of the sample plates were not exposed to the UV bulbs.

Table I.3.14 Appearance of Pultruded Sample Plates after Subjection to the Weathering Treatments of UV and Water Spray, and Exterior Exposure

1,000 Cycles UV and Water Spray	2,000 Cycles UV and Water Spray	1 Year Exterior Exposure
Exposed surface turned brown	Exposed surface turned brown	Yellow/brownish color where exposed and the edge sealant was of brownish color.

I.3.1.4.2 Mass Change

Table I.3.15 is a summary of the change in mass of the pultruded sample plates after the weathering treatments of UV and water spray and exterior exposure. The sample plates showed a slight increase in mass of 0.03% for the exterior exposure treatment while decreasing progressively by 0.26% for the treatment of 2,000 cycles of UV and water spray. The data from the monitoring of the sample plates during the exposure process are located in Wood and Lopez-Anido (2000).

Table I.3.15 Mass Change of the Pultruded Sample Plates after the Weathering Treatments of UV and Water Spray, Exterior Exposure

Average Mass Change after Environmental Exposure Treatment (%)		
1,000 Cycles UV and Spray	2,000 Cycles UV and Spray	1 Year Exterior Exposure
-0.15	-0.26	0.03

I.3.1.4.3 Tensile Strength

The results of the tension tests of the coupons cut from the sample plates after the weathering treatments are summarized in Table I.3.16 and Table I.3.17. A one-way analysis of variance was used to compare all possible pairs of the mechanical test results (strength and elastic modulus) for each freeze-thaw treatment, baseline control, and aged control. The results of the individual tensile tests and the statistical analysis for coupons are located in Wood and Lopez-Anido (2000).

The longitudinal tension coupons showed a statistically significant decrease of 6.8 and 6.9% for 2,000 cycles of UV and water spray and 1 year of exterior exposure, respectively. The transverse tensile strength and the modulus of elasticity in both directions were unaffected by the treatments.

Table I.3.16 Tensile Strength Results for Coupons Cut from the Pultruded Sample Plates after the Environmental Exposure Treatments of UV and Water Spray, and Exterior Exposure

Direction	Treatment	Test Duration	Sample Size	Ultimate Tensile Strength MPa (ksi)	Residual Strength (%)	COV (%)	Strength Statistic Level
Longitudinal	UV and Water Spray	1,000 Cyc	5	283 (41.2)	96.7	6.67	ABC
		2,000 Cyc	5	274 (39.7)	93.2	5.99	BC
	Exterior	1 Year	5	274 (39.8)	93.1	5.37	BC
Transverse	UV and Water Spray	1,000 Cyc	4	144 (20.9)	96.0	4.35	A
		2,000 Cyc	4	146 (21.2)	97.3	3.04	A
	Exterior	1 Year	7	139 (20.2)	92.7	6.81	A

Table I.3.17 Modulus of Elasticity Results for Coupons Cut from the Pultruded Sample Plates after the Environmental Exposure Treatments of UV and Water Spray, and Exterior Exposure

Direction	Treatment	Test Duration	Sample Size	Modulus of Elasticity GPa (msi)	Residual Modulus (%)	COV (%)	Strength Statistic Level
Longitudinal	UV and Water Spray	1,000 Cyc	5	23.0 (3.36)	103	2.16	A
		2,000 Cyc	5	22.8 (3.30)	102	2.26	A
	Exterior	1 Year	5	23.0 (3.33)	102	5.01	A
Transverse	UV and Water Spray	1,000 Cyc	5	16.7 (2.42)	105	2.76	A
		2,000 Cyc	5	16.8 (2.44)	106	6.06	A
	Exterior	1 Year	7	16.2 (2.35)	102	4.42	A

The mode of failure of the tension coupons was unaffected by the freeze-thaw cycling treatments. Typical failures of the tension coupons are shown Figure I.3.6.

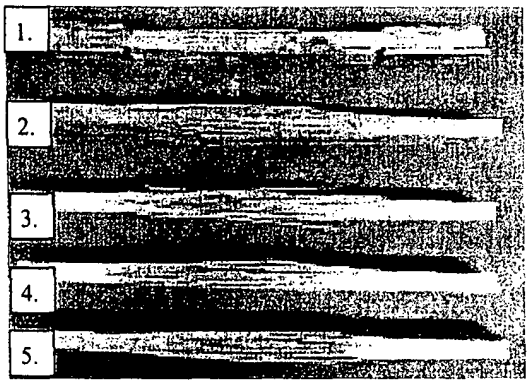

1. Baseline Control, 2. 1000 Cycles UV and Water Spray, 3. 2000 Cycles UV and Water Spray, 4. 1-Year Exterior Exposure, 5. Aged Control

(a)

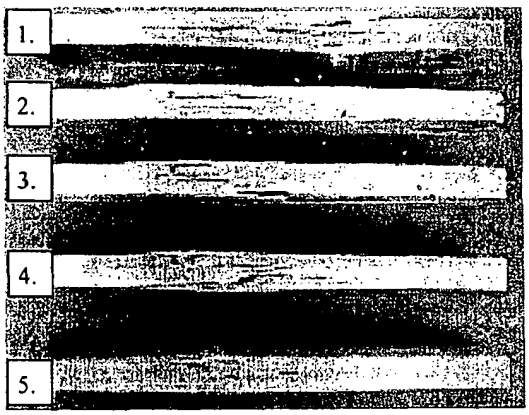

1. Baseline Control, 2. 1000 Cycles UV and Water Spray, 3. 2000 Cycles UV and Water Spray, 4. 1-Year Exterior Exposure, 5. Aged Control

(b)

Figure I.3.6 Pultruded Weathering Coupons: (a) Longitudinal, (b) Transverse

I.3.1.4.4 Interlaminar Shear Strength

The results of the interlaminar shear strength for the coupons from the sample plates for weathering treatments are summarized in Table I.3.18. A one-way analysis of variance was used to compare all possible pairs of the interlaminar shear test results for each freeze-thaw treatment, baseline control, and aged control. The results of the individual interlaminar shear test and the corresponding statistical analysis are located in Wood and Lopez-Anido (2000).

The response of the interlaminar shear strength to the weathering treatments was statistically unaffected by the treatments. The mode of failure of the interlaminar shear coupons did not change with the weathering treatments

Table I.3.18 Interlaminar Shear Strength for the Longitudinal Coupons Cut from the Pultruded Sample Plates after the Environmental Exposure Treatments of UV and Water Spray, and Exterior Exposure

Treatment	Test Duration	Sample Size	Interlaminar Shear Strength MPa (ksi)	Interlaminar Shear Residual (%)	COV (%)	ILSS Statistic Level
UV and Spray	1,000 Cyc	10	27.8 (4.03)	104	6.67	A
	2,000 Cyc	10	26.9 (3.90)	101	5.99	A
Exterior	1 Year	10	27.2 (3.94)	101	7.96	A

I.3.1.5 Summary

The responses of the pultruded material to all the environmental exposure treatments were very similar. The composite laminate showed statistically significant decreases of 6.8–9.8% in the longitudinal direction, depending on the treatment. However, there were no statistically significant decreases in the transverse tensile strength, the interlaminar shear strength, or the modulus of elasticity in either of the primary directions. The sealant resin did not withstand the immersion and freeze-thaw exposure treatments and flaked off over time.

I.3.2 FRP Material Fabricated by Pultrusion Used in Concrete Bridge Decks (DFI)

I.3.2.1 Control (unexposed)

This section is a summary of the results from the control tests conducted on the DFI pultruded laminates prior to subjecting them to the environmental exposure treatments and for the aged control samples. Baseline properties were established for appearance, longitudinal and transverse tensile strength, longitudinal and transverse tensile modulus of elasticity, and longitudinal interlaminar shear strength. The results of the ignition loss tests were used for verification of the results from the laminate analysis.

I.3.2.1.1 Appearance

The pultruded sample plates were black. Longitudinal stitch lines were apparent on both faces. Only the ends of the sample plates were sealed with resin since the material was pultruded to the 152.4-mm width. The sample plates had consistent dimensions.

I.3.2.1.2 Tensile Strength

The tensile strength of the control coupons was measured before and after environmental exposure to determine the effects of further curing during the exposure process. Table I.3.19 and Table I.3.20 summarize the results of the tension tests for the baseline control and aged control coupons. A one-way ANOVA was performed on the tension test data (strength and elastic modulus) to determine differences between the baseline control and aged results. The results of the individual tension tests and the statistical analysis for the control condition are given in Wood and Lopez-Anido (2000).

The values for 0.75 years of exposure were the baseline control values established for the 12.7-mm-wide coupons. The width of the tension coupons was narrowed to allow testing in the 100-kN Instron to minimize compression of the tab area during testing.

Table I.3.19 Ultimate Tensile Strength Results of Control Coupons for the Pultruded Material

Direction	Time (years)	Sample Size	Ultimate Tensile Strength MPa (ksi)	Residual Strength (%)	COV (%)	Statistical Level
Longitudinal	0	7	664 (96.3)	-	3.15	A
	0.75*	6	595 (86.4)	98.7	4.01	B
	1.5*	8	587 (85.2)		3.07	B
Transverse	0	5	28.1 (4.02)	110	8.79	B
	1.5	5	30.9 (4.48)		2.07	A

*12.7-mm- (0.5-in.-) wide samples

Table I.3.20 Modulus of Elasticity Results of Control Coupons for the Pultruded Material

Direction	Time (years)	Sample Size	Modulus of Elasticity GPa (msi)	Residual Modulus (%)	COV (%)	Statistical Level
Longitudinal	0	7	39.5 (5.73)	98.7	3.21	A
	0.75*	6	39.0 (5.65)		2.66	AB
	1.5*	8	40.8 (5.92)	103	3.08	A
Transverse	0	5	9.05 (1.31)	104	7.26	A
	1.5	5	9.40 (1.36)		1.36	A

*12.7-mm- (0.5-in.-) wide samples

The results of the tension tests conducted on the baseline control coupons and the aged control coupons showed decreases in the longitudinal tensile strength due to the change in coupon width and increases in transverse tensile strength. The decrease between the 25.4-mm and 12.7-mm longitudinal tension coupons was 10%, and the increase in the transverse tensile strength of the aged control coupons was 10%.

The modulus of elasticity in the longitudinal direction of the aged control coupons was not statically different from the baseline control. However, the two sets of 12.7-mm-wide coupons were statistically different from each other by 4.6%. The transverse modulus of elasticity of the aged control samples increased 3.9% but was not statistically different from the baseline control.

The mode of failure of the aged control tension coupons was not different from the control. The longitudinal tension coupons failed in an explosive manner typical of most unidirectional composites. Typical failures of the longitudinal tension coupons are shown in Figure I.3.7.

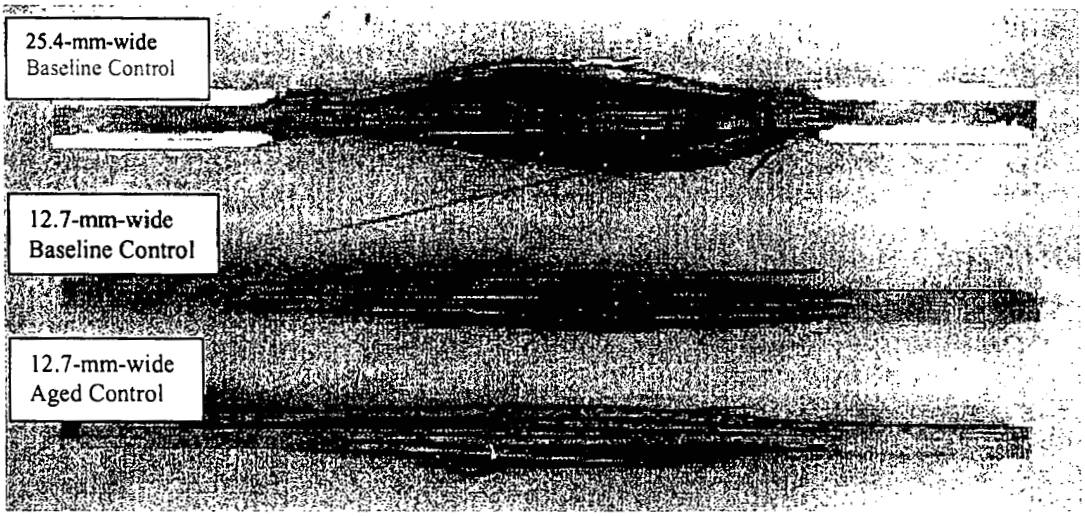

Figure I. 3.7 Control Longitudinal Tension Coupons for the Pultruded Material

The failure of the transverse tension coupons was characterized as a lateral failure within the unidirectional core followed by a diagonal failure of the ±45° fabric on the face of the laminate. The location of the failure within the gauge line was sporadic because the failure occurred at the weakest point within the unidirectional core and then at the weakest point in the fabric. Typical failures of the transverse control coupons are shown in the Figure I.3.8.

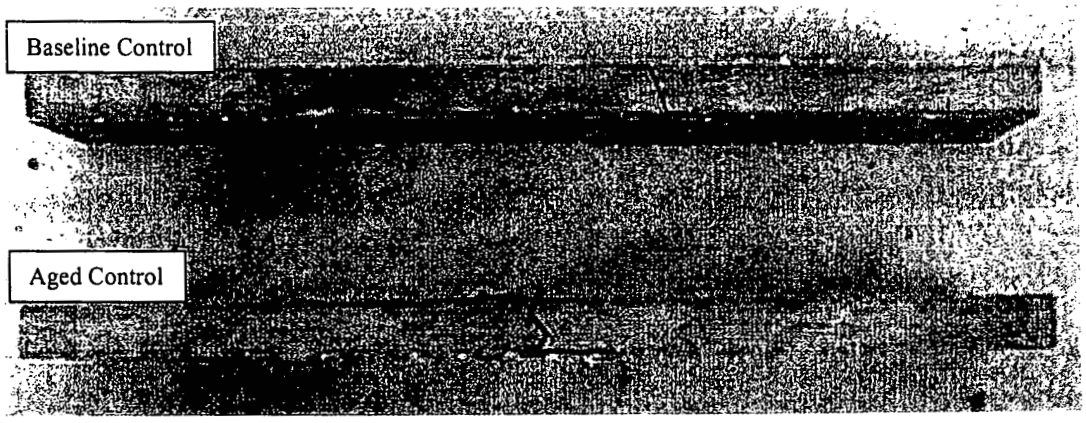

Figure I.3.8 Control Transverse Tension Coupons for the Pultruded Material

I.3.2.1.3 Interlaminar Shear Strength

Interlaminar shear tests were conducted before and after environmental exposure to evaluate the interface between the fibers and the matrix. Table I.3.21 summarizes the results of the interlaminar shear tests of the control coupons before and after the environmental exposure period. A one-way ANOVA was performed on the interlaminar shear test data to determine differences between the baseline control and aged results. The results of the individual interlaminar shear test and the corresponding statistical analysis are located in Wood and Lopez-Anido (2000).

There was no statistically significant change in the interlaminar shear strength between the baseline control and the aged control sample sets. The interlaminar shear coupons failed in a typical interlaminar shear manner between the individual rovings in the core of the laminate.

Table I.3.21 Interlaminar Shear Strength Results of Control Coupons for the Pultruded Material

Aging Time (years)	Sample Size	Interlaminar Shear Strength MPa (ksi)	Residual Interlaminar Shear Strength (%)	COV (%)	Statistical Level
0	10	38.5 (5.59)	98.7	3.63	A
1.5	10	38.0 (5.51)		2.53	A

I.3.2.1.4 Ignition Loss

Ignition loss tests (ASTM D 2548) were conducted to verify the volume fractions used in the laminate analysis. Ignition loss tests were conducted on ten specimens, and the average fiber volume fraction was 61.5% with a COV of 0.78%. The results of the individual ignition loss tests are located in Wood and Lopez-Anido (2000).

I.3.2.2 Immersion Treatments

This section summarizes the results of the pultruded samples plates subjected to the environmental exposure treatments of immersion in water, salt water, and alkali solutions for 1,000, 3,000, and 10,000 hours

I.3.2.2.1 Appearance

The appearance of the pultruded sample plates subjected to the immersion treatments did not change over the course of the exposure period of 10,000 hours.

I.3.2.2.2 Mass Change

Table I.3.22 summarizes the average change in mass of the sample plates after the immersion treatments. The changes in mass of the sample plates subjected to the water and alkali treatments were very similar. The mass change of the salt water sample plates was higher than for the water or alkali plates after 10,000 hours, but the rate of change was much slower than for the other two conditions. The sample plates coated with epoxy had a rate of mass change similar to that of the salt water plates, but the mass change of the epoxy-coated plate was higher than for all the rest at 10,000 hours. The weight data from the monitoring of the sample plates during the exposure process are located in Wood and Lopez-Anido (2000).

Table I.3.22 Mass Change of the Pultruded Immersion Plates after Environmental Exposure Treatments of Water and Salt Water

Treatment	Average Mass Change after Environmental Exposure (%)		
	1,000 Hours	3,000 Hours	10,000 Hours
Water	1.67	2.10	2.10
Salt Water	0.39	1.49	2.25
Alkali	1.56	2.10	2.10
Alkali (DFI-E)	0.66	1.31	2.41

I.3.2.2.3 Tensile Strength

Table I.3.23 is a summary of the results from the tension tests of the pultruded coupons from the sample plates for the water, salt water, and alkali treatments. Also included are the results of the epoxy-coated pultruded coupons from the epoxy-coated pultruded sample plates for the alkali condition only. A one-way analysis of variance was used to compare all possible pairs of the mechanical test results (strength and elastic modulus) for each treatment of a particular exposure, baseline control, and aged control. A two-way analysis of variance was used to determine the dependency (time, treatment, or interaction of time and treatment) of the mechanical response. The results of the individual tensile tests and the statistical analysis for tension coupons are located in Wood and Lopez-Anido (2000).

Table I.3.23 Tensile Strength Results for the Coupons Cut from the Pultruded Sample Plates after the Environmental Exposure Treatments of Water, Salt Water, and Alkali Immersion

Direction	Treatment	Time (hrs)	Sample Size	Ultimate Tensile Strength MPa (ksi)	Retained Strength (%)	COV (%)	Strength Statistic for Treat.	Depend. System Statistic
Long.	Water	1,000	5	517 (74.9)	77.8	5.79	BC	COND. (C)
		3,000	6*	505 (73.2)	84.8	8.19	B	
		10,000	6*	409 (59.3)	68.7	6.94	BC	
	Salt Water	1,000	5	577 (83.7)	86.9	10.46	B	COND. (B)
		3,000	6*	610 (88.6)	103	1.87	A	
		10,000	7*	475 (68.9)	79.7	1.57	B	
	Alkali	1,000	5	535 (77.7)	80.6	9.00	B	COND. (C)
		3,000	0	NDA**	-	-	-	
		10,000	7*	431 (62.5)	72.3	2.83	B	
	DFI-E (Alkali)	1,000	5	620 (89.9)	93.4	3.47	A	COND. (B)
		3,000	7*	500 (72.5)	83.9	6.13	B	
		10,000	7*	488 (70.8)	82.0	4.57	B	
Trans.	Water	1,000	7	29.5 (4.28)	105	2.81	A	INTER-ACTION
		3,000	0	NDA*	-	-	-	
		10,000	7	26.9 (3.91)	95.9	2.65	A	
	Salt Water	1,000	7	30.6 (4.44)	108	5.46	A	
		3,000	0	NDA*	-	-	-	
		10,000	6	22.4 (3.26)	79.4	46.7	B	

* 12.7-mm- (0.5-in.-) wide samples
NDA** = No Data Available

The tension coupons cut from the pultruded sample plates for the immersion conditions of water, salt water, and alkali all showed statistically significant decreases in longitudinal tensile strength. The coupons from the water plates showed an initial decrease in longitudinal tensile strength of the 12%, followed by a slight increase of 8.3% and another decrease of 20%, resulting in a total decrease in longitudinal tensile strength of 31%. These decreases were statistically significant from the baseline control but were not different from each other. The slight increase at 3000 hours was presumably due to the change in size of the tension coupons and any dry-out that may have occurred in the samples while dealing with the tabbing problem. The transverse tensile strength of the coupons from the sample plates from the water treatment was statistically unaffected by the treatment.

The coupons cut from the salt water plates showed a 13% decrease in longitudinal tensile strength after 1,000 hours, which was followed by an 18% increase after 3,000 hours and another decrease of 22% after 10,000 hours. This resulted in a 20% decrease from the baseline control after 10,000 hours. The decreases at 1,000 and 10,000 hours were statistically different from the baseline control, but they were not statistically different from each other. The increase at 3,000 hours is presumably due to the change in coupon size and any dry-out that may have occurred in the samples while dealing with the tabbing problem. The transverse tension coupons showed a statistically significant decrease in tensile strength of 20% after 10,000 hours of the salt water treatment.

The pultruded and epoxy-coated pultruded longitudinal coupons that were cut from the sample plates for the alkali condition both showed statistically significant decreases from the baseline control. However, the epoxy-coated coupons showed a smaller decrease in strength after 10,000 hours. The pultruded coupons showed an initial decrease of 19% after 10,000 hours and a total decrease of 28% after 10,000 hours. The epoxy-coated pultruded coupons showed a statistically insignificant decrease of 7% after 1,000 hours, followed by another decrease of 10% after 3,000 hours and a total decrease of 18% after 10,000 hours.

The mode of failure of the longitudinal and transverse tension coupons did not change due to any of the three treatments. The mode of failure of the longitudinal coupons was always an explosive failure, while the transverse sample always failed abruptly at the weakest point in the matrix. Figure I.3.9, Figure I.3.10, and Figure I.3.11 show typical failures of the tension coupons in both directions for the water, salt water, and alkali immersion treatments.

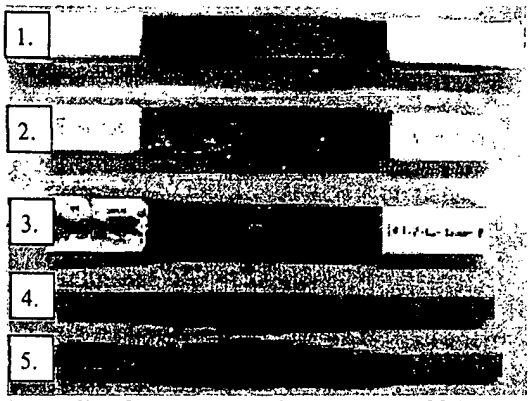

1. Baseline Control, 2. 1,000 Hours, 3. 3,000 Hours, 4. 10,000 Hours 5. Aged Control

(a)

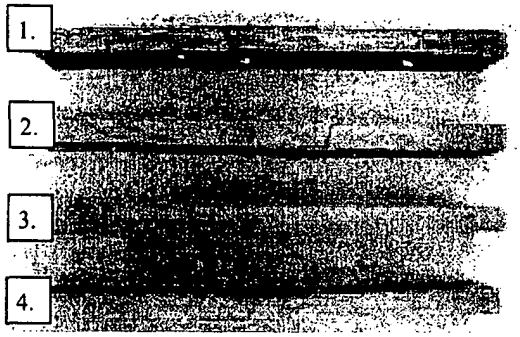

1. Baseline Control, 2. 1,000 Hours, 3. 3,000 Hours, 4. 10,000 Hours 5. Aged Control

(b)

Figure I.3.9 Pultruded Water Immersion Coupons: (a) Longitudinal, (b) Transverse

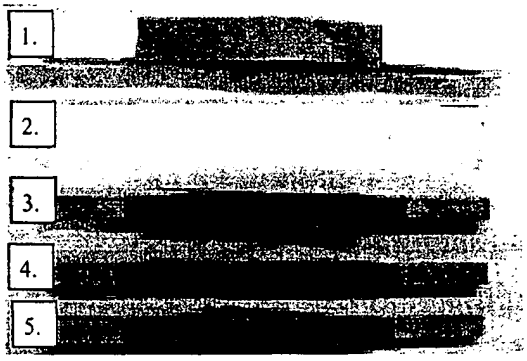

1. Baseline Control, 2. 1,000 Hours, 3. 3,000 Hours, 4. 10,000 Hours 5. Aged Control

(a)

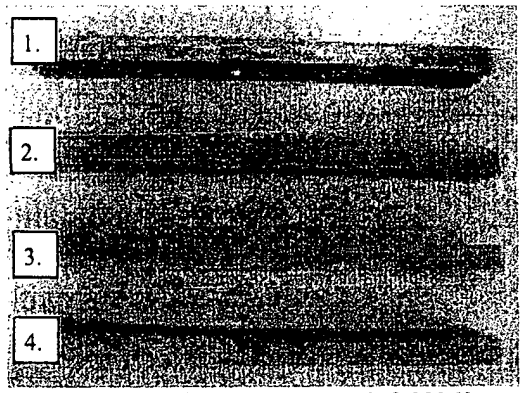

1. Baseline Control, 2. 1,000 Hours, 3. 3,000 Hours, 4. 10,000 Hours 5. Aged Control

(b)

Figure I.3.10 Pultruded Salt Water Immersion Coupons: (a) Longitudinal, (b) Transverse

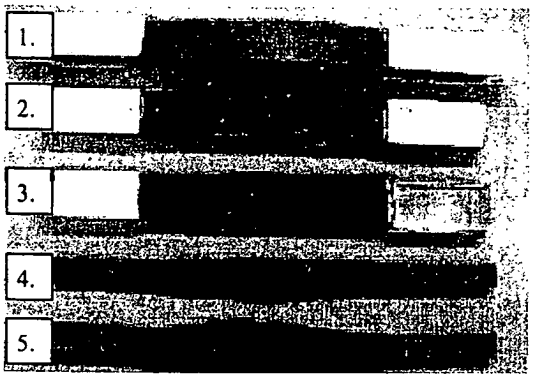

1. Baseline Control, 2. 1,000 Hours, 3. 3,000 Hours, 4. 10,000 Hours 5. Aged Control

(a)

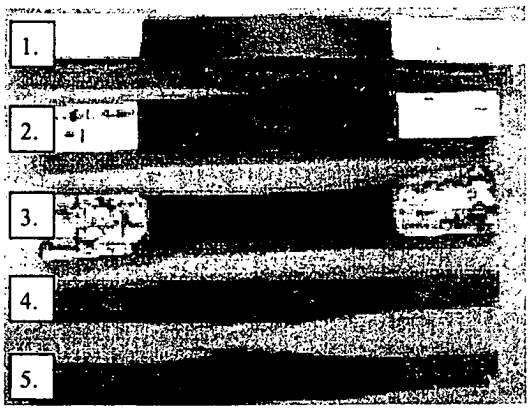

1. Baseline Control, 2. 1,000 Hours, 3. 3,000 Hours, 4. 10,000 Hours 5. Aged Control

(b)

Figure I.3.11 Pultruded Alkali Immersion Coupons: (a) Non-Epoxy Coated, (b) Epoxy Coated

The modulus of elasticity in the longitudinal direction of the non-epoxy-coated coupons was unaffected by the immersion treatments. The results for the elastic modulus are shown in Table I.3.24. The modulus of elasticity results for 1,000 hours of immersion in water and salt water were lost due to a bad extensometer. The changes in modulus of elasticity were only ±4% from the control value. Thus, they were statistically insignificant. The modulus of elasticity of the longitudinal coupons from the epoxy-coated plates did show a statistically significant decrease of 9% for 3000 hours. The initial increase of 12% was not statistically significant.

The transverse coupons showed consecutive statistically significant decreases in the transverse modulus of elasticity for 1,000 and 10,000 hours. The coupons from the water immersion sample showed decreases of 13 and 31% after 1,000 and 10,000 hours, respectively, and the salt water coupons showed decreases of 9 and 28% after 1,000 and

10,000 hours, respectively. The 3,000 hours of immersion sample plates were sacrificed for longitudinal tension coupons after those coupons failed in the grips.

Table I.3.24 Modulus of Elasticity Results for the Coupons Cut from the Pultruded Sample Plates after the Environmental Exposure Treatments of Water, Salt Water and Alkali Immersion

Direction	Treat.	Time (hrs)	Sample Size	Modulus of Elasticity GPa (msi)	Retained Strength (%)	COV (%)	Strength Statistic for Treatment	Depend. System Statistic
Long.	Water	1,000	0	NDA**	-	-	-	NONE
		3,000	6*	39.1 (5.66)	98.8	2.57	A	
		10,000	6*	38.9 (5.63)	98.4	2.58	A	
	Salt Water	1,000	0	NDA**	-	-	-	
		3,000	6*	39.3 (5.71)	99.6	2.51	A	
		10,000	7*	37.8 (5.48)	95.7	3.77	A	
	Alkali	1,000	5	40.4 (5.86)	102	4.60	A	
		3,000	0	NDA**	-	-	-	
		10,000	7*	38.1 (5.52)	96.4	1.88	A	
	DFI-E (Alkali)	1,000	5	44.0 (6.39)	112	9.36	AB	INTER-ACTION
		3,000	7*	35.9 (5.20)	90.8	7.80	D	
		10,000	7*	39.8 (5.77)	101	3.36	BC	
Trans.	Water	1,000	5	7.50 (1.09)	82.8	11.86	B	INTER-ACTION
		3,000	0	NDA**	-	NDA	-	
		10,000	7	6.22 (0.902)	68.7	7.05	C	
	Salt Water	1,000	5	8.27 (1.06)	91.4	8.83	BC	
		3,000	0	NDA**	-	NDA	-	
		10,000	6	6.49 (0.942)	71.7	3.56	D	

* 12.7-mm- (0.5-in.-) wide samples
NDA** = No Data Available

I.3.2.2.4 Interlaminar Shear Strength

The results of the interlaminar shear tests conducted on the coupons cut from the sample plates for the immersion treatments are summarized in Table I.3.25. A one-way analysis of variance was used to compare all possible pairs of the interlaminar shear test results for each treatment of a particular exposure, baseline control, and aged control. The results of the individual interlaminar shear tests and the corresponding statistical analysis are located in Wood and Lopez-Anido (2000).

Table I.3.25 Interlaminar Shear Strength Results for the Coupons Cut from the Pultruded Sample Plates after the Environmental Exposure Treatments of Water, Salt Water, and Alkali Immersion

Treatment	Time (hours)	Sample Size	Interlaminar Shear Strength MPa (ksi)	Residual Interlaminar Shear Strength (%)	COV (%)	ILSS Statistic for Treatment	Depend. System
Water	1,000	10	33.6 (4.87)	87.1	1.44	B	TIME & COND (B)
	3,000	10	39.2 (5.69)	102	2.53	A	
	10,000	10	30.5 (4.42)	79.1	3.37	C	
Salt Water	1,000	10	37.3 (5.41)	96.8	2.01	B	TIME & COND (AB)
	3,000	10	39.8 (5.79)	103	3.07	A	
	10,000	10	31.9 (4.62)	82.7	2.03	C	
Alkali	1,000	4	38.4 (5.58)	99.8	3.61	A	TIME & COND (B)
	3,000	8	39.7 (5.75)	103	2.56	A	
	10,000	10	30.0 (4.35)	77.9	5.19	B	
Alkali (DFI-E)	1,000	5	35.6 (5.17)	96.3	3.58	A	TIME & COND (B)
	3,000	10	37.4 (5.42)	97.1	9.75	A	
	10,000	10	32.1 (4.65)	83.3	7.32	B	

The response of the interlaminar shear strength of the laminates was a function of treatment time and condition and was similar to the tensile strength response. The water and salt water coupons showed statistically significant decreases in interlaminar shear strength for 1,000 hours, followed by a recovery of the loss after 3,000 hours. The loss at 1,000 hours was 13% and 3% for the water and salt water treatments, respectively. The final loss of interlaminar shear strength at 10,000 hours was statistically greater than the loss of interlaminar shear strength at 1,000 hours. The final loss of interlaminar shear strength at 10,000 hours was 21% and 17% for the water and salt water treatments, respectively. The recovery of interlaminar shear strength was presumably due to dry-out of the coupons between removal from the treatment and testing.

The interlaminar shear strength of the epoxy-coated and non-epoxy-coated coupons from the sample plates from the alkali immersion treatment showed the same response. Neither set of coupons for the treatment times of 1,000 and 3,000 hours showed any statistically significant response to the alkali treatment. At 10,000 hours,

both sets of coupons showed statistically significant decreases of 22% and 17% for the non-epoxy-coated and epoxy-coated coupons, respectively. However, the decreases were not statistically different from each other.

I.3.2.3 Freeze-Thaw Cycling Treatment

This section is a summary of the results from monitoring of the pultruded sample plates during the freeze-thaw treatments and the mechanical tests performed on the coupons cut from the plates after the treatments.

I.3.2.3.1 Appearance

The appearance of the pultruded sample plates did not change during the treatments of freeze-thaw cycles.

I.3.2.3.2 Mass Change

The change in mass of the pultruded sample plates after the 21-day conditioning period was 1.78% and the sample plates continued to absorb water during the tests, reaching a maximum mass change of 2.16% after 60 freeze-thaw cycles. The total change in mass of the sample plates after 60 freeze-thaw cycles was comparable to the total change of the immersion plates after 10,000 hours. In addition, the mass change after the 21-day conditioning period was comparable to the mass change of the water immersion plates after 1,000 hours. The change in mass of the pultruded sample plates for the freeze-thaw treatments is summarized in Table I.3.26. The weight data from the monitoring of the sample plates during the exposure process are located in Wood and Lopez-Anido (2000).

Table I.3.26 Average Mass Change of the Pultruded Sample Plates after the Environmental Exposure Treatments of Freeze-Thaw Cycling

Average Mass Change after Environmental Exposure (%)			
Immersion for 21 Days	**20 Cycles**	**40 Cycles**	**60 Cycles**
1.78	1.95	2.05	2.16

I.3.2.3.3 Tensile Strength

Table I.3.27 and I.3.28 summarize the results of the tension tests of the coupons from the sample plates for the freeze-thaw cycling treatments. A one-way analysis of variance was used to compare all possible pairs of the mechanical test results (strength and elastic modulus) for each freeze-thaw treatment, baseline control, and aged control. The results of the individual interlaminar shear tests and the corresponding statistical analysis are located in Wood and Lopez-Anido (2000).

The coupons tested in the longitudinal direction showed a statistically significant decrease relative to the control for 20 and 40 cycles of freeze-thaw treatments. The coupons showed a decrease of 19% and 16% from the baseline control for 20 and 40 cycles of freeze-thaw, respectively. The longitudinal coupons for 60 cycles of freeze-thaw were lost due to crushing of the sample by the grips. The transverse coupons showed a statistically significant increase of 18% relative to the control for 40 cycles of freeze-thaw. However, the minor decreases in tensile strength for 20 and 60 cycles of freeze-thaw were statistically insignificant.

Table I.3.27 Tensile Strength Results for Coupons Cut from the Pultruded Sample Plates after the Environmental Exposure Treatments of Freeze-Thaw Cycling

Direction	Time (cycles)	Sample Size	Ultimate Tensile Strength MPa (ksi)	Retained Strength (%)	COV (%)	Strength Statistic Level
Longitudinal	20	5	538 (78.1)	81.1	2.67	B
	40	5*	503 (72.9)	84.4	5.09	B
	60	0	NDA**	-	-	-
Transverse	20	7	27.2 (3.94)	96.8	3.59	A
	40	7	33.0 (4.79)	118	3.69	B
	60	7	27.6 (4.01)	98.4	2.46	A

* 12.7-mm- (0.5-in.-) wide samples
NDA** = No Data Available

Table I.3.28 Modulus of Elasticity Results for the Tension Coupons Cut from the Pultruded Sample Plates after the Environmental Exposure Treatments of Freeze-Thaw Cycling

Direction	Time (cycles)	Sample Size	Modulus of Elasticity GPa (msi)	Retained Strength (%)	COV (%)	Modulus Statistic Level
Longitudinal	20	5	38.4 (5.58)	97.3	6.54	A
	40	5*	37.6 (5.45)	95.2	4.63	A
	60	0	NDA**	-	-	-
Transverse	20	7	6.91 (1.00)	76.4	10.8	B
	40	7	8.69 (1.26)	94.7	11.2	A
	60	7	7.25 (1.05)	80.1	4.31	B

* 12.7-mm- (0.5-in.-) wide samples
NDA** = No Data Available

The longitudinal modulus of elasticity of the tension coupons cut from the sample plates was statistically unaffected by the freeze-thaw cycles. The data showed a slight decrease of 3% and 5% for 20 and 40 freeze-thaw cycles, respectively, which were statistically insignificant. The transverse coupons showed statistically significant decreases for 40 and 60 cycles of freeze-thaw of 24% and 20%, respectively. The decrease in transverse modulus was 5.3%, which was statistically insignificant.

The mode of failure of the tension samples did not change with the freeze-thaw treatments. Figure I.3.12 shows typical failure for the freeze-thaw coupons in the longitudinal and transverse directions.

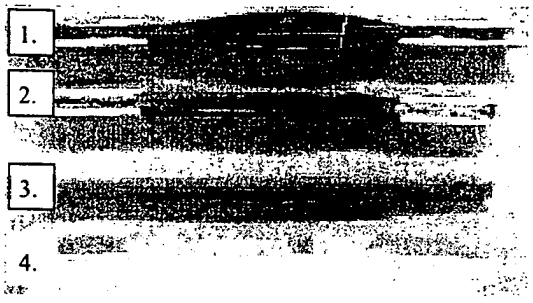

1. Baseline Control, 2. 20 Freeze-Thaw Cycles, 3. 40 Freeze-Thaw Cycles, and 4. 40 Freeze-Thaw Cycles

(a)

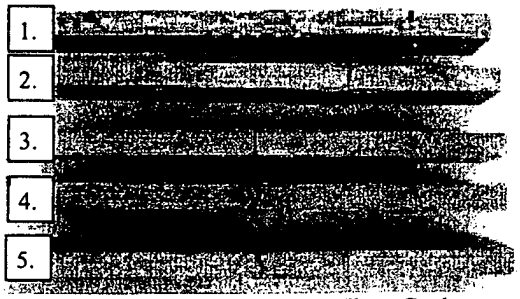

1. Baseline Control, 2. 20 Freeze-Thaw Cycles, 3. 40 Freeze-Thaw Cycles, and 4. 40 Freeze-Thaw Cycles

(b)

Figure I.3.12 Pultruded Freeze-Thaw Cycling Coupons: (a) Longitudinal, (b) Transverse

I.3.2.3.4 Interlaminar Shear Strength

The results of the interlaminar shear tests conducted on the coupons cut from the sample plates from freeze-thaw treatments are summarized in Table I.3.29. A one-way analysis of variance was used to compare all possible pairs of the interlaminar shear test results for each freeze-thaw treatment, baseline control, and aged control. The results of the individual interlaminar shear tests and the corresponding statistical analysis are located in Wood and Lopez-Anido (2000).

The interlaminar shear coupons from the sample plates for 20 freeze-thaw treatments showed a statistically significant decrease of 18% relative to the control. However, there were no strength reductions for the coupons from the plates for 40 and 60 freeze-thaw treatments. The recovery of interlaminar shear strength of the samples for 40 and 60 freeze-thaw treatments could be attributed to the dry-out of the sample between

the end of the treatments and the testing the samples. Finally, the mode of failure of the interlaminar shear coupons was not affected by the freeze-thaw treatments.

Table I.3.29 Interlaminar Shear Strength for the Longitudinal Coupons Cut from the Pultruded Sample Plates after the Environmental Exposure Treatments of Freeze-Thaw Cycling

Time (Cycles)	Sample Size	Interlaminar Shear Strength (MPa) (ksi)	Retained ILS Strength (%)	COV (%)	ILSS Statistic Level
20	10	31.5 (4.57)	81.8	1.73	B
40	10	39.7 (5.76)	103	2.71	A
60	10	38.7 (5.61)	100	1.38	A

I.3.2.4 Weathering Treatments

This section is a summary of the results of the weathering treatments and the mechanical tests performed on the coupon cut from the pultruded sample plates after the treatments.

I.3.2.4.1 Appearance

The appearance of the sample plates after the weathering treatments is summarized in Table I.3.30. Very small amounts of fibers were exposed on the surface of the sample plates after the UV and water spray treatments. The UV and water spray sample plates were the only plates to show any visible changes after the environmental exposure treatments.

Table I.3.30 Appearance of the Pultruded Sample Plates after the Environmental Exposure Treatments of UV and Water Spray, and Exterior Exposure

1,000 Cycles UV and Spray	2,000 Cycles UV and Spray	1 Year Exterior Exposure
Very small amounts of exposed fibers	Very small amounts of exposed fibers	The stitching lines were more prominent

I.3.2.4.2 Mass Change

The mass change was minimal for the weathering conditions. The UV and water spray samples showed minor decreases of 0.04% and 0.05%, respectively, which corresponded to the exposure of the fibers, and the exterior exposure samples showed an increase of 0.12%. The mass change of the sample plates for the weathering treatments is summarized in Table I.3.31. The weight data from the monitoring of the sample plates during the exposure process are located in Wood and Lopez-Anido (2000).

Table I.3.31 Average Mass Change of the Pultruded Sample Plates after the Environmental Exposure Treatments of UV and Water Spray, and Exterior Exposure

Average Mass Change after Environmental Exposure (%)		
1,000 Cycles UV and Water Spray	2,000 Cycles UV and Water Spray	1 Year Exterior Exposure
–0.04	–0.05	0.12

I.3.2.4.3 Tensile Strength

The results of the tension tests on the coupons from the sample plates for the weathering tests are summarized in Table I.3.32 and Table I.3.33. A one-way analysis of variance was used to compare all possible pairs of the mechanical test results (strength and elastic modulus) for each treatment of a particular exposure, baseline control, and aged control. The results of the tension tests and statistical analysis for the weathering coupons are located in Wood and Lopez-Anido (2000).

The longitudinal samples showed a statistically significant increase of 3% for 1,000 cycles of UV and water spray treatments. However, the slight increase of 1% for 2,000 cycles of UV and water spray treatments and the 3% decrease for the exterior exposure treatment were statistically insignificant. The transverse samples showed

statistically significant increases of 15%, 13%, and 15% with respect to the control coupons for the weathering treatments of 1,000 and 2,000 cycles of UV and water spray treatments and exterior exposure treatment, respectively.

The longitudinal modulus of elasticity of the tension coupons was not affected by the weathering treatments. The increases of 2% and 3% for the 2,000 cycles of UV and water spray treatments and the exterior exposure treatment, respectively, were statistically insignificant. The transverse tension coupons showed decreases of 10% relative to the baseline control for 1,000 cycles of UV and water spray treatments and the exterior exposure treatment. These decreases were statistically significant.

Table I.3.32 Tensile Strength Results for Coupons Cut from the Pultruded Sample Plates after the Environmental Exposure Treatments of UV and Water Spray, and Exterior Exposure

Direction	Treatment	Test Duration	Sample Size	Ultimate Tensile Strength MPa (ksi)	Residual Tensile Strength (%)	COV (%)	Strength Statistic Level
Longitudinal	UV and Water Spray	1,000 Cyc	6*	614 (89.1)	103	1.13	A
		2,000 Cyc	5*	600 (87.0)	101	2.39	AB
	Exterior	1 Year	6*	579 (83.9)	97.1	3.03	AB
Transverse	UV and Water Spray	1,000 Cyc	5	32.5 (4.71)	115	5.24	A
		2,000 Cyc	5	31.3 (4.53)	113	4.10	A
	Exterior	1 Year	7	32.3 (4.68)	115	4.84	A

*12.7-mm-wide tension samples

Table I.3.33 Modulus of Elasticity Results for Coupons Cut from the Pultruded Sample Plates after the Environmental Exposure Treatments of UV and Water Spray, and Exterior Exposure

Direction	Treatment	Test Duration	Sample Size	Modulus of Elasticity GPa (msi)	Residual Modulus (%)	COV (%)	Strength Statistic Level
Longitudinal	UV and Water Spray	1,000 Cyc	7*	39.6 (5.74)	100	2.31	A
		2,000 Cyc	5*	40.9 (5.93)	103	3.36	A
	Exterior	1 Year	7*	39.5 (5.74)	102	8.36	A
Transverse	UV and Water Spray	1,000 Cyc	5	8.16 (1.18)	90.2	4.03	BC
		2,000 Cyc	5	9.25 (1.34)	102	9.19	AB
	Exterior	1 Year	7	8.17 (1.19)	90.3	6.98	BC

The mode of failure of the tension coupons was not affected by the weathering treatments. Figure I.3.13 shows typical failures of the tension coupons from sample plates for the weathering treatments.

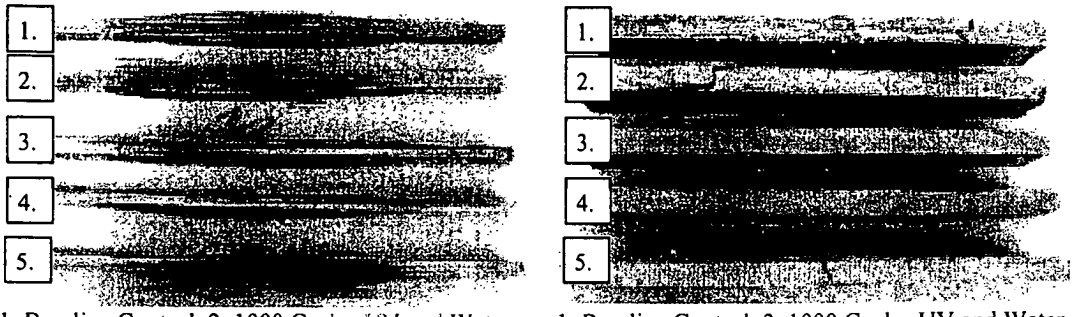

1. Baseline Control, 2. 1000 Cycles UV and Water Spray, 3. 2000 Cycles UV and Water Spray, 4. 1-Year Exterior Exposure, 5. Aged Control

(a)

1. Baseline Control, 2. 1000 Cycles UV and Water Spray, 3. 2000 Cycles UV and Water Spray, 4. 1-Year Exterior Exposure, 5. Aged Control

(b)

Figure I.3.13 Pultruded Weathering Coupons: (a) Longitudinal, (b) Transverse

I.3.2.4.4 Interlaminar Shear Strength

The results of the interlaminar shear tests conducted on the coupons from the weathering sample plates are summarized in Table I.3.34. A one-way analysis of variance was used to compare all possible pairs of the interlaminar shear test for each treatment of a particular exposure, baseline control, and aged control. The results of the tension tests and statistical analysis for the weathering coupons are located in Wood and Lopez-Anido (2000).

The interlaminar shear coupons showed statistically significant increases in interlaminar shear strength for all three treatments. The increases were 4%, 6%, and 3% relative to the baseline control for the treatments of 1,000 and 2,000 cycles of UV and water spray treatments and the exterior exposure treatment. The mode of failure of the interlaminar shear samples was unaffected by the weathering treatments.

Table I.3.34 Interlaminar Shear Strength for the Longitudinal Coupons Cut from the Pultruded Sample Plates after the Environmental Exposure Treatments of UV and Water Spray, and Exterior Exposure

Treatment	Test Duration	Sample Size	Interlaminar Shear Strength MPa (ksi)	Interlaminar Shear Strength Residual (%)	COV (%)	ILSS Statistic
UV and Water Spray	1,000 Cyc	10	39.9 (5.79)	104	1.13	ABC
	2,000 Cyc	10	40.9 (5.93)	106	2.39	AB
Exterior	1 Year	10	39.8 (5.78)	103	2.17	ABC

I.3.2.5 Summary

The response of the pultruded laminates to the exposure treatments with immersion baths was much different from the weathering exposure response. The longitudinal tensile strength was severely degraded for the treatments in water, salt water, alkali, and freeze-thaw. The longitudinal modulus of elasticity was degraded for the epoxy-coated coupons for the alkali condition but increased for the UV and water spray and exterior exposure treatments.

The retained values of the transverse properties of the laminate were more variable than the longitudinal ones. The transverse tensile strength was degraded for the salt water treatments but increased for the freeze-thaw treatments. However, there was not a decrease in the response of either of the weathering treatments. The response of the transverse modulus was very similar the strength response. The coupons showed decreases for the water, salt water, freeze-thaw, exterior exposure, and UV and water spray treatments.

The interlaminar shear strength of the coupons was degraded for the water, salt water, alkali, and freeze-thaw treatments but increased for the exterior exposure and UV

and water spray treatments. The interlaminar shear response was also unpredictable. The water and salt water specimens decreased initially, then regained the lost strength, and then subsequently lost the strength again after 10,000 hours. However, the alkali coupons showed continuous degradation with time.

I.3.3 FRP Material Fabricated by VARTM Used in Bridge Decks (HCC)

I.3.3.1 Control (Unexposed)

This section is a summary of the results from the control tests conducted on the VARTM laminates prior to subjecting them to the environmental exposure treatments and for the aged control samples. Baseline properties were established for appearance, longitudinal and transverse tensile strength, longitudinal and transverse tensile modulus of elasticity, and longitudinal interlaminar shear strength. The results of the ignition loss tests were obtained for verification of the results from the laminate analysis.

I.3.3.1.1 Appearance

Observations of the appearance of the sample plates were made before and after environmental exposure. The VARTM material was of greenish color with all four edges sealed with a clear resin. The laminate had one flat side, while the other was of wave-like appearance. The fiber direction was apparent on flat side and the stitching was visible on the wavy side. These observations served as a reference for evaluating the environmentally aged samples.

I.3.3.1.2 Tensile Strength

The tensile strength of the control coupons was measured before and after environmental exposure to determine the effects of further curing during the exposure process. Table I.3.35 and TableI.3.36 summarize the results of the tension tests for the baseline control and aged control coupons. A one-way ANOVA was performed on the tension test data (strength and elastic modulus) to determine differences between the baseline control and aged results. The results of the individual tensile tests and the statistical analysis for tension coupons are located in Wood and Lopez-Anido (2000).

Table I.3.35 Ultimate Tensile Strength Results of the Control Coupons for the VARTM Material

Direction	Time (years)	Sample Size	Ultimate Tensile Strength MPa (ksi)	Residual Strength (%)	COV (%)	Statistical Level
Longitudinal	0	7	434 (63.0)	116	7.86	B
	1.5	6	503 (72.9)		2.94	A
Transverse	0	7	288 (41.8)	96.5	4.37	A
	1.5	8	278 (40.3)		8.09	A

Table I.3.36 Modulus of Elasticity of Results of the Control Coupons for the VARTM Material

Direction	Time (years)	Sample Size	Modulus of Elasticity GPa (msi)	Residual Modulus (%)	COV (%)	Statistical Level
Longitudinal	0	7	23.6 (3.42)	102	9.51	A
	1.5	8	24.1 (3.49)		5.17	A
Transverse	0	7	19.6 (2.84)	103	3.85	A
	1.5	8	20.2 (2.93)		2.93	A

The results of the longitudinal tension tests on the two sets of control coupons are statistical different. The longitudinal strength of the VARTM samples increased 16% over the time for the environmental exposure treatments. Thus, the baseline longitudinal strength of the material changes with respect to time. However, the modulus of elasticity

in both directions and the transverse tensile strength of the laminate was unaffected by the exposure in air. The other minor changes in the values from the baseline control to the aged control are within the coefficient of variation of the baseline controls.

The mode of failure of the longitudinal and transverse tensile samples was very different. The mode of failure for the longitudinal tension coupons was characterized as an explosive failure of the longitudinal fibers on the non-tool side of the coupons in the middle of the gauge line. This failure was initiated by the straightening of the unidirectional fibers along the non-tool side of the coupon. The failure of the outer unidirectional fibers was followed by the progressive failure of the coupon through the thickness in an explosive manner. Typical failures of the baseline and aged control samples are shown in Figure I.3.14.

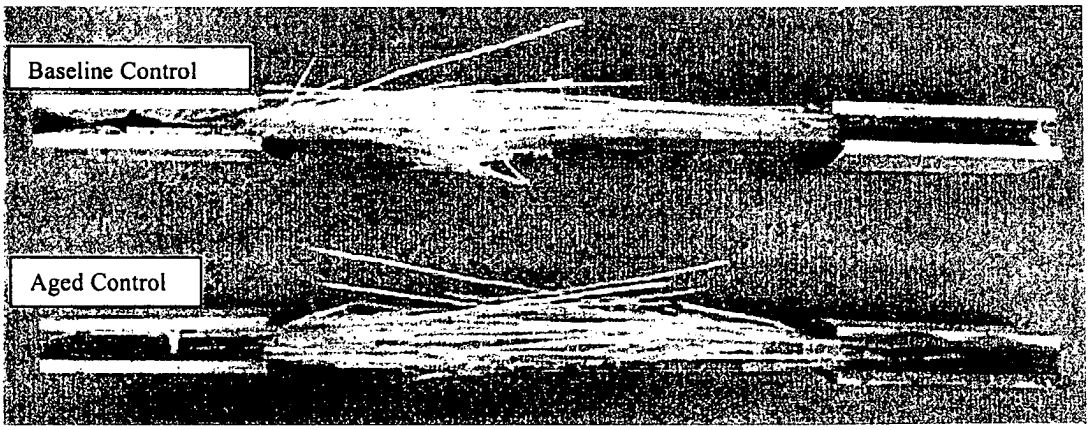

Figure I.3.14 Control Longitudinal Tension Coupons for the VARTM Material

The transverse samples failed in a less explosive manner. A 45° break on the tool side of the material and a transverse failure on the non-tool side of the coupons characterized the failure of the transverse coupons. The location of the failure was not always in the center of the gauge line. Typical failures of the transverse coupons are shown in Figure I.3.15.

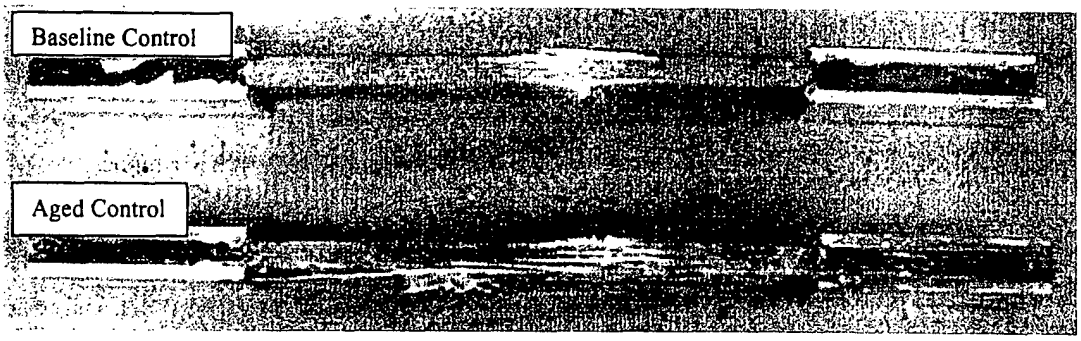

Figure I.3.15 Control Transverse Tension Coupons for the VARTM Material

I.3.3.1.3 Interlaminar Shear Strength

Interlaminar shear tests were conducted before and after environmental exposure to evaluate the interface between the fibers and the matrix. Table I.3.37 summarizes the results of the interlaminar shear tests of the control coupons before and after the environmental exposure period. A one-way ANOVA was performed on the interlaminar shear test data to determine differences between the baseline control and aged results. The results of the individual interlaminar shear test and the corresponding statistical analysis are located in Wood and Lopez-Anido (2000).

There was no statistically significant change in the interlaminar shear strength between the baseline control and the aged control sample sets. The control coupons were taken apart to determine the location of failure of the samples. It was observed that most of the interlaminar shear failures occurred at the CSM layers and then propagated into the fabric layers. Thus, the test result did not give a true indication of the interface properties of directional fibers and the matrix but of the weak link in the laminate due to bending.

Table I.3.37 Interlaminar Shear Strength of the VARTM Material Control Coupons in the Longitudinal Direction

Aging Time (yr.)	Sample Size	Interlaminar Shear Strength MPa (ksi)	Residual ILSS (%)	COV (%)	Statistical Level
0	10	44.2 (6.41)	104	2.84	A
1.5	10	45.8 (6.64)		4.87	A

I.3.3.1.4 Ignition Loss

Ignition loss tests (ASTM D 2548) were conducted to verify the volume fractions used in the laminate analysis. Ignition loss tests were conducted on ten specimens, and the average fiber volume fraction was 56.0% with a COV of 2.33%. The ignition loss test data are located in Wood and Lopez-Anido (2000).

I.3.3.2 Immersion Treatments

This section summarizes the results of the VARTM samples plates subjected to the environmental exposure treatments of immersion in water, salt water, and alkali solutions for 1,000, 3,000, and 10,000 hours

I.3.3.2.1 Appearance

The appearance of the sample plates after the immersion tests is summarized in Table I.3.38. The general appearance of the samples after the environmental exposure treatment was characterized by delamination of the edges of the sample plates after the water immersion treatments.

Table I.3.38 Appearance of the VARTM Material Immersion Sample Plates after Immersion Treatments

Condition	1,000 Hours	3,000 Hours	10,000 Hours
Water	Delamination along the edges of the material (less than ½ in.)	Delamination along the edges of the material (less than ½ in.)	Edge resin is white. ¼-in. delamination on the edges and ¼- to ¾-in. delamination on the ends.
Salt Water	No visible changes	No visible changes	No visible changes

I.3.3.2.2 Mass Change

The change in mass of the sample plates was larger for the salt water treatment at the end of each exposure period. The immersion sample plates showed total mass changes of 0.12% and 0.18% for 10,000 hours of immersion in water and salt water, respectively. Table I.3.39 summarizes the average change in mass of the sample plates after the environmental exposure treatments. The weight data from the monitoring of the sample plates during the exposure process are located in Wood and Lopez-Anido (2000).

Table I.3.39 Mass Change of the VARTM Material Immersion Plates after Environmental Exposure Treatments of Water and Salt Water

Treatment	Average Mass Change (%) after Environmental Exposure		
	1,000 Hours	3,000 Hours	10,000 Hours
Water	–0.03	0.06	0.12
Salt Water	0.06	0.14	0.18

I.3.3.2.3 Tensile Strength

Table I.3.40 and Table I.3.41 summarize the results of the tension tests for the coupons subjected to the environmental exposure treatments of water and salt water immersion. A one-way analysis of variance was used to compare the mechanical test results for each exposure to the baseline and aged control. A two-way analysis of variance was used to determine the dependency (time, treatment, or interaction of time

and treatment) of the mechanical response. The results of the individual tensile tests and the statistical analysis for tension coupons are located in Wood and Lopez-Anido (2000)

The response of the longitudinal tensile coupons was statistically a function of the interaction of the treatments and the exposure time. The VARTM material was not degraded because of the treatments. Instead the coupons showed statistically significant increases in longitudinal tensile strength of 12% for 3,000 hours of water immersion and 12% and 14% increases for 3,000 and 10,000 hours of immersion in salt water, respectively. These increases coincided with the increases in the aged control coupons relative to the baseline control.

The response of the tensile coupons in the transverse direction was statistically unaffected by the environmental exposure treatments. Although the coupons from 3,000 hours of immersion in water showed a decrease of 6.6% relative to the control, the decrease was not statistically significant. Thus, the material was unaffected by the treatments.

Table I.3.40 Tensile Strength Results for Coupons Cut from the VARTM Material Sample Plates after the Environmental Exposure Treatments of Water and Salt Water

Direction	Treatment	Time (hrs)	Sample Size	Ultimate Tensile Strength MPa (ksi)	Residual Tensile Strength (%)	COV (%)	Strength Statistic Level	Depend. System Statistic
Long.	Water	1,000	5	442 (64.1)	102	4.03	B	INTER-ACTION
		3,000	5	486 (70.5)	112	2.68	A	
		10,000	7	425 (61.6)	97.7	8.52	B	
	Salt Water	1,000	5	423 (61.3)	97.3	5.87	B	
		3,000	5	492 (71.5)	110	3.33	A	
		10,000	6	495 (71.8)	114	6.33	A	
Trans.	Water	1,000	5	277 (40.1)	95.9	2.24	A	NONE
		3,000	5	269 (39.1)	93.4	4.89	A	
		10,000	5	269 (39.1)	93.5	4.42	A	
	Salt Water	1,000	7	273 (39.6)	95.7	4.27	A	
		3,000	5	270 (39.2)	93.7	5.81	A	
		10,000	5	277 (40.2)	96.2	2.83	A	

Table I.3.41 Modulus of Elasticity Results for the Tension Coupons Cut from the VARTM Material Sample Plates after the Environmental Exposure Treatments of Water and Salt Water Immersion

Direction	Treatment	Time (hrs)	Sample Size	Modulus of Elasticity GPa (msi)	Residual Modulus (%)	COV (%)	Modulus Statistic Level	Depend. System
Long.	Water	1,000	5	22.1 (3.19)	93.6	4.03	B	TIME
		3,000	9	25.2 (3.66)	107	3.53	A	
		10,000	8	25.3 (3.67)	107	4.08	A	
	Salt Water	1,000	5	21.8 (3.16)	92.5	10.26	B	
		3,000	8	25.1 (3.63)	106	6.27	A	
		10,000	7	25.4 (3.69)	108	4.12	A	
Trans.	Water	1,000	5	19.5 (2.83)	99.6	3.82	A	NONE
		3,000	5	19.3 (2.81)	98.8	4.12	A	
		10,000	5	20.5 (2.97)	105	3.73	A	
	Salt Water	1,000	5	19.1 (2.78)	98.0	9.10	A	
		3,000	5	19.3 (2.80)	98.5	5.23	A	
		10,000	5	20.6 (2.99)	105	2.89	A	

The longitudinal modulus of elasticity of the coupons did not show a statistically significant decrease relative to the baseline control samples. However, there was a statistically significant increase in the longitudinal modulus of elasticity for 3,000 and 10,000 hours of immersion in water and salt water. The increase was between 6% and

8%, depending upon the condition, but was statistically the same as the increase in the aged control samples. The treatments or exposure periods did not affect the transverse modulus of elasticity.

Finally, the mode of failure of the tension coupons was not affected by the immersion treatments. Figure I.3.16 and Figure I.3.17 show typical failures of the tension coupons.

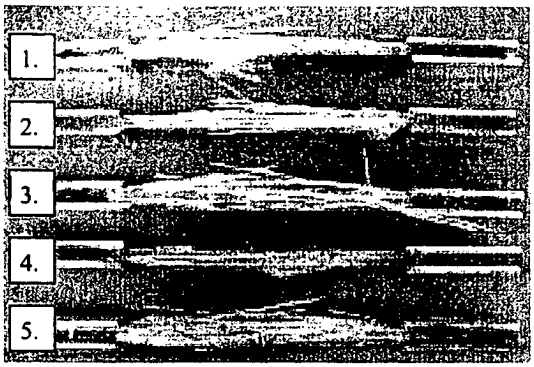

1. Baseline Control, 2. 1,000 Hours, 3. 3,000 Hours, 4. 10,000 Hours 5. Aged Control

(a)

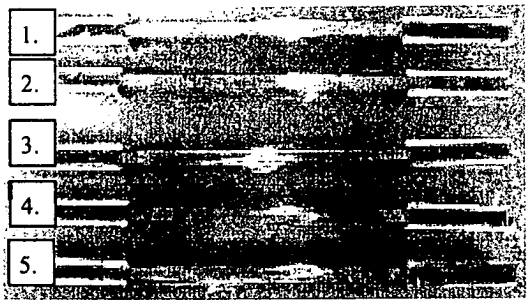

1. Baseline Control, 2. 1,000 Hours, 3. 3,000 Hours, 4. 10,000 Hours 5. Aged Control

(b)

Figure I. 3.16 VARTM Material Water Immersion Coupons: (a) Longitudinal, (b) Transverse

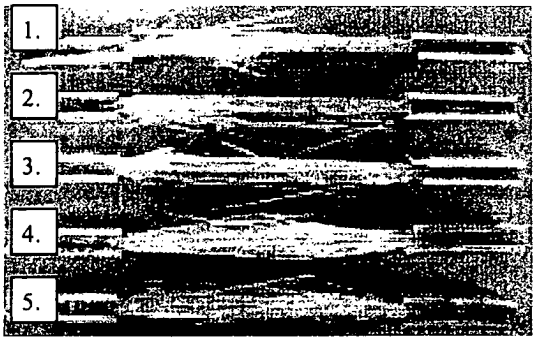

1. Baseline Control, 2. 1,000 Hours, 3. 3,000 Hours, 4. 10,000 Hours 5. Aged Control

(a)

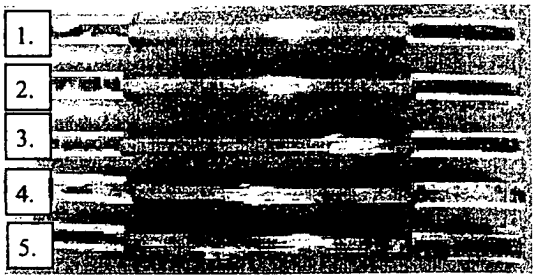

1. Baseline Control, 2. 1,000 Hours, 3. 3,000 Hours, 4. 10,000 Hours 5. Aged Control

(b)

Figure I. 3.17 VARTM Material Salt Water Immersion Coupons: (a) Longitudinal, (b) Transverse

I.3.3.2.4 Interlaminar Shear Strength

The results of the interlaminar shear tests conducted on the coupons cut from the VARTM sample plates after the immersion treatments are summarized in Table I.3.42. A one-way analysis of variance was used to compare all possible pairs of the interlaminar shear test results for each treatment of a particular exposure, baseline control, and aged control. The data from the interlaminar shear tests are located in Wood and Lopez-Anido (2000).

The interlaminar shear strength of the VARTM was not affected by the immersion treatments. The minor changes in strength were not statistically significant. In addition, the mode of failure of the interlaminar shear coupons was not affected by the immersion treatments.

Table I.3.42 Interlaminar Shear Strength for the Longitudinal Coupons Cut from the VARTM Material Sample Plates after the Environmental Exposure Treatments of Water and Salt Water Immersion

Treatment	Time (hours)	Sample Size	Interlaminar Shear Strength (MPa) (ksi)	Residual Interlaminar Shear Strength (%)	COV (%)	ILS Strength Statistic Level	Depend. System Statistic
Water	1,000	9	43.4 (6.29)	98.1	5.60	A	NONE
	3,000	10	45.7 (6.64)	104	3.10	A	
	10,000	10	45.6 (6.61)	103	5.18	A	
Salt Water	1,000	8	44.3 (6.42)	100	4.68	A	
	3,000	10	44.6 (6.46)	100	4.76	A	
	10,000	10	45.8 (6.65)	103	6.55	A	

I.3.3.3 Freeze-Thaw Cycling Treatment

This section summarizes the results and observations from the freeze-thaw treatments on the VARTM sample plates.

I.3.3.3.1 Appearance

The effect of the freeze-thaw treatments on the appearance was similar to the water immersion. The sample plates showed increasing amounts of edge delamination with each set of freeze-thaw treatments. Table I.3.43 summarizes the appearance of the VARTM sample plates after each set of freeze-thaw treatments.

Table I.3.43 Appearance of VARTM Material Sample Plates after the Freeze Thaw Cycling Treatments

20 Cycles	40 Cycles	60 Cycles
Slight edge delamination (less than ¼ in.).	Greater amounts of edge delamination at the ends of the samples, roughly ¼ to ¾ in.	Same amounts of edge delamination as 40 cycles, and samples are darker in color.

I.3.3.3.2 Mass Change

The mass change of the sample plates was 0.10% for the per-cycling conditioning period, and the sample plates maintained the change in mass over the time period for the 60 freeze-thaw treatments. Table I.3.44 summarizes the mass change of the freeze-thaw sample plates after the pre-cycling conditioning period and after each set of freeze-thaw treatments. The weight data from the monitoring of the sample plates during the exposure process are located in Wood and Lopez-Anido (2000).

Table I.3.44 Average Mass Change of VARTM Material Samples Plates after the Freeze-Thaw Cycling Treatments

Average Mass Change (%) after Treatment			
Immersion for 21 Days	**20 Cycles**	**40 Cycles**	**60 Cycles**
0.10	0.11	0.10	0.11

I.3.3.3.3 Tensile Strength

Table I.3.45 and Table I.3.46 summarize the results of the tension tests conducted on the sample plates from the freeze-thaw treatments. A one-way analysis of variance was used to compare all possible pairs of the mechanical test results (strength and elastic modulus) for each freeze-thaw treatment, baseline control, and aged control. The results of the individual tensile tests and the statistical analysis for tension coupons are located in Wood and Lopez-Anido (2000).

The tension coupons showed a statistically significant increase of 13% and 11% in longitudinal tensile strength for 40 and 60 cycles of freeze-thaw treatments, respectively. The transverse coupons showed a statistically significant decrease of 8.3% for the coupons from the sample plates for 20 freeze-thaw treatments.

Table I.3.45 Tensile Strength Results for Coupons Cut from the VARTM Material Sample Plates after the Environmental Exposure Treatments of Freeze-Thaw Cycling

Direction	Time (cycles)	Sample Size	Ultimate Tensile Strength MPa (ksi)	Residual Tensile Strength (%)	COV (%)	Strength Statistic
Longitudinal	20	5	464 (67.3)	107	4.16	ABC
	40	5	491 (71.2)	113	5.51	BC
	60	5	480 (69.7)	111	2.27	BC
Transverse	20	6	265 (38.4)	91.7	1.87	B
	40	5	282 (41.0)	98.0	6.82	A
	60	5	284 (41.2)	98.4	2.84	A

Table I.3.46 Modulus of Elasticity Results for the Tension Coupons Cut from the VARTM Material Sample Plates after the Environmental Exposure Treatments of Freeze-Thaw Cycling

Direction	Time (cycles)	Sample Size	Modulus of Elasticity GPa (msi)	Residual Modulus (%)	COV (%)	Modulus Statistic
Longitudinal	20	5	25.1 (3.63)	106	2.45	A
	40	7	24.9 (3.61)	106	5.86	A
	60	5	25.5 (3.70)	108	3.40	A
Transverse	20	5	19.5 (2.83)	99.6	7.73	A
	40	5	20.9 (3.03)	107	1.52	A
	60	5	20.5 (2.97)	105	3.79	A

The modulus of elasticity of the VARTM sample plates was not statistically affected by the freeze-thaw treatments. The maximum increases of 8% and 7% in the longitudinal and transverse directions were not statistically significant. Finally, the mode of failure of the tension coupons was not affected by the freeze-thaw treatments. Figure I.3.18 shows typical failures of the tension coupons.

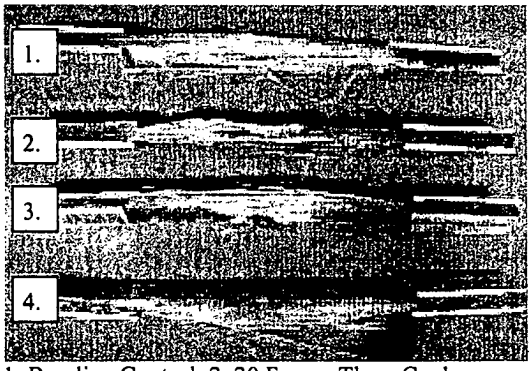

1. Baseline Control, 2. 20 Freeze-Thaw Cycles, 3. 40 Freeze-Thaw Cycles, and 4. 40 Freeze-Thaw Cycles -

(a)

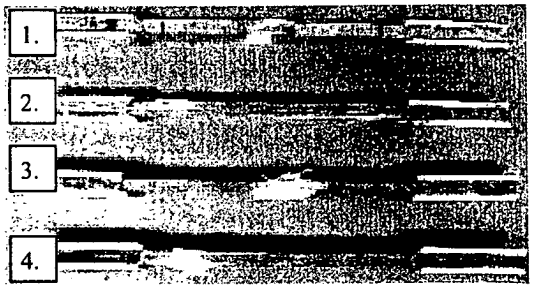

1. Baseline Control, 2. 20 Freeze-Thaw Cycles, 3. 40 Freeze-Thaw Cycles, and 4. 40 Freeze-Thaw Cycles

(b)

Figure I.3.18 VARTM Material Freeze-Thaw Coupons: (a) Longitudinal, (b) Transverse

I.3.3.3.4 Interlaminar Shear Strength

Table I.3.47 summaries the result of the interlaminar shear tests on the coupons from the sample plates for the freeze-thaw treatments. A one-way analysis of variance was used to compare all possible pairs of the interlaminar shear test results for each freeze-thaw treatment, baseline control, and aged control. The results of the individual tensile tests and the statistical analysis for tension coupons are located in Wood and Lopez-Anido (2000).

The coupons for 40 and 60 freeze-thaw treatments showed statistically significant increases of 7% and 9%, respectively. The 5% increase for 20 freeze-thaw treatments was not statistically significant.

Table I.3.47 Interlaminar Shear Strength for the Longitudinal Coupons Cut from the VARTM Material Sample Plates after the Environmental Exposure Treatments of Freeze-Thaw Cycling

Aging Time (Cycles)	Sample Size	Interlaminar Shear Strength (MPa) (ksi)	Residual ILS Strength (%)	COV (%)	ILSS Statistic
20	10	46.2 (6.71)	105	4.99	ABC
40	10	47.5 (6.89)	107	6.76	AB
60	10	48.0 (6.96)	109	6.34	AB

I.3.3.4 Weathering Treatments

This section summarizes the observations and results of the mechanical tests conducted on the coupons from the weathering treatments.

I.3.3.4.1 Appearance

Table I.3.48 summarizes the appearance of the sample plates after the weathering treatments. The appearance of the sample plates after the weathering treatments was

characterized by the exposure of the CSM layer on the tool side of the samples and small amounts of the unidirectional fibers on the non-tool side.

Table I.3.48 Appearance of VARTM Material Sample Plates after Subjection to the Weathering Treatments of UV and Water Spray, and Exterior Exposure

1,000 Cycles UV and Spray	2,000 Cycles UV and Spray	1 Year Exterior Exposure
Exposed surfaces turned brown, and small amounts of fibers were exposed on tool side.	Exposed surfaces turned brown, and CSM fibers were exposed on tool side.	The fibers were exposed on tool side

I.3.3.4.2 Mass Change

Table I.3.49 summarizes the change in mass of the VARTM sample plates for the weathering treatments. The exterior exposure treatment did affect the sample plates, but the UV and water spray treatments progressively decreased the mass of the material by 0.35% for 2,000 cycles. The weight data from the monitoring of the sample plates during the exposure process are located in Wood and Lopez-Anido (2000).

Table I.3.49 Mass Change of the VARTM Material Sample Plates after the Weathering Treatments of UV and Water Spray, Exterior Exposure

Average Mass Change after Environmental Exposure Treatment (%)		
1,000 Cycles UV and Spray	2,000 Cycles UV and Spray	1 Year Exterior Exposure
–0.17	–0.35	–0.02

I.3.3.4.3 Tensile Strength

Table I.3.50 and Table I.3.51 are summaries of the results of the tension tests conducted on the coupons from the sample plates for the weathering tests. A one-way analysis of variance was used to compare all possible pairs of the mechanical test results (strength and elastic modulus) for each treatment of a particular exposure, baseline

control, and aged control. The results of the individual tensile tests and the statistical analysis for tension coupons are located in Wood and Lopez-Anido (2000).

The mechanical properties (tensile strength and elastic modulus) of the VARTM sample plates were not degraded by the weathering treatments. The longitudinal couples from the sample plates for 2,000 cycles of UV and water spray showed a statistically significant increase in longitudinal elastic modulus of 11% from the baseline control. The longitudinal coupons also showed an increase in tensile strength of 10%; however, the increase was not statistically significant. The transverse coupons showed an increase of 17% in longitudinal modulus, which was statistically significant. However, there was a maximum decrease of 6% in transverse strength that was not statistically significant.

Table I.3.50 Tensile Strength Results for Coupons Cut from the VARTM Material Sample Plates after the Environmental Exposure Treatments of UV and Water Spray, and Exterior Exposure

Direction	Treatment	Test Duration	Sample Size	Ultimate Tensile Strength MPa (ksi)	Residual Tensile Strength (%)	COV (%)	Strength Statistic Level
Longitudinal	UV and Water Spray	1,000 Cyc	8	459 (66.6)	106	13.17	ABC
		2,000 Cyc	5	479 (69.5)	110	3.19	ABC
	Exterior	1 Year	5	472 (68.5)	109	3.89	ABC
Transverse	UV and Water Spray	1,000 Cyc	5	277 (40.2)	96.2	6.36	A
		2,000 Cyc	4	272 (39.4)	94.2	5.43	A
	Exterior	1 Year	5	282 (40.8)	97.9	6.28	A

Table I.3.51 Modulus of Elasticity Results for Coupons Cut from the VARTM Material Sample Plates after the Environmental Exposure Treatments of UV and Water Spray, and Exterior Exposure

Direction	Treatment	Test Duration	Sample Size	Modulus of Elasticity GPa (msi)	Residual Modulus (%)	COV (%)	Strength Statistic Level
Longitudinal	UV and Water Spray	1,000 Cyc	7	25.4 (3.69)	108	4.93	ABC
		2,000 Cyc	4	26.1 (3.81)	111	3.64	AB
	Exterior	1 Year	5	24.1 (3.49)	102	5.63	BC
Transverse	UV and Water Spray	1,000 Cyc	5	20.6 (2.99)	105	7.91	A
		2,000 Cyc	5	22.9 (3.33)	117	12.6	A
	Exterior	1 Year	5	21.0 (3.05)	107	3.60	A

Finally, the mode of failure of the tension coupons was not effected by the weathering treatments. Figure I.3.19 shows typical failures of the tension coupons.

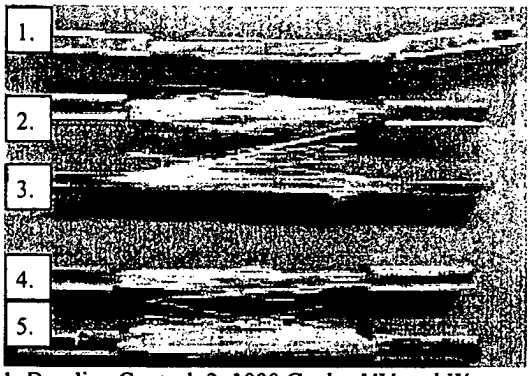

1. Baseline Control, 2. 1000 Cycles UV and Water Spray, 3. 2000 Cycles UV and Water Spray, 4. 1-Year Exterior Exposure, 5. Aged Control

(a)

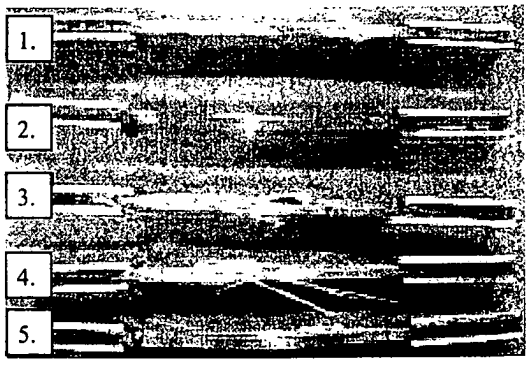

Baseline Control, 2. 1000 Cycles UV and Water Spray, 3. 2000 Cycles UV and Water Spray, 4. 1-Year Exterior Exposure, 5. Aged Control

(b)

Figure I.3.19 VARTM Material Weathering Coupons: (a) Longitudinal, (b) Transverse

I.3.3.4.4 Interlaminar Shear Strength

Table I.3.52 summarizes the results of the interlaminar shear tests conducted on the coupons from the sample plates for the weathering treatments. A one-way analysis of variance was used to compare all possible pairs of the interlaminar shear test results for each treatment of a particular exposure, baseline control, and aged control. The results of the individual tensile tests and the statistical analysis for tension coupons are located in Wood and Lopez-Anido (2000).

The coupons from the sample plates for 1,000 showed a statistically significant increase in interlaminar shear strength of 16%. The 10% increase in interlaminar shear strength after 2,000 cycles of UV and water spray was statistically insignificant.

Table I.3.52 Interlaminar Shear Strength for the Longitudinal Coupons Cut from the VARTM Material Sample Plates after the Environmental Exposure Treatments of UV and Water Spray, and Exterior Exposure

Treatment	Test Duration	Sample Size	Interlaminar Shear Strength MPa (ksi)	Residual Interlaminar Shear Strength (%)	COV (%)	ILSS Statistic
UV and	1,000 Cyc	8	51.2 (7.48)	116	13.17	AB
Water Spray	2,000 Cyc	10	48.2 (7.03)	110	7.27	ABC
Exterior	1 Year	4	45.1 (4.72)	102	10.46	ABC

I.3.3.5 Summary

The interlaminar shear and tensile properties of the VARTM sample plates were not significantly degraded after the environmental exposure treatments. The only statistically significant decreases in mechanical properties were the 6% and 7% decreases in longitudinal modulus elasticity for 1,000 hours of water and salt water immersion, respectively. Otherwise, the sample plates were not negatively affected or even showed increases in mechanical properties.

The tensile strength of the VARTM sample plates in the longitudinal direction showed statistically significant increases for the aged control, water, salt water, and freeze-thaw of 16%, 12%, 14%, and 13%, respectively. The increases in strength correlated with the increases in the aged control coupons. Thus, the increases were attributed to the further cure of the resin matrix with time.

The transverse tensile and longitudinal interlaminar shear properties were not affected as much as the tensile strength of the sample plates. The transverse tensile strength of the coupons was not affected statistically by the environmental exposure treatments. The interlaminar shear strength of the material showed statistically

significant increases of 9% and 16% for the freeze-thaw and UV and water spray treatments.

I.3.4 FRP Material Fabricated by Contact Molding Hand Lay-Up Used in Bridge Decks (ICI)

I.3.4.1 Control (unexposed)

This section is a summary of the results from the control tests conducted on the contact molding hand lay-up laminates prior to subjecting them to the environmental exposure treatments and for the aged control samples. Baseline properties were established for appearance, longitudinal and transverse tensile strength, longitudinal and transverse tensile modulus of elasticity, and longitudinal interlaminar shear strength. The results of the ignition loss tests were used for verification of the results from the laminate analysis.

I.3.4.1.1 Appearance

Observations of the appearance of the sample plates were made before and after environmental exposure. The ICI-B hand lay-up sample plates were a brown/tan material with all four edges sealed with an opaque-colored resin. The sample plates had one flat side and one slightly undulating side. The stitching was visible on the flat side, while the off-axis fibers along with the stitching were visible on the undulating side. The ICI-C hand lay-up sample plates were a brown/tan material with all four edges sealed with an opaque-colored resin. They had one flat side and one slightly undulating side. The primary-axis and off-axis fibers were visible from the flat side, along with voids in the

resin. The primary and off-axis fibers were visible on the undulating side. These observations served as a reference for evaluating the environmentally aged samples.

I.3.4.1.2 Tensile Strength

The tensile strength of the control coupons was measured before and after environmental exposure to determine the effects of further curing during the exposure process. Table I.3.53 and Table I.3.54 summarize the results of the tension tests for the baseline control and aged control coupons. A one-way ANOVA was performed on the tension test data (strength and elastic modulus) to determine differences between the baseline control and aged results. The results of the individual tensile tests and the statistical analysis for tension coupons are located in Wood and Lopez-Anido (2000).

Table I.3.53 Ultimate Tensile Strength Results of the Control Coupons for the Hand Lay-Up Material

Deck Laminate	Time (years)	Sample Size	Ultimate Tensile Strength MPa (ksi)	Residual Strength (%)	COV (%)	Statistical Level
ICI-B	0	6	271 (39.9)	103	11.08	A
	1.5	7	278 (40.4)		4.39	A
ICI-C	0	7	194 (28.1)	101	9.58	A
	1.5	6	196 (28.4)		10.21	A

Table I.3.54 Modulus of Elasticity of Results of the Control Coupons for the Hand Lay-Up Material

Deck Laminate	Time (years)	Sample Size	Modulus of Elasticity GPa (msi)	Residual Modulus (%)	COV (%)	Statistical Level
ICI-B	0	6	16.4 (2.39)	115	5.03	B
	1.5	7	18.8 (2.72)		2.57	A
ICI-C	0	7	13.4 (1.94)	101	6.01	A
	1.5	8	13.6 (1.97)		3.78	A

The results of the tension tests on the two sets of control samples are not statistically different for tensile strength. Thus, the baseline strength of the material does

change with respect to time. The other minor changes in the strength values from the baseline control to the aged control are within the coefficient of variation of the baseline controls.

The modes of failure of the ICI-B hand lay-up and ICI-C hand lay-up control tension coupons were very different. The mode of failure of the ICI-B hand lay-up coupons was an explosive failure of the fabric layers within the gauge line. Typical failures of the baseline and aged ICI-B hand lay-up control coupons are shown in Figure I.3.20.

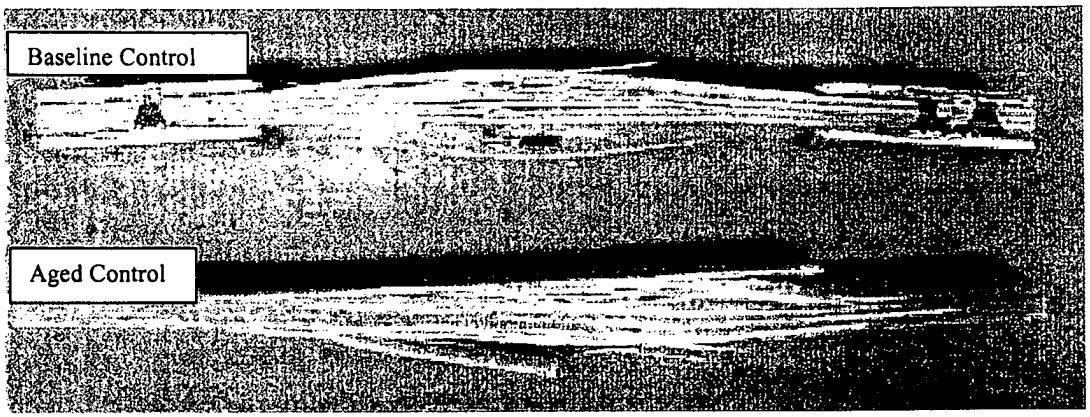

Figure I.3.20 Control Longitudinal Tension Coupons for the Hand Lay-Up ICI-B

The ICI-C hand lay-up coupons failed in a less explosive manner. The mode of failure of the ICI-C hand lay-up coupons was characterized by a transverse to diagonal failure of the coupons. The failure was not explosive relative to the ICI-B hand lay-up coupons. The location of the failure was not always in the center of the gauge line. Typical failures of the ICI-C coupons are shown in Figure I.3.21.

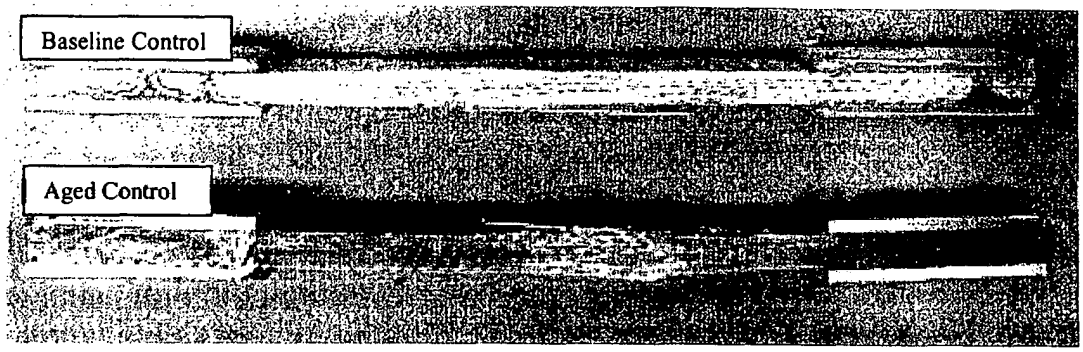

Figure I.3.21 Control Longitudinal Tension Coupons for the Hand Lay-Up ICI-C

I.3.4.1.3 Interlaminar Shear Strength

Interlaminar shear tests were conducted before and after environmental exposure to evaluate the interface between the fibers and the matrix. Table I.3.55 summarizes the results of the interlaminar shear tests of the control coupons before and after the environmental exposure period. The results of the individual tensile tests and the statistical analysis for tension coupons are located in Wood and Lopez-Anido (2000).

There was no significant change in the interlaminar shear strength between the baseline control and the aged control sample sets of the ICI-C hand lay-up coupons. However, the interlaminar shear strength of the ICI-B hand lay-up coupons increased with time.

Table I.3.55 Interlaminar Shear Strength of the Control Coupons in the Longitudinal Direction for the Hand Lay-Up Material

Deck Laminate	Time (years)	Sample Size	Interlaminar Shear Strength MPa (ksi)	Residual ILSS (%)	COV (%)	Statistical Level
ICI-B	0	10	23.9 (3.47)	109	5.14	B
	1.5	10	26.1 (3.79)		7.46	A
ICI-C	0	10	21.7 (3.15)	101	5.74	A
	1.5	10	21.9 (3.18)		7.60	A

The modes of failure of the interlaminar shear coupons were distinctly different for the two different laminates. The ICI-B hand lay-up coupons failed in an interlaminar shear manner in the resin-rich area between the layers of fabric. The ICI-C hand lay-up coupons did not fail in an interlaminar shear manner but instead failed in pure shear. The length of the coupons was adjusted in an attempt to initiate an interlaminar shear failure, but this was not successful.

I.3.4.1.4 Ignition Loss

Ignition loss tests (ASTM D 2548) were conducted to verify the volume fractions used in the laminate analysis. Table I.3.56 summaries the results of the ignition loss test for the ICI samples. The ignition loss test data are located in Wood and Lopez-Anido (2000).

Table I.3.56 Ignition Loss Results for the Hand Lay-Up Material Samples

Deck Laminate	Property	Sample Size	Average	COV (%)
ICI-B	Fiber Volume Fraction (%)	10	37.1	3.31
ICI-C	Fiber Volume Fraction (%)	10	24.5	1.16

I.3.4.2 Immersion Treatments

This section summarizes the results of the contact molding hand lay-up samples plates subjected to the environmental exposure treatments of immersion in water and salt water solutions for 1,000, 3,000, and 10,000 hours

I.3.4.2.1 Appearance

The appearance of the sample plates after the immersion treatments is summarized in Table I.3.57. The darkening of the tool side and the whitening of the non-

tool side of the sample plates characterized the general appearance of the samples after the environmental exposure treatments. There was also a noticeable change in the appearance of the resin that sealed the edges of the sample plates.

Table I.3.57 Appearance of the Hand Lay-Up Immersion Sample Plates after Environmental Exposure Treatments

Deck Laminate	Treatment	1,000 Hours	3,000 Hours	10,000 Hours
ICI-B	Water	Non-tool sides turned very white. Resin used to seal edges turned white.	Same as 1,000 hours	Edges resin changed color for a length of ¼ to ¾ in. but was still translucent. Some white scratches on the front and back.
	Salt Water	Non-tool side turned white/yellow. Tool side of the samples turned darker/brown. Resin used to seal the edges turned white/opaque.	Same as 1,000 hours except the tool side was darker and the non-tool side was whiter.	Same as 3,000 hours except the tool side was darker and the non-tool side was whiter.
ICI-C	Water	Non-tool side turned very white. Resin used to seal edges turned white.	Same as 1,000 hours	Edge resin changed color for a length of ¼ to ½ in. and the non-tool side was all white scratches.
	Salt Water	Non-tool side turned white. Resin used to seal the edges turned white/opaque. Tool side of the samples turned darker/brown.	Same as 1,000 hours except the tool side was darker and the non-tool side was whiter.	Same as 3,000 hours except the tool side was darker and the non-tool side was whiter.

I.3.4.2.2 Mass Change

The average change in mass of the sample plates after the immersion treatments is shown in Table I.3.58. The change in mass of the sample plates was similar for each treatment and exposure period. The weight data from the monitoring of the sample plates during the exposure process are located in Wood and Lopez-Anido (2000).

Table I.3.58 Mass Change of the Hand Lay-Up Immersion Plates after Environmental Exposure Treatments of Water and Salt Water

Deck Laminate	Treatment	Average Mass Change (%) after Environmental Exposure		
		1,000 Hours	3,000 Hours	10,000 Hours
ICI-B	Water	0.15	0.28	0.47
	Salt Water	0.20	0.36	0.52
ICI-C	Water	0.11	0.43	0.68
	Salt Water	0.27	0.47	0.65

I.3.4.2.3 Tensile Strength

Table I.3.59 and Table I.3.60 summarize the results of the tension tests for the coupons subjected to the environmental exposure treatments of water and salt water immersion. A one-way analysis of variance was used to compare all possible pairs of the mechanical test results (strength and elastic modulus) for each treatment of a particular exposure, baseline control, and aged control. A two-way analysis of variance was used to determine the dependency (time, treatment, or interaction of time and treatment) of the mechanical response. The results of the individual tensile tests and the statistical analysis for tension coupons are located in Wood and Lopez-Anido (2000).

The responses of the two deck systems to the immersion treatments were very different. The tensile strength of the ICI-B hand lay-up was statistically unaffected by the immersion treatments. The 7% decrease in tensile strength after 3,000 hours of

immersion in salt water was statistically insignificant, since the coefficient of variation of the control samples was 11%.

Table I.3.59 Tensile Strength Results for Coupons Cut from the Hand Lay-Up Sample Plates after the Environmental Exposure Treatments of Water and Salt Water

Deck Laminate	Treat.	Time (hrs)	Sample Size	Ultimate Tensile Strength MPa (ksi)	Residual Tensile Strength (%)	COV (%)	Strength Statistic	Depend. System Statistic
ICI-B	Water	1,000	7	263 (38.1)	97.2	8.04	A	NONE
		3,000	5	276 (40.0)	102	2.71	A	
		10,000	5	268 (38.9)	96.4	6.21	A	
	Salt Water	1,000	5	261 (37.8)	96.3	1.79	A	
		3,000	5	267 (38.7)	93.0	3.53	A	
		10,000	7	273 (39.6)	101	3.51	A	
ICI-C	Water	1,000	5	193 (28.0)	99.7	4.63	A	INTER-ACTION
		3,000	5	214 (31.0)	110	4.76	A	
		10,000	5	166 (24.1)	85.9	3.80	B	
	Salt Water	1,000	5	198 (28.7)	102	1.92	B	
		3,000	5	225 (32.7)	117	1.89	A	
		10,000	7	204 (29.6)	105	3.85	AB	

Table I.3.60 Modulus of Elasticity Results for the Tension Coupons Cut from the Hand Lay-Up Sample Plates after the Environmental Exposure Treatments of Water and Salt Water Immersion

Deck Laminate	Treat.	Time (hrs)	Sample Size	Modulus of Elasticity GPa (msi)	Residual Modulus (%)	COV (%)	Modulus Statistic	Depend. System
ICI-B	Water	1,000	0	NDA**	-	-	-	TIME
		3,000	5	17.5 (2.54)	106	1.79	AB	
		10,000	5	17.1 (2.48)	103	5.39	B	
	Salt Water	1,000	5	NDA**	-	-	-	
		3,000	5	16.6 (2.41)	100	7.11	A	
		10,000	7	17.1 (2.48)	103	3.94	A	
ICI-C	Water	1,000	3	13.5 (1.96)	102	3.56	ABC	INTER-ACTION
		3,000	5	14.1 (2.05)	105	1.96	AB	
		10,000	5	12.3 (1.78)	91.9	3.50	BC	
	Salt Water	1,000	5	13.3 (1.92)	103	8.80	A	
		3,000	7	13.4 (1.94)	103	4.94	A	
		10,000	7	14.0 (2.03)	105	3.90	A	

NDA** - No Data Available

The responses of the coupons from the ICI-C hand lay-up sample plates were different for the water and salt water treatments. The coupons from the water treatments

showed a statistically insignificant 10% increase in tensile strength after 3,000 hours but a 14% decrease relative to the baseline control after 10,000 hours. The salt water coupons only showed a statistically significant increase in tensile strength of 17% after 3,000 hours.

The response of the modulus of elasticity of the two deck systems was very similar to the tensile strength response. The ICI-B hand lay-up coupons did not show any statistically significant reductions relative to the baseline control but did show reductions relative to the aged control. The retained modulus of elasticity for the water treatment of 10,000 hours and the salt water treatments of 3,000 and 10,000 hours were statistically different from the aged control. The 3% increase shown by the 3,000 hours of water treatment coupons was statistically the same as both controls.

The longitudinal modulus of elasticity of the contact molding hand lay-up coupons was not statistically affected by the immersion treatments relative to the baseline control. The only statistical significant change was the 13% loss of modulus between 3,000 and 10,000 hours of water immersion.

The mode of failure of the tension coupons was not affected by the immersion treatments. Figure I.3.22 and Figure I.3.23 show typical failures of the tension coupons for the water and salt water immersion treatments in comparison to the control coupons.

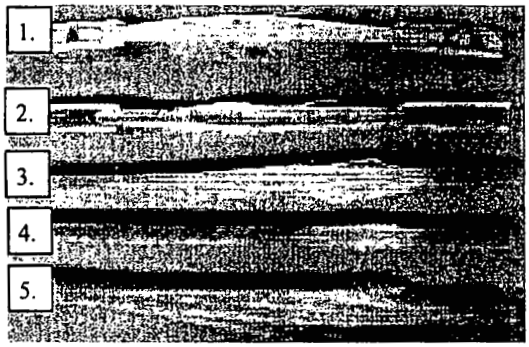

1. Baseline Control, 2. 1,000 Hours, 3. 3,000 Hours, 4. 10,000 Hours 5. Aged Control

(a)

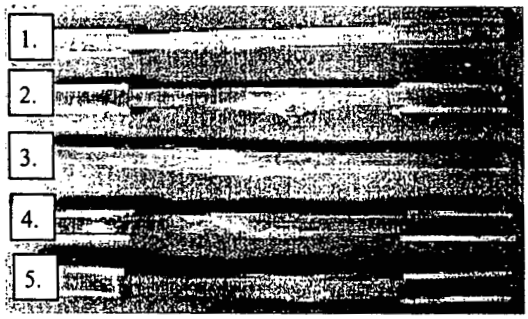

1. Baseline Control, 2. 1,000 Hours, 3. 3,000 Hours, 4. 10,000 Hours 5. Aged Control

(b)

Figure I.3.22 Hand Lay-Up Tension Coupons for Water Immersion: (a) ICI-B, (b) ICI-C

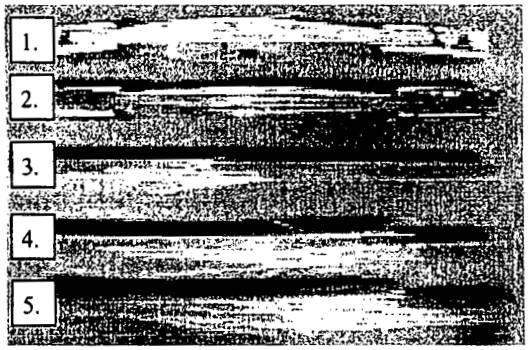

1. Baseline Control, 2. 1,000 Hours, 3. 3,000 Hours, 4. 10,000 Hours 5. Aged Control

(a)

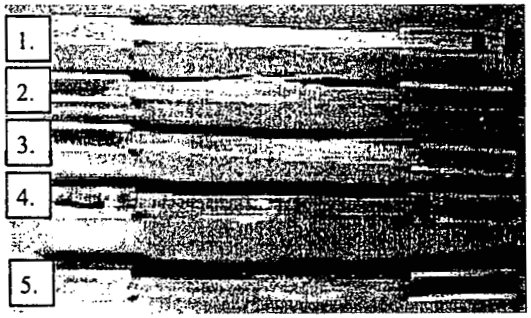

1. Baseline Control, 2. 1,000 Hours, 3. 3,000 Hours, 4. 10,000 Hours 5. Aged Control

(b)

Figure I. 3.23 Hand Lay-Up Tension Coupons for Salt Water Immersion: (a) ICI-B, (b) ICI-C

I.3.4.2.4 Interlaminar Shear Strength

The response of the interlaminar shear strengths of the two deck systems were a function of time. Table I.3.61 summarizes the results of the interlaminar shear tests conducted on the coupons from the immersion plates. A one-way analysis of variance was used to compare all possible pairs of the interlaminar shear test results (strength and elastic modulus) for each treatment of a particular exposure, baseline control, and aged

control. The results of the individual interlaminar shear tests and the corresponding statistical analysis are located in Wood and Lopez-Anido (2000).

The mode of failure of the interlaminar shear coupons from either deck was not affected by the immersion treatments. The interlaminar shear strength of the ICI-B coupons increased with tim, while that of the ICI-C coupons decreased with time. The ICI-B coupons showed statistically significant increases of 11% and 10% in interlaminar shear strength for 3,000 hours of immersion in water and 10,000 hours of immersion in salt water, respectively. The ICI-C coupons showed statistically significant decreases of 11% and 16% for 10,000 hours of water and salt water immersion, respectively.

Table I.3.61 Interlaminar Shear Strength for the Longitudinal Coupons Cut from the Hand Lay-Up Sample Plates after the Environmental Exposure Treatments of Water and Salt Water Immersion

Deck Laminate	Treat.	Time (hrs)	Sample Size	Interlaminar Shear Strength MPa (ksi)	Residual ILS Strength (%)	COV (%)	ILS Strength Statistic	Depend. System Statistic
ICI-B	Water	1,000	10	25.6 (3.72)	106	8.66	ABC	TIME
		3,000	10	26.5 (3.85)	111	7.06	AB	
		10,000	10	25.8 (3.74)	108	5.75	ABC	
	Salt Water	1,000	10	25.4 (3.69)	107	6.77	ABC	
		3,000	10	25.9 (3.76)	109	3.92	ABC	
		10,000	10	26.3 (3.81)	110	3.60	AB	
ICI-C	Water	1,000	10	21.5 (3.12)	98.9	4.18	A	TIME
		3,000	10	22.1 (3.21)	102	6.61	A	
		10,000	10	19.4 (2.82)	89.4	4.61	B	
	Salt Water	1,000	10	21.1 (3.06)	97.1	5.60	A	
		3,000	10	23.2 (3.36)	107	2.27	A	
		10,000	10	18.2 (2.64)	83.7	6.60	B	

I.3.4.3 Freeze-Thaw Cycling Treatments

This section summarizes the results of the hand lay-up samples plates subjected to the environmental exposure treatment of freeze-thaw cycling for 20, 40, and 60 cycles.

I.3.4.3.1 Appearance

The appearance of the sample plates after the freeze-thaw treatments is summarized in Table I.3.62. The darkening of the tool side and the whitening of the non-tool side of the sample plates characterized the general appearance of the samples after the freeze-thaw treatments. There was also a noticeable change in the appearance of the resin that sealed the edges of the sample plates.

Table I.3.62 Appearance of Hand Lay-Up Sample Plates after the Freeze-Thaw Cycling Treatments

	20 Cycles	40 Cycles	60 Cycles
ICI-B	The non-tool sides of the sample faded to a whitish color, and the tool sides became more of an orange/brown. Resin used to seal the edges turned whiter (less than ¼ in.).	The non-tool sides of the samples were whiter than the samples for 20 cycles, and the tool sides were darker than for 20 cycles. White lines appeared on the tool side in the longitudinal direction. Resin used to seal the edges was white for ¼ to ½ in.	The non-tool side of the sample turned to a yellow white, especially where the fibers were, and the tool side turned to a darker brown/ yellow. The width of the resin used to seal the edges remained the same, and the amount of white lines on the tool sides increased.
ICI-C	The non-tool sides of the sample faded to a whitish color, and the tool sides became more of an orange/brown. Resin used to seal the edges turned whiter.	The non-tool sides of the samples were whiter than the samples for 20 cycles, and the tool sides were darker than for 20 cycles. Wavy white lines appeared on the tool side in the longitudinal direction. Resin used to seal the edges was white for less than ¼ in.	The non-tool side of the sample turned to a yellow white, especially where the fibers were, and the tool side turned to a darker brown/ yellow. The width of the resin used to seal the edges and the number of longitudinal lines remained the same.

I.3.4.3.2 Mass Change

Table I.3.63 summarizes the average change in mass of the sample plates after the immersion treatments. The change in mass of the sample plates was similar for each set of freeze-thaw treatments. The mass change ICI-B sample plates was 0.30% for the pre-cycling conditioning period and 0.36% for 60 freeze-thaw treatments. The mass change ICI-B sample plates was 0.39% for the pre-cycling conditioning period and 0.49% for 60 freeze-thaw treatments. The data from the monitoring of the sample plates during the exposure process are located in Wood and Lopez-Anido (2000).

Table I.3.63 Average Mass Change of Hand Lay-Up Sample Plates after the Freeze-Thaw Cycling Treatments

	Average Mass Change after Environmental Exposure Treatments (%)			
	Immersion for 21 Days	20 Cycles	40 Cycles	60 Cycles
ICI-B	0.30	0.28	0.33	0.36
ICI-C	0.39	0.39	0.46	0.49

I.3.4.3.3 Tensile Strength

Table I.3.64 and Table I.3.65 summarize the results of the tension tests for the coupons subjected to the freeze-thaw cycling treatments. A one-way analysis of variance was used to compare all possible pairs of the mechanical test results (strength and elastic modulus) for each freeze-thaw treatment, baseline control, and aged control. The results of the individual tensile tests and the statistical analysis for tension coupons are located in Wood and Lopez-Anido (2000).

The longitudinal tensile strength of the ICI coupons from the sample plates for the freeze-thaw treatments was statistically unaffected. The longitudinal modulus of elasticity of the ICI-B coupons was also statistically unaffected by the exposure

treatments. However, the ICI-C coupons showed a statistically significant increase of 7% in the longitudinal modulus of elasticity for 60 freeze-thaw treatments.

Table I.3.64 Tensile Strength Results for Coupons Cut from the Hand Lay-Up Sample Plates after the Environmental Exposure Treatments of Freeze-Thaw Cycling

Deck Laminate	Time (cycles)	Sample Size	Ultimate Tensile Strength MPa (ksi)	Residual Tensile Strength (%)	COV (%)	Strength Statistic
ICI-B	20	5	274 (39.8)	101	4.45	A
	40	5	271 (39.3)	100	3.16	A
	60	5	266 (38.5)	98.1	2.37	A
ICI-C	20	5	209 (30.4)	108	6.10	A
	40	5	209 (30.3)	107	4.06	A
	60	5	195 (28.3)	100	6.49	A

Table I.3.65 Modulus of Elasticity Results for the Tension Coupons Cut from the Hand Lay-Up Sample Plates after the Environmental Exposure Treatments of Freeze-Thaw Cycling

Deck Laminate	Time (cycles)	Sample Size	Modulus of Elasticity GPa (msi)	Residual Modulus (%)	COV (%)	Modulus Statistic
ICI-B	20	5	17.9 (2.60)	108	3.26	A
	40	5	17.3 (2.51)	104	6.66	A
	60	5	17.4 (2.52)	105	3.49	A
ICI-C	20	5	13.8 (2.00)	103	2.46	ABC
	40	4	13.9 (2.02)	104	2.66	ABC
	60	9	14.3 (2.08)	107	4.68	AB

The mode of failure of the tension coupons was not affected by the freeze-thaw treatments. Figure I.3.24 shows typical failures of the tension coupons from the freeze-thaw cycling treatments.

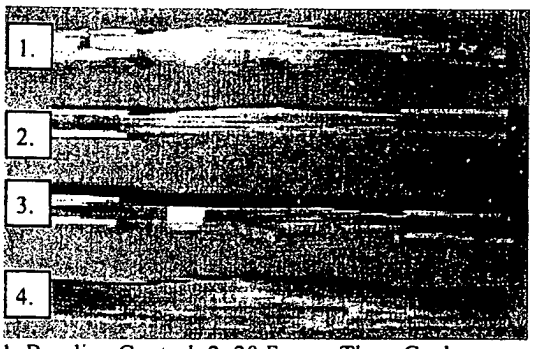

1. Baseline Control, 2. 20 Freeze-Thaw Cycles, 3. 40 Freeze-Thaw Cycles, and 4. 40 Freeze-Thaw Cycles

(a)

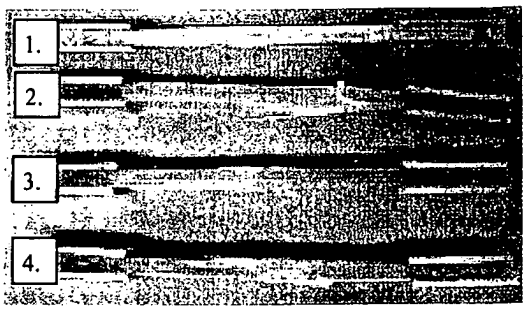

1. Baseline Control, 2. 20 Freeze-Thaw Cycles, 3. 40 Freeze-Thaw Cycles, and 4. 40 Freeze-Thaw Cycles

(b)

Figure I.3.24 Hand Lay-Up Tension Coupons for Freeze-Thaw Cycling: (a) ICI-B, (b) ICI-C

I.3.4.3.4 Interlaminar Shear Strength

Table I.3.66 summarizes the results of the interlaminar shear tests conducted on the coupons from the sample plates for the freeze-thaw treatments. A one-way analysis of variance was used to compare all possible pairs of the interlaminar shear test results for each freeze-thaw treatment, baseline control, and aged control. The results of the individual interlaminar shear tests and the corresponding statistical analysis are located in Wood and Lopez-Anido (2000).

The ICI-B coupons showed a statistically significant increase for 20, 40, and 60 freeze-thaw treatments. Statistically, the increases of 14%, 14%, and 8% for 20, 40, and 60 freeze-thaw treatments, respectively, were the same increase. The ICI-C coupons were statistically affected by the freeze-thaw treatments. The mode of failure of the interlaminar shear coupons was not affected by the freeze-thaw treatments

Table I.3.66 Interlaminar Shear Strength for the Longitudinal Coupons Cut from the Hand Lay-Up Sample Plates after the Environmental Exposure Treatments of Freeze-Thaw Cycling

Deck Laminate	Time (cycles)	Sample Size	Interlaminar Shear Strength MPa (ksi)	Residual Interlaminar Shear Strength (%)	COV (%)	ILS Strength Statistic
ICI-B	0	10	23.9 (3.47)	100	5.14	B
	20	10	27.3 (3.95)	114	5.72	A
	40	10	27.2 (3.94)	114	7.56	A
	60	10	25.8 (3.75)	108	5.66	A
ICI-C	20	10	21.6 (3.13)	99.4	2.96	A
	40	10	22.1 (3.22)	102	8.00	A
	60	10	21.8 (3.17)	101	7.54	A

I.3.4.4 Weathering Treatments

This section is a summary of the observations and results of the mechanical tests conducted on the ICI-B hand lay-up coupons from the weathering treatments. The ICI-C hand lay-up coupons were not subjected to the weathering treatments due to the availability of space on the exterior exposure apparatus and the time and space required in the QUV machine.

I.3.4.4.1 Appearance

The appearance of the ICI-B hand lay-up sample plates after the weathering treatments is summarized in Table I.3.67. The darkening of the tool side and the yellowing of the non-tool side of the sample plates characterized the general appearance of the samples after the freeze-thaw treatments. The fibers from the CSM layers were also exposed on the tool side of the sample plates. There was also a noticeable change in the appearance of the resin that sealed the edges of the sample plates.

Table I.3.67 Appearance of Hand Lay-Up ICI-B Sample Plates after Subjection to the Weathering Treatments of UV and Water Spray, and Exterior Exposure

1,000 Cycles UV and Spray	2,000 Cycles UV and Spray	1 Year Exterior Exposure
Fibers from the CSM were exposed on the tool side. The non-tool side turned yellow.	Fibers from the CSM were exposed on the tool side. The non-tool side turned yellow.	The fibers were exposed on the tool side. The tool side was a darker brown, and the non-tool side was yellowish.

I.3.4.4.2 Mass Change

The mass change response of the ICI-B hand lay-up sample plates was not very consistent. The mass change of the samples for the UV and water spray treatments showed an increase of 0.16% for 1,000 cycles but a decrease of 0.38% for 2,000 cycles. The sample plates for the exterior exposure treatment showed an increase of 0.12%. Table I.3.68 summarizes the average mass change of the ICI-B hand lay-up sample plates after the weathering treatments. The data from the monitoring of the sample plates during the exposure process are located in Wood and Lopez-Anido (2000).

Table I.3.68 Mass Change of the Hand Lay-Up ICI-B Sample Plates after the Weathering Treatments of UV and Water Spray, Exterior Exposure

Average Mass Change after Environmental Exposure (%)		
1,000 Cycles UV and Spray	2,000 Cycles UV and Spray	1 Year Exterior Exposure
0.16	–0.38	0.12

I.3.4.4.3 Tensile Strength

Table I.3.69 and Table I.3.70 summarize the results of the tensile tests conducted on the coupons from the sample plates for the weathering treatments. A one-way analysis of variance was used to compare all possible pairs of the mechanical test results (strength and elastic modulus) for each treatment of a particular exposure, baseline control, and

aged control. The results of the individual tensile tests and the statistical analysis for tension coupons are located in Wood and Lopez-Anido (2000).

The longitudinal tensile strength and modulus of elasticity were not statistically affected by the weathering treatments. The decreases in tensile strength and increases in modulus of elasticity were not statistically significant. However, the increases in modulus were statistically similar to the increases in the control coupons.

Table I.3.69 Tensile Strength Results for Coupons Cut in the Longitudinal Direction from the Hand Lay-Up ICI-B Sample Plates after the Environmental Exposure Treatments of UV and Water Spray, and Exterior Exposure

Treatment	Test Duration	Sample Size	Ultimate Tensile Strength MPa (ksi)	Residual Tensile Strength (%)	COV (%)	Strength Statistic
UV and Water	1,000 Cyc	5	248 (3.60)	91.7	6.77	AB
Spray	2,000 Cyc	5	256 (3.71)	93.9	9.14	AB
Exterior	1 Year	6	260 (37.7)	95.9	3.27	AB

Table I.3.70 Modulus of Elasticity Results for Coupons Cut in the Longitudinal Direction from the Hand Lay-Up ICI-B Sample Plates after the Environmental Exposure Treatments of UV and Water Spray, and Exterior Exposure

Treatment	Test Duration	Sample Size	Modulus of Elasticity GPa (msi)	Residual Modulus (%)	COV (%)	Strength Statistic
UV and Water	1,000 Cyc	5	18.2 (2.65)	110	8.09	ABC
Spray	2,000 Cyc	5	17.8 (2.58)	107	10.16	ABC
Exterior	1 Year	7	18.0 (2.61)	110	7.84	ABC

The mode of failure of the tension coupons was not affected by the weathering treatments. Figure I.3.25 shows typical failures of the tension coupons from the weathering treatments.

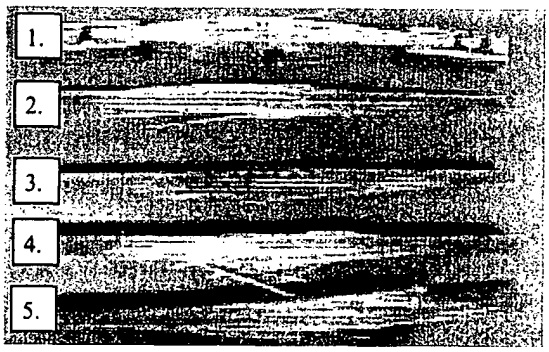

1. Baseline Control, 2. 1000 Cycles UV and Water Spray, 3. 2000 Cycles UV and Water Spray, 4. 1-Year Exterior Exposure, 5. Aged Control

Figure I.3.25 Hand Lay-Up ICI-B Tension Coupons for the Weathering Treatments

I.3.4.4.4 Interlaminar Shear Strength

Table I.3.71 summarizes the results of the interlaminar shear tests conducted on the coupons from the sample plates for the weathering treatments. A one-way analysis of variance was used to compare all possible pairs of the interlaminar shear test results for each treatment of a particular exposure, baseline control, and aged control. The results of the individual interlaminar shear tests and the corresponding statistical analysis are located in Wood and Lopez-Anido (2000).

The coupons showed statistically significant increases in interlaminar shear strength of 14% and 10% for 1,000 cycles of UV and water spray and one year of exterior exposure, respectively. In addition, the mode of failure of the interlaminar shear coupons was unaffected by the weathering treatments.

Table I.3.71 Interlaminar Shear Strength for the Longitudinal Coupons Cut from the Hand Lay-Up ICI-B Sample Plates after the Environmental Exposure Treatments of UV and Water Spray, and Exterior Exposure

Treatment	Test Duration	Sample Size	Interlaminar Shear Strength MPa (ksi)	Residual Interlaminar Shear Strength (%)	COV (%)	ILSS Statistic
UV and Water Spray	1,000 Cyc	10	27.2 (3.95)	114	6.77	A
	2,000 Cyc	10	25.1 (3.64)	105	9.14	AB
Exterior	1 Year	10	26.2 (3.80)	110	4.05	A

I.3.4.5 Summary

The responses of the two sets of contact molding hand lay-up sample plates to the environmental exposure treatments were not the same. The ICI-B hand lay-up samples showed increases in mechanical properties with time, while the ICI-C hand lay-up showed initial increases in properties, but the increases were followed by large decreases at the end of the exposure periods. Thus, the deck with the stitched fabric (ICI-B) is the preferred alternative.

The ICI-B deck showed an increase in the mechanical properties of the control, immersion, freeze-thaw, and weathering coupons. The aged control coupons showed increases of 9% and 15% in the longitudinal tensile strength and modulus, respectively. The coupons from the immersion treatments showed increases of 11% and 10% for the water and salt water immersion treatments, respectively. The interlaminar shear coupons from the freeze-thaw treatments showed increases of 10%. Finally, the coupons from the weathering tests showed increases of 10% and 14% for the longitudinal modulus of elasticity and the interlaminar shear strength, respectively.

The ICI-C coupons did show increases in tensile strength of 10% and 17% for 3,000 hours of immersion in water and salt water, respectively. However, the strength of the coupons from the water treatment decreased by 22% between 3,000 and 10,000 hours. In addition, the longitudinal modulus of elasticity decreased by 9% relative to the baseline control for 10,000 hours of immersion in water. There was also a corresponding decrease in interlaminar shear strength of 11% and 16% for 10,000 hours of water and salt water immersion, respectively. Finally, the modulus of elasticity increased 7% for 60 freeze-thaw cycles.

I.4 Discussion of Results

This chapter discusses the results of the durability characterization of the FRP composite materials used in bridge decks. Subjects covered are: 1) Correlation between laminate analysis and experimental elastic modulus and fiber volume fraction; 2) Application of the acceptance criteria proposed by the HITEC evaluation panel; 3) Model of the mass change (moisture diffusion) for the laminated composite plates based on Fickian diffusion; 4) Kinetic model of degradation; and 5) Material capacity reduction factors. The analytical work contributed to the understanding and characterization of the effects of environmental exposures on the mechanical properties.

I.4.1 Correlation with Laminate Analysis

Laminate analysis was applied to predict the modulus of elasticity and fiber volume fraction of the composite laminates based upon the properties of the constituent materials (fibers and matrix). The comparison of the fiber volume fractions predicted by the laminate analysis and the results of the ignition tests allow for the validation of the laminate analysis input for properties. To allow for the direct comparison of the predicted and the laboratory values, the weight fraction of the CSM layers within each laminate was iterated within the laminate analysis until a constant fiber volume fraction for the laminate was achieved. Table I.4.1 compares the predicted fiber volume fractions to the results of the ignition loss tests. All of the values from the ignition loss tests are within 6% except for the lay-up material with stitched fabric, which is about 9% different from the predicted value. Most fiber-reinforcement manufacturers can produce reinforcing fabrics within ±6% of the desired value. Thus, the fiber inputs into the

laminate analysis were reasonable since the fiber volume fractions were all within 6% of the predicted except for one case.

Table I.4.1 Comparison of Predicted and Actual Fiber Volume Fractions

Deck Laminate	Predicted Fiber Volume Fraction (%)	Fiber Volume Fraction from Ignition Test (%)	Difference from Predicted (%)
CPI	51.5	54.1	5.05
DFI	62.2	61.5	1.13
HCC	55.7	56.0	0.54
ICI-B	34.0	37.1	9.12
ICI-C	25.7	24.5	4.67

The predicted modulus of elasticity from the laminate analysis was compared to the baseline and age control values in Table I.4.2.

Table I.4.2 Comparison of Control Modulus of Elasticity with Predicted Value from the Laminate Analysis

Direction	Deck Laminate	Predicted Modulus (GPa)	Baseline Control Modulus (GPa)	Difference from Predicted (%)	Aged Control Modulus (GPa)	Difference from Predicted (%)
Long.	CPI	22.86	22.4	2.01	22.2	2.89
	DFI	40.33	39.5	2.06	40.8	1.17
	HCC	25.51	23.6	7.49	24.1	5.53
	ICI-B	17.18	16.4	4.54	18.8	9.43
	ICI-C	14.15	13.4	5.30	13.6	3.89
Trans.	CPI	18.71	15.9	15.0	16.3	12.9
	DFI	16.08	9.05	43.7	9.40	41.5
	HCC	21.76	19.6	9.93	20.2	7.17

All of the values for longitudinal modulus of elasticity were within 10% of the predicted value. The transverse modulus of elasticity for the pultruded laminates exhibited higher differences. In particular the pultruded material with no directional reinforcement in the transverse direction, DFI, resulted in predicted values of transverse tensile modulus considerably higher than the experimental ones. This difference is

attributed to uncertainties in the elastic properties specified for the resin matrix of this composite material.

I.4.2 Acceptance Criteria

The acceptance criteria proposed by the HITEC Panel on FRP Bridge Decks were applied to evaluate the residual strength and modulus after environmental exposure, as shown in Table I.4.3. The HITEC Panel's evaluation criteria consider retained strength after 36 months (26,280 hours) of exposure (Seible et al. 2000). Specimens must average 85% retention of as-received test values, and no single test value can be below 75% of the as-received value. On the other hand, the acceptance criteria for AC 125 consider 90% retention of average values after 3,000 hours and 85% retention after 10,000 hours as acceptable (ICB0 1997).

I.4.2.1 FRP Material Fabricated by Pultrusion for Bridge Decks (CPI)

This pultruded laminate had two outliers that appeared for 20 cycles of freeze-thaw and 1,000 hours of water immersion exposure, which fail the 75% individual rule.

Table I.4.3 HITEC Acceptance Criteria Failure to Meet Requirements (CPI)

		Exposure	Time Period
Longitudinal Tensile Strength	85% Average	M.R.	
	75% Individual	M.R.	
Transverse Tensile Strength	85% Average	M.R.	
	75% Individual	Water	1,000
Longitudinal Modulus of Elasticity	85% Average	M.R.	
	75% Individual	M.R.	
Transverse Modulus of Elasticity	85% Average	M.R.	
	75% Individual	Freeze-Thaw	20
Interlaminar Shear Strength	85% Average	M.R.	
	75% Individual	M.R.	

Note: M.R. means meet requirement.

I.4.2.2 FRP Material Fabricated by Pultrusion for Reinforcing-Concrete Bridge Decks (DFI)

This pultruded material does not meet the criteria for any of the immersion exposures (Table I.4.4). The epoxy coating applied to the samples for the alkali exposure only decreased the time to failure. However, the epoxy coating did not contribute to increases in the long-term residual properties.

Table I.4.4 HITEC Acceptance Criteria Failure to Meet Requirements (DFI)

		Uncoated		Epoxy Coated	
		Exposure	**Time Period**	**Exposure**	**Time Period**
Longitudinal Tensile Strength	85% Average	Water	1,000	Alkali	3,000
		Water	3,000	Alkali	10,000
		Water	10,000		
		Salt Water	10,000		
		Alkali	1,000		
		Alkali	10,000		
		Freeze-Thaw	20		
		Freeze-Thaw	40		
	75% Individual	Water	1,000		
		Water	10,000		
		Alkali	1,000		
		Alkali	10,000		
Transverse Tensile Strength	85% Average	Salt Water	10,000		
	75% Individual	Water	1,000		
		Salt Water	10,000		
Longitudinal Modulus of Elasticity	85% Average	M.R.			
	75% Individual	M.R.			
Transverse Modulus of Elasticity	85% Average	Water	1,000		
		Water	10,000		
		Salt Water	10,000		
		Freeze-Thaw	20		
		Freeze-Thaw	60		
	75% Individual	Water	1,000		
		Water	10,000		
		Salt Water	10,000		
		Freeze-Thaw	20		
		Freeze-Thaw	60		
Interlaminar Shear Strength	85% Average	Water	10,000		
		Alkali	10,000		
		Salt Water	10,000		
		Freeze-Thaw	20		
	75% Individual	Alkali	10,000		

Note: M.R. means meet requirement.

I.4.2.3 FRP Material Fabricated by VARTM for Bridge Decks (HCC)

The VARTM laminates meet the HITEC panel requirements for all the environmental exposure treatments for the time period studied.

I.4.2.4 FRP Material Fabricated by Contact Molding Hand Lay-Up for Bridge Decks (ICI)

The hand lay-up laminates with knitted fabric, ICI-C, failed the 85% average for interlaminar shear in salt water after 10,000 hours but previously showed increases in interlaminar shear strength for 1,000 and 3,000 hours (Table I.4.5). The actual fabric reinforcement used for the bridge deck was stitched, ICI-B.

Table I.4.5 HITEC Acceptance Criteria Failure to Meet Requirements of Hand Lay-Up Material

		Stitched Fabric Reinforcement		Knitted Fabric Reinforcement	
		Exposure	Time Period	Exposure	Time Period
Longitudinal Tensile Strength	85% Average	M.R.		M.R.	
	75% Individual	M.R.		M.R.	
Transverse Tensile Strength	85% Average	M.R.		M.R.	
	75% Individual	M.R.		M.R.	
Longitudinal Modulus of Elasticity	85% Average	M.R.		M.R.	
	75% Individual	M.R.		M.R.	
Transverse Modulus of Elasticity	85% Average	M.R.		M.R.	
	75% Individual	M.R.		M.R.	
Interlaminar Shear Strength	85% Average	M.R.		Salt Water	10,000
	75% Individual	M.R.		M.R.	

Note: M.R. means meet requirement.

I.4.3 Moisture Absorption

Most polymer matrix composites are capable of absorbing relatively small but potentially significant amounts of moisture from the surrounding environment (Composite Materials Handbook-MIL-17, 1999). The physical mechanism for moisture gain is generally assumed to be mass diffusion following Fick's Law. The governing partial differential equation for Fick's Law is similar to the ones describing other transport phenomena (i.e., heat conduction) (See for example, Sih et al. 1986). However, this model for mass diffusion assumes there are no matrix cracks, voids, or other seepage paths. For this reason, a limit condition for the application of moisture diffusion to exposure treatments was established based on first ply failure (e.g., matrix cracking).

In polymer matrix composites, the moisture diffusion rate is many orders of magnitude slower than heat flow in thermal conductivity (Composite Materials Handbook-MIL-17, 1999). However, after a long-term exposure to a humid environment, the polymer matrix composite will absorb moisture. As a result of moisture absorption the following effects may occur: a) dimensional changes (swelling), b) reduction in the glass transition temperature of the polymer matrix (Mallick 1993), c) degradation of mechanical properties dependent on the matrix and fiber/matrix interface, and d) reduction of fiber strength due to chemical attack on the fibers (e.g., leaching of glass fibers). Therefore, moisture absorption is a design concern for construction applications, and residual mechanical properties need to be evaluated after representative moisture exposure treatments.

There are two moisture properties of a Fickian material: moisture diffusivity and moisture equilibrium content (weight percent moisture). The most commonly used test

method to determine these two properties using gravimetric techniques is ASTM D 5229/D 5229M Procedure A. Under this test protocol, specimens that are initially dry are exposed to a humid environment, and moisture mass gain versus the square root of time response is documented. The initial moisture mass gain versus the square root of time response will be linear, and the slope is related to the rate of absorption (the moisture diffusivity). The slope of the moisture mass gain versus the square root of time curve becomes smaller as the moisture content in the exterior of the polymer matrix composite begins to approach equilibrium. As time progresses, the interior of the polymer matrix material will approach equilibrium, and thus the difference between individual weights with respect to time and the slope of the moisture mass gain versus the square root of time will approach zero. The weight percent mass gain, where the slope of the response is zero, is known as the moisture equilibrium content.

For this study the suggested ASTM procedure was modified to apply to the sample plates for the immersion exposures of water and salt water at an ambient temperature of 23°C. The moisture mass gain versus the square root of time response was monitored according to the test protocols developed in Chapter 4. The results of the monitoring were fitted to a moisture mass gain versus the square root of time curve to determine the applicability of Fick's diffusion law.

I.4.3.1 Moisture Diffusion

The rate of moisture absorption is controlled by the moisture diffusivity. Moisture diffusivity is usually only weakly related to relative humidity and is often assumed to be a function only of temperature, usually following an Arrhenius-type exponential relation with inverse absolute temperature (Composite Materials Handbook-MIL-17, 1999).

Moisture diffusivity is the rate of moisture adsorption measured in mm^2/s. The moisture diffusivity coefficient, D, is calculated as follows:

$$D = \pi \cdot \left(\frac{h}{4 \cdot M_m} \right)^2 \cdot \left(\frac{M_2 - M_1}{\sqrt{t_2} - \sqrt{t_1}} \right)^2 \qquad \text{(I-4-1)}$$

where h is the thickness of the laminate exposed on both flat surfaces, M_m is the moisture equilibrium content, (M_1, t_1) and (M_2, t_2) are points on the linear portion of the moisture mass gain versus the square root of time curve. Alternatively, the slope of the linear portion, S, can be computed by doing a least-square linear regression analysis, and therefore the diffusivity can be computed as

$$D = \pi \cdot \left(\frac{h}{4 \cdot M_m} \right)^2 \cdot (S)^2 \qquad \text{(I-4-2)}$$

For this study the diffusivity coefficient was calculated for the water and salt water immersion exposures. Moisture mass gain versus the square root of time curves for these two exposures are shown in Figure I.4.1 and Figure I.4.2. These curves follow the typical trend of Fickian diffusion models only in an approximate way. It is worth noting that deviations in Fickian diffusion can occur for composite materials immersed in liquids (Springer 1988). The slope of the linear portion of the graphs was taken as the best fit of a linear trend line to the portion of the curves after the noise in initial data was removed. The initial data were ignored since it was felt that the noise was due to washing of dust and other particles off the sample plates. The linear range considered was between 1,000 and 3,000 hours, except for the pultruded DFI materials in water immersion that exhibited an initial linear response between 50 and 300 hours. The moisture diffusivity

coefficients were calculated using equation I.4.2, and the results of the calculations are shown in Table I.4.6.

Table I.4.6 Moisture Diffusivity Coefficients (*D*) for Water and Salt Water Immersion

Material/ Treatment	Diffusivity Coefficient in (mm^2/s)	
	Water Immersion	Salt Water Immersion
CPI	26.1	10.2
DFI	113	20.8
HCC	44.0	28.5
ICI-B	15.7	10.7
ICI-C	15.0	14.9

The moisture diffusivity coefficients are in the range of 10 to 44 mm^2/s for all of the laminates except for the pultruded DFI laminates from the salt water immersion exposure. The hand lay-up material samples with same resin matrix and different types of fiber reinforcement have a similar diffusivity coefficient for water immersion. In all the cases, the diffusivity coefficient in salt water is smaller than in reagent water. In order to compare the range of diffusivity coefficient with data from the literature, we consider the following example. The diffusivity coefficients for desorption and absorption of epoxy resins at 100% relative humidity and 25°C are 17 and 21 mm^2/s, respectively (Mallick 1993).

Based on the experience gained from these tests, it is suggested to expose the materials to 100% relative humidity (or as close as possible) instead of doing water immersion to estimate diffusivity coefficients.

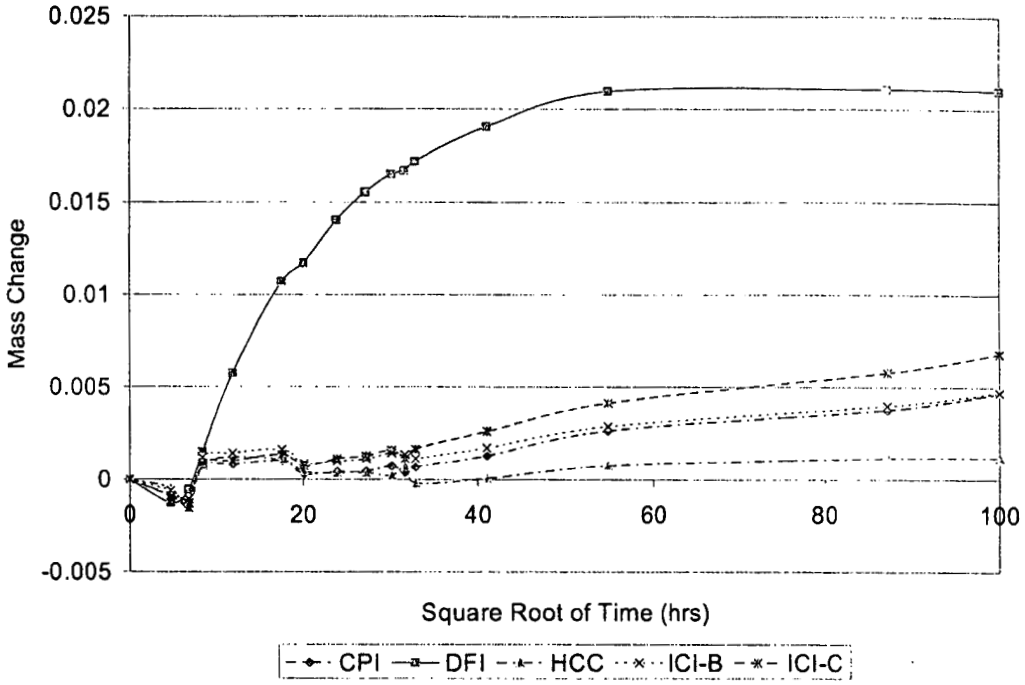

Figure I.4.1 Moisture Mass Gain versus the Square Root of Time Curves for the Water Immersion Tests

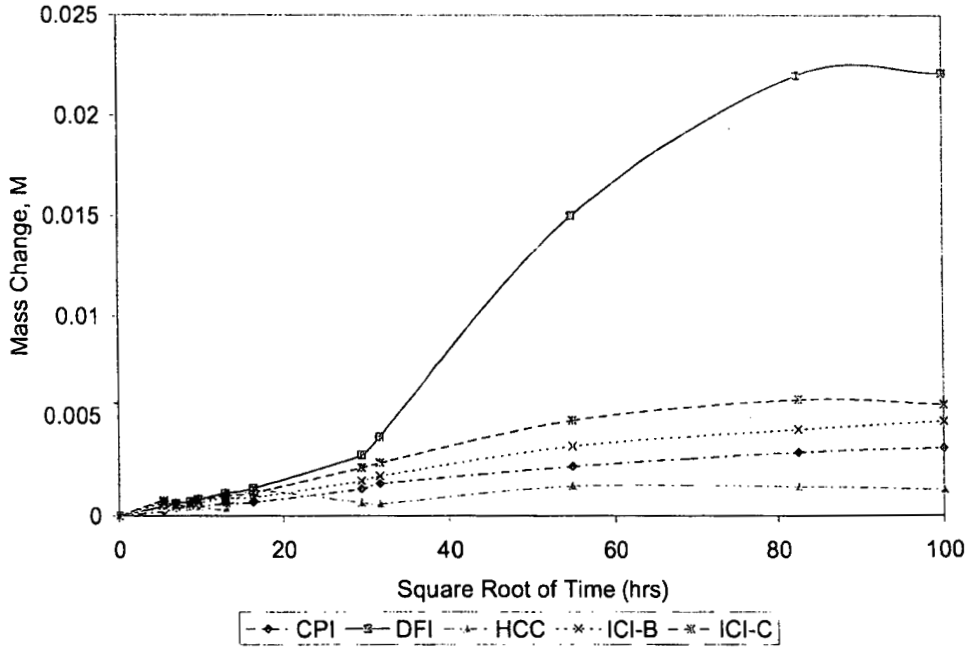

Figure I.4.2 Moisture Mass Gain versus the Square Root of Time Curves for the Salt Water Immersion Tests

I.4.3.2 Moisture Equilibrium Content

The moisture equilibrium content values found in the literature for E-glass/polyester and E-glass/vinyl ester composites were compared with the experimental data. Table I.4.7 summarizes the maximum moisture content of materials covered in the pertinent literature. These values ranged from a low of 0.2% for a unidirectional E-glass/vinyl ester material fabricated by the SCRIMP process to a high of 1.35% for an E-glass/polyester molded material. However, it is difficult to make comparisons due to the many variables involved, such as fiber content, laminate configuration, exposure, temperature, and fabrication process. The results selected from the literature were approximate comparisons to the materials and exposures for this study.

Table I.4.7 Moisture Equilibrium Contents for FRP Materials Studied by Other Researchers

Material (fiber, matrix, V_f or W_f)	Ref	Laminate	RH (%)	Temp (°C)	Moisture Equilibrium Content (%)
E-glass/ Polyester (W_f = 50%)	Springer et al., 1980	SMC-R50	100	23	1.35
E-glass/ Vinyl Ester (W_f = 50%)	Springer et al., 1980	SMC-R50	100	23	0.63
E-glass/ Vinyl Ester	Steckel et al., 1999	G3 Fabricated by SCRIMP	100	38	0.2
E-glass/ Vinyl Ester	Gentry et al., 1999	VGR pultruded rod	Deionized Water Immersion	80	0.32 for 922 hrs
E-glass/ Vinyl Ester	Liao et al., 1999	Extren® 625 fabricated by pultrusion 0 & 90° coupons unsealed	Deionized Water Immersion	25	0.68-0.82 for 10,000 hrs

In general, the results of this study are consistent with the results from the literature. The results of this study relative to the exposure and material properties are summarized in Table I.4.8 and Table I.4.9. The vinyl ester resin composites have an approximate moisture equilibrium content at room temperature (23°C) of 0.12% to 0.43%. The composites with polyester resins have higher moisture equilibrium contents at room temperature ranging from 0.47% to 2.25%.

Table I.4.8 Moisture Equilibrium Contents for Water Immersion Tests

Fabrication Process	Material (fiber, matrix, V_f or W_f)	Exposure	Temp (°C)	Moisture Equilibrium Content (%)
Putrusion (CPI)	E-glass/Vinyl ester (V_f = 49.2%)	Immersion in Type IV Reagent Water	23	0.43
Pultrusion (DFI)	E-glass/Vinyl ester/ Polyester Blend (V_f = 60.6%)	Immersion in Type IV Reagent Water	23	2.10
VARTM (HCC)	E-glass/Vinyl ester (V_f = 55.6%)	Immersion in Type IV Reagent Water	23	0.12
Contact Molding Hand Lay-Up (ICI)	E-glass-Isophthalic/ Terephthalic Polyester Stitched Fabric (V_f = 34.2%)	Immersion in Type IV Reagent Water	23	0.47
Contact Molding Hand Lay-Up (ICI)	E-glass-Isophthalic/ Terephthalic Polyester Knitted Fabric (V_f = 25.7%)	Immersion in Type IV Reagent Water	23	0.68

Table I.4.9 Moisture Equilibrium Contents for Salt Water Immersion Tests

Fabrication Process	Material (fiber, matrix, V_f or W_f)	Exposure	Temp (°C)	Moisture Equilibrium Content (%)
Putrusion (CPI)	E-glass/Vinyl ester (V_f = 49.2%)	Immersion in Salt Water	23	0.37
Pultrusion (DFI)	E-glass/Vinyl ester/ Polyester Blend (V_f = 60.6%)	Immersion in Salt Water	23	2.25
VARTM (HCC)	E-glass/Vinyl ester (V_f = 55.6%)	Immersion in Salt Water	23	0.18
Contact Molding Hand Lay-Up (ICI)	E-glass-Isophthalic/ Terephthalic Polyester Stitched Fabric (V_f = 34.2%)	Immersion in Salt Water	23	0.52
Contact Molding Hand Lay-Up (ICI)	E-glass-Isophthalic/ Terephthalic Polyester Knitted Fabric (V_f = 25.7%)	Immersion in Salt Water	23	0.65

Although the values of moisture equilibrium content or mass change appear to be consistent with the values provided by the literature, there are inherent sources of variability in the data. First, the sample plates were weighed as received with dust and other residues present, which contributed to the initial weight of the sample plates. Second, the relative amount of water present on the surface after drying could modify the mass after the initial change. These two occurrences are considered responsible for the initial variations in mass, as shown in Figure I.4.1 and Figure I.4.2.

It is also worth noting that the moisture concentration in a laminate may exceed the moisture equilibrium content if micro cracks develop in the material (Mallick 1993). The moisture adsorption is then accelerated due to the capillary action, which occurs at the micro cracks and the exposure of the fiber/matrix interface at the edges of the laminates. However, there also may appear to be a reduction in the moisture

concentration after the occurrence of micro cracks if there is the loss of material due to leaching or the cracking itself (Mallick 1993).

I.4.4 Degradation Kinetics

An attempt was made to model the residual material properties with degradation kinetics. First-order kinetics was applied to the experimental results that showed degradation beyond 5% of the control values. It was found that kinetic models did not appear to match closely the response of the materials over the entire period of study, i.e., rapid decrease in properties between 0 and 3,000 hours followed by a much slower change in properties between 3,000 and 10,000 hours. However, for the degradation of tensile strength up to 3,000 hours, and interlaminar shear up to 10,000 hours, a first-order kinetics model predicted the results with reasonable accuracy.

To characterize the kinetic response of the composite laminates subjected to the environmental treatments, a modified version of ASTM D 4502 was applied to the strength results. The response of the laminates was characterized as one of the four possible behaviors presented in the ASTM Standard. Table I.4.10, Table I.4.11, Table I.4.12, Table I.4.13, and Table I.4.14 summarize the kinetic response of the composite laminates subjected to the environmental treatments. The kinetic response is classified as follows: (A) is the ideal first-order kinetic response; (B) is a rapid initial strength loss or gain; (C) is variability; and (D) is a change in the visible aging rate as shown in Figure I.4.3.

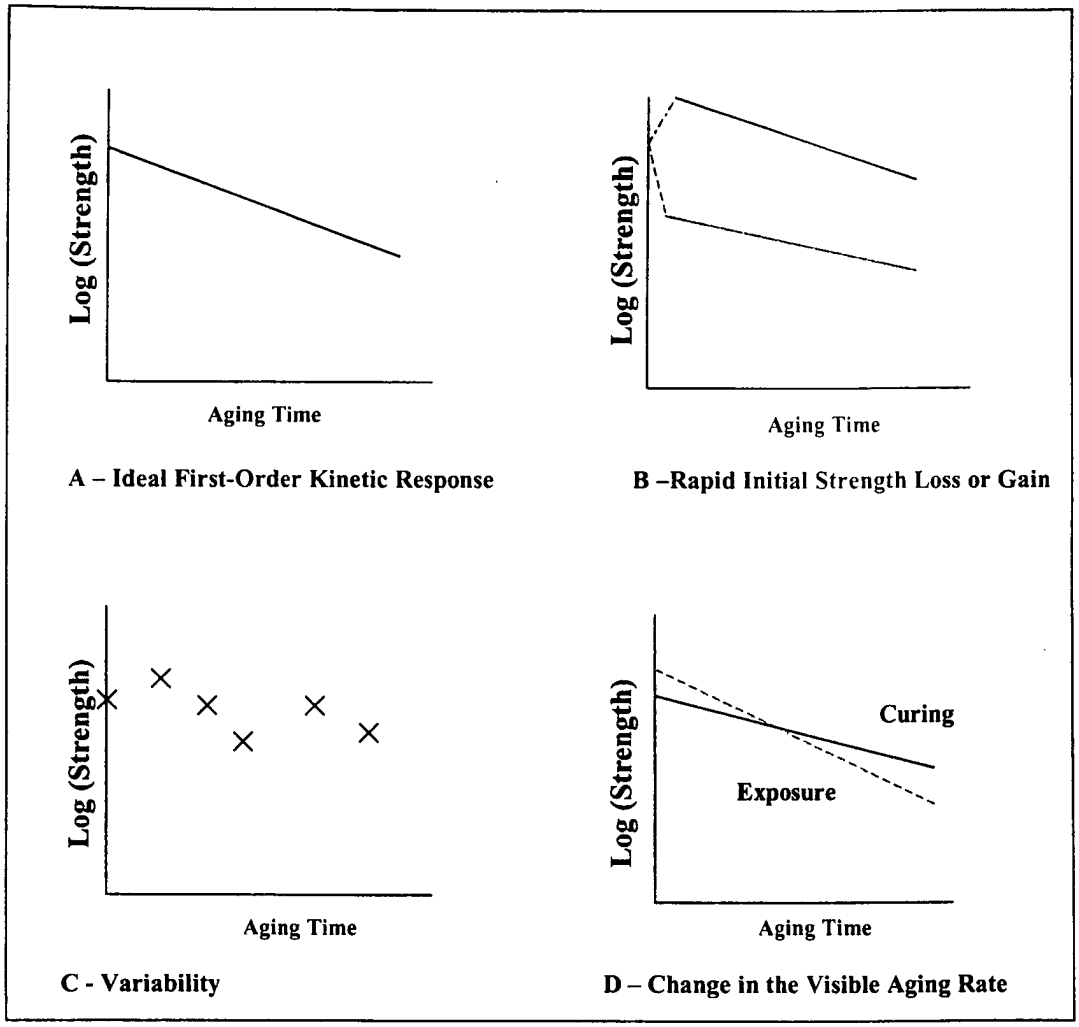

Figure I.4.3 Possible Kinetic Responses of the Strength Properties of the FRP Laminates

Table I.4.10 Characterization of the CPI Kinetic Response

Treatment	Tensile Strength		Interlaminar Shear Strength
	Longitudinal	Transverse	
Water	C	D	D
Salt Water	C	C	D
Freeze-Thaw	D	D	C
UV and Water Spray	A	C	D

Table I.4.11 Characterization of the DFI Kinetic Response

Treatment	Tensile Strength		Interlaminar Shear Strength
	Longitudinal	Transverse	
Water	C	C	C
Salt Water	C	C	C
Alkali	C	---	C
Alkali w/ Epoxy	D	---	C
Freeze-Thaw	C	C	C
UV and Water Spray	C	C	A

Table I.4.12 Characterization of the VARTM Material Kinetic Response

Treatment	Tensile Strength		Interlaminar Shear Strength
	Longitudinal	Transverse	
Water	C	D	C
Salt Water	C	D	A
Freeze Thaw	D	C	A
UV and Water Spray	C	C	C

Table I.4.13 Characterization of the Hand Lay-Up Material ICI-B Kinetic Response

Treatment	Longitudinal Tensile Strength	Interlaminar Shear Strength
Water	C	C
Salt Water	C	C
Freeze-Thaw	D	B
UV and Water Spray	C	C

Table I.4.14 Characterization of the Hand Lay-Up Material ICI-C Kinetic Response

Treatment	Longitudinal Tensile Strength	Interlaminar Shear Strength
Water	D	C
Salt Water	D	C
Freeze-Thaw	C	C

The kinetic characterization of the laminates showed that an ideal kinetic response was only possible for the treatments with short durations. For the treatments with longer durations, the results were typically variable. However, in some cases there was an indication of a change in kinetic behavior with respect to time. In some cases the laminates usually showed one response between 0 and 3,000 hours and another between 3,000 and 10,000 hours. The freeze-thaw treatment was the only treatment for which the results showed rapid increases or losses in strength.

A first-order kinetics model was applied to the residual tensile strengths for the pultruded CPI coupons in the longitudinal direction for the UV and water spray treatment and the salt water immersion treatment for the transverse coupons for the first 3,000 hours. The model was also applied to the epoxy-coated pultruded material, DFI-E, longitudinal tensile strength coupons for the alkali exposure. The kinetics model was applied by fitting a least-squares regression line to the data for 0, 1,000, and 3,000 hours and plotting the log of the residual strengths versus normal time. These three linear trends are shown in Figure I.4.4, Figure I.4.5, and Figure I.4.6.

A first-order kinetics model was also applied to the interlaminar shear strength response of the VARTM material for the salt water and the freeze-thaw cycling exposures. Degradation kinetics was also applied to the interlaminar shear strength response of the pultruded DFI laminates to UV and water spray exposure for the entire exposure period. These three linear trends are shown in Figure I.4.7, Figure I.4.8, and Figure I.4.9.

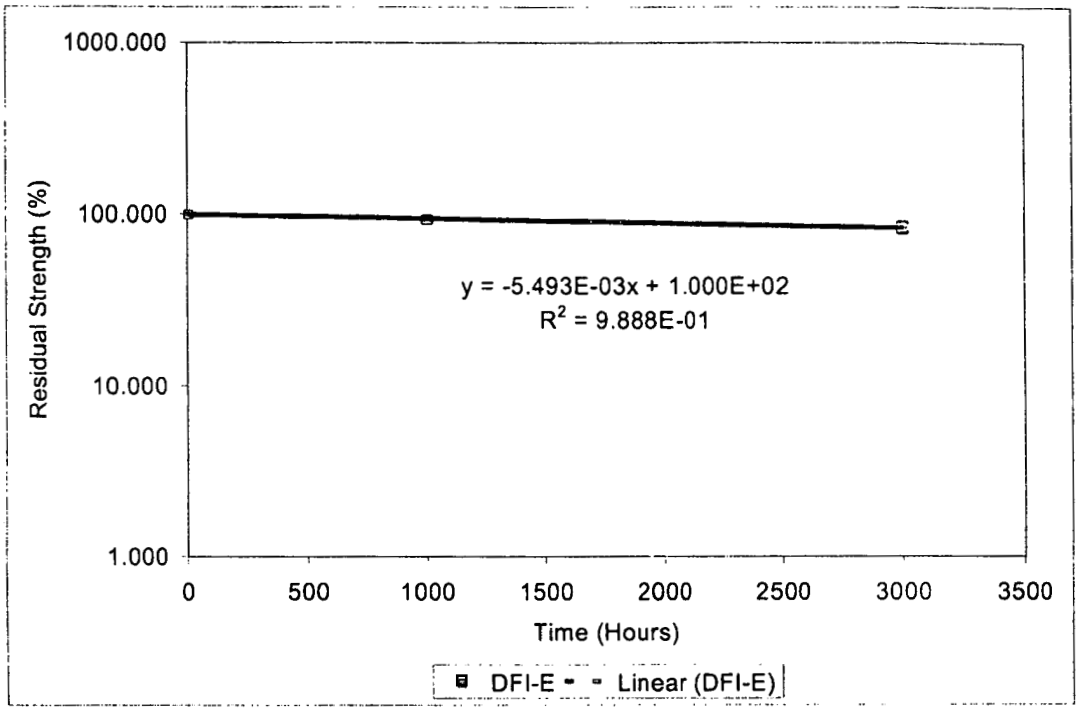

Figure I.4.4 First-Order Kinetics Model for the Tensile Strength of the Pultruded Material with Epoxy Coating (DFI-E) in the Longitudinal Direction for the Alkali Immersion Exposure

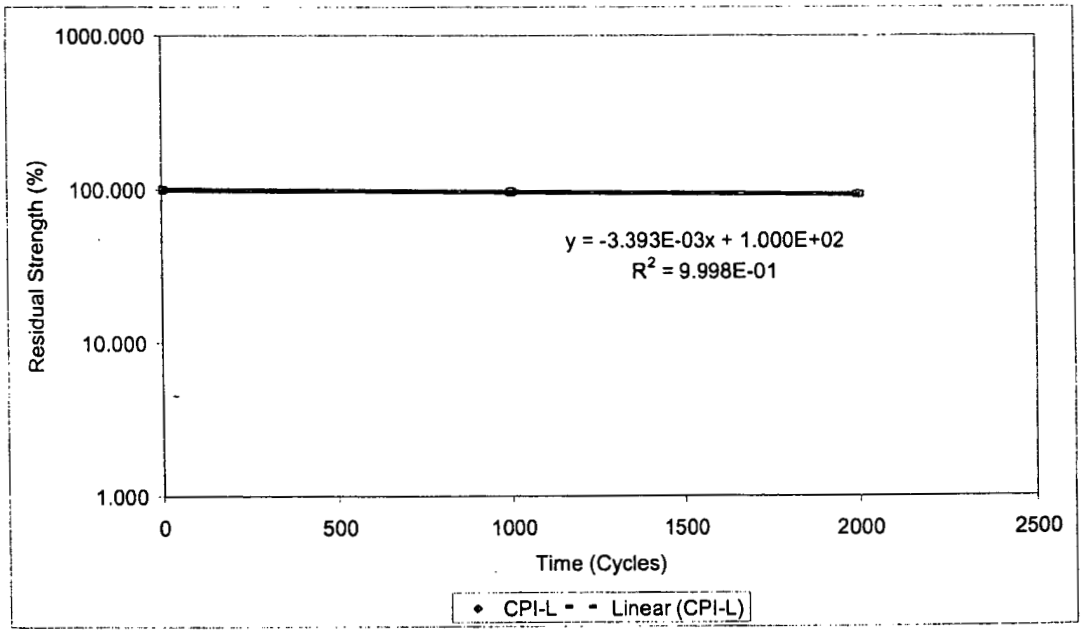

Figure I.4.5 First-Order Kinetics Model for the Tensile Strength of the Pultruded Material (CPI) in the Longitudinal Direction for the UV and Spray Exposure

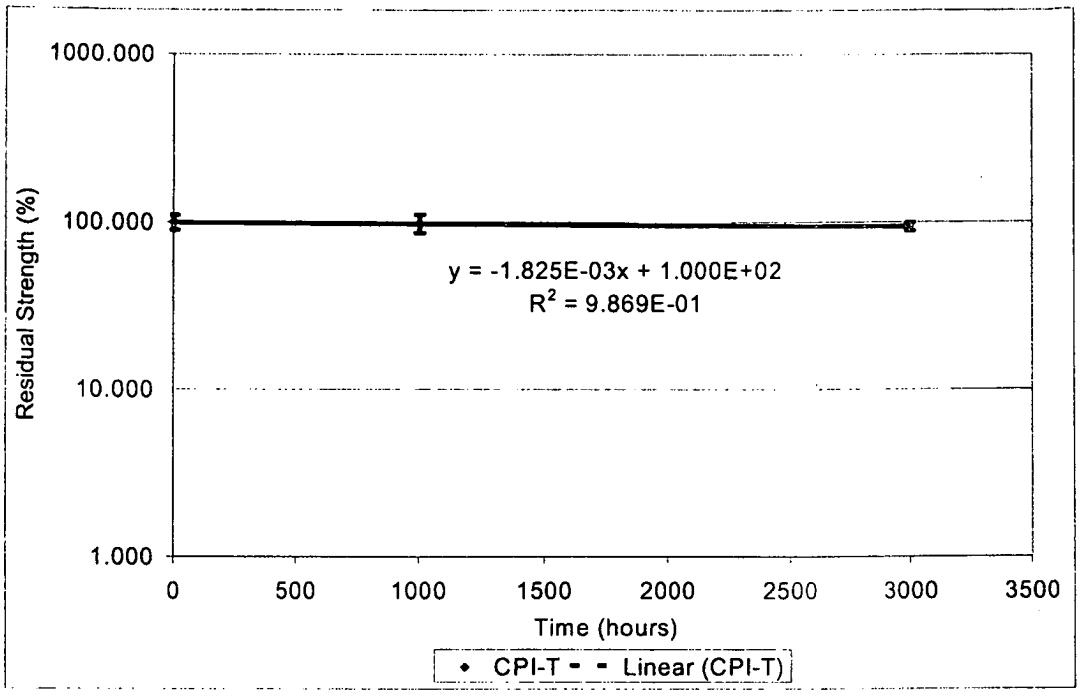

Figure I.4.6 First-Order Kinetics Model for the Tensile Strength of the Pultruded Material (CPI) in the Transverse Direction for the Salt Water Immersion Exposure

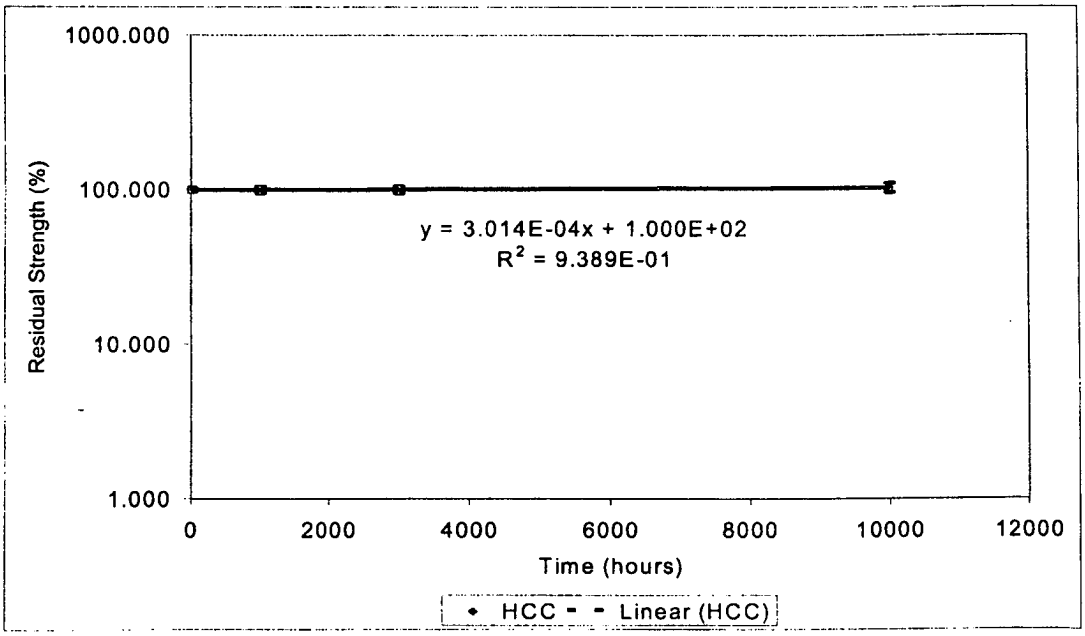

Figure I.4.7 First-Order Kinetics Model for the Interlaminar Shear Strength of the VARTM Material in the Longitudinal Direction for the Salt Water Immersion Exposure

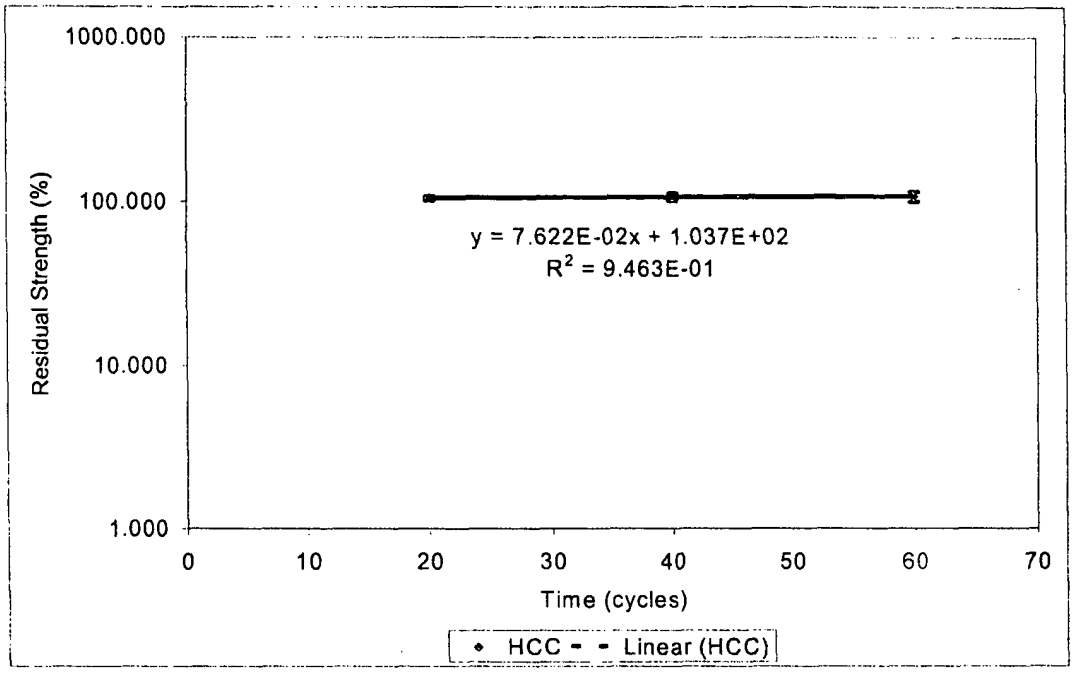

Figure I.4.8 First-Order Kinetics Model for the Interlaminar Shear Strength of the VARTM Material in the Longitudinal Direction for Freeze-Thaw Cycling

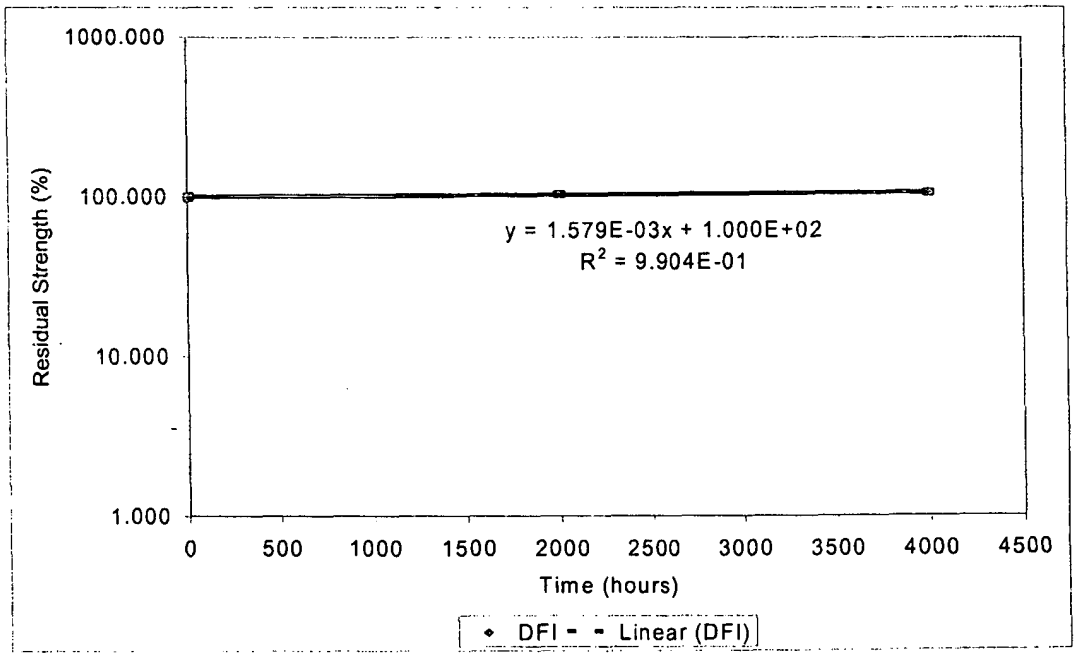

Figure I.4.9 First-Order Kinetics Model for the Interlaminar Shear Strength of the VARTM Material in the Longitudinal Direction for the UV and Water Spray Exposure

The application of first-order degradation kinetics results in the computation of rate parameters. The degradation rate parameters are obtained as the slope of the least-square linear regression analysis of the experimental values of residual strength. The rates of degradation in tensile strength range from –5.49%/1000 hours for the tensile strength of the pultruded material from DFI in the alkali solution to –1.8%/1000 hours for the tensile strength of the pultruded material CPI in the salt water solution. The rates of interlaminar strength increases are 0.76%/10 cycles of freeze-thaw, 0.3%/1000 hours of salt water immersion, and 1.6%/1000 hours of UV and water spray exposure, respectively. Thus, the rates of increase and decrease in material properties vary depending upon the material and fabrication process.

The degradation kinetics model provides a tool to predict residual tensile strength for medium-term exposures (i.e., 3,000 hours). For longer exposure times, the extrapolation of results will lead to conservative estimates of residual strength. On the other hand, for interlaminar shear strength, degradation kinetics can be used for predictions of long-term residual strength (i.e., 10,000 hours) under severe environmental exposure. Based on these results, it is hypothesized that chemical kinetics can provide a better prediction model for degradation of strength properties controlled by the polymer matrix and the matrix-fiber interface (i.e., interlaminar shear strength) than for properties controlled by the fiber reinforcement (i.e., longitudinal tensile strength).

I.4.5 Material Capacity Reduction Factors

This section summarizes the design approach to account for the environmental effects the material will encounter in service. The safety factors reported in this section are highly conservative due to the relatively small sample sizes for the control and

environmentally treated coupons. To determine more reliable safety factors, a statistically significant value for design strength needs to be determined as explained in Composite Materials Handbook-MIL-17 (Composite Materials Handbook-MIL-17, 1999). It is worth noting that the proposed safety factors only apply to the material in the uncracked state and for the first monotonic loading of the laminates past the cracking load.

I.4.5.1 Design Approach

The design approach for environmental knock-down factors for strength properties was to determine the 5% lower tolerance limit of the residual strength property (tensile strength and interlaminar shear strength) after exposure to each treatment period. The knock-down factor was defined as the residual strength with respect to the baseline control. The 5% lower tolerance limit of the residual mechanical properties after the environmental exposure treatments was divided into the 5% lower tolerance limit of the baseline control to determine the multiplier, R_F, for environmental effects.

In this study the lower tolerance limit is defined as a 5% lower tolerance limit (LTL) with 95% confidence. The 5% lower tolerance limit is based upon the Student's *t*-distribution with the sample size minus one degrees of freedom. A student's *t*-distribution is used instead of a normal distribution due to the small sample sizes. The student's *t*-distribution is symmetrical about zero but has thicker tails than a normal distribution.

The 5% lower tolerance limit of the baseline and residual strengths was chosen as the design criterion based upon the design approaches proposed by code authorities for other relevant materials. The following were considered: 1) ASTM guidelines for wood design properties, 2) ACI guidelines for the strength of FRP unidirectional reinforcements (rebars) for concrete, and 3) Composite Materials Handbook-MIL-17

recommendations for the strength of composites. The design approach proposed by these three reference materials are correlated with the proposed design approach for FRP materials used in composite bridge decks in Table I.4.15.

Table I.4.15 Comparison of Evaluation Criteria

	Wood (ASTM, NDS)	FRP Bars (ACI)	MIL-HDBK-17	Proposed for FRP Bridge Decks
Confidence Level	95%	99%	90% and 95%	95%
Sample Size	>100	20	30	5-10
Statistical Distribution	Student's *t*-Distribution	Normal Distribution	Depends on sample size	Student's *t*-Distribution
COV	16% MOR 22% MOE	- - -	- - -	10% UTS 10% ILSS

The characteristic strength property of the baseline control material (unexposed) is computed as

$$F_K^o = F_m^o - K_o \cdot S_o \tag{I-4-3}$$

where F_m^o is the mean strength property, S_o is the standard deviation of the sample, and K_o is the statistical factor that accounts for the sample size and the tolerance interval.

The characteristic strength property of the degraded material (exposed) is computed as

$$F_K^d = F_m^d - K_d \cdot S_d \tag{I-4-4}$$

where F_m^d is the mean strength property, S_d is the standard deviation of the sample, and K_d is the statistical factor.

The residual strength factor is computed as

$$R_F = \frac{F_K^d}{F_K^o} \leq 1 \qquad \text{(I-4-5)}$$

The approach for the elastic modulus properties is to compute the residual property based on mean values to have an accurate prediction of stiffness, buckling, and vibration responses. The residual modulus factor is computed as

$$R_E = \frac{E_m^d}{E_m^o} \leq 1 \qquad \text{(I-4-6)}$$

where E_m^o is the mean elastic modulus of the baseline control material (unexposed) and E_m^d is the mean elastic modulus of the degraded material (exposed).

The knock-down factors that follow can only be used with design strength and modulus values that were derived in the same manner. The knock-down factors for modulus can only be used with design values derived based on the mean to the sample set. The knock-down factors for tensile and interlaminar shear strength can only be used in conjunction with design values derived from 5% lower tolerance limits of the sample set.

I.4.5.2 Knock-Down Factors

The following sections list the knock-down factors for strength and modulus of the five deck systems.

I.4.5.2.1 FRP Material Fabricated by Pultrusion for Bridge Decks (CPI)

The knock-down factors for strength and elastic modulus are shown in Table I.4.16 and Table I.4.17. The knock-down factors for tensile strength are in the range of

0.85 to 0.95 for longitudinal direction and are above 0.95 for transverse tensile strength except for the water exposure, which is 0.74. The knock-down factors for tensile strength are all in a group and less than one due to the low COVs for the baseline and residual strengths. The knock-down factors for transverse tensile strength are all close to one except for water exposure due to the higher amounts of variability in the transverse direction, especially in the baseline sample set. The knock-down factors for interlaminar shear strength are in the range of 0.85 to 1.00 due to the larger sample size.

Table I.4.16 Knock-Down Factors for the Strength Properties of the Pultruded Material (CPI)

	Longitudinal Tensile Strength		Transverse Tensile Strength		Interlaminar Shear Strength	
	Character-istic (MPa)	Residual Factor	Character-istic (MPa)	Residual Factor	Character-istic (MPa)	Residual Factor
Control	273	1.00	117	1.00	24.4	1.00
Water	252	0.92	92.4	0.79	22.4	0.92
Salt Water	246	0.91	112	0.96	24.2	0.99
Freeze-Thaw	243	0.89	117	1.00	20.7	0.85
UV and Spray	260	0.95	117	1.00	23.9	0.98
Exterior Exposure	243	0.89	117	1.00	23.4	0.96

Table I.4.17 Knock-Down Factors for the Modulus Properties of the Pultruded Material (CPI)

	Longitudinal Tensile Modulus		Transverse Tensile Modulus	
	Mean (GPa)	Residual Factor	Mean (GPa)	Residual Factor
Control	22.4	1.00	15.9	1.00
Water	21.5	0.96	15.7	0.99
Salt Water	22.0	0.98	15.5	0.98
Freeze-Thaw	22.4	1.00	15.3	0.96
UV and Spray	22.4	1.00	15.9	1.00
Exterior Exposure	22.4	1.00	15.9	1.00

The knock-down factors for modulus are in the range of 0.96 to 1.00. These factors are small because of the slight changes in modulus due to the small sample sizes and the use of average values to compute the knock-down factors.

I.4.5.2.2 FRP Material Fabricated by Pultrusion for Reinforcing Concrete Bridge Decks (DFI)

The knock-down factors for strength and elastic modulus are shown in Table I.4.18 and Table I.4.19. The knock-down factors for longitudinal tensile strength are in the range of 0.63 to 1.00. The values for the exposures with immersion baths are in the range of 0.63 to 0.80. These values accurately take into account the large decreases in longitudinal tensile strength for these exposures. The knock-down factors agree with the statistical analysis of the test results since the knock-down factors for water and alkali exposure are greater than salt water.

Table I.4.18 Knock-Down Factors for the Strength Properties of the Pultruded Material (DFI)

	Longitudinal Tensile Strength		Transverse Tensile Strength		Interlaminar Shear Strength	
	Character-istic (MPa)	Residual Factor	Character-istic (MPa)	Residual Factor	Character-istic (MPa)	Residual Factor
Control	559	1.00	22.8	1.00	35.8	1.00
Water	352	0.63	22.8	1.00	28.6	0.80
Salt Water	403	0.72	10.5	0.46	30.8	0.86
Alkali	386	0.69	22.8	1.00	27.5	0.77
Freeze-Thaw	447	0.80	22.8	1.00	30.4	0.85
UV and Spray	553	0.99	22.8	1.00	35.8	1.00
Exterior Exposure	535	0.99	22.8	1.00	27.2	0.76

Table I.4.19 Knock-Down Factors for the Modulus Properties of the Pultruded Material (DFI)

	Longitudinal Tensile Modulus		Transverse Tensile Modulus	
	Mean (GPa)	Residual Factor	Mean (GPa)	Residual Factor
Control	39.5	1.00	9.05	1.00
Water	38.7	0.98	6.24	0.69
Salt Water	37.9	0.96	6.52	0.72
Alkali	37.9	0.96		
Freeze-Thaw	37.5	0.95	6.89	0.76
UV and Spray	39.5	1.00	8.15	0.90
Exterior Exposure	39.5	1.00	8.15	0.90

The knock-down factors for transverse tensile strength were all 1.00 except for the salt water exposure. The 0.46 knock-down factor for the salt-water exposure was due to a very large standard deviation in the test results for 10,000 hours. All the other knock-down factors are 1.00 because the 5% lower tolerance limit of the baseline control was smaller than the 5% lower tolerance limits of the exposed sample sets.

The knock-down factors for interlaminar shear strength are very similar to the factors for longitudinal tensile strength. The factors are very representative of the actual decreases in interlaminar shear strength due to the large sample size. The knock-down factors for water and alkali are less than salt water, which agrees with the statistical analysis.

The knock-down factors for longitudinal tensile strength are in the range of 0.96 to 1.00. These values accurately represent the actual tensile modulus of the material, and the small range of values agrees with the statistical analysis, which showed that the longitudinal modulus was statistically unaffected by the exposure treatments. The knock-down factors for transverse modulus of elasticity are in the range of 0.69 to 1.00. These

factors account for the large amounts of variability in the transverse modulus of elasticity after environmental exposure.

I.4.5.2.3 FRP Material Fabricated by VARTM for Bridge Decks (HCC)

The knock-down factors for strength and elastic modulus are shown in Table I.4.20 and Table I.4.21. The knock-down factors for longitudinal tensile strength are all very close to one since the material showed increases in strength for most of the exposure treatments. The knock-down factors for transverse tensile strength are in the range of 0.89 to 0.92. The transverse knock-down factors account for the slight decreases in tensile strength reasonable well.

Table I.4.20 Knock-Down Factors for the Strength Properties of the VARTM Material

	Longitudinal Tensile Strength		Transverse Tensile Strength		Interlaminar Shear Strength	
	Character-istic (MPa)	Residual Factor	Character-istic (MPa)	Residual Factor	Character-istic (MPa)	Residual Factor
Control	369	1.00	265	1.00	42.0	1.00
Water	354	0.96	241	0.91	39.0	0.93
Salt Water	369	1.00	236	0.89	39.9	0.95
Freeze-Thaw	369	1.00	241	0.91	41.6	0.99
UV and Spray	369	1.00	236	0.89	38.6	0.92
Exterior Exposure	369	1.00	244	0.92	34.0	0.81

Table I.4.21 Knock-Down Factors for the Modulus Properties of VARTM Material

	Longitudinal Tensile Modulus		Transverse Tensile Modulus	
	Mean (GPa)	Residual Factor	Mean (GPa)	Residual Factor
Control	23.6	1.00	19.6	1.00
Water	22.2	0.94	19.2	0.98
Salt Water	21.7	0.92	18.6	0.97
Freeze-Thaw	23.6	1.00	19.4	0.99
UV and Spray	23.6	1.00	19.6	1.00
Exterior Exposure	23.6	1.00	19.6	1.00

The knock-down factors for elastic modulus in the longitudinal and transverse directions were in the range of 0.92 to 1.00. These factors account for the initial decreases in elastic modulus for the immersion exposure well. However, most of the knock-down factors are relatively close to 1.00 to the increases in elastic modulus with time.

I.4.5.2.4 FRP Material Fabricated by Contact Molding Hand Lay-Up for Bridge Decks (ICI)

I.4.5.2.4.1 Hand Lay-Up Material with Stitched Fabric Reinforcement

The knock-down factors for strength and elastic modulus are shown in Table I.4.22 and Table I.4.23. The knock-down factors for tensile and interlaminar shear strength and elastic modulus are in the range of 0.96 to 1.00. These factors are close to one due to the larger coefficients of variation as a result to the fabrication process and the increase in properties with time.

Table I.4.22 Knock-Down Factors for the Strength Properties of Hand Lay-Up Material with Stitched Fabric Reinforcement

	Longitudinal Tensile Strength		Interlaminar Shear Strength	
	Characteristic (MPa)	Residual Factor	Characteristic (MPa)	Residual Factor
Control	211	1.00	21.7	1.00
Water	208	0.99	21.5	0.99
Salt Water	208	0.99	21.7	1.00
Freeze-Thaw	211	1.00	21.7	1.00
UV and Spray	211	1.00	20.7	0.96
Exterior Exposure	211	1.00	21.7	1.00

Table I.4.23 Knock-Down Factors for the Modulus Properties of Hand Lay-Up Material with Stitched Fabric Reinforcement

	Longitudinal Tensile Modulus	
	Mean (GPa)	Residual Factor
Control	16.4	1.00
Water	16.4	1.00
Salt Water	16.4	1.00
Freeze-Thaw	16.4	1.00
UV and Spray	16.4	1.00
Exterior Exposure	16.4	1.00

I.4.5.2.4.2 Hand Lay-Up Material with Knitted Fabric Reinforcement

The knock-down factors for strength and elastic modulus are shown in Table I.4.24 and Table I.4.25. The knock-down factors for longitudinal tensile strength and elastic modulus are in the range of 0.92 to 1.00. The knock-down factors that are less than one account for the decreases in properties at 10,000 hours of environmental exposure.

Table I.4.24 Knock-Down Factors for the Strength Properties of Hand Lay-Up Material with Knitted Fabric Reinforcement

	Longitudinal Tensile Strength		Interlaminar Shear Strength	
	Characteristic (MPa)	Residual Factor	Characteristic (MPa)	Residual Factor
Control	159	1.00	19.3	1.00
Water	155	0.98	17.8	0.92
Salt Water	159	1.00	16.0	0.83
Freeze-Thaw	159	1.00	18.9	0.98

Table I.4.25 Knock-Down Factors for the Modulus Properties of Hand Lay-Up Material with Knitted Fabric Reinforcement

	Longitudinal Tensile Modulus	
	Mean (GPa)	Residual Factor
Control	13.4	1.00
Water	12.3	0.92
Salt Water	13.4	1.00
Freeze-Thaw	13.4	1.00

I.5 Summary, Conclusions, and Recommendations for Future Work

This chapter summaries the methods, results, and conclusions of this study and provides recommendations for future work on the durability of fiber-reinforced composites for bridge decks.

I.5.1 Summary

The main objective of this study was to determine the effects of harsh environments on the stiffness and strength of four different FRP materials used for bridge deck systems. This study had two main objectives: 1) development of an environmental exposure test protocol to evaluate the durability of FRP materials used for bridge deck construction; and 2) characterization of the effects of environmental exposure on the mechanical properties of FRP materials through correlations of experimental results and mechanics modeling.

I.5.1.1 Development of Test Methods

A test method to study the effects of harsh environments on the stiffness and strength of the four FRP materials used in bridge deck systems was developed based upon the prior research of Steckel et al. (1999) and the acceptance criteria AC 125, from ICBO (1997). The test methods were adapted for FRP deck materials. Sample plates from each manufacturer were subjected to the test matrix in Table I.5.1.

Table I.5.1 Environmental Test Matrix

Environmental Durability Test	Test Conditions	Test Duration
Water Resistance	Immersion in reagent water at 23°C	1,000, 3,000 and 10,000 hours
Salt Water Resistance	Immersion in salt water at 23°C	1,000, 3,000 and 10,000 hours
Alkali Resistance	Immersion in calcium carbonate with pH of 9.5 at 23°C (pultruded materials from DFI only)	1,000, 3,000 and 10,000 hours
Freeze-Thaw Resistance	Water immersion at 38°C followed by consecutive cycles of 12 hours of freeze at –18°C and 12 hours of water immersion at 38°C	21 days conditioning followed by 20, 40, and 60 cycles of FT
Exterior Exposure Resistance	Natural environmental conditions	1 year
QUV Resistance	Cycles of 1 hour and 42 minutes of light followed by 18 minutes of spray and light	1,000 and 2,000 cycles

I.5.1.2 Characterization of the Effects of the Environmental Exposure Treatments

To characterize the effects of the environmental exposures, baseline properties were determined for appearance, density, fiber volume fraction, longitudinal tensile strength and modulus, transverse tensile strength and modulus, and longitudinal interlaminar shear strength. The longitudinal tensile strength and modulus, transverse tensile strength and modulus, and longitudinal interlaminar shear strength were evaluated after each preset exposure duration. The mass change of the sample plates was also monitored throughout the aging process.

I.5.1.3 Degradation Kinetics and Material Capacity Reduction Factors

First-order kinetics was applied to compute the initial degradation rate, which followed a linear trend. The importance of the initial degradation rate was to correlate the

residual properties with the exposure time and provide an indication of the resistance of the material to the selective treatments. However, after 3,000 hours of exposure a typical non-linear response was observed. The long-term characterization of degradation kinetics requires extensive experimental work and different temperature treatments, which were beyond the scope of this study.

Material capacity reduction factors for strength were developed based upon the 5% lower tolerance limit of the residual material properties after aging. The 5% lower tolerance limit was used since it was a conservative estimate of the reduction in material properties.

I.5.2 Conclusions

The following conclusions were drawn for each of the two main objectives.

I.5.2.1 Development of Test Methods

The environmental exposure treatments that the sample plates were subjected to appear to be accelerated forms of aging. The degradation of the samples subjected to the immersion conditions was much greater than the weathering samples. However, the salt water condition could be eliminated since it was statistically less severe when compared to the water and alkali conditions. In addition, the use of the artificial weathering machine to produce the UV and water spray exposure appears to accelerate the rate of degradation relative to the exterior exposure condition.

For calculation of statistically based materials properties, the procedure presented in the MIL-HDBK-17 is recommended (e.g., 30 specimens from at least five batches of a material per environment and direction). This procedure is required to establish "basis

values" that provide a reasonable evaluation of material variation. This research work focused on characterizing environmental treatments for four different FRP materials. Hence, establishing basis values was beyond the scope of the research effort. For this reason, fewer replicates (e.g., 5 to 7 for tension and 8 to 10 for interlaminar shear) from one processing batch were studied for each material and treatment.

I.5.2.2 Characterization of the Effects of the Environmental Exposure Treatments

The tension and interlaminar shear tests provided a reliable evaluation method for the composite laminates. The intent of the study was to characterize composite laminates with multi-axial reinforcement, which are representative of the actual laminates used in the FRP bridge decks.

To characterize reinforcing fibers, resin matrix, and fiber-matrix interfaces, other test procedures should be followed (see, for example, MIL-HDBK-17), which were beyond the scope of this research work. Experimental characterization of fiber and matrix properties is required to apply micro-mechanics models for predicting unidirectional composite lamina response. Furthermore, unidirectional composite lamina testing is useful to apply laminate analysis for predicting multi-axial laminate response.

In multi-axial composite laminates, directional properties (e.g., longitudinal tensile strength) can only be partially related to the material constituents (e.g., longitudinal fiber reinforcement). For example, in materials with relatively high fiber reinforcement in the longitudinal direction (e.g., pultruded material by DFI), the laminate response becomes closer to an equivalent unidirectional composite lamina. In this case it is possible to associate the longitudinal tensile strength with a "fiber-dominated" property

and the transverse tensile strength with a "matrix-dominated" property. However, in materials with a more balanced directional reinforcement (e.g., VARTM or hand lay-up), both the fiber and matrix contribute to longitudinal and transverse properties. Furthermore, the short-beam shear test provides a strength indicator that is only partially related to the actual interlaminar shear strength. Other factors such as resin-rich areas and directional reinforcement affect the "apparent" interlaminar shear strength of multi-axial composites. For example, the hand lay-up samples with relatively high matrix content experienced inclined shear failure as opposed to horizontal interlaminar failure.

Two control samples sets were used: baseline (tested as received) and aged in air at ambient conditions (tested after one and a half years). The mechanical properties of both control sets were compared. It was found that the longitudinal and transverse tensile properties (modulus and strength) of the two FRP materials fabricated by pultrusion had no statistical difference between both controls. The interlaminar shear strength of one of the pultruded materials control sets (DFI) changed with aging time, while the other pultruded material did not (CPI).

On the other hand, the VARTM and hand lay-up materials experienced changes on some modulus and strength properties with the aging time. It is worth noting that while the pultruded materials were cured at high temperature in the die during fabrication, the VARTM and hand lay-up materials were cured at ambient temperature. It is hypothesized that the higher temperature during fabrication favored a more complete degree of curing. To account for varying properties with aging time as further curing takes places, it is necessary to test control samples for all the time periods used in the treatment periods. This was beyond the scope of this research work. Therefore, the

baseline control properties were adopted as reference values and applied to compute residual properties.

One important observation of this study was the determination of the first-ply failure (FPF) of multi-axially reinforced laminates, which is clearly defined by a change in the slope of the stress-strain curve during tension tests. FPF is associated with matrix cracking and takes place in the 0.3 to 0.5% strain range depending on the material systems, while the strain to failure is typically around 2%. This implies that beyond FPF, although the fiber-reinforced composite is structurally sound, the matrix has micro-cracks that can favor water ingress and expose the fibers to environmental attack. The characterization of the FPF limit, which is not evident in typical unidirectional composite laminas, highlights the importance of conducting tests on multi-axial composite laminates. The determination of FPF also provides a service limit for environmental durability. In this sense the durability characterization presented in this study only applies to uncracked materials, which are loaded below FPF. For loads beyond FPF, the durability of the material is uncertain and therefore is not recommended for exterior applications.

I.5.2.3 Summary of Conclusions

1. Mechanical test indicators for multi-axial composite laminates (tensile strength, ILS strength, tensile modulus) allow for characterization of durability response.
2. The environmental exposure test protocol combined with the mechanical test indicators serves to characterize the in-service response of FRP materials for bridge decks. The test protocol was implemented with the HITEC criteria.

3. Water and alkali immersion are the most severe exposure treatments. Salt water is less severe than other immersion treatments. Immersion treatments are more severe than weathering.
4. The FPF limit (matrix cracking) provides an upper bound for the applicability of the environmental exposure results. Loading beyond FPF will be detrimental for durability. FPF is proposed as a serviceability limit state.
5. A set of laminate analysis tools has been developed to predict fiber volume fraction and elastic modulus for orthotropic directions. Modulus prediction is more reliable for orthotropic directions with relatively high fiber content. The laminate analysis tool can be applied to predict the elastic properties of FRP deck parts.
6. The experimental evaluation and analysis performed was at the composite laminate level (multi-axial fiber reinforcement). The advantages of this approach are a) ti accounts for the effects of processing parameters (defects, degree of curing, compaction, geometric tolerances); b) it detects non-linearity in the stress-strain curves (FPF limit); and c) it allows for easier scale-up to predict structural response. For micro-mechanics-based degradation models, the experimental response of individual constituents (fiber and matrix) and unidirectional composite laminas needs to be characterized.
7. Linear degradation kinetics applied to the following treatments and indicators: a) tensile strength for medium-term immersion exposure (3,000 to 4,000 hours); and b) interlaminar shear response for long-term exposure (which is matrix dominated).

8. A statistically based methodology to compute material capacity reduction factors that account for environmental exposure degradation was proposed: a) strength factors were based on tolerance limits; and b) modulus factors were based on mean values.

I.5.3 Recommendations and Future work

1. Study the long-term freeze-thaw cycling response of FRP materials similarly to current practice with other construction materials (e.g., freeze-thaw of concrete).
2. Track the effects of matrix curing for all the time periods studied in the exposure treatments by aging multiple sets of control samples in air at ambient conditions.
3. Characterize the change in FPF with the exposure time for various treatments. This requires collecting strain data with strain gages beyond the range specified by ASTM D3039 to determine the modulus of elasticity.
4. Specify a standard and durable sealant resin for the exposed laminate edges.
5. Eliminate salt water treatment, since it is statistically the same as the water treatment or even more benign.
6. Characterize the durability response of FRP composite material that was pre-cracked beyond FPF by conducting a quasi-static tensile test prior to the environmental exposure treatments.
7. Study the synergistic effects of freeze-thaw cycling and artificial weathering.
8. Study the synergistic effects of load cycling (fatigue damage accumulation) and environmental exposure.
9. Develop a methodology to correlate standard environmental exposure treatments in the lab environment with the actual degradation in the field.

10. Assess methods to accelerate aging and predict residual strength based on increasing temperatures (Arrhenius relationships).
11. Investigate the effects of material property recovery after dry-out.

I.6 REFERENCES

American Society for Testing and Materials. (1995). Standard Test Method for Tensile Properties of Polymer Matrix Composite Materials. ASTM D 3039/D3039M – 95a. Philadelphia, PA.

American Society for Testing and Materials. (1995). Standard Test Method for Apparent Interlaminar Shear Strength of Parallel Fiber Composites by Short-Beam Method. Philadelphia, PA.

American Society for Testing and Materials. (1991). Standard Specifications for Reagent Water. ASTM D 1193-91. Philadelphia, PA

American Society for Testing and Materials. (1994). Standard Practice for Testing Water Resistance of Coatings in 100% Relative Humidity. ASTM D 2247-94. Philadelphia, PA.

American Society for Testing and Materials. (1991). Standard Specifications for Substitute Ocean Water. ASTM D 1141-90. Philadelphia, PA.

American Society for Testing and Materials. (1992). Standard Test Method for Resistance of Concrete to Rapid freezing and Thawing. ASTM C 666 – 92. Philadelphia, PA.

American Society for Testing and Materials. (1996). Standard Practice for Operating Light-Exposure Apparatus (Carbon-Arc Type) With and Without Water for Exposure of Nonmetallic Materials. ASTM G 23-96. Philadelphia, PA.

American Society for Testing and Materials. (1996). Standard Practice for Operating Light- and Water-Exposure Apparatus (Fluorescent and Condensation Type) for Exposure of Nonmetallic Materials. ASTM G 53-96. Philadelphia, PA.

American Society for Testing and Materials. (1994). Standard Test Method for Ignition Loss of Cured Reinforced resins. ASTM D 2584 – 94. Philadelphia, PA.

American Society for Testing and Materials. (1994). Standard Test Method Void Content of Reinforced Plastics. ASTM D 2734 – 94. Philadelphia, PA.

Apicella, F., Imbrogno, M. (2000, February). Closing in on Approval. Civil Engineering. Vol. 70. No. 3, pp. 42-45.

Ashland Chemical. (1998). Hetron® and Aropol™ Resin Selection Guide For Corrosion Resistant FRP Applications. Composites Polymers Division of Ashland Chemical.

Barbero, E. J. (1998). Introduction to Composite Materials Design. Ann Arbor, MI: Edwards Brothers.

Bakeri, P.A., Sunder, S.S. (1990). "Concepts for Hybrid FRP Bridge Deck Systems," Serviceability and Durability of Construction Materials, B.A. Suprenant (ed.), Proceedings of the First Materials Engineering Congress Vol. 2 (pp. 1006-1014). Denver, Colorado; ASCE.

Buck, S. E., Lischer, D.W., Nemat-Nasser, S. (1999). The Combined Effects of Load, Temperature, and Moisture on the Durability of E-glass/Vinyl Ester Composite materials. Proceedings of the 44th International SAMPE Symposium - Exhibition Evolving and Revolutionary Technologies for the New Millennium, May 23- 27 V 44 (II) (pp. 1495-1506). Covina, CA; SAMPE.

Composite Materials Handbook-MIL-17. (1999). Polymer Matrix Composites Handbook, MIL-HDBK-17 PMC, Vol. 1-3. Army Research Laboratory, Aberdeen Proving Ground, MD.

DFI Pultruded Composites. (1998). Report to Mr. Steve Morton, Ohio Department of Transportation. DFI Pultruded Composites and Miller Valentine Group, Inc.

Dow Plastics. (1992). DURAKANE Epoxy Vinyl Ester Resins Technical Product Information. The Dow Chemical Company.

Gentry, R. T., Bank, L. C., Brakatt, A., Prain, L., Wang, F. (1999). Development of Accelerated Test Methods to Determine the Durability of Composites Subject to Environmental Loading. Proceedings of the 1999 International Composites Expo, Cincinnati, OH, May 10-12. (Session 5-D. pp. 1-11). The Composites Institute.

Gentry, R. T., Bank, L. C., Barkatt, A., Prain, L. (1998, January). Accelerated Test Methods to Determine the Long-term Behavior of Composite Highway Structures Subject to Environmental Loading. Journal of Composites Technology & Research, Vol. 20, No. 1, pp. 38-50.

Gomez, J., Casto, B., (1996). Freeze-Thaw Durability of Composites Materials. Proceedings of the First International Conference on Composites in Infrastructure, Tucson, AZ (pp. 947-955).

Hardcore Composites. (1998). Ohio Department of Transportation Composite Deck Project Layout of the Test Sections and Finite Element Analysis. Hardcore Composites.

International Conference of Building Officials April. (1997). Acceptance Criteria for Concrete and Reinforced and Unreinforced Masonry Strengthening Using Fiber-Reinforced, Composite Systems AC125. ICBO; Whittier, CA.

Jones, R. M. (1999). Mechanics of Composite Materials. Philadelphia, PA; Talyor & Francis. Inc.

Karbhari, V. (1999). Material Design Considerations for the Use of FRP Composites for Renewal of Civil Infrastructure. Proceedings for International Composites Expo 99, May 10-12, 1999 Cincinnati, Ohio. USA (Session 22A pp. 1-6). The Composites Institute.

Liao, K., Schultheisz, C. R., Hunston, D. L. (1999). Effects of Environmental Aging on the Properties of Pultruded GFRP. Composites: Part B, Vol. 30, No. 5, pp. 485-493.

Mallick, R. K. (1993). Fiber-Reinforced Composite Materials, Manufacturing, and Design. New York: Marcel Decker, Inc.

McGhee, K.K., Barton, F.W., McKeel, W.T. (1991). Optimum Design of Composite Bridge Deck Panels. Advanced Composites Materials in Civil Engineering Structures, Proceedings. Specialty Conference (pp. 360-370). Las Vegas, Nevada; ASCE.

Nagy, G., Kunz, J. (1998). Preliminary Design of Composite Bridge Deck System and Test Panels for the First Salem Bridge in Dayton Ohio. Infrastructure Composites International, LLC.

Plecnik, J.M., Azar, W.A. (1991). Structural Components, Highway Bridge Deck Applications. International Encyclopedia of Composites. I. Lee and M. Stuart (eds), Vol. 6, pp. 430-445.

Schwatrz, M. M. (1997). Composite Materials, Volume II: Processing, Fabrication, and Applications. Upper Saddle River, New Jersey: Prentice Hall PTR.

Seible, F., Christie, R., Hiel, C., Hooks, J., Karbhari, V., Karshenas, M., Liles, P., Lopez-Anido, R., Morton, S., Post, T., Schutte, C., Seim, C., Till, R., Williams, D., and Yannotti, A. (2000). FRP Bridge Decks Evaluation Panel, "FRP Composite Bridge Decks," HITEC Evaluation Plan., Washington, DC; Civil Engineering Research Foundation.

Sih, G. C., Michopoulus, J. G., Chou, S. C. (1986). Hydrothermoelasticity. Dordrecht; Martinus Nijhoff Publishers.

Sotiropoulos, S.N., GangaRao, H.V.S., Mongi, A.N.K. (1994). Theoretical and Experimental Evaluation of FRP Composites and Systems. ASCE Journal of Structural Engineering, Vol. 120, pp. 464-485.

Steckel, G. L., Hawkins, G. F., Bauer, J. L. Jr. (1999). Durability Issues for Composites in Infrastructure. Proceedings of the 1999 44th International SAMPE Symposium and Exhibition 'Evolving and Revolutionary Technologies for the New Millennium' May 23-May 27 1999 Long Beach, CA, USA (Vol. 44 II pp. 2194-2208). Covina CA; SAMPE.

Springer, G. S., Sanders, B. A., Tung, R. W., Loos, A. C. (1980, April). "Moisture Absorption of Polyester-E Glass Composites." Journal of Composite Materials. Vol. 14, pp. 142-154.

Springer, G. S. (1988). Environmental Effects on Composite Materials. Lancaster, Pennsylvania; Technomic Publishing Company, Inc.

Triandafilou, L. (2000) The Great Miami FRP Composite Bridge Deck Project. Presented at the 5th World Pultrusion Conference, Berlin, April 13, 2000. pp. 1-9.

Zureick, Abdul-Hamid., Shih, B., Munley, E. (1995, August). Fiber-Reinforced Polymeric Bridge Decks. Structural Engineering Review. Vol. 7, No. 3, pp. 257-266.

Wood, K., Lopez-Anido, R. (2000). AEWC Technical Report #00-011, Experimental Data for Characterizing Environmental Exposure of Fiber Reinforced Polymer Materials Used in Bridge Decks. Advanced Engineered Wood Composites Center, University of Maine.

I.7 ACKNOWLEDGMENTS

The authors thank the Ohio Department of Transportation and the Federal Highway Administration for providing the funding for this project. The authors also thank Dr. Habib Dagher, Dr. Douglas Gardner, and Dr. Stephen Shaler, faculty members of the AEWC Center at the University of Maine, for their input and assistance with this project. The authors thank the staff at the AEWC Center for their assistance with this project: Donald Strong, Gregory Perkins, Shane O'Neill, Marcy Smith, and Doreen Parent.

Section II

Static and Failure Tests of F Deck Panels

Contributors

P. Alagusundaramoorthy, I. Harik, and R. Siddiqui

University of Kentucky

Abstract

The objective of this study is to evaluate the static load-deflection response of FRP deck panels supplied by the following manufacturers: Creative Pultrusions (CP), Composite Deck Solutions (CDS), Hardcore Composites (HP) and Infrastructure Composites International (ICI). Tests are conducted up to failure on sixteen FRP deck panels. Five additional reinforced concrete (RC) conventional deck panels are tested, and are used as "baseline" panels. The test panels are ented with Linear Variable Deflection Transducers (LVDT) and strain gages to measure the out-of-plane deflections and strains. The panels are subjected to four loading steps to establish the baseline curve, to predict the responses under cyclic loading, and to study the behavior up to failure. The test results of FRP deck panels are compared with the deflection criteria, flexure criteria, and shear criteria specified by the Ohio Department of Transportation (ODOT), and with the test results from the reinforced concrete (RC) conventional deck panels. The flexural rigidities (EI) and shear rigidities (GA_w) of FRP deck panels are calculated using the first-order shear deformation beam equations, and by conducting a linear regression analysis on the load vs deflection relationship for the baseline curve. The flexural rigidity (EI) is also calculated using (i) the first order beam equation without considering the shear deformation, and (ii) the moment-curvature relationship on the load vs deflection relationship for the baseline curve. The conclusions and recommendations drawn from this study are reported.

T LE OF CONTENTS

LIST OF FIG S

LIST OF TABLES

II.1 SUMMARY

II.1.1 Introduction

Sixteen fiber reinforced polymer (FRP) and five reinforced concrete (RC) conventional deck panels were supplied to the University of Kentucky for static testing. The manufactures of the FRP deck panels are: Creative Pultrusions (CP), Composite Deck Solutions (CDS), Hardcore Composites (HP), and Infrastructure Composites International (ICI). The RC panels are used as "baseline" panels.

II.1.2 Objectives

The objectives of this study are to evaluate the static load-deflection response of deck panels supplied by four manufacturers, and to compare the test results with the deflection criteria, flexure criteria, and shear criteria specified by the Ohio Department of Transportation (ODOT), and with the test results from reinforced concrete conventional deck panels. Based on the test data the flexural and shear rigidities (EI and GA_w respectively) of these panels will be determined.

II.1.3 Scope of the Work

In order to achieve the objectives of this study, the following tasks were conducted.

(i) Static testing of deck panels under the factored load of 115.7 kN (26 kips) (89 kN (20 kips) + 30% for impact) for the AASHTO standard HS25 truck wheel load.

(ii) Cyclic loading of the deck panels under the service load of 53.4 kN (12 kips) (or 58.4 kN/m (4 kips/ft) of width) and factored load of 115.7 kN (26 kips) for the AASHTO standard HS25 truck wheel load.

(iii) Loading to failure.

(iv) Comparison of deflection of the deck panels with the deflection criteria specified by ODOT, and the reinforced concrete conventional deck panels.

(v) Comparison of strain and ultimate load of the deck panels with the flexure criteria specified by ODOT.

(vi) Comparison of shear capacity of the deck panels with the shear criteria specified by ODOT.

(vii) Calculation of flexural rigidities (EI) and shear rigidities (GA_w).

II.1.4 Deck Panels

The reinforced concrete (RC) conventional deck panels or baseline panels are cast of concrete reinforced with steel rebars. The single span deck panels are designated as RC1, RC*, RC2 and RC3, and the double span deck panel is designated as RC4 (Table II.1.1).

The Pultruded FRP Deck - Creative Pultrusions (CP) panels consist of pultruded components that are placed transversely to the traffic direction and supported by longitudinal beams. The CP-FRP deck panels are made of double trapezoid and hexagonal pultruded components (Figure II.1.1). The pultruded components are bonded and interlocked to form a deck panel. The single span deck panels are designated as CP1, CP2 and CP3, and the double span deck panel is designated as CP4 (Table II.1.1).

The Hybrid FRP - Concrete Deck - Composite Deck Solutions (CDS) panels are fabricated of concrete reinforced with Glass Fiber Reinforced Polymer (GFRP) rebars, and cast over pultruded GFRP tubular sections (Figure II.1.1). The single span deck panels are designated as CDS1, CDS2 and CDS3, and the double span deck panel is designated as CDS4 (Table II.1.1).

The Scrimp FRP Deck - Hardcore Composites fiberglass panels are fabricated using the "cell core" technology in conjunction with SCRIMP (Seeman Composite Resin Infusion Molding Process). The cell core is a foam or plastic form that is wrapped with fiberglass fabric to create an internal lattice structure for the composite deck. The composite deck is comprised of multiple wrapped cells with upper and lower fiberglass fabric skin faces (Figure II.1.1). The multiple wrapped cells form the longitudinal and transverse stiffening webs to create a deck with bi-directional stiffness. The single span deck panels are designated as HC1, HC2 and HC3, and the double span deck panel is designated as HC4 (Table II.1.1).

The Contact Molding Hand Lay-up FRP deck - Infrastructure Composites International (ICI) fiberglass panels consist of the core craft corrugated core sandwich system. The basic system is a single-tier sandwich panel with a standard core configuration (Figure II.1.1). The flats of the core will be in the direction normal to traffic flow. The single span deck panels are designated as ICI1, ICI2 and ICI3, and the double span deck panel is designated as ICI4 (Table II.1.1).

The length, effective length (distance between centerlines of supports), width and thickness of all single span and double span deck panels are presented in Table II.1.1.

II.1.5 Performance Criteria

The Ohio Department of Transportation (ODOT) specified the deflection, flexure and shear criteria.

II.1.5.1 Deflection Criteria

The deflection limits for the FRP Decks are based on deflection calculations/limits for conventional reinforced concrete decks. These limits are presented in Table II.1.2.

II.1.5.2 Flexure Criteria

(i) Maximum allowable strain is limited to 20% of the ultimate strain under service load of LL+IM+DL, in which LL = Live Load, IM = Impact load and DL = Dead Load.

(ii) Maximum allowable dead load strain is limited to 10% of the ultimate strain. This includes 2.87×10^{-3} MPa (60 psf) of future wearing surface.

(iii) Maximum factored load of 1.3[1.67(LL+IM)+DL] < 50% of ultimate load capacity for all FRP decks.

(iv) Maximum factored load of 1.3[1.67(LL+IM)+DL] < 100% of ultimate load capacity for hybrid FRP/concrete decks.

II.1.5.3 Shear Criteria

(i) Shear capacity shall be equal to or greater than that of a reinforced concrete (RC) conventional deck. For this deck the shear capacity is 145.9 kN/m (10,000 lb/ft) of width.

(ii) The maximum allowable shear for a factored load of 1.3[1.67(LL+IM)+DL] shall be <45% of the ultimate shear load capacity for the "all" FRP decks (i.e. non hybrid FRP/concrete decks).

(iii) The allowable shear for a factored load of 1.3[1.67(LL+IM)+DL] shall be <100% of the ultimate shear capacity for the hybrid FRP/concrete decks.

II.1.6 Experimental Results

II.1.6.1 Comparison of Experimental Results with Performance Criteria

The load vs strain curves and load vs deflection curves for loading to failure are presented at the end of chapters II.3 to II.7.

The measured deflection at applied service load of 58.4 kN/m (4,000 lb/ft) of width, baseline deflection, and allowable deflections are presented in Table II.1.3. The measured strain

under service loads of (LL+IM+DL) and DL, and allowable strain are also presented in Table II.1.3.

The ultimate load, required load, maximum deflection at ultimate load, and mode of failure are presented in Table II.1.4.

The following observations are made based upon the test results (Tables II.1.3 and II.1.4) and without any account for the "knock down" factors.

(i) None of the panels supplied by the FRP manufacturers failed in shear, and all panels satisfy the shear criteria.

(ii) The single and double span Pultruded FRP Deck - Creative Pultrusions (CP) panels satisfy the deflection criteria and flexure criteria.

(iii) The single and double span Hybrid FRP - Concrete Deck - Composite Deck Solutions (CDS) panels satisfy the deflection criteria and flexure criteria.

(iv) The single span Scrimp FRP Deck - Hardcore Composites (HC) panels satisfy the flexure-strain criteria but do not satisfy the deflection criteria (Measured deflection/allowable deflection = 1.029 to 1.059, Table II.1.3). The double span deck panel satisfies the deflection criteria and flexure criteria.

(v) The single span Contact Molding Hand Lay-up FRP deck - Infrastructure Composites International (ICI) panels satisfy the deflection criteria and flexure criteria. The double span deck panel satisfies the deflection criteria and strain limits specified in the flexure criteria but does not satisfy the required ultimate load specified in the flexure criteria (Measured ultimate load = 483,473 N (108,689 lb), required ultimate load = 528,431 N (118,796 lb), Table II.1.4).

The load at failure and maximum deflection at failure are also compared with their respective baseline failure load and maximum deflection in Table II.1.4.

II.1.6.2 Flexural and Shear Rigidities

The flexural and shear rigidities (EI and GA_w respectively) for the deck panels are determined using different techniques:

(i) Linear regression analysis of the load vs deflection relationship for the baseline curve using the first-order shear deformation beam equations.

(ii) First order beam equation without considering the shear deformation on the load vs deflection relationship for the baseline curve.

(iii) Moment-curvature relationship of the load vs strain relationship for the baseline curve.

The calculated values of flexural and shear rigidities for the single and double span deck panels are presented in Tables II.1.5 and II.1.6.

II.1.7 Conclusions and Recommendations for the First Salem Bridge

The following conclusions are drawn based upon the static testing, and without any account for the " knock down" factors. The double span deck panels are assumed to be representative of the panels placed on the First Salem bridge.

(i) The double span deck panels provided by Creative Pultrusions (CP), Composite Deck Solutions (CDS) and Hardcore Composites (HP) satisfy the deflection criteria and flexure criteria.

(ii) The double span deck panel provided by Infrastructure Composites International (ICI) satisfies the deflection criteria and strain limits specified in flexure criteria but does not satisfy the required ultimate load specified in the flexure criteria (Measured ultimate load = 483,473 N (108,689 lb), required ultimate load = 528,431 N (118,796 lb), Table II.1.4)

The following flexural rigidities (EI) and shear rigidities (GA_w) are recommended for use in modeling the First Salem Bridge.

Creative Pultrusions panels (CP): $EI = 2.428 \times 10^7$ N-m^2 (8.461×10^9 lb-in^2) and $GA_w = 1.120 \times 10^7$ N (2.518×10^6 lb.)

Composite Deck Solutions panels (CDS): $EI = 1.588 \times 10^7$ N-m^2 (5.532×10^9 lb-in^2) and $GA_w = 3.358 \times 10^7$ N (7.550×10^6 lb.)

Hardcore Composites panels (HC): $EI = 1.157 \times 10^7$ N-m^2 (4.031×10^9 lb-in^2) and $GA_w = 1.394 \times 10^7$ N (3.134×10^6 lb.)

Infrastructure Composites International panels (ICI): $EI = 1.665 \times 10^7$ N-m^2 (5.802×10^9 lb-in^2) and $GA_w = 1.809 \times 10^7$ N (4.066×10^6 lb.)

These rigidities are obtained by calculating the average values of the rigidities in span 1 and span 2 for the double span panels. They are based on first-order shear deformation beam equations, and are derived by conducting a linear regression analysis on the load vs deflection relationship for the baseline curve.

Table II.1.1 Bridge Deck Panels

Details	Reinforced Concrete Panels					Creative Pultrusions Panels				Composite Deck Solutions Panels				Hardcore Composites Panels				Infrastructure Composites International Panels			
	RC1	RC*[a]	RC2	RC3	RC4[b]	CP1	CP2	CP3	CP4[b]	CDS1	CDS2	CDS3	CDS4[b]	HC1	HC2	HC3	HC4[b]	IC11	IC12	IC13	IC14[b]
	(1)	(2)	(3)	(4)	(5)	(6)	(7)	(8)	(9)	(10)	(11)	(12)	(13)	(14)	(15)	(16)	(17)	(18)	(19)	(20)	(21)
Length (m)	2.74	3.05	3.35	3.96	5.79[c]	2.74	3.35	3.96	5.79[c]	2.74	3.35	3.96	6.10[c]	2.74	3.35	3.96	6.10[c]	2.74	3.35	3.96	6.10[c]
Effective[d] Length (m)	2.44	2.74	3.05	3.66	2.74[e]	2.44	3.05	3.66	2.74[e]	2.44	3.05	3.66	2.74[e]	2.44	3.05	3.66	2.74[e]	2.44	3.05	3.66	2.74[e]
Width (m)	0.91	0.91	0.91	0.91	1.07	0.91	0.91	0.91	0.91	0.91	0.91	0.91	0.91	0.91	0.91	0.91	0.91	0.91	0.91	0.91	0.91
Thickness[f] (m)	0.19	0.19	0.20	0.22	0.19	0.20	0.20	0.20	0.20	0.20	0.24	0.25	0.20	0.22	0.23	0.24	0.20	0.21	0.24	0.25	0.20
Remarks	Each specimen possessed some minor deformations (waviness) over the top and bottom surfaces.					Each specimen possessed some minor deformations (waviness) over the top and bottom surfaces.				Specimens CDS1, CDS2, and CDS3 possessed some minor deformations (waviness) over the top and bottom surfaces. A crack of width = 0.076 mm was observed at midspan of the CDS4 panel when it was unloaded from the delivery truck.				Each specimen possessed some minor deformations (waviness) over the top and bottom surfaces.				Each specimen possessed some minor deformations (waviness) over the top and bottom surfaces.			

[a] Specimen RC* is not used as a baseline specimen since no FRP composite panels of the same dimensions are provided or tested.
[b] Double span panel.
[c] Total length of the double span panel.
[d] Distance between centerline of supports.
[e] Effective length in each span of the double span panel.
[f] Average thickness
Note: The effective span is 2.667 m (105 in) for the First Salem Bridge over the Great Miami River in Montgomery County, Ohio.

Table II.1.2 Deflection Limits for the Deck Panels Specified by Ohio Department of Transportation

Span [a] (m)	Clear Span used for Design (m)	Deck Thickness [b] (m)	Applied Service Load [c] (kN/m)	Single Span Deflection [d] (mm)	Continuous Span Deflection (mm)
2.44	2.29	2.44	58.38	3.175	2.540
2.74	2.59	2.44	58.38	4.572	2.540
3.05	2.90	2.74	58.38	4.318	2.794
3.66	3.51	2.90	58.38	6.096	4.318

[a] Distance between center to center of beams.
[b] Manufacturers are permitted to increase the depth of their decks within + 12.7 mm (½") of the thickness shown for the 3.05 m (10'0'') and 3.66 m (12'0") span lengths.
[c] Load is to be applied over a 0.229m x 0.559m (9" x 22") contact area.
[d] Simple span values are to be used during testing to evaluate the FRP decks relative to an RC deck.

Table II.1.3 Comparison of Deflections and Strains for the FRP Deck Panels with Deflection Criteria and Flexure Criteria

Specimen Identification [a]	Centerline Deflection @ Applied Service Load of 58.38 kN/m of Width (mm)			Maximum Strain @ (LL+IM+DL)		Maximum Strain @ DL	
	Measured[b]	Baseline[c]	Allowable[d]	Measured[e]	Allowable[f]	Measured[e]	Allowable[f]
(1)	(2)	(3)	(4)	(5)	(6)	(7)	(8)
CP1 (2.44 m)	2.286	3.607	3.175	0.000808	0.003200	0.000080	0.001600
CP2 (3.05 m)	4.064	5.029	4.318	0.000969	0.003200	0.000071	0.001600
CP3 (3.66 m)	6.071	6.731	6.096	0.001399	0.003200	0.000125	0.001600
CP4 Span1[g] (2.74 m)	2.184	1.372	4.572	0.000660[h]	0.003200	0.000092[h]	0.001600
CP4 Span2[g] (2.74 m)	2.616	1.499	4.752				
CDS1 (2.44 m)	0.965	3.607	3.175	0.000659	0.003400	0.000042	0.001700
CDS2 (3.05 m)	1.321	5.029	4.318	0.000727	0.003400	0.000117	0.001700
CDS3 (3.66 m)	2.540	6.731	6.096	0.001027	0.003400	0.000202	0.001700
CDS4 Span1[g] (2.74 m)	1.321	1.372	4.572	0.000827[h]	0.003400	0.000193[h]	0.001700
CDS4 Span2[g] (2.74 m)	1.346	1.499	4.572				
HC1 (2.44 m)	3.353	3.607	3.175	0.001230	0.004100	0.000091	0.002050
HC2 (3.05 m)	4.572	5.029	4.318	0.001188	0.004100	0.000102	0.002050
HC3 (3.66 m)	6.274	6.731	6.096	0.001400	0.004100	0.000156	0.002050
HC4 Span1[g] (2.74 m)	2.515	1.372	4.572	0.001205[h]	0.004100	0.000176[h]	0.002050
HC4 Span2[g] (2.74 m)	2.565	1.499	4.572				
ICI1 (2.44 m)	2.311	3.607	3.175	0.000974	0.004200	0.000069	0.002100
ICI2 (3.05 m)	3.277	5.029	4.318	0.001011	0.004200	0.000094	0.002100
ICI3 (3.66 m)	4.394	6.731	6.096	0.001118	0.004200	0.000118	0.002100
ICI4 Span1[g] (2.74 m)	1.854[g]	1.372	4.572	0.000932[h]	0.004200	0.000130[h]	0.002100
ICI4 Span2[g] (2.74 m)	1.905[g]	1.499	4.572				

[a] Effective span is shown in parentheses.
[b] The centerline deflections are derived by interpolation from the baseline deflection curves.
[c] The baseline deflection is obtained from tests conducted on the baseline panels (Table II.3.2).
[d] The allowable deflections are provided by the Ohio Department of Transportation.
[e] The centerline strains are derived by interpolation from the baseline strain curves*.
[f] The allowable strain = 20% of maximum strain of the FRP coupon test (Refer Section I, Tables I.8.1 and I.8.2)
[g] Span 1 and span 2 for the two span panel are shown in Figure II.2.5.
[h] The maximum strain is measured along the middle support in the double span panel *.
* The strains are measured at 285.8 mm (11.25 in) on both sides from the centerline of the panels (Figures II.2.4 and II.2.5)
Note: The effective span for the First Salem Bridge is 2.667 m (105 in).

Table II.1.4 Ultimate Load, Maximum Deflection , and Mode of Failure for the Deck Panels

Specimen Identification[a]	Ultimate Load (N)			Maximum Deflection at Ultimate Load[c] (mm)		Mode of Failure
	Measured	Baseline	Required[b]	Measured	Baseline	
(1)	(2)	(3)	(4)	(5)	(6)	(7)
CP1 (2.44 m)	659,436	189,859	524,561	39.116	29.794	Punching
CP2 (3.05 m)	654,000	197,781	530,166	61.163	33.350	Punching
CP3 (3.66 m)	646,731	181,652	535,762	98.603	41.605	Punching
CP4 Span1[d] (2.74 m)	659,903	243,380	527,363	35.408	29.185	Punching
CP4 Span2[d] (2.74 m)	659,903	243,380	527,363	35.306	21.920	
CDS1 (2.44 m)	402,146	189,859	273,290	19.609	29.794	Flexure-Shear
CDS2 (3.05 m)	435,361	197,781	282,093	22.784	33.350	Flexure-Shear
CDS3 (3.66 m)	348,420	181,652	289,597	38.989	41.605	Flexure-Shear
CDS4 Span1[d] (2.74 m)	374,829	243,380	276,066	25.222	29.185	Flexure-Shear
CDS4 Span2[d] (2.74 m)	374,829	243,380	276,066	25.400	21.920	
HC1 (2.44 m)	885,717	189,859	524,552	65.964	29.794	Web buckling and delamination
HC2 (3.05 m)	819,394	197,781	530,575	74.143	33.350	Web buckling and delamination
HC3 (3.66 m)	762,074	181,652	536,758	98.984	41.605	Web buckling and delamination
HC4 Span1[d] (2.74 m)	946,195	243,380	526,972	50.190	29.185	Web buckling and delamination
HC4 Span2[d] (2.74 m)	946,195	243,380	526,972	51.740	21.920	
ICI1 (2.44 m)	593,540	189,859	525,762	26.645	29.794	Delamination
ICI2 (3.05 m)	719,313	197,781	532,915	49.276	33.350	Delamination
ICI3 (3.66 m)	833,592	181,652	539,436	76.352	41.605	Web-buckling and delamination
ICI4 Span1[d] (2.74 m)	483,473	243,380	528,431	17.602	29.185	Delamination
ICI4 Span2[d] (2.74 m)	483,473	243,380	528,431	17.501	21.920	

[a] Effective span is shown in parentheses.

[b] Required ultimate load = 1.3[1.67(LL+IM)+DL)] for CDS panels and = 2*1.3[1.67(LL+IM)+DL)] for CP, HC, and ICI panels.

[c] The measured and baseline maximum deflections do not occur under the same load. Refer to columns (2) and (3) of this table for the magnitude of load at failure.

[d] Span 1 and span 2 for the two span panel are shown in Figure II.2.5.

Note: The effective span for the First Salem Bridge is 2.667 m (105 in).

Table II.1.5 Flexural and Shear Rigidities for Single Span FRP Deck Panels

Specimen	Effective Span = 2.44 m				Effective Span = 3.05 m				Effective Span = 3.66 m			
	Flexural Rigidity			Shear Rigidity	Flexural Rigidity			Shear Rigidity	Flexural Rigidity			Shear Rigidity
	EI^{1} ($N\text{-}m^2$)	EI^{2} ($N\text{-}m^2$)	EI^{3} ($N\text{-}m^2$)	GA_w (N)	EI^{1} ($N\text{-}m^2$)	EI^{2} ($N\text{-}m^2$)	EI^{3} ($N\text{-}m^2$)	GA_w (N)	EI^{1} ($N\text{-}m^2$)	EI^{2} ($N\text{-}m^2$)	EI^{3} ($N\text{-}m^2$)	GA_w (N)
CP	7.612×10^6	9.368×10^6	6.590×10^6	9.893×10^7	1.004×10^7	9.884×10^6	7.287×10^6	3.438×10^7	2.324×10^7	9.055×10^6	8.047×10^6	1.103×10^7
CDS	1.615×10^7	1.452×10^7	1.619×10^7	-[4]	2.664×10^7	1.996×10^7	2.388×10^7	2.970×10^8	2.796×10^7	1.395×10^7	2.134×10^7	8.078×10^7
HC	5.614×10^6	6.288×10^6	4.784×10^6	6.530×10^7	8.481×10^6	9.279×10^6	6.851×10^6	4.604×10^7	9.864×10^6	1.033×10^7	8.687×10^6	6.526×10^7
ICI	9.405×10^6	9.658×10^6	6.963×10^6	5.409×10^7	1.068×10^7	1.190×10^7	9.612×10^6	1.237×10^8	1.430×10^7	1.344×10^7	1.242×10^7	8.456×10^7

[1] Flexural rigidity by considering shear deformation.
[2] Flexural rigidity from moment-curvature relationships.
[3] Flexural rigidity without considering shear deformation.
[4] The GA_w value derived from substituting the experimental data into analytical equations is negative.
Note: The effective span is 2.667 m (105 in) for the First Salem Bridge over the Great Miami River in Montgomery County, Ohio.

Table II.1.6 Flexural and Shear Rigidities for Double Span FRP Deck Panels

Specimen	Span 1 = 2.74 m				Span 2 = 2.74 m			
	Flexural Rigidity			Shear Rigidity	Flexural Rigidity			Shear Rigidity
	EI [1] (N-m^2)	EI [2] (N-m^2)	EI [3] (N-m^2)	GA_w (N)	EI [1] (N-m^2)	EI [2] (N-m^2)	EI [3] (N-m^2)	GA_w (N)
CP	3.046×10^7	1.157×10^7	4.213×10^6	1.114×10^7	1.810×10^7	1.201×10^7	3.883×10^6	1.126×10^7
CDS	1.644×10^7	8.452×10^6	7.603×10^6	3.222×10^7	1.531×10^7	9.224×10^7	7.663×10^6	3.494×10^7
HC	1.213×10^7	6.021×10^6	3.984×10^6	1.351×10^7	1.101×10^7	7.052×10^7	4.009×10^6	1.437×10^7
ICI	1.586×10^7	9.307×10^6	5.444×10^6	1.888×10^7	1.744×10^7	8.934×10^6	5.289×10^6	1.729 x 10

[1] Flexural rigidity by considering shear deformation.
[2] Flexural rigidity from moment-curvature relationships.
[3] Flexural rigidity without considering shear deformation.
Note: The effective span is 2.667 m (105 in) for the First Salem Bridge over the Great Miami River in Montgomery County, Ohio.

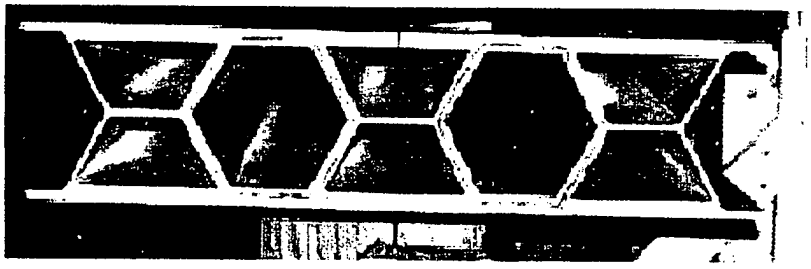

(a) Creative Pultrusions (CP)

(b) Composite Deck Solutions (CDS)

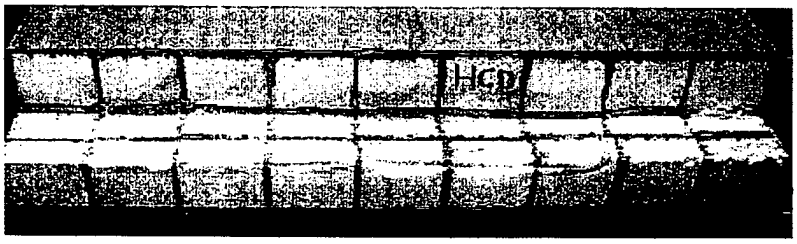

(c) Hardcore Composites (HC)

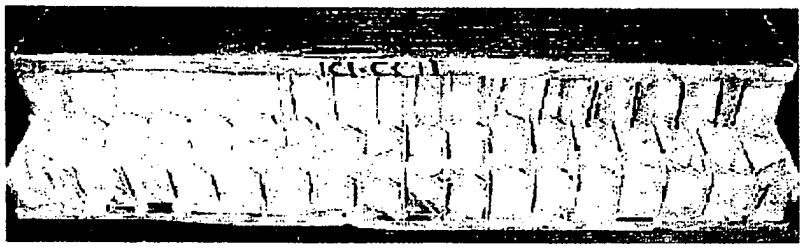

(d) Infrastructure Composites International (ICI)

Figure II.1.1 Cross Sections of the FRP Deck

II.2 EXPE NTAL SETUP AND PROCEDU

II.2.1 Introduction

Tests are conducted up to failure on sixteen FRP deck panels supplied by the following manufacturers: Creative Pultrusions (CP), Composite Deck Solutions (CDS), Hardcore Composites (HP) and Infrastructure Composites International (ICI), and five reinforced concrete (RC) conventional panels (Table II.1.1). The test panels are instrumented with Linear Variable Deflection Transducers (LVDT) and strain gages to measure the out-of-plane deflections and strains and are loaded as per the loading pattern given in chapter II.2.3. This chapter briefly describes the test setup, loading pattern and the instrumentation on the test panels. The equations used to calculate the flexural and shear rigidities (EI and GA_w respectively) are also presented.

II.2.2 Test Setup

A test setup for a capacity of 3558.6 kN (800,000 lb) has been designed and fabricated (Figure II.2.1) to test the deck panels. The test setup is capable of testing single and double span panels up to a maximum length of 13.7 m (45 ft) and breadth of 1.5 m (5 ft), and is made up of independent loading frames. Each independent loading frame consists of built-up tubular sections (A, B, C, D and E) and threaded bars as shown in Figure II.2.1. The threaded bars are anchored to the test floor. The span length for testing the deck panels can be varied by changing the positions of the threaded bars along the holes in the test floor. The height of the loading frames is also adjustable.

II.2.3 Loading Pattern

The specimens are initially loaded gradually up to 8.90 kN and then the load is released. This operation is repeated twice in order to ensure the loading edges (rubber pad) remained in proper contact with the specimen. Then the specimens are loaded as per the following order.

Step 1. Load from zero to 115.7 kN (26 kips) and release the load back to zero in order to establish a baseline curve. The 115.7 kN load represents the factored load for the AASHTO standard HS25 truck wheel load (89.0 kN + 30% for impact).

Step 2. Load from zero to 53.4 kN (12 kips) and back to zero, and repeat the cycle five times. The 53.4 kN load represents the service load for the AASHTO HS25 truck (58.38 kN/m (4 kips/ft) width).

Step 3. Load from zero to 115.7 kN and back to zero, and repeat the cycle five times. Note: Following step 3 the data is reduced and checked prior to executing step 4.

Step 4. Load from zero to failure.

The load is applied using hydraulic jacks of 1779.3 kN (400,000 lb) capacity. The load is transmitted through a rectangular plate of size 0.559m x 0.229m x 0.051m (22 in x 9 in x 2

in) to the deck panel in order to represent the AASHTO HS25 standard truck wheel load. Hydraulic jacks having 183.9 mm (7.24 in) ram and 149.9 mm (5.9 in) stroke are used for testing. The top of the ram is provided with a spherical cap so that if any tilting of the plate occurs while loading, the spherical cap adjusts in such a way that only a perpendicular load is applied to the deck panel. Load cell measures the load applied by the jack. A rubber pad having the same dimensions as the steel plate and a thickness of 12.7 mm (0.5 in) is placed between the deck panel and the steel plate in order to ... the abrasion between the steel plate and the deck panel. The details of the test setup for single and double span panels, along with the supports, are shown in Figures II.2.2 and II.2.3.

II.2.4 Instrumentation

Electrical resistance disposable strain gages 6.35 mm (0.25 in) long, manufactured by Vishay, Measurements Group, are fixed across the mid section on the FRP side of CP, CDS, HC, and ICI panels and reusable strain gages of 76.2 mm (3 in) long, manufactured by Bridge Diagnostics, on the concrete side of CDS and RC deck panels in order to measure the tensile and compressive strains. Out-of-plane deflections at three points along the mid-section and at quarter span from both supports are measured by using Linear Variable Deflection Transducers (LVDT) manufactured by Sensotec, Ohio. The position of strain gages on single and double span panels are shown in Figures II.2.4 and II.2.5 and the position of LVDT's are shown in Figures II.2.6 and II.2.7. The strain gages, linear variable deflection transducers and load cell are connected to a data acquisition system and the data is recorded and stored in a computer at an interval of 1 sec. during loading.

II.2.5 Flexural and Shear Rigidities

Using different techniques the flexural and shear rigidities (EI and GA_w respectively) are calculated.

(i) By conducting a linear regression analysis on the load vs deflection relationship for the baseline curve (Load step 1). The first-order shear deformation beam equations II.2.1 and II.2.2 for single span panels and equations II.2.3 and II.2.4 for double span panels are used, and are shown below:

Single Span

$$\ddot{a}_{1/2} = \frac{PL^3}{48EI} + \frac{PL}{4GA_w} \qquad \text{(II.2.1)}$$

$$\ddot{a}_{1/4} = \frac{11PL^3}{768EI} + \frac{PL}{8GA_w} \qquad \text{(II.2.2)}$$

Double Span

$$\ddot{a}_{1/2} = \frac{7PL^3}{768EI} + \frac{5PL}{32GA_w} \qquad \text{(II.2.3)}$$

$$\ddot{a}_{1/4} = \frac{43PL^3}{6144EI} + \frac{5PL}{64GA_w} \qquad \text{(II.2.4)}$$

in which

$\delta_{1/2}$ - deflection at a distance of L/2 from support A (Figures II.2.2 and II.2.3)
$\delta_{1/4}$ - deflection at a distance of L/4 from support A (Figures II.2.2 and II.2.3)
P - patch load distributed over a region of 0.229m x 0.559m (9 in x 22 in) at the center of the panel (Figures II.2.2 and II.2.3)
L - effective span length

(ii) The first order beam equations II.2.5 and II.2.6 for single and double span panels without considering the shear deformations are used to calculate the flexural rigidity (EI) from the load vs deflection relationship for the baseline curve (Load step 1).

$$\delta_{1/2} = \frac{PL^3}{48EI} \qquad \text{Single span} \qquad \text{(II.2.5)}$$

$$\delta_{1/2} = \frac{7PL^3}{768EI} \qquad \text{Double span} \qquad \text{(II.2.6)}$$

(iii) The flexural rigidity (EI) is also calculated using the load vs strain relationship for the baseline curve (Load step 1). The moment-curvature relationship (Eqn. II.2.7) is used.

$$\frac{M}{I} = \frac{\sigma}{y} \qquad \text{(II.2.7)}$$

M - bending moment
I - moment of Inertia
σ - bending stress
y - distance of outer most fiber from neutral axis

The neutral axis is located by using the strains on the top and bottom faces of the panel.

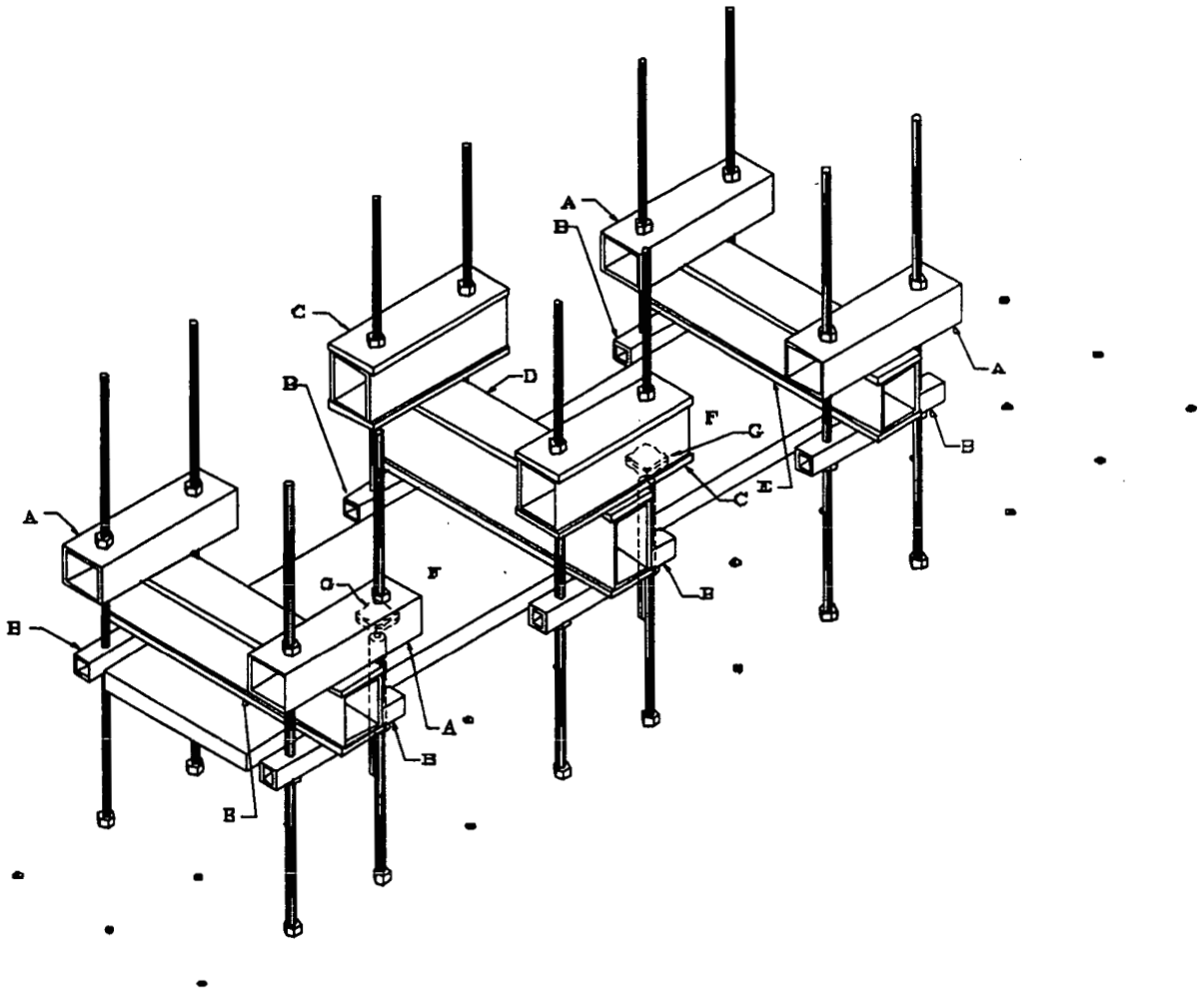

Figure II.2.1 Loading Frame Showing the Tubular Sections A, B, C, D and E, Deck Panel F, and the Jacks G.

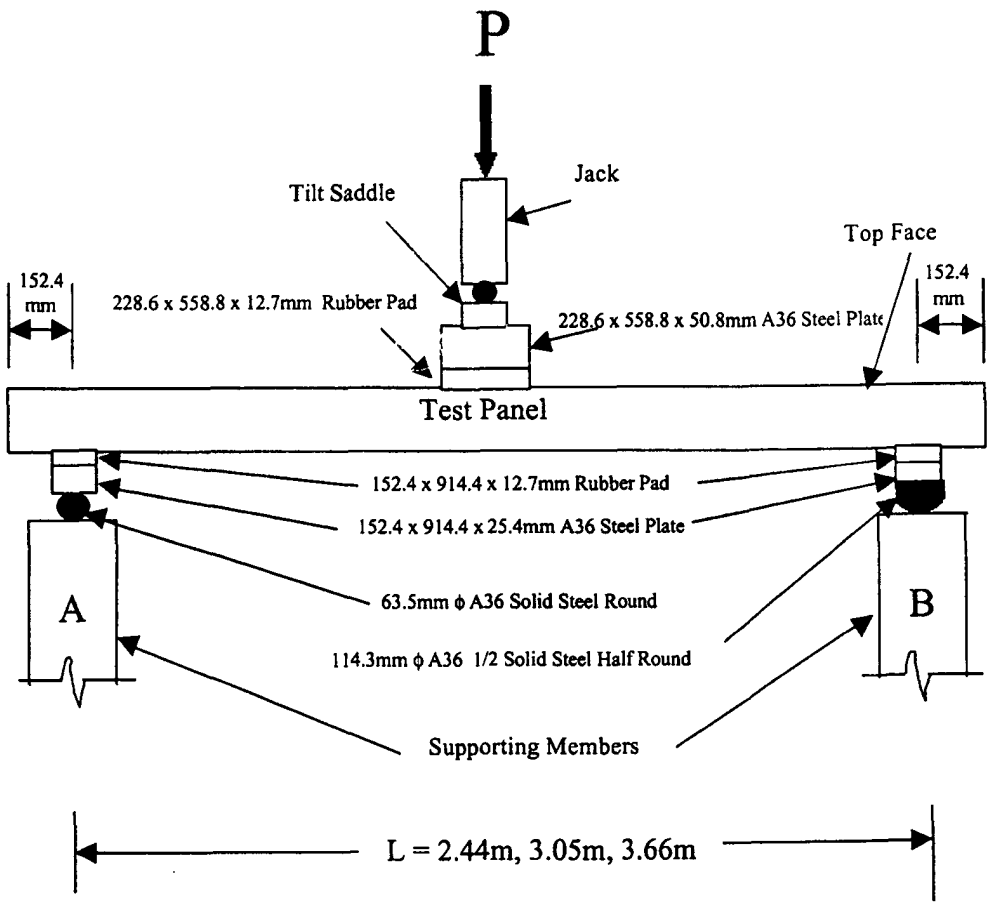

Figure II.2.2 Test Setup for Single Span Deck Panels

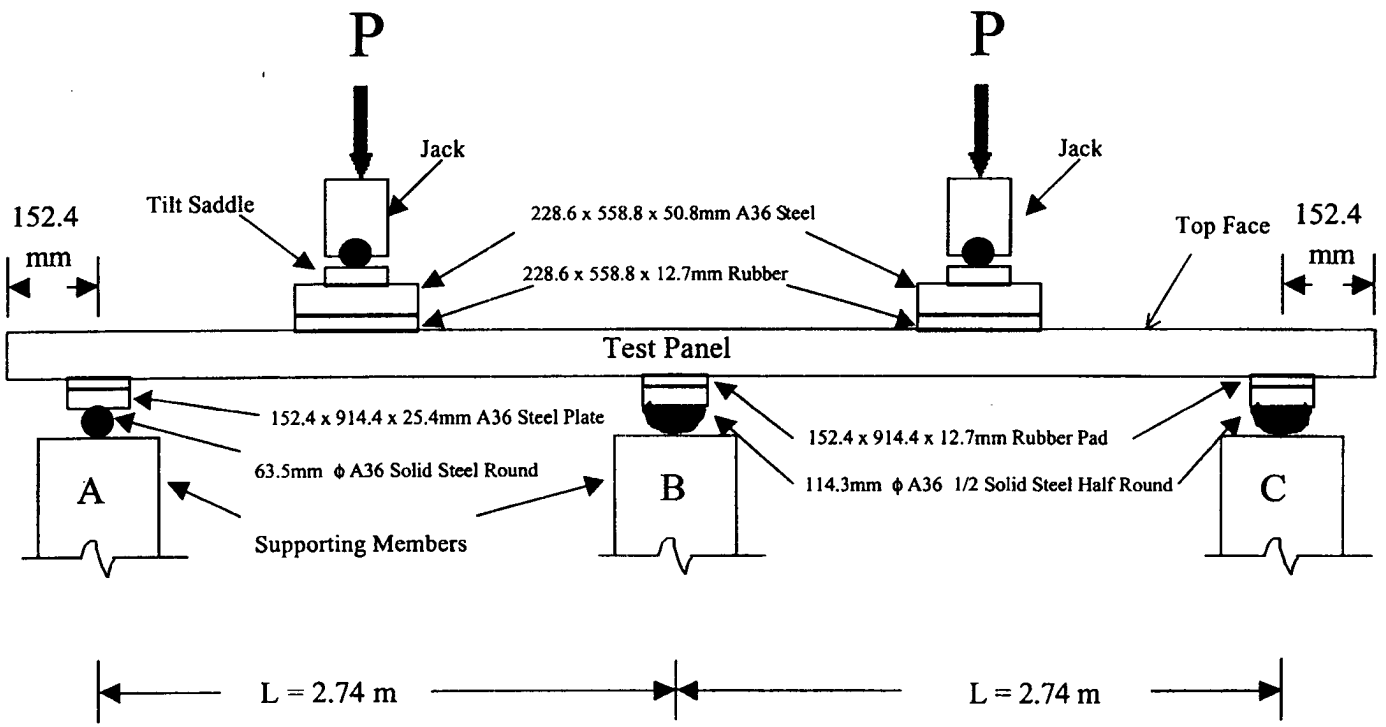

Figure II.2.3 Test Setup for Double Span Deck Panels

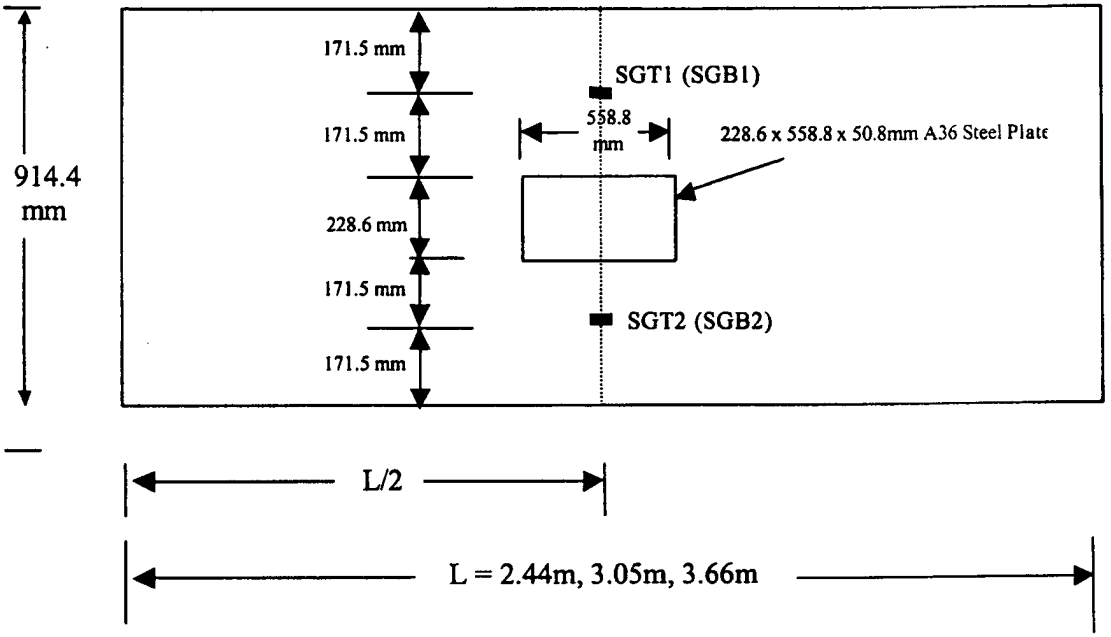

Note: Strain gages SGB1 and SGB2 are on the bottom side of the panel

Figure II.2.4 Location of Strain Gages on Single Span Deck Panels

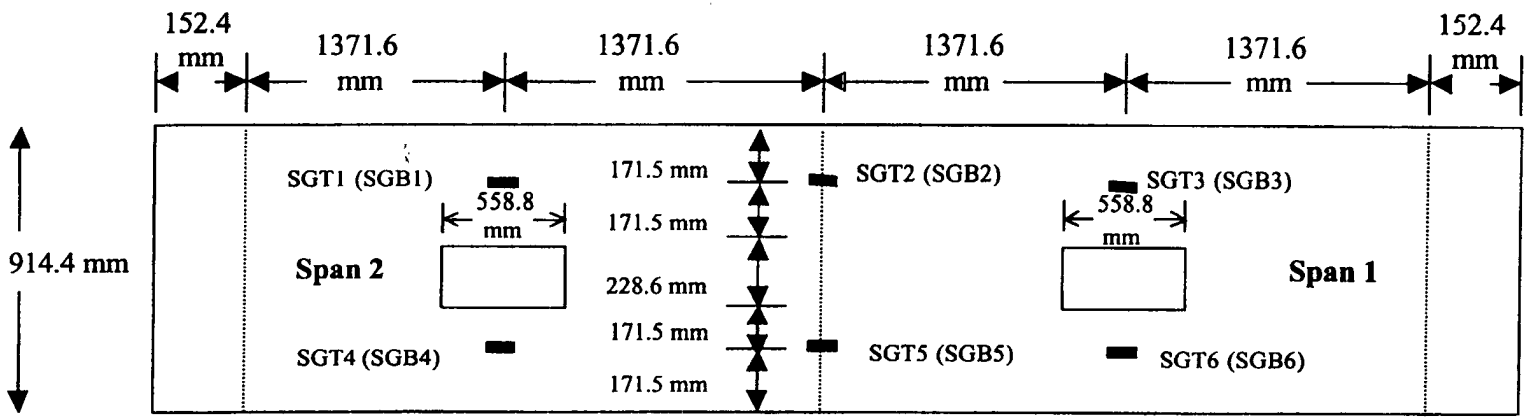

Note: Strain gages SGB1 to SGB6 are on the bottom side of the panel

Figure II.2.5 Location of Strain Gages on Double Span Deck Panels

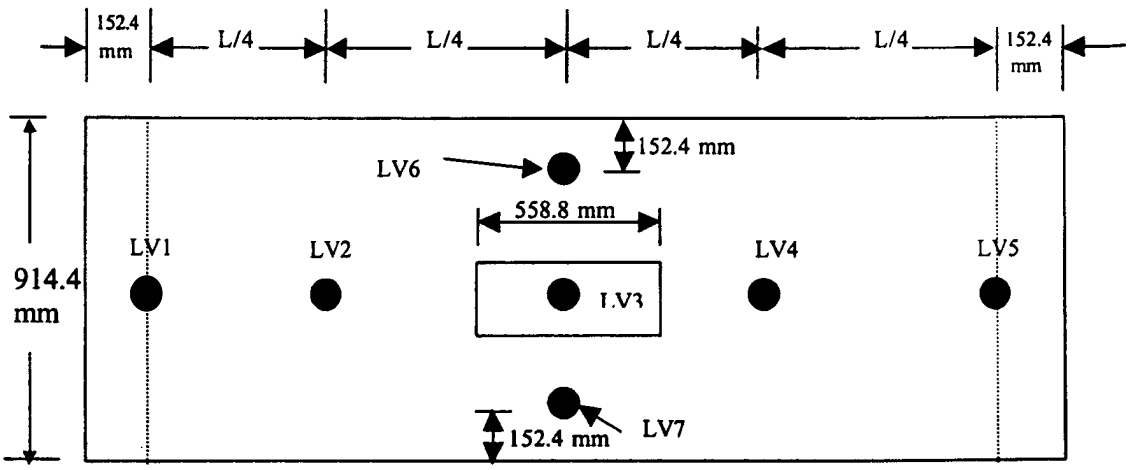

Note: Measurements from LV1 and LV5 are used to interpolate the readings from other LVDTs

Figure II.2.6 Location of LVDTs on Single Span Deck Panels

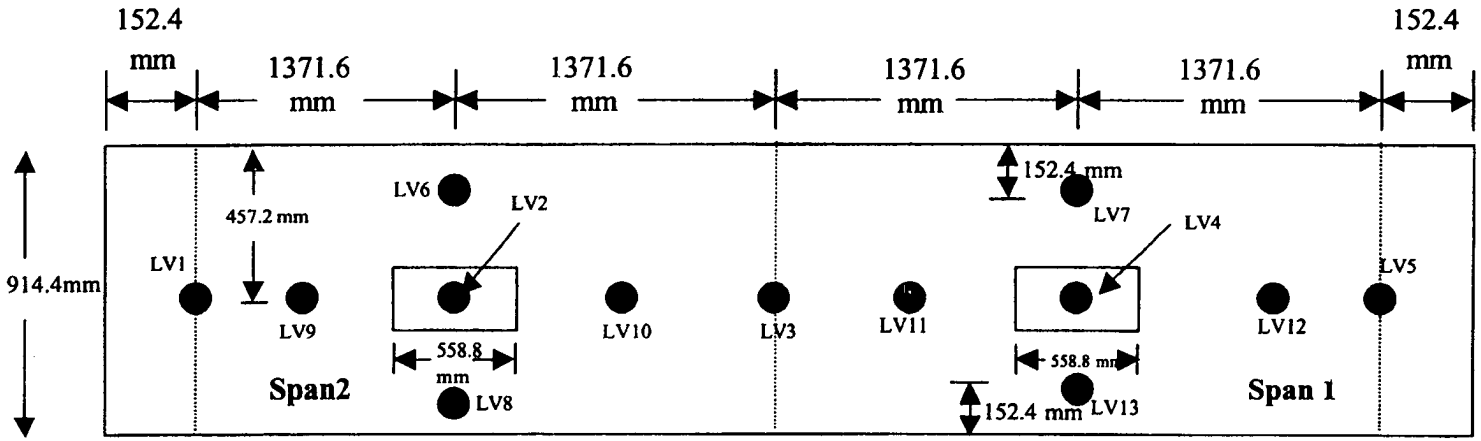

Note: Measurements from LV1, LV3 and LV5 are used to interpolate the readings from other LVDTs

Figure II.2.7 Location of LVDTs on Double Span Deck Panels

II.3 INFORCED CONC TE CONVENTIONAL DECK

II.3.1 Summary

The reinforced concrete (RC) conventional deck double span panel satisfies the deflection criteria for the First-Salem Bridge over the Great Miami River in Montgomery County, Ohio.

II.3.2 Introduction

The reinforced concrete (RC) conventional deck panels are cast of concrete reinforced with steel rebars (Figure II.3.1). The length, effective length (distance between centerlines of supports), width and thickness of single span and double span deck panels are presented in Table II.3.1. The single span deck panels are designated as RC1, RC*, RC2 and RC3, and the double span deck panel is designated as RC4 (Table II.3.1). The single and double span deck panels are loaded as per the steps outlined in section II.2.3.

II.3.3 Specimen RC1 – 2.44 m (8 ft) Panel

The load vs deflection curves for loading step 4 are presented for the specimen RC1 in Figure II.3.2. The maximum centerline deflection at applied service load of 58.38 kN/m (4,000 lb/ft) of width, the maximum strain on steel rebars at service load (LL+IM+DL) and maximum strain at dead load (DL) are presented in Table II.3.2. The allowable deflections as per the deflection criteria specified by ODOT are also presented in Table II.3.2.

The load at failure, maximum deflection at failure and mode of failure are presented in Table II.3.3.

The load vs deflection plots show that the stiffness of the deck remains constant during the cyclic loading. For the failure load in step 4, the load vs deflection curve (Figure II.3.2) indicates that the specimen fails at 189.9 kN (42,682 lb). While loading the specimen, flexural cracks are formed initially in the concrete tension zone, and then throughout the length of the panel. As the load is further increased, the flexural crack width and depth increases, and the specimen collapsed in flexure (Figure II.3.3). The specimen starts load shedding as soon as it reaches its collapse load and failure is observed to be sudden. Crushing of concrete at the loading point is observed after failure.

II.3.4 Specimen RC2 - 2.74 m (9 ft) Panel

The load vs deflection curves for loading step 4 are presented for specimen RC2 in Figure II.3.4. The maximum centerline deflection at applied service load of 58.38 kN/m (4,000 lb/ft) of width, the maximum strain on steel rebars at service load (LL+IM+DL) and maximum strain at dead load (DL) are presented in Table II.3.2. The allowable deflections as per the deflection criteria specified by ODOT are also presented in Table II.3.2.

The load at failure, maximum deflection at failure and mode of failure are presented in Table II.3.3.

The load vs deflection plots show that the stiffness of the deck remains constant during the cyclic loading. For the failure load in step 4, the load vs deflection curve (Figure II.3.4) indicates that the specimen fails at 197.8 kN (44,463 lb). While loading the specimen, flexural cracks are formed initially in the concrete tension zone, and then throughout the length of the panel. As the load is further increased, the flexural crack width and depth increases, and the specimen collapsed in flexure (Figure II.3.5). The specimen starts load shedding as soon as it reaches its collapse load and failure is observed to be sudden. Crushing of concrete at the loading point is observed after failure.

II.3.5 Specimen RC3 - 3.05 m (10 ft) Panel

The load vs strain curves and load vs deflection curves for loading step 4 are presented for specimen RC3 in Figures II.3.6 and II.3.7. The maximum centerline deflection at applied service load of 58.38 kN/m (4,000 lb/ft) of width, the maximum strain on steel rebars at service load (LL+IM+DL) and maximum strain at dead load (DL) are presented in Table II.3.2. The allowable deflections as per the deflection criteria specified by ODOT are also presented in Table II.3.2.

The load at failure, maximum deflection at failure and mode of failure are presented in Table II.3.3.

The load vs deflection plots show that the stiffness of the deck remains constant during the cyclic loading. For the failure load in step 4, the load vs deflection curve (Figure II.3.7) indicates that the specimen fails at 181.7 kN (40,837 lb). While loading the specimen, flexural cracks are formed initially in the concrete tension zone, and then throughout the length of the panel. As the load is further increased, the flexural crack width and depth increases, and the specimen collapsed in flexure (Figure II.3.8). The specimen starts load shedding as soon as it reaches its collapse load and failure is observed to be sudden. Crushing of concrete at the loading point is observed after failure

II.3.6 Specimen RC4 - Double Span Panel

The load vs strain curves and load vs deflection curves for loading step 4 are presented for specimen RC4 in Figures II.3.9 and II.3.10. The maximum centerline deflections at applied service load of 58.38 kN/m (4,000 lb/ft) of width, the maximum strain on steel rebars at service load (LL+IM+DL) and maximum strain at dead load (DL) are presented in Table II.3.2. The allowable deflections as per the deflection criteria specified by ODOT are also presented in Table II.3.2.

The load at failure, maximum deflection at failure and mode of failure are presented in Table II.3.3.

The load vs deflection plots show that the stiffness of the deck remains constant during the cyclic loading. For the failure load in step 4, the load vs deflection curve (Figure II.3.10) indicates that the specimen fails at 243.4 kN (54,714 lb). While loading the specimen, flexural cracks are formed initially in the concrete tension zone in span 1 and span 2, and then throughout the length of the panel. As the load is increased, the flexural crack width and depth increases, shear cracks initiates and the specimen collapsed due to flexure-shear nearer to the middle support (Figure II.3.11). The specimen starts load shedding as soon as it reaches its collapse load and failure is observed to be sudden. At the time of failure a blast like sound is heard. Crushing of concrete at the loading point is observed after failure.

Table II.3.1 Reinforced Concrete Conventional Deck Panels

Specimen Identification	Length (m)	Effective Length[a] (m)	Width (m)	Thickness[b] (m)	Remarks
(1)	(2)	(3)	(4)	(5)	(6)
RC1	2.74	2.44	0.91	0.188	Each specimen possessed some minor deformations (waviness) along the top and bottom surfaces.
RC* [c]	3.05	2.74	0.91	0.185	
RC2	3.35	3.05	0.91	0.203	
RC3	3.96	3.66	0.91	0.224	
RC4 (Double Span)	5.79	2.74 (each span)	1.07	0.185	

[a] Distance between centerline of supports (Figures II.2.2 and II.2.3).
[b] Average thickness.
[c] Specimen RC* is not used as a baseline specimen since no composite panel of the same dimensions is provided or tested
Note: The effective span is 2.667 m (105 in) for the First Salem Bridge over the Great Miami River in Montgomery County, Ohio.

Table II.3.2 Deflections and Strains for Reinforced Concrete Conventional Deck Panels

Specimen Identification[a]	Centerline Deflection @ Applied Service Load of 58.38 kN/m Width (mm)		Maximum Strain @ (LL+IM+DL) [d]	Maximum Strain @ DL[d]
	Baseline[b]	Allowable[c]		
(1)	(2)	(3)	(4)	(5)
RC1 (2.44 m)	3.607	3.175	*	0.000431
RC* [e] (2.74 m)	5.486	4.572	*	0.000202
RC2 (3.05 m)	5.029	4.318	*	0.000519
RC3 (3.66 m)	6.731	6.096	0.004361	0.000750
RC4 Span1 [f] (2.74 m)	1.372	4.572	0.002430	0.000463
RC4 Span 2 [f] (2.74 m)	1.499		0.001770	0.000543

[a] Effective span is shown in parentheses.
[b] The centerline deflections are derived by interpolation from the baseline deflection curves.
[c] The allowable deflections are provided by the Ohio Department of Transportation.
[d] The strain on steel rebar is derived by interpolation from the baseline strain curves.
[e] Specimen RC* is not used as a baseline specimen since no composite panel of the same dimensions is provided or tested.
[f] Span 1 and span 2 for the two span panel are shown in Figure II.2.5.
* The steel bars yielded at the service load (LL+IM+DL).
Note: The effective span for the First Salem Bridge is 2.667 m (105 in).

Table II.3.3 Load at Failure, Maximum Deflection, and Mode of Failure for Reinforced Concrete Conventional Deck Panels

Specimen Identification[a]	Load at Failure (kN)	Maximum Deflection at Failure (mm)	Mode of Failure
(1)	(2)	(3)	(4)
RC1 (2.44 m)	189.9	29.79	Flexure
RC* [b] (2.74 m)	153.8	35.94	Flexure
RC2 (3.05 m)	197.8	33.35	Flexure
RC3 (3.66 m)	181.7	41.61	Flexure
RC4 Span 1 [c] (2.74 m)	243.4	29.18	Flexure-Shear
RC4 Span 2 [c] (2.74 m)	243.4	21.92	

[a] Effective span is shown in parentheses.
[b] Specimen RC* is not used as a baseline specimen since no composite panels of the same dimensions were provided or tested
[c] Span 1 and span 2 for the two span panel are shown in Figure II.2.5.
Note: The effective span for the First Salem Bridge is 2.667 m (105 in).

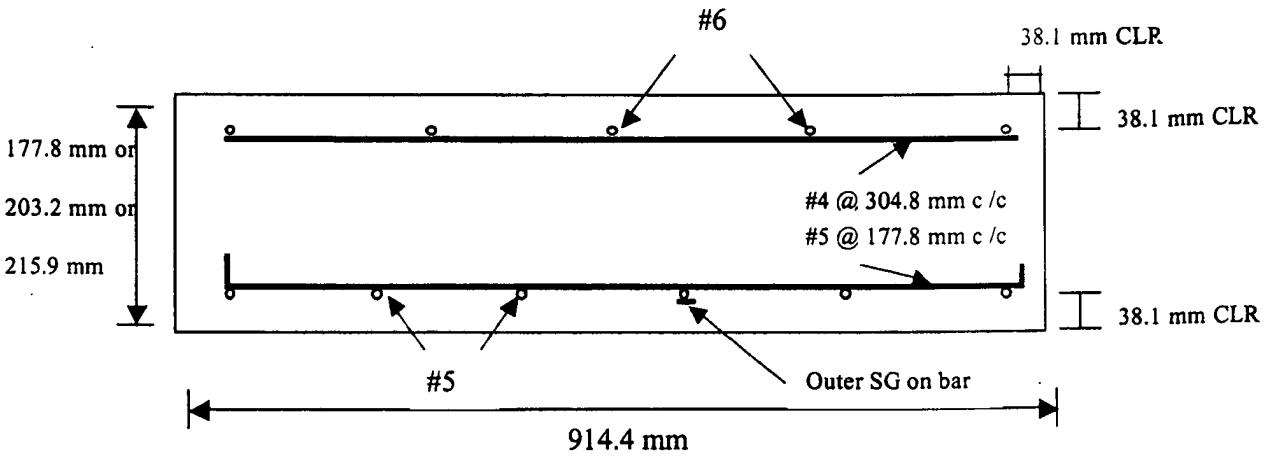

II.3.1 (a): Reinforcement Details

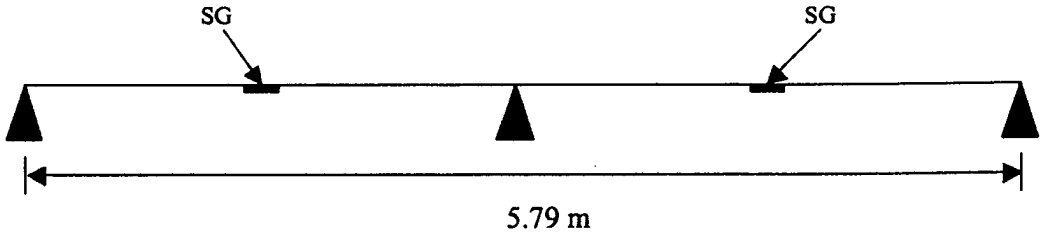

II.3.1 (b): Position of Strain Gages on Steel Rebars in Double Span Panel

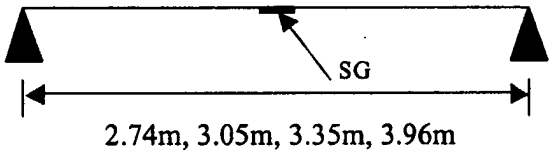

II.3.1 (c): Position of Strain Gages on Steel Rebars in Single Span Panel

Figure II.3.1 RC Panels - Location of Strain Gages (SG) on Steel Rebars; (a) Panel Cross Section; (b) Double Span Panel; and (c) Single Span Panel.

(Note: Strain gages on concrete are not shown)

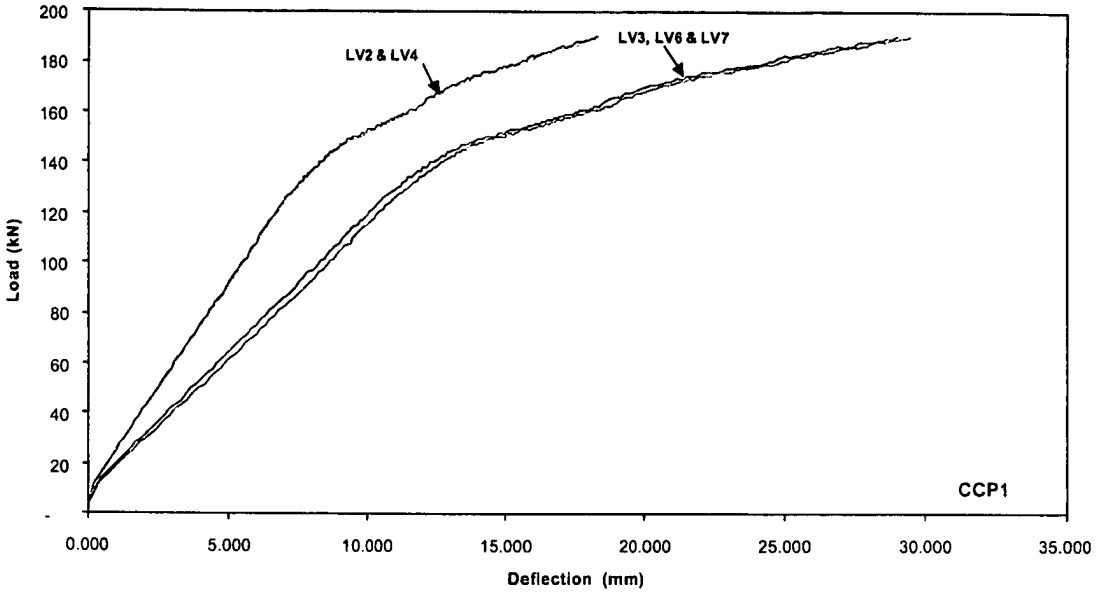

Fig. A8 Load vs Deflection for Failure

Figure II.3.2 Load vs Deflection for Loading to Failure for the Deck Panel RC1

(Refer to Figure II.2.6 for the location of LVDT's LV2, LV3, LV4, LV6 and LV7, and refer to Table II.3.1 for the properties of the RC1 Panel)

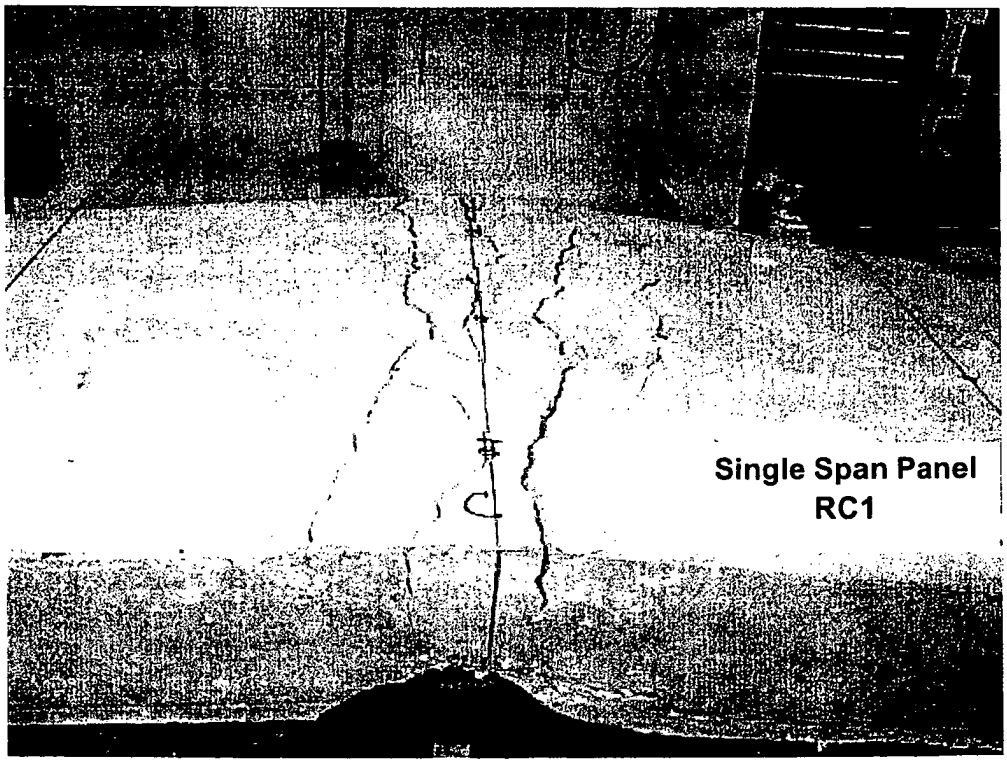

Figure II.3.3 Failure Pattern of the Deck Panel RC1

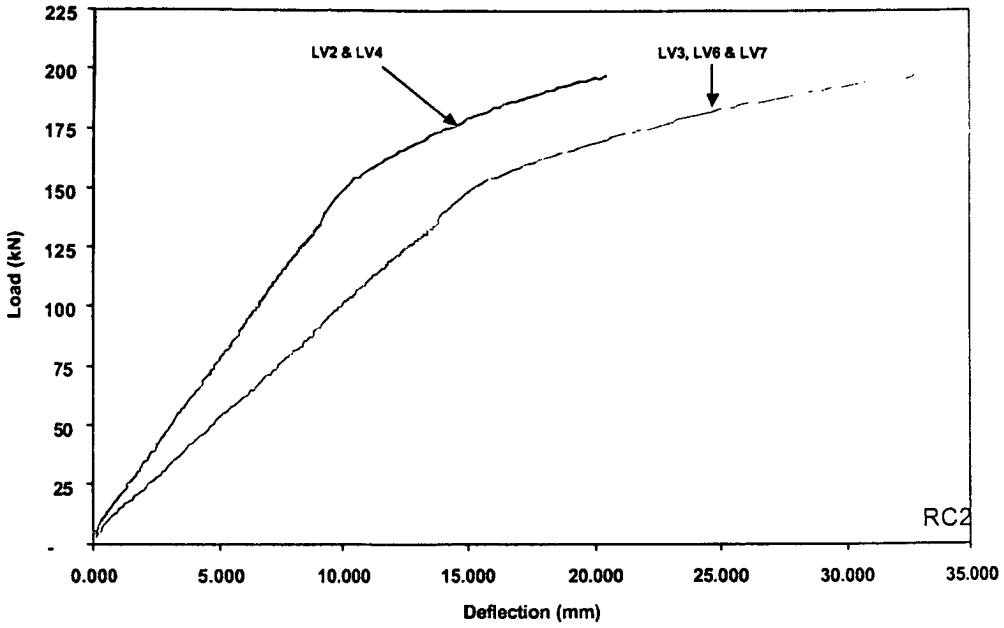

Figure II.3.4 Load vs Deflection for Loading to Failure for the Deck Panel RC2
(Refer to Figure II.2.6 for the location of LVDT's LV2, LV3, LV4, LV6 and LV7, and refer to Table II.3.1 for the properties of the RC2 Panel)

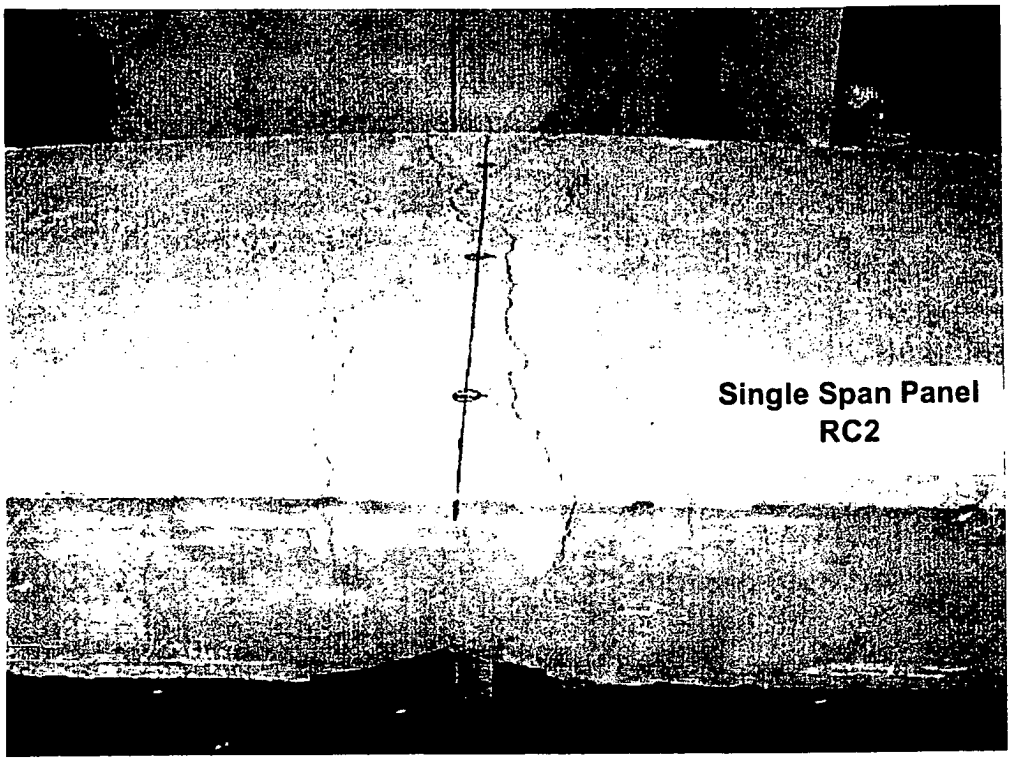

Figure II.3.5 Failure Pattern of the Deck Panel RC2

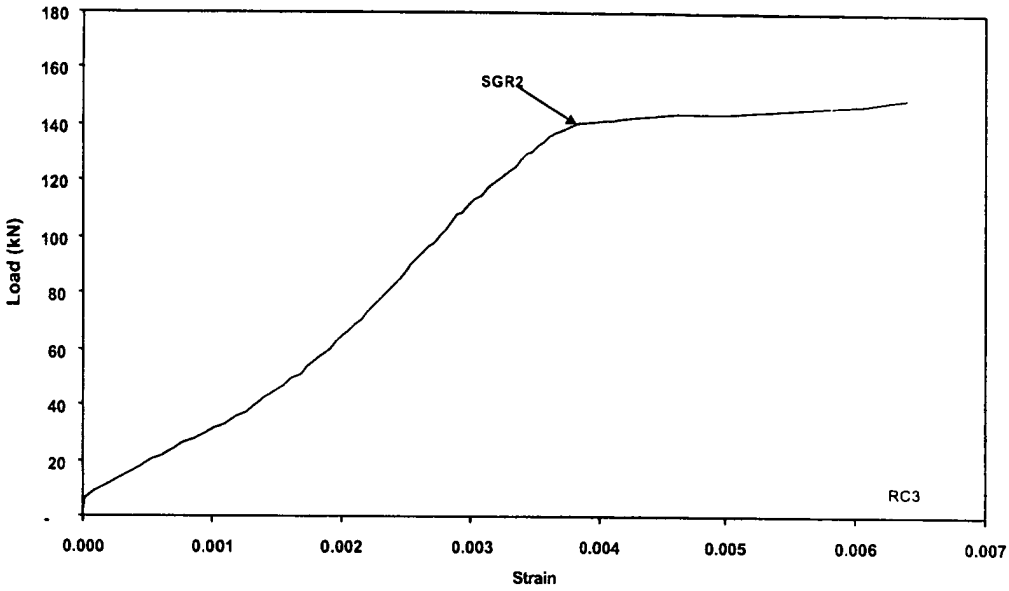

Figure II.3.6 Load vs Strain for Loading to Failure for the Deck Panel RC3
(SGR2 is the strain gage fixed on the rebar, and refer to Table II.3.1 for the properties of the RC3 Panel)

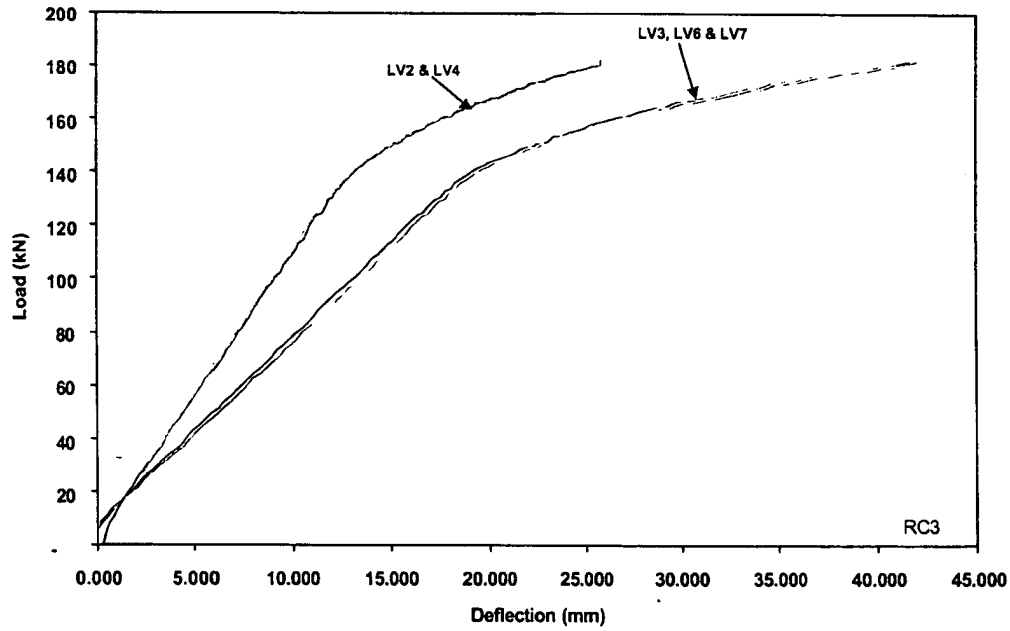

Figure II.3.7 Load vs Deflection for Loading to Failure for the Deck Panel RC3
(Refer to Figure II.2.6 for the location of LVDT's LV2, LV3, LV4, LV6 and LV7, and refer to Table II.3.1 for the properties of the RC3 Panel)

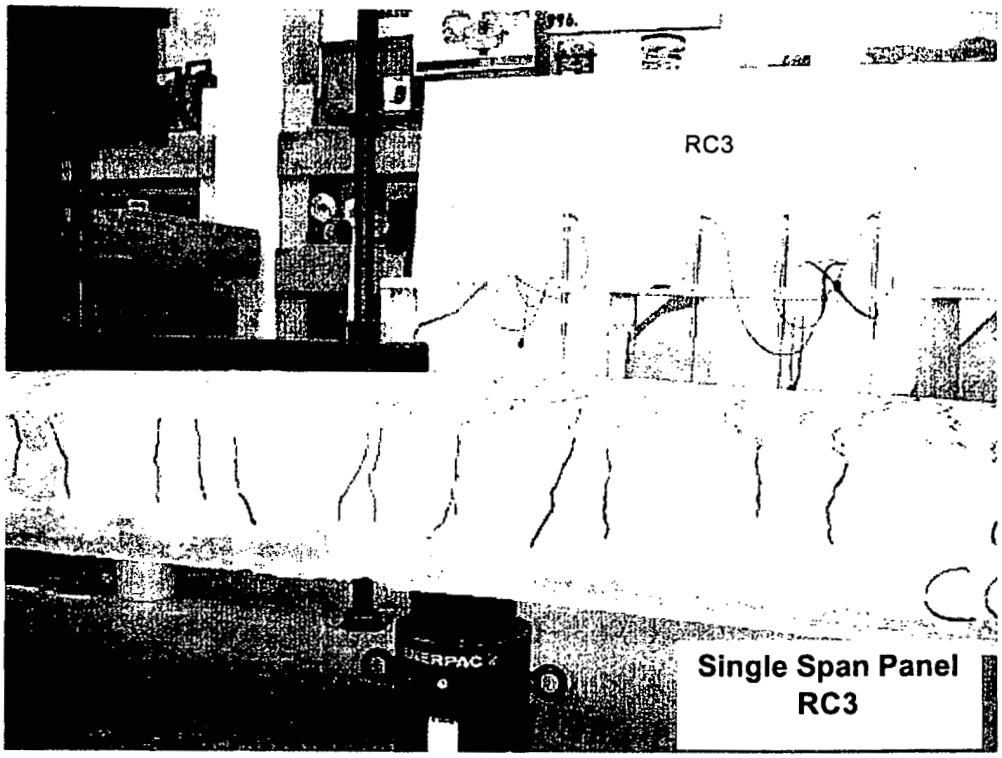

Figure II.3.8 Failure Pattern of the Deck Panel RC3

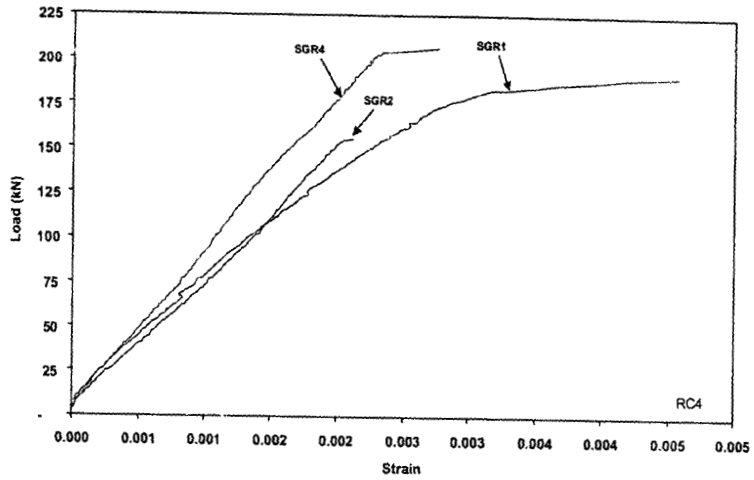

Figure II.3.9 Load vs Strain for Loading to Failure for the Deck Panel RC4
(SGR1, SGR2 and SGR4 are the strain gages fixed on the rebars, and refer to Table II.3.1 for the properties of RC4 Panel)

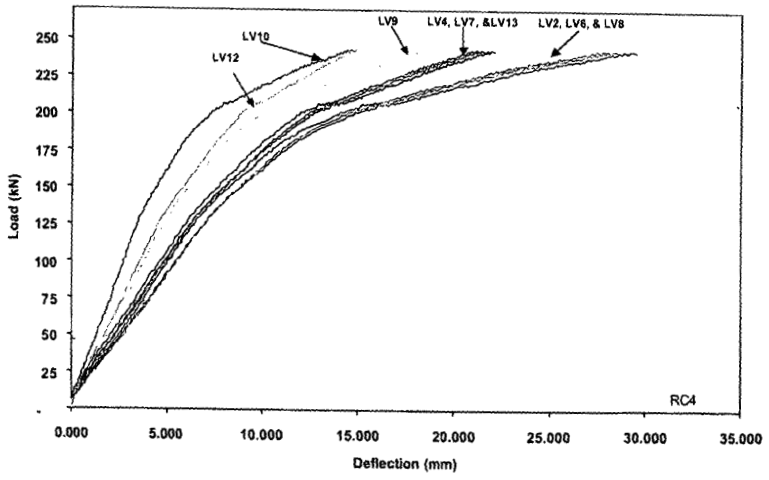

Figure II.3.10 Load vs Deflection for Loading to Failure for the Deck Panel RC4
(Refer to Figure II.2.7 for the location of LVDT's LV2, LV4, LV6, LV7, LV8, LV9, LV10, LV11, LV12 and LV13, and refer to Table II.3.1 for the properties of the RC4 Panel)

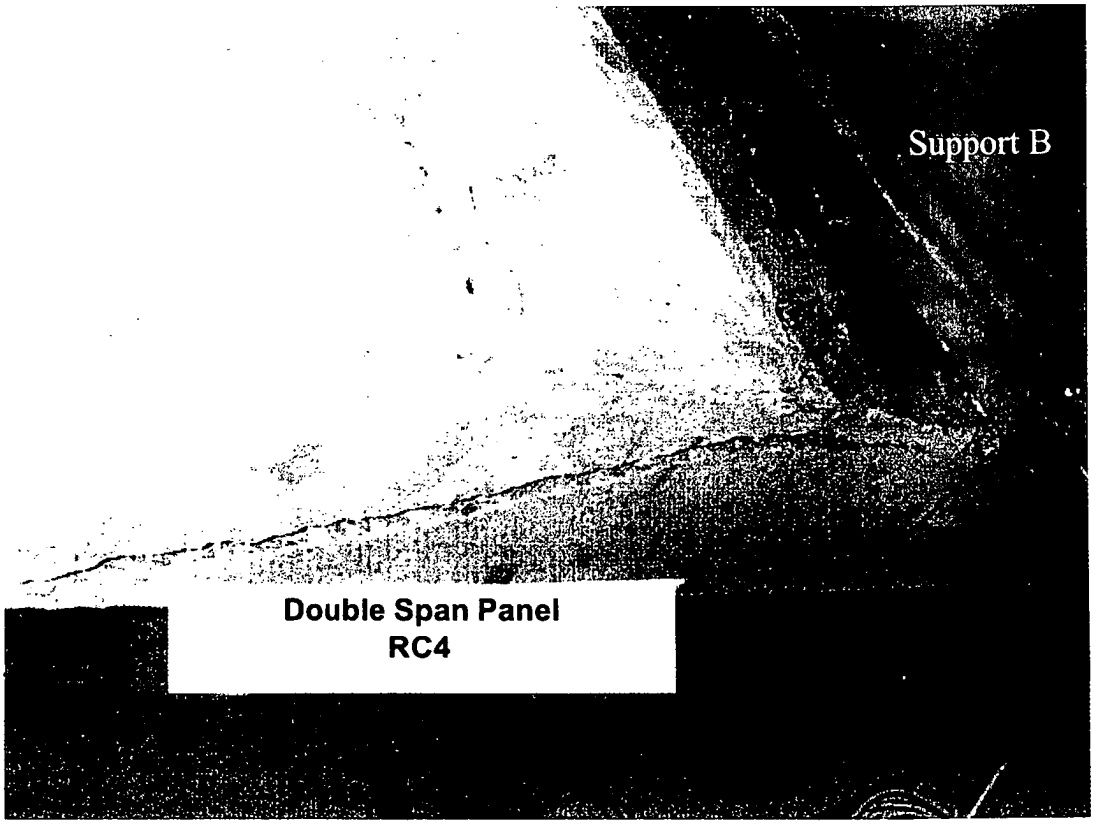

Figure II.3.11 Failure Pattern of the Deck Panel RC4

II.4 PULTRUDED F DECK - C ATIVE PULTRUSIONS

II.4.1 Summary

The single and double span Pultruded FRP Deck - Creative Pultrusions (CP) panels satisfy the deflection criteria and flexure criteria.

The following flexural rigidity (EI) and shear rigidity (GA_w) are recommended for use in modeling the First Salem Bridge: EI = 2.428 x 10^7 N-m^2 (8.461 x 10^9 lb-in^2) and GA_w= 1.120 x 10^7 N (2.518 x 10^6 lb).

II.4.2 Introduction

The Pultruded FRP Deck - Creative Pultrusions (CP) panels consist of pultruded components that are placed transversely to the traffic direction and supported by longitudinal beams. The CP-FRP deck panels are made of double trapezoid and hexagonal pultruded components. The pultruded components are bonded and interlocked to form a deck module as shown in Figure II.4.1. The length, effective length (distance between centerlines of supports), width and thickness of single and double span panels are presented in Table II.4.1. The single span panels are designated as CP1, CP2 and CP3, and the double span panel is designated as CP4 (Table II.4.1). The single and double span panels are loaded as per the steps outlined in section II.2.3.

II.4.3 Specimen CP1 – 2.44 m (8 ft) Panel

The load vs strain curves and load vs deflection curves for loading step 4 are presented for the deck panel CP1 in Figures II.4.2 and II.4.3.

The maximum centerline deflection at applied service load of 58.38 kN/m (4,000 lb/ft) of width, the maximum strain at service load (LL+IM+DL) and maximum strain at dead load (DL) are presented in Table II.4.2. The baseline deflection, allowable deflection as per deflection criteria and allowable strain as per the flexure criteria specified by ODOT are also presented in Table II.4.2.

The ultimate load, maximum deflection at ultimate load and mode of failure are presented in Table II.4.3. The ultimate load is compared with the required load in Table II.4.3 as per the flexure criteria specified by ODOT. The ultimate load and maximum deflection at ultimate load are also compared with their respective baseline ultimate load and maximum deflection (Table II.4.3).

The load vs deflection plots show that the stiffness of the deck remains constant during the cyclic loading. For the failure load in step 4, the load vs deflection curve (Figure II.4.3) indicates that the deck panel fails at 659,436 N (148,247 lb).

While loading cracking sound resulting from the delamination of the panel is observed starting at a load of 284,686 N (64,000 lb), to failure. At the time of failure, a blast like sound is heard and the deck panel started load shedding immediately. Buckling of the web is seen above the loading point when viewed through the end sections of the deck panel. After releasing the load, deck panel returned to its original shape and the top and bottom surfaces look almost like the original untested specimen. Failure of the deck panel is due to punching at the loading point, and due to delamination between the pultruded components surrounding the loaded region. The deck panel starts load shedding as soon as it reaches its collapse load and failure is observed to be sudden. The flexural and shear rigidities (EI and GA_w respectively) for the deck panel are determined by different techniques (Refer chapter II.2.5 for the equations used). The calculated values are presented in Table II.4.4.

II.4.4 Specimen CP2 – 2.74 m (9 ft) Panel

The load vs strain curves and load vs deflection curves for loading step 4 are presented for the deck panel CP2 in Figures II.4.4 and II.4.5.

The maximum centerline deflection at applied service load of 58.38 kN/m (4,000 lb/ft) of width, the maximum strain at service load (LL+IM+DL) and maximum strain at dead load (DL) are presented in Table II.4.2. The baseline deflection, allowable deflection as per deflection criteria and allowable strain as per the flexure criteria specified by ODOT are also presented in Table II.4.2.

The ultimate load, maximum deflection at ultimate load and mode of failure are presented in Table II.4.3. The ultimate load is compared with the required load in Table II.4.3 as per the flexure criteria specified by ODOT. The ultimate load and maximum deflection at ultimate load are also compared with their respective baseline ultimate load and maximum deflection (Table II.4.3).

The load vs deflection plots show that the stiffness of the deck remains constant during the cyclic loading. For the failure load in step 4, the load vs deflection curve (Figure II.4.5) indicates that the deck panel fails at 654,000 N (147,025 lb).

While loading cracking sound resulting from the delamination of the panel is observed starting at a load of 266,893 N (60,000 lb), to failure. At the time of failure, a blast like sound is heard and the deck panel started load shedding immediately. Buckling of the web is seen above the loading point when viewed through the end sections of the deck panel. Delamination of the panel at the end of a section is observed after failure. After releasing the load, the deck panel did not return to its original shape. Failure of the deck panel is due to punching at the loading point, and due to delamination between the pultruded components surrounding the loaded region. The deck panel starts load shedding as soon as it reaches its collapse load and failure is observed to be sudden. The flexural and shear rigidities (EI and GA_w respectively) for the deck panel are determined by different techniques (Refer chapter II.2.5 for the equations used). The calculated values are presented in Table II.4.4.

II.4.5 Specimen CP3 – 3.05 m (10 ft) Panel

The load vs strain curves and load vs deflection curves for loading step 4 are presented for deck panel CP3 in Figures II.4.6 and II.4.7.

The maximum centerline deflection at applied service load of 58.38 kN/m (4,000 lb/ft) of width, the maximum strain at service load (LL+IM+DL) and maximum strain at dead load (DL) are presented in Table II.4.2. The baseline deflection, allowable deflection as per deflection criteria and allowable strain as per the flexure criteria specified by ODOT are also presented in Table II.4.2.

The ultimate load, maximum deflection at ultimate load and mode of failure are presented in Table II.4.3. The ultimate load is compared with the required load in Table II.4.3 as per the flexure criteria specified by ODOT. The ultimate load and maximum deflection at ultimate load are also compared with their respective baseline ultimate load and maximum deflection (Table II.4.3).

The load vs deflection plots show that the stiffness of the deck remains constant during the cyclic loading. For the failure load in step 4, the load vs deflection curve (Figure II.4.7) indicates that the deck panel fails at 646,731 N (145,391 lb).

While loading cracking sound resulting from the delamination of the panel is observed starting at a load of 209,066 N (47,000 lb), to failure. At the time of failure, a blast like sound is heard and the deck panel started load shedding immediately. Buckling of the web is seen above the loading point when viewed through the end sections of the deck panel. Delamination of the panel at the end of a section is observed after failure. After releasing the load, the deck panel did not return to its original shape. Failure of the deck panel is due to punching at the loading point, and due to delamination between the pultruded components surrounding the loaded region. The deck panel starts load shedding as soon as it reaches its collapse load and failure is observed to be sudden. The punching failure of the deck panel is shown in Figure II.4.8. The flexural and shear rigidities (EI and GA_w respectively) for the deck panel are determined by different techniques (Refer chapter II.2.5 for the equations used). The calculated values are presented in Table II.4.4.

II.4.6 Specimen CP4 – Double Span Panel

The load vs strain curves and load vs deflection curves for loading step 4 are presented for deck panel CP4 in Figures II.4.9 and II.4.10.

The maximum centerline deflections at applied service load of 58.38 kN/m (4,000 lb/ft) of width, the maximum strain at service load (LL+IM+DL) and maximum strain at dead load (DL) are presented in Table II.4.2. The baseline deflection, allowable deflection as per deflection criteria and allowable strain as per the flexure criteria specified by ODOT are also presented in Table II.4.2.

The ultimate load, maximum deflection at ultimate load and mode of failure are presented in Table II.4.3. The ultimate load is compared with the required load in Table II.4.3 as per the flexure criteria specified by ODOT. The ultimate load and maximum deflection at ultimate load are also compared with their respective baseline ultimate load and maximum deflection (Table II.4.3).

The load vs deflection plots show that the stiffness of the deck remains constant during the cyclic loading. For the failure load in step 4, the load vs deflection curve (Figure II.4.10) indicates that the deck panel fails at 659,903 N (148,352 lb).

While loading cracking sound resulting from the delamination of the panel is observed starting at a load of 127,929 N (40,000 lb), to failure. At the time of failure, a blast like sound is heard and the deck panel started load shedding immediately. Buckling of the web is seen above the loading point when viewed through the end sections of the deck panel. After releasing the load, deck panel returned to its original shape and the top and bottom surfaces in span 1 and span 2 look almost like the original untested specimen. Failure of the deck panel is due to punching at the loading point, and due to delamination between the pultruded components surrounding the loaded region. The deck panel starts load shedding as soon as it reaches its collapse load and failure is observed to be sudden. The failure pattern of the deck panel CP4 is shown in Figure II.4.11. The flexural and shear rigidities (EI and GA_w respectively) for the deck panel are determined by different techniques (Refer chapter II.2.5 for the equations used). The calculated values are presented in Table II.4.4.

Table II.4.1 Pultruded FRP Deck - Creative Pultrusions Panels

Specimen Identification	Length (m)	Effective Length[a] (m)	Width (m)	Thickness[b] (m)	Remarks
(1)	(2)	(3)	(4)	(5)	(6)
CP1	2.74	2.44	0.91	0.203	Each specimen possessed some minor deformations (waviness) along the top and bottom surfaces.
CP2	3.35	3.05	0.91	0.203	
CP3	3.96	3.66	0.91	0.203	
CP4 (Double Span)	5.79	2.74 (each span)	0.91	0.203	

[a] Distance between centerline of supports (Figures II.2.2 and II.2.3).

[b] Average thickness.

Note: The effective span is 2.667 m (105 in) for the First Salem Bridge over the Great Miami River in Montgomery County, Ohio.

Table II.4.2 Deflections and Strains for Pultruded FRP Deck - Creative Pultrusions Panels

Specimen Identification[a]	Centerline Deflection @ Applied Service Load of 58.38 kN/m of Width (mm)			Maximum Strain @ (LL+IM+DL)		Maximum Strain @ DL	
	Measured[b]	Baseline[c]	Allowable[d]	Measured[e]	Allowable[f]	Measured[e]	Allowable[f]
(1)	(2)	(3)	(4)	(5)	(6)	(7)	(8)
CP1 (2.44 m)	2.286	3.607	3.175	0.000808	0.003200	0.000080	0.001600
CP2 (3.05 m)	4.064	5.029	4.318	0.000969	0.003200	0.000071	0.001600
CP3 (3.66 m)	6.071	6.731	6.096	0.001399	0.003200	0.000125	0.001600
CP4 Span1[g] (2.74 m)	2.184	1.372	4.572	0.000660[h]	0.003200	0.000092[h]	0.001600
CP4 Span2[g] (2.74 m)	2.616	1.499	4.572				

[a] Effective span is shown in parentheses.
[b] The centerline deflections are derived by interpolation from the baseline deflection curves.
[c] The baseline deflection is obtained from tests conducted on the baseline panels (Table II.3.2).
[d] The allowable deflections are provided by the Ohio Department of Transportation.
[e] The centerline strains are derived by interpolation from the baseline strain curves*.
[f] The allowable strain = 20% of maximum strain of the FRP coupon test (Refer Section I, Tables I.8.1 and I.8.2)
[g] Span 1 and span 2 for the two span panel are shown in Figure II.2.5.
[h] The maximum strain is measured along the middle support in the double span panel *.
* The strains are measured at 285.8 mm (11.25 inches) on both sides from the centerline of the panels (Figures II.2.4 and II.2.5)
Note: The effective span for the First Salem Bridge is 2.667 m (105 in).

Table II.4.3 Load at Failure, Maximum Deflection, and Mode of Failure for Pultruded FRP Deck - Creative Pultrusions Panels

Specimen Identification[a]	Ultimate Load (N)			Maximum Deflection at Ultimate Load [c] (mm)		Mode of Failure
	Measured	Baseline	Required [b]	Measured	Baseline	
(1)	(2)	(3)	(4)	(5)	(6)	(7)
CP1 (2.44 m)	659,436	189,859	524,561	39.12	29.79	Punching
CP2 (3.05 m)	654,000	197,781	530,166	61.16	33.35	Punching
CP3 (3.66 m)	646,731	181,652	535,762	98.60	41.61	Punching
CP4 Span1 [d] (2.74 m)	659,903	243,380	527,363	35.41	29.19	Punching
CP4 Span2 [d] (2.74 m)	659,903	243,380	527,363	35.31	21.92	

[a] Effective span is shown in parentheses.
[b] Required ultimate load = 2 x 1.3 [1.67(LL+IM)+DL)].
[c] The measured and baseline maximum deflections do not occur under the same load. Refer to columns (2) and (3) of this table for the magnitude of load at failure.
[d] Span 1 and span 2 for the two span panel are shown in Figure II.2.5.
Note: The effective span for the First Salem Bridge is 2.667 m (105 in).

Table II.4.4 Flexural and Shear Rigidities for Pultruded FRP Deck - Creative Pultrusions Panels

Specimen Identification	Effective Length (m)	Flexural Rigidity			Shear Rigidity
		EI [1] ($N\text{-}m^2$)	EI [2] ($N\text{-}m^2$)	EI [3] ($N\text{-}m^2$)	GA_w [4] (N)
(1)	(2)	(3)	(4)	(5)	(6)
CP1	2.44	7.611×10^6	9.367×10^6	6.589×10^6	9.893×10^7
CP2	3.05	1.004×10^7	9.884×10^6	7.286×10^6	3.438×10^7
CP3	3.66	2.324×10^7	9.054×10^6	8.047×10^6	1.103×10^7
CP4 (Double Span Panel)	2.74 (Span 1)	3.046×10^7	1.157×10^7	4.213×10^6	1.114×10^7
	2.74 (Span 2)	1.810×10^7	1.200×10^7	3.883×10^6	1.126×10^7
	Average of Spans 1 & 2	2.428×10^7 (recommended [5])	1.179×10^7	4.049×10^6	1.120×10^7 (recommended [6])

[1] Flexural rigidity by considering shear deformation (derived from experimental deflection).
[2] Flexural rigidity from moment-curvature relationship (derived from experimental strain).
[3] Flexural rigidity without considering shear deformation (derived from experimental deflection).
[4] Shear rigidity based on first order shear deformation equation (derived from experimental deflection)
[5] This flexural rigidity is recommended for use in modeling the First Salem Bridge.
[6] This shear rigidity is recommended for use in modeling the First Salem Bridge.
Note: The effective span is 2.667 m (105 in) for the First Salem Bridge over the Great Miami River in Montgomery County, Ohio.

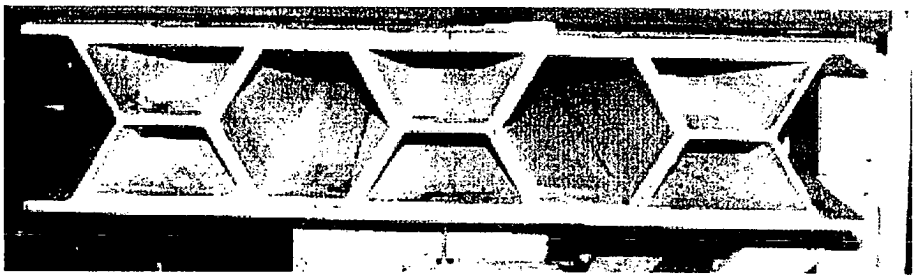

Figure II.4.1 Cross Section of Pultruded FRP Deck – Creative Pultrusions Panel

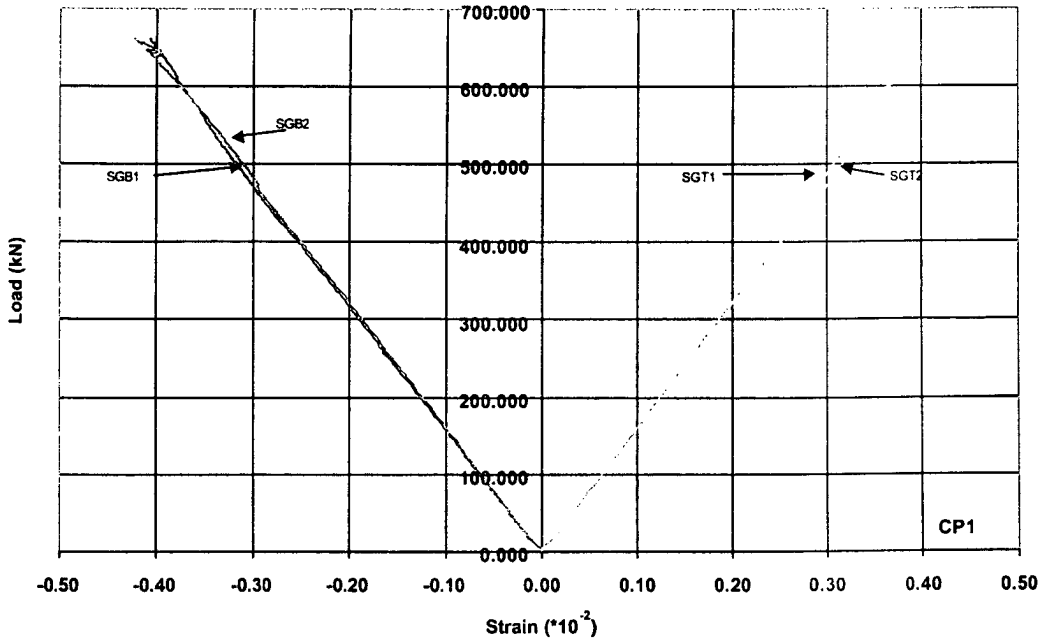

Figure II.4.2 Load vs Strain for Loading to Failure for the Deck Panel CP1
(Refer to Figure II.2.4 for the location of strain gages SGT1 and SGT2, and refer to Table II.4.1 for the properties of the CP1 Panel)

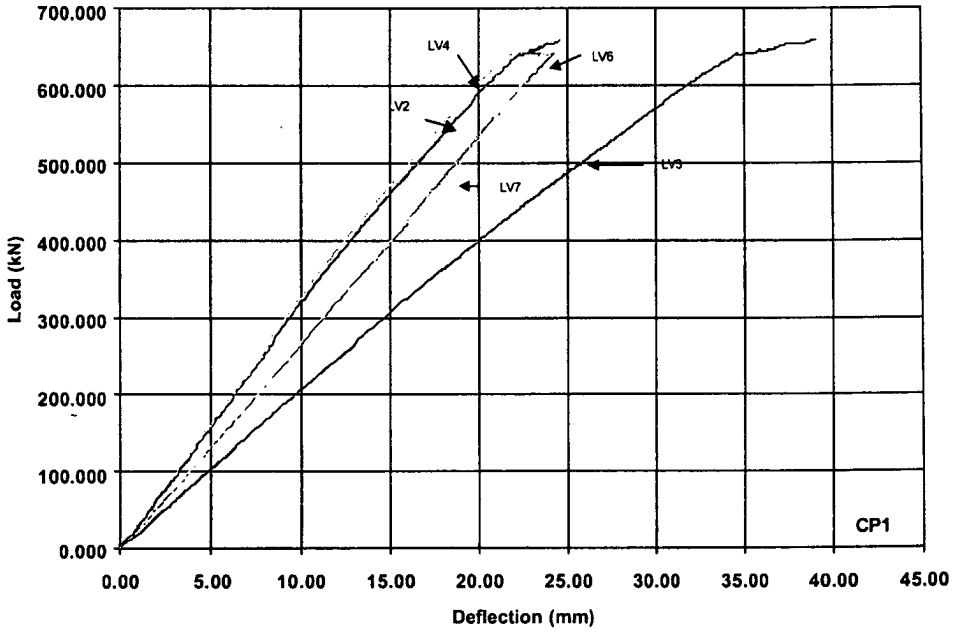

Figure II.4.3 Load vs Deflection for Loading to Failure for the Deck Panel CP1
(Refer to Figure II.2.6 for the location of LVDT's LV2, LV3, LV4, LV6 and LV7, and refer to Table II.4.1 for the properties of the CP1 Panel)

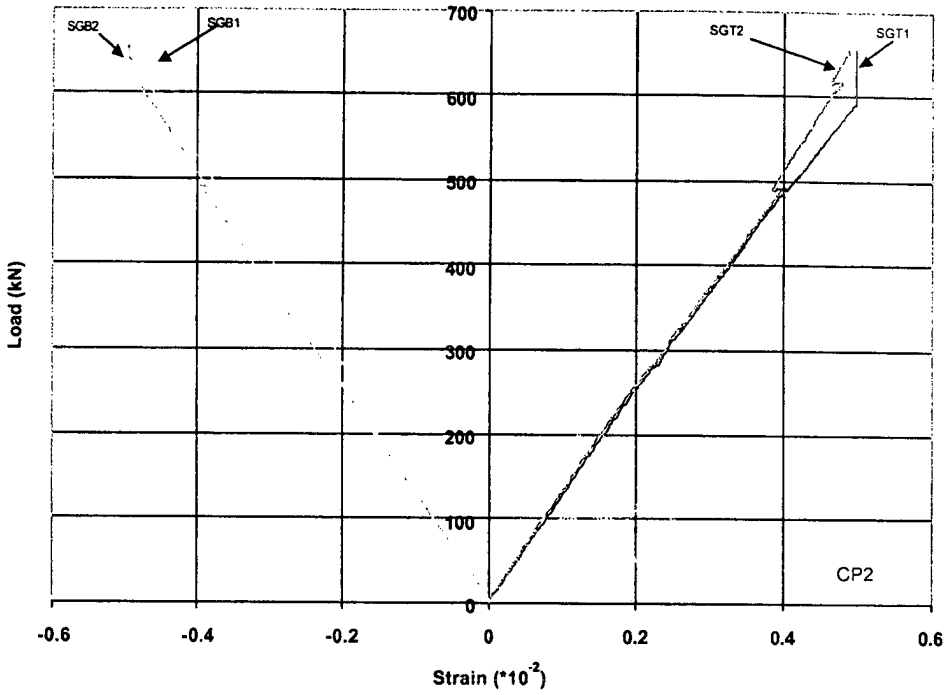

Figure II.4.4 Load vs Strain for Loading to Failure for the Deck Panel CP2
(Refer to Figure II.2.4 for the location of strain gages SGT1 and SGT2, and refer to Table II.4.1 for the properties of the CP2 Panel)

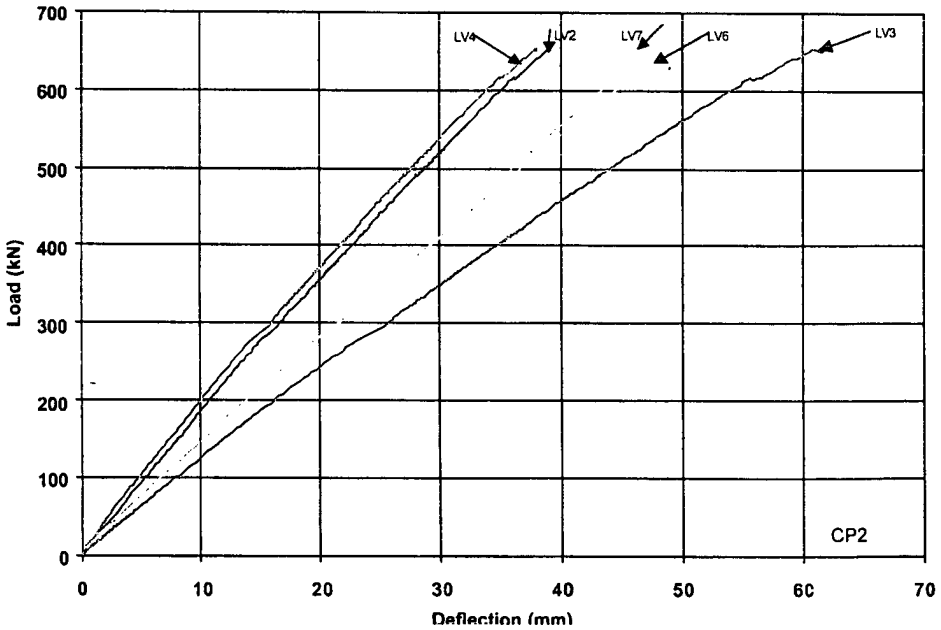

Figure II.4.5 Load vs Deflection for Loading to Failure for the Deck Panel CP2
(Refer to Figure II.2.6 for the location of LVDT's LV2, LV3, LV4, LV6 and LV7, and refer to Table II.4.1 for the properties of the CP2 Panel)

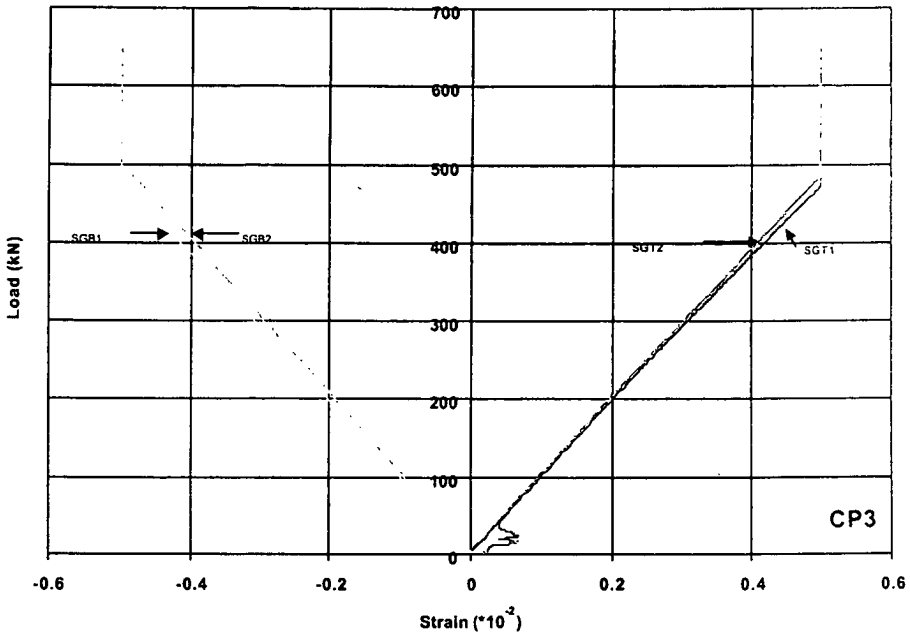

Figure II.4.6 Load vs Strain for Loading to Failure for the Deck Panel CP3
(Refer to Figure II.2.4 for the location of strain gages SGT1 and SGT2, and refer to Table II.4.1 for the properties of the CP3 Panel)

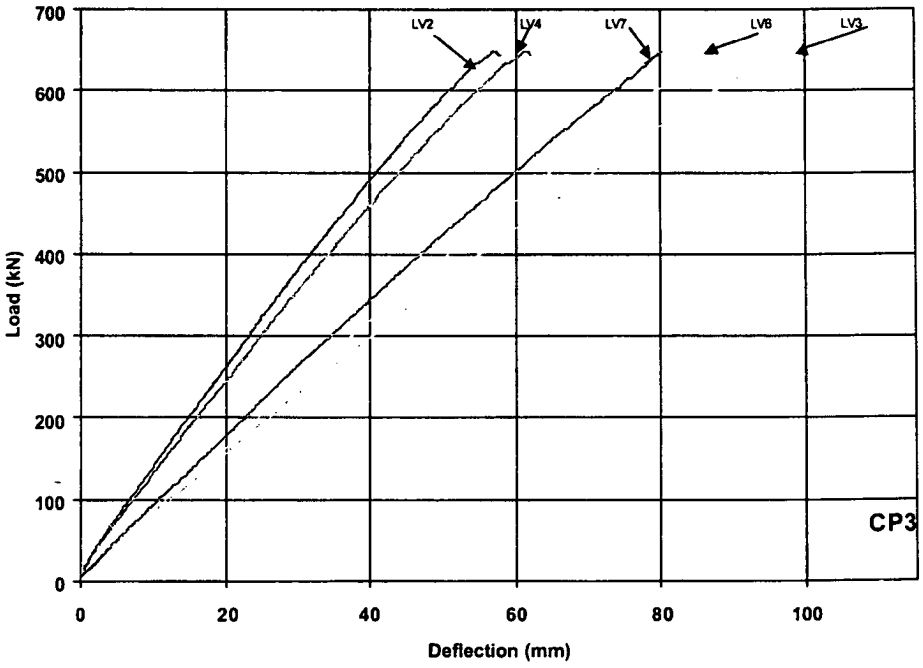

Figure II.4.7 Load vs Deflection for Loading to Failure for the Deck Panel CP3
(Refer to Figure II.2.6 for the location of LVDT's LV2, LV3, LV4, LV6 and LV7, and refer to Table II.4.1 for the properties of the CP3 Panel)

Figure II.4.8 Punching Failure at the Loading Point in Deck Panel CP3

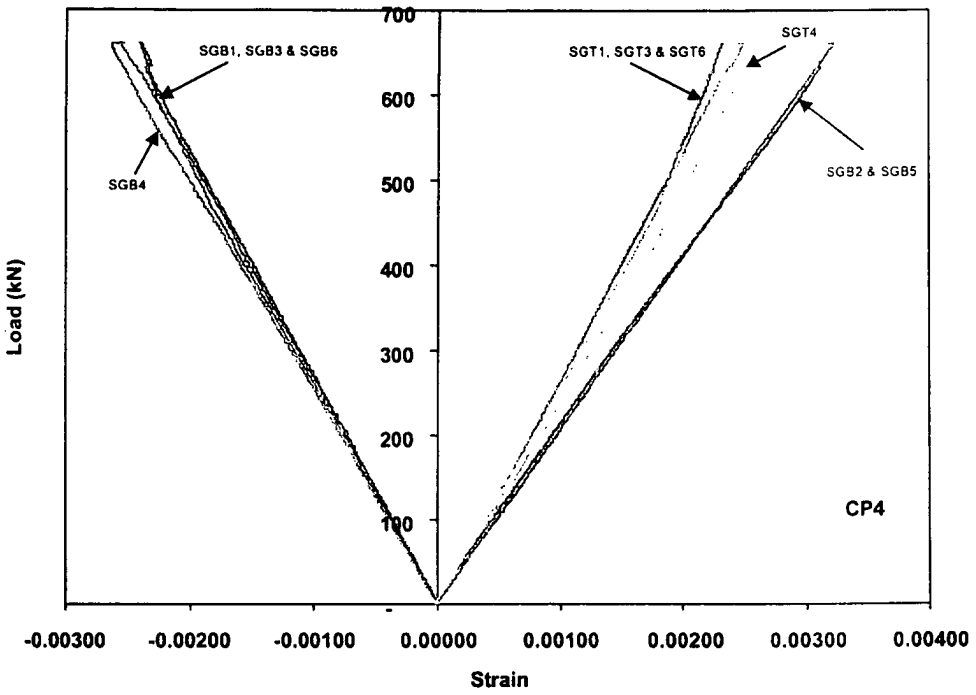

Figure II.4.9 Load vs Strain for Loading to Failure for the Deck Panel CP4
(Refer to Figure II.2.5 for the location of strain gages SGT1 and SGT2, and refer to TableII.4.1 for the properties of the CP4 Panel)

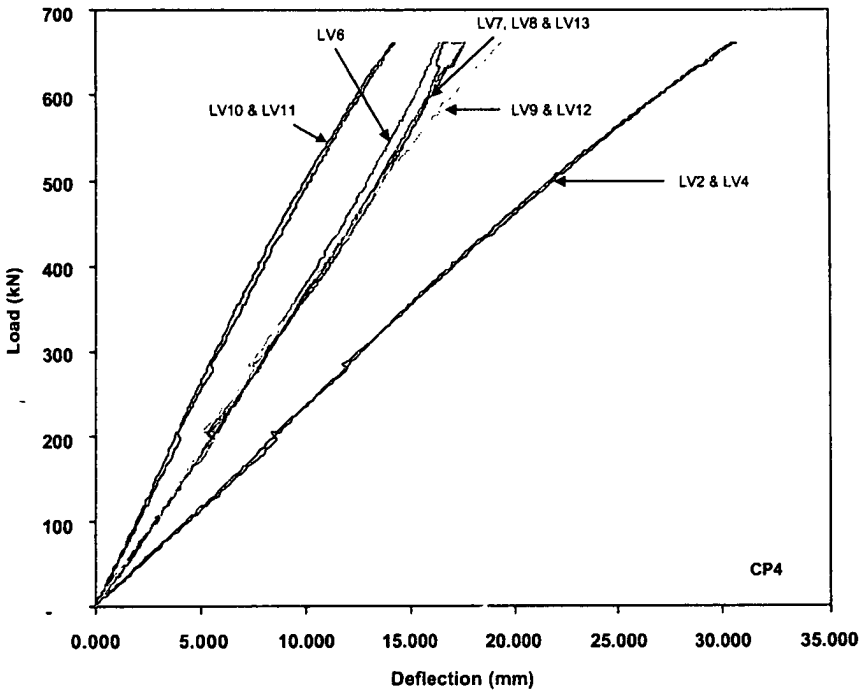

Figure II.4.10 Load vs Deflection for Loading to Failure for the Deck Panel CP4
(Refer to Figure II.2.7 for the location of LVDT's LV2, LV4, LV6, LV7, LV8, LV9, LV10, LV11, LV12 and LV13, and refer to Table II.4.1 for the properties of the CP4 Panel)

Figure II.4.11 Punching Failure at the Loading Point in Deck Panel CP4

II.5 HYBRID F - CONC TE DECK - COMPOSITE DECK SOLUTIONS

II.5.1 Summary

The single and double span Hybrid FRP - Concrete Deck - Composite Deck Solutions (CDS) panels satisfy the deflection criteria and flexure criteria.

The following flexural rigidity (EI) and shear rigidity (GA_w) are recommended for use in modeling the First Salem Bridge: EI = 1.588 x 10^7 N-m^2 (5.532 x 10^9 lb-in^2) and GA_w= 3.358 x 10^7 N (7.550 x 10^6 lb).

II.5.2 Introduction

The Hybrid FRP - Concrete Deck - Composite Deck Solutions (CDS) Panels are fabricated of concrete reinforced with Glass Fiber Reinforced Polymer (GFRP) rebars, and cast over pultruded GFRP tubular sections (Figure II.5.1). The length, effective length (distance between centerlines of supports), width and thickness of all single span and double span deck panels are presented in Table II.5.1. The single span panels are designated as CDS1, CDS2 and CDS3, and the double span panel is designated as CDS4 (Table II.5.1). The single and double span panels are loaded as per the steps outlined in section II.2.3.

II.5.3 Specimen CDS1 - 2.44 m (8 ft) Panel

The load vs strain curves and load vs deflection curves for loading step 4 are presented for deck panel CDS1 in Figures II.5.2 and II.5.3.

The maximum centerline deflection at the applied service load of 58.38 kN/m (4,000 lb/ft) of width, the maximum strain on FRP side at service load (LL+IM+DL) and maximum strain at dead load (DL) are presented in Table II.5.2. The baseline deflection, allowable deflection as per deflection criteria and allowable strain as per the flexure criteria specified by ODOT are also presented in Table II.5.2.

The ultimate load, maximum deflection at ultimate load, and mode of failure are presented in Table II.5.3. The ultimate load is compared with the required load in Table II.5.3 as per the flexure criteria specified by ODOT. The ultimate load and maximum deflection at ultimate load are also compared with their respective baseline ultimate load and maximum deflection (Table II.5.3).

The bad vs deflection plots show that the stiffness of the deck remains constant during the cyclic loading. For the failure load in step 4, the load vs deflection curve (Figure II.5.3) indicates that the deck panel fails at 402,146 N (90,406 lb).

While loading the deck panel, flexural cracks are formed initially in the concrete tension zone, and then throughout the length of the panel. As the load is further increased, the flexural crack width and depth increases, shear cracks initiate, and eventually intersect with the flexural cracks. Debonding of the GFRP tubular sections from concrete is observed at failure. The deck panel starts load shedding as soon as it reaches its collapse load and failure is observed to be sudden. The flexural and shear rigidities (EI and GA_w respectively) for the deck panel are determined by different techniques (Refer chapter II.2.5 for the equations used). The calculated values are presented in Table II.5.4.

II.5.4 Specimen CDS2 - 2.74 m (9 ft) Panel

The load vs strain curves and load vs deflection curves for loading step 4 are presented for deck panel CDS2 in Figures II.5.4 and II.5.5.

The maximum centerline deflection at the applied service load of 58.38 kN/m (4,000 lb/ft) of width, the maximum strain on FRP side at service load (LL+IM+DL) and maximum strain at dead load (DL) are presented in Table II.5.2. The baseline deflection, allowable deflection as per deflection criteria and allowable strain as per the flexure criteria specified by ODOT are also presented in Table II.5.2.

The ultimate load, maximum deflection at ultimate load and mode of failure are presented in Table II.5.3. The ultimate load is compared with the required load in Table II.5.3 as per the flexure criteria specified by ODOT. The ultimate load and maximum deflection at ultimate load are also compared with their respective baseline ultimate load and maximum deflection (Table II.5.3).

The load vs deflection plots show that the stiffness of the deck remains constant during the cyclic loading. For the failure load in step 4, the load vs deflection curve (FigureII.5.5) indicates that the deck panel fails at 435,361 N (97,873 lb).

While loading the deck panel, flexural cracks are formed initially in the concrete tension zone, and then throughout the length of the panel. As the load is further increased, the flexural crack width and depth increases, shear cracks initiate, and eventually intersect with the flexural cracks. Debonding of the GFRP tubular sections from concrete is observed at failure. The deck panel starts load shedding as soon as it reaches its collapse load and failure is observed to be sudden. The flexural and shear rigidities (EI and GA_w respectively) for the deck panel are determined by different techniques (Refer chapter II.2.5 for the equations used). The calculated values are presented in Table II.5.4.

II.5.5 Specimen CDS3 - 3.05 m (10 ft) Panel

The load vs strain curves and load vs deflection curves for loading step 4 are presented for deck panel CDS3 in Figures II.5.6 and II.5.7.

The maximum centerline deflection at the applied service load of 58.38 kN/m (4,000 lb/ft) of width, the maximum strain on FRP side at service load (LL+IM+DL) and maximum strain at dead load (DL) are presented in Table II.5.2. The baseline deflection, allowable deflection as per deflection criteria and allowable strain as per the flexure criteria specified by ODOT are also presented in Table II.5.2.

The ultimate load, maximum deflection at ultimate load and mode of failure are presented in Table II.5.3. The ultimate load is compared with the required load in Table II.5.3 as per the flexure criteria specified by ODOT. The ultimate load and maximum deflection at ultimate load are also compared with their respective baseline ultimate load and maximum deflection (Table II.5.3).

The load vs deflection plots show that the stiffness of the deck remains constant during the cyclic loading. For the failure load in step 4, the load vs deflection curve (Figure II.5.7) indicates that the deck panel fails at 348,420 N (78,328 lb).

While loading the deck panel, flexural cracks are formed initially in the concrete tension zone, and then throughout the length of the panel. As the load is further increased, the flexural crack width and depth increases, shear cracks initiate, and eventually intersect with the flexural cracks. Debonding of the GFRP tubular sections from concrete is observed at failure. The deck panel starts load shedding as soon as it reaches its collapse load and failure is observed to be sudden. The failure pattern of the deck panel CDS3 is shown in Figure II.5.8. The flexural and shear rigidities (EI and GA_w respectively) for the deck panel are determined by different techniques (Refer chapter II.2.5 for the equations used). The calculated values are presented in Table II.5.4.

II.5.6 Specimen CDS4 - Double Span Panel

The load vs strain curves and load vs deflection curves for loading step 4 are presented for deck panel CDS4 in Figures II.5.9 and II.5.10.

The maximum centerline deflections at the applied service load of 58.38 kN/m (4,000 lb/ft) of width, the maximum strain on FRP side at service load (LL+IM+DL) and maximum strain at dead load (DL) are presented in Table II.5.2. The baseline deflection, allowable deflection as per deflection criteria and allowable strain as per the flexure criteria specified by ODOT are also presented in Table II.5.2.

The ultimate load, maximum deflection at ultimate load and mode of failure are presented in Table II.5.3. The ultimate load is compared with the required load in Table II.5.3 as per the flexure criteria specified by ODOT. The ultimate load and maximum deflection at ultimate load are also compared with their respective baseline ultimate load and maximum deflection (Table II.5.3).

The load vs deflection plots show that the stiffness of the deck remains constant during the cyclic loading. For the failure load in step 4, the load vs deflection curve (Figure II.5.10) indicates that the deck panel fails at 374,829 N (84,265 lb).

While loading the deck panel, flexural cracks are formed initially in the concrete tension zone in span 1 and span 2 , and then throughout the length of the panel. As the load is increased, the flexural crack width and depth increases, shear cracks initiate, and eventually intersect with the flexural cracks in span 1 and span 2. Debonding of the GFRP tubular sections from concrete is observed at failure in span 1 and span 2. The deck panel starts load shedding as soon as it reaches its collapse load and failure is observed to be sudden. The failure pattern of the deck panel CDS4 is shown in Figure II.5.11. The flexural and shear rigidities (EI and GA_w respectively) for the deck panel are determined by different techniques (Refer chapter II.2.5 for the equations used). The calculated values are presented in Table II.5.4.

Table II.5.1 Hybrid FRP - Concrete Deck - Composite Deck Solutions Panels

Specimen Identification	Length (m)	Effective Length[a] (m)	Width (m)	Thickness[b] (m)	Remarks
(1)	(2)	(3)	(4)	(5)	(6)
CDS1	2.74	2.44	0.91	0.203	Specimens CDS1, CDS2, and CDS3 possessed some minor deformations (waviness) along the top and bottom surfaces. A crack width of 0.0762 mm was observed at midspan of the CDS4 panel when it was unloaded from the delivery truck.
CDS2	3.35	3.05	0.91	0.241	
CDS3	3.96	3.66	0.91	0.254	
CDS4 (Double Span)	6.10	2.74 (each span)	0.91	0.203	

[a] Distance between centerline of supports (Figures II.2.2 and II.2.3).

[b] Average thickness.

Note: The effective span is 2.667 m (105 in) for the First Salem Bridge over the Great Miami River in Montgomery County, Ohio.

Table II.5.2 Deflections and Strains for Hybrid FRP - Concrete Deck - Composite Deck Solutions Panels

Specimen Identification[a]	Centerline Deflection @ Applied Service Load of 58.38 kN/m of Width (mm)			Maximum Strain @ (LL+IM+DL)		Maximum Strain @ DL	
	Measured[b]	Baseline[c]	Allowable[d]	Measured[e]	Allowable[f]	Measured[e]	Allowable[f]
(1)	(2)	(3)	(4)	(5)	(6)	(7)	(8)
CDS1 (2.44 m)	0.965	3.607	3.175	0.000659	0.003400	0.000042	0.001700
CDS2 (3.05 m)	1.321	5.029	4.318	0.000727	0.003400	0.000117	0.001700
CDS3 (3.66 m)	2.540	6.731	6.096	0.001027	0.003400	0.000202	0.001700
CDS4 Span1[g] (2.74 m)	1.321	1.372	4.572	0.000827[h]	0.003400	0.000193[h]	0.001700
CDS4 Span2[g] (2.74 m)	1.346	1.499	4.572				

[a] Effective span is shown in parentheses.
[b] The centerline deflections are derived by interpolation from the baseline deflection curves.
[c] The baseline deflection is obtained from tests conducted on the baseline panels (Table II.3.2).
[d] The allowable deflections are provided by the Ohio Department of Transportation.
[e] The centerline strains are derived by interpolation from the baseline strain curves*.
[f] The allowable strain = 20% of maximum strain of the FRP coupon test (Refer section I, Tables I.8.1 and I.8.2)
[g] Span 1 and span 2 for the two span panel are shown in Figure II.2.5.
[h] The maximum strain is measured along the middle support in the double span panel *.
* The strains are measured at 285.8 mm (11.25 inches) on both sides from the centerline of the panels (Figures II.2.4 and II.2.5)
Note: The effective span for the First Salem Bridge is 2.667 m (105 in).

Table II.5.3 Load at Failure, Maximum Deflection , and Mode of Failure for Hybrid FRP - Concrete Deck - Composite Deck Solutions Panels

Specimen Identification[a]	Ultimate Load (kN)			Maximum Deflection at Ultimate Load [c] (mm)		Mode of Failure
	Measured	Baseline	Required[b]	Measured	Baseline	
(1)	(2)	(3)	(4)	(5)	(6)	(7)
CDS1 (2.44 m)	402,146	189,859	273,290	19.609	29.794	Flexure-Shear
CDS2 (3.05 m)	435,361	197,781	282,093	22.784	33.350	Flexure-Shear
CDS3 (3.66 m)	328,420	181,652	289,597	38.989	41.605	Flexure-Shear
CDS4 Span1 [d] (2.74 m)	347,829	243,380	276,066	25.222	29.185	Flexure-Shear
CDS4 Span2 [d] (2.74 m)	347,829	243,380	276,066	25.400	21.920	

[a] Effective span is shown in parentheses.

[b] Required ultimate load = 1.3[1.67(LL+IM)+DL).

[c] The measured and baseline maximum deflections do not occur under the same load. Refer to columns (2) and (3) of this table for the magnitude of load at failure.

[d] Span 1 and span 2 for the two span panel are shown in Figure II.2.5.

Note: The effective span for the First Salem Bridge is 2.667 m (105 in).

Table II.5.4 Flexural and Shear Rigidities for Hybrid FRP- Concrete Deck - Composite Deck Solutions Panels

Specimen Identification	Effective Length (m)	Flexural Rigidity			Shear Rigidity
		EI [1] ($N\text{-}m^2$)	EI [2] ($N\text{-}m^2$)	EI [3] ($N\text{-}m^2$)	GA_w [4] (N)
(1)	(2)	(3)	(4)	(5)	(6)
CDS1	2.44	1.615×10^7	1.452×10^7	1.619×10^7	- [5]
CDS2	3.05	2.664×10^7	1.996×10^7	2.387×10^7	2.970×10^8
CDS3	3.66	2.796×10^7	1.395×10^7	2.133×10^7	8.078×10^7
CDS4 (Double Span Panel)	2.74 (Span 1)	1.644×10^7	8.452×10^6	7.602×10^6	3.222×10^7
	2.74 (Span 2)	1.531×10^7	9.224×10^6	7.662×10^6	3.494×10^7
	Average of Spans 1 & 2	1.588×10^7 (recommended [6])	8.839×10^6	7.634×10^6	3.358×10^7 (recommended [7])

[1] Flexural rigidity by considering shear deformation (derived from experimental deflection).
[2] Flexural rigidity from moment-curvature relationship (derived from experimental strain).
[3] Flexural rigidity without considering shear deformation (derived from experimental deflection).
[4] Shear rigidity based on first order shear deformation equation (derived from experimental deflection)
[5] The GA_w value derived from substituting the deflections into analytical equations is negative.
[6] This flexural rigidity is recommended for use in modeling the First Salem Bridge.
[7] This shear rigidity is recommended for use in modeling the First Salem Bridge.
Note: The effective span is 2.667 m (105 in) for the First Salem Bridge over the Great Miami River in Montgomery County, Ohio.

Figure II.5.1 Cross Section of Composite Deck Solutions Deck Panel

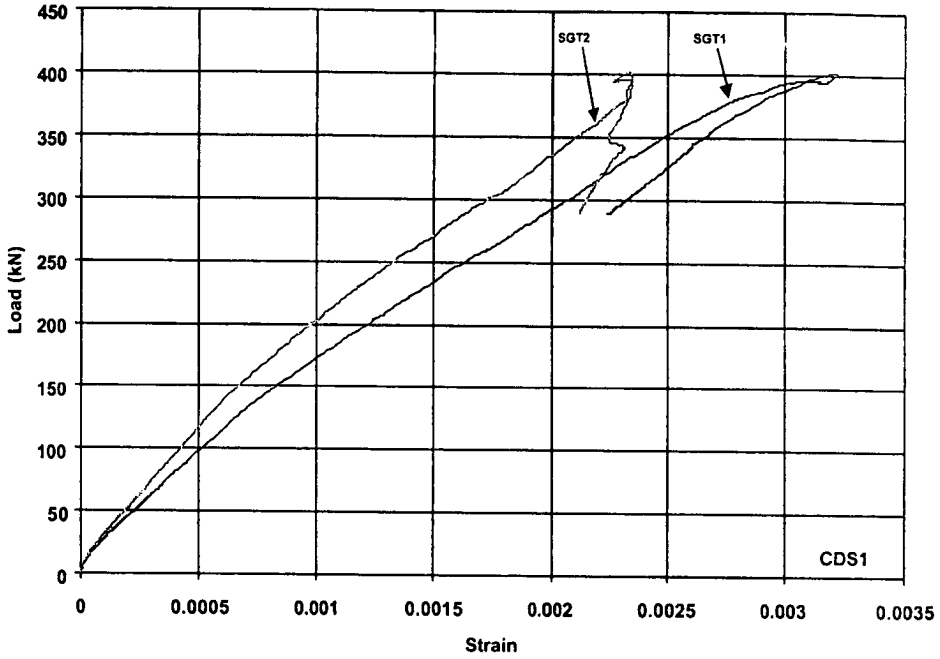

Figure II.5.2 Load vs Strain for Loading to Failure for the Deck Panel CDS1

(Refer to Figure II.2.4 for the location of strain gages SGT1 and SGT2, and refer to Table II.5.1 for the properties of the CDS1 Panel)

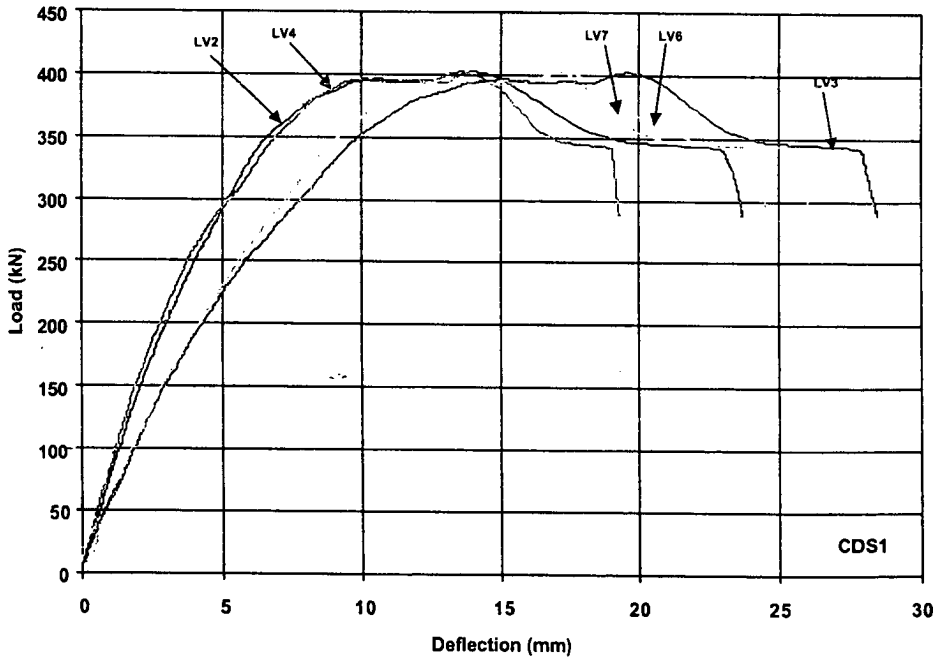

Figure II.5.3 Load vs Deflection for Loading to Failure for the Deck Panel CDS1

(Refer to Figure II.2.6 for the location of LVDT's LV2, LV3, LV4, LV6 and LV7, and refer to Table II.5.1 for the properties of the CDS1 Panel)

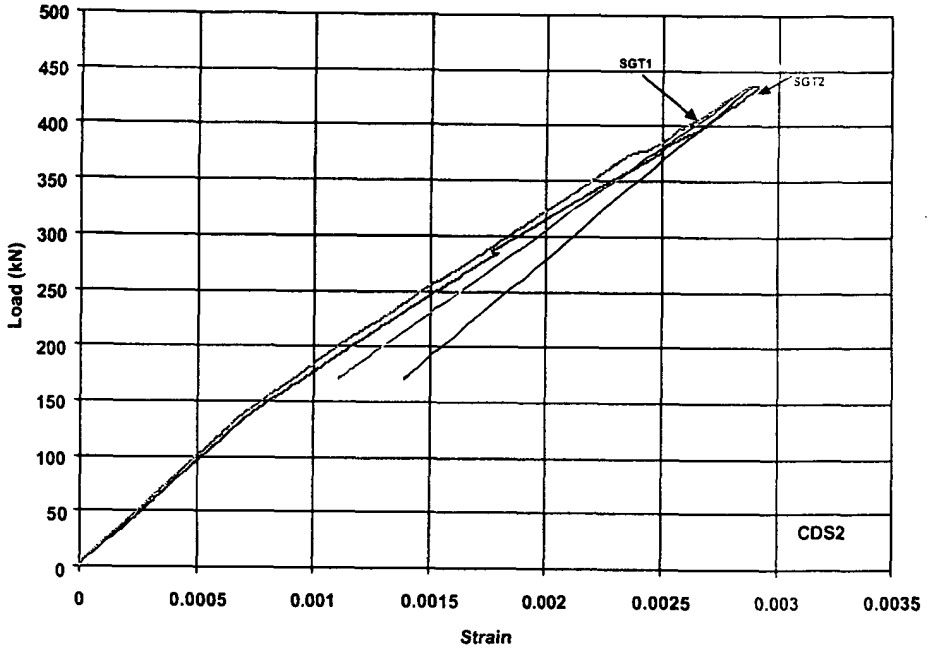

Figure II.5.4 Load vs Strain for Loading to Failure for the Deck Panel CDS2

(Refer to Figure II.2.4 for the location of strain gages SGT1 and SGT2, and refer to Table II.5.1 for the properties of the CDS2 Panel)

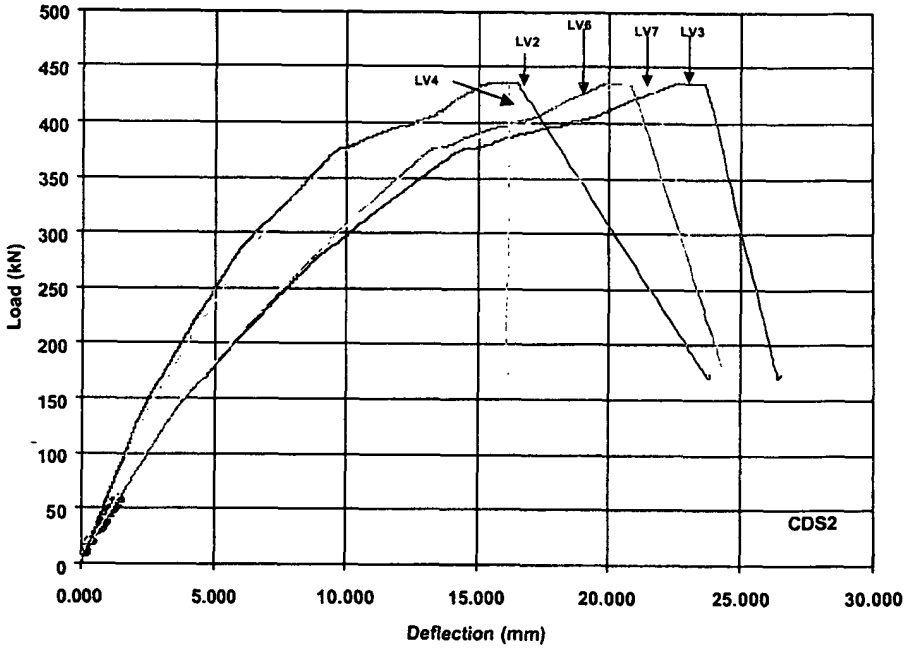

Figure II.5.5 Load vs Deflection for Loading to Failure for the Deck Panel CDS2

(Refer to Figure II.2.6 for the location of LVDT's LV2, LV3, LV4, LV6 and LV7, and refer to Table II.5.1 for the properties of the CDS2 Panel)

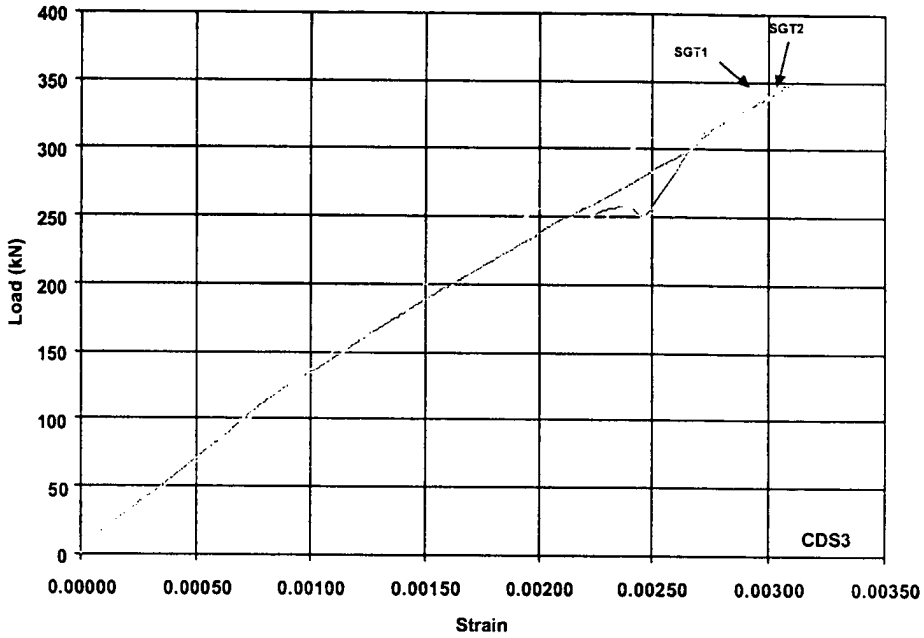

Figure II.5.6 Load vs Strain for Loading to Failure for the Deck Panel CDS3
(Refer to Figure II.2.4 for the location of strain gages SGT1 and SGT2, and refer to Table II.5.1 for the properties of the CDS3 Panel)

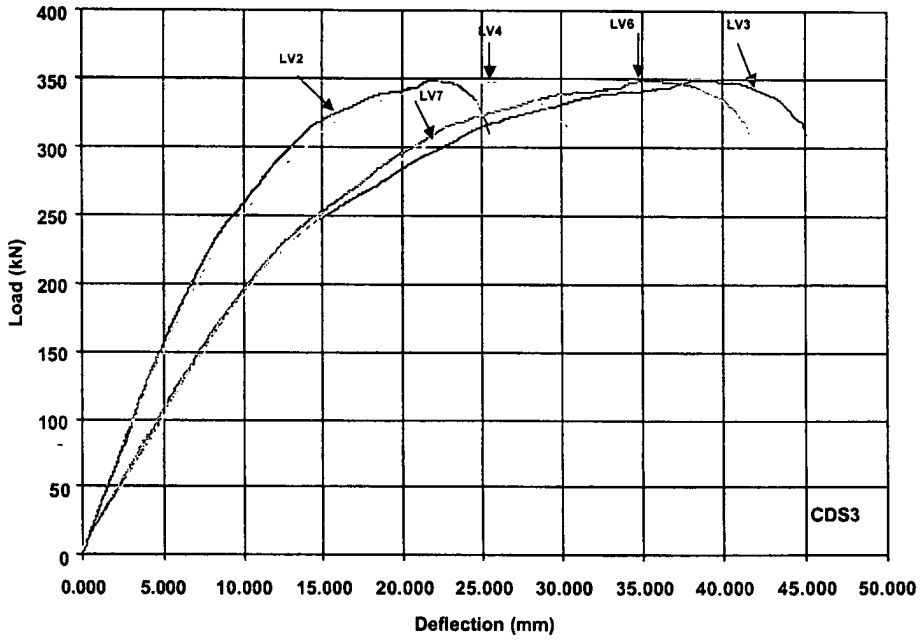

Figure II.5.7 Load vs Deflection for Loading to Failure for the Deck Panel CDS3
(Refer to Figure II.2.6 for the location of LVDT's LV2, LV3, LV4, LV6 and LV7, and refer to Table II.5.1 for the properties of the CDS3 Panel)

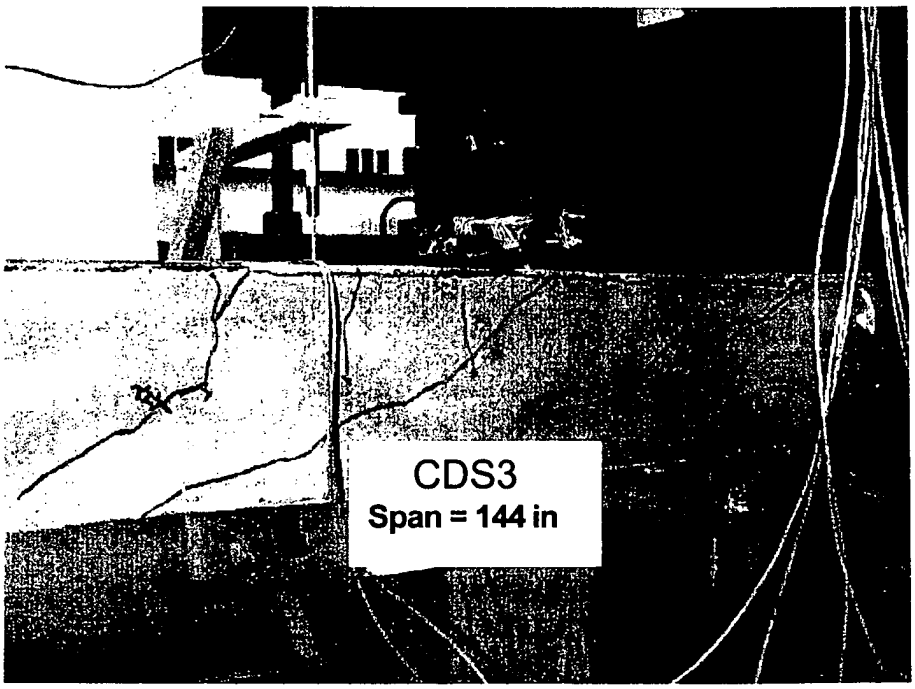

Figure II.5.8 Failure Pattern of the Deck Panel CDS3

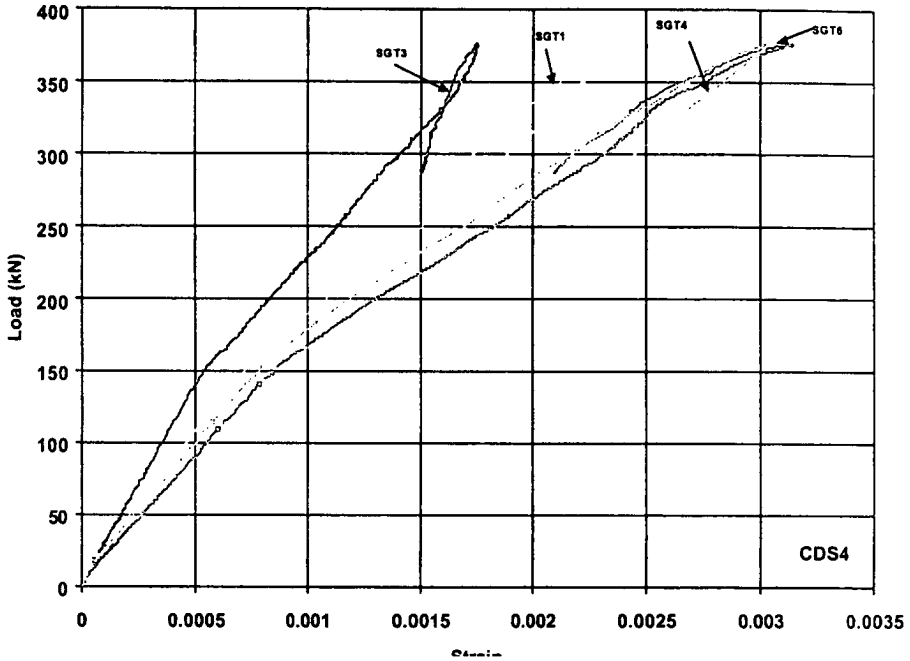

Figure II.5.9 Load vs Strain for Loading to Failure for the Deck Panel CDS4
(Refer to Figure II.2.5 for the location of strain gages SGT1 and SGT2, and refer to Table II.5.1 for the properties of the CDS4 Panel)

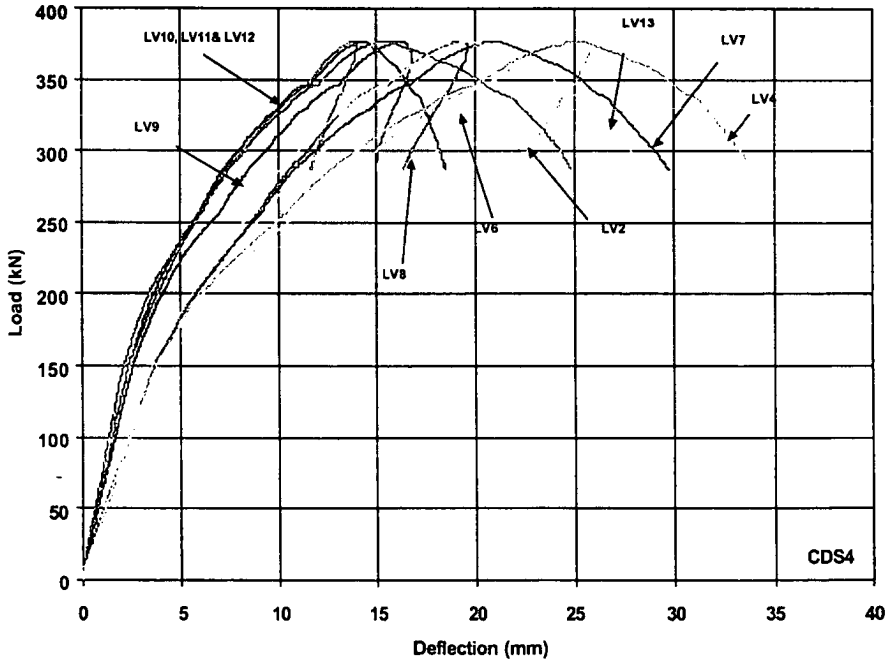

Figure II.5.10 Load vs Deflection for Loading to Failure for the Deck Panel CDS4
(Refer to Figure II.2.7 for the location of LVDT's LV2, LV4, LV6, LV7, LV8, LV9, LV10, LV11, LV12 and LV13, and refer to Table II.5.1 for the properties of the CDS4 Panel)

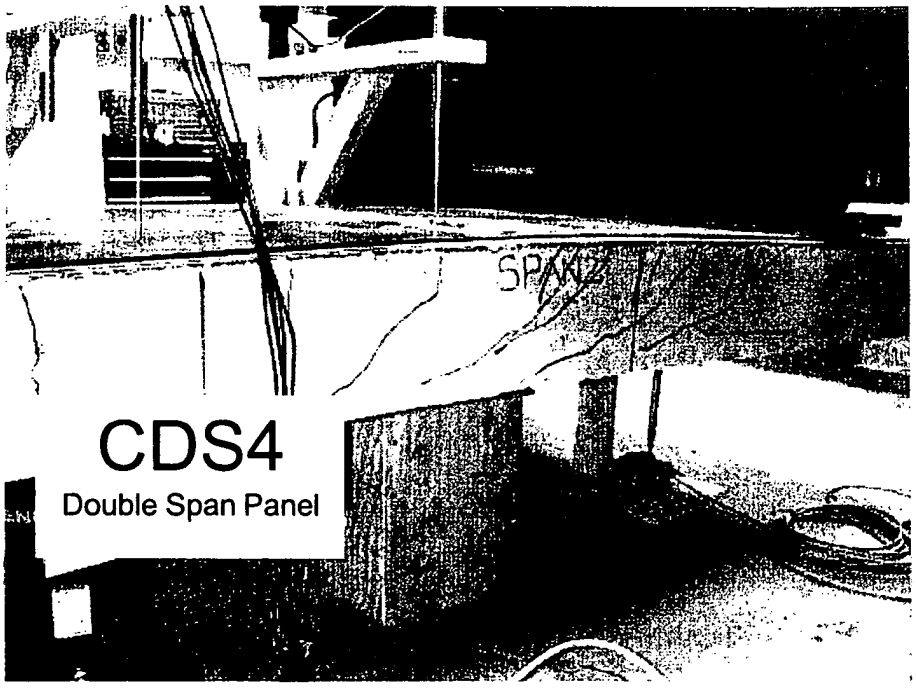

Figure II.5.11 Failure Pattern of the Deck Panel CDS4

II.6 SCRIMP F DECK - HA CO COMPOSITES

II.6.1 Summary

The single span Scrimp FRP Deck - Hardcore Composites (HC) panels satisfy the flexure-strain criteria but do not satisfy the deflection criteria (Measured deflection/allowable deflection = 1.029 to 1.059, Table II.6.2). The double span deck panel satisfies the deflection criteria and flexure criteria.

The following flexural rigidity (EI) and shear rigidity (GA_w) are recommended for use in modeling the First Salem Bridge: EI = 1.157 x 10^7 N-m^2 (4.031 x 10^9 lb-in^2) and GA_w = 1.394 x 10^7 N (3.134 x 10^6 lb).

II.6.2 Introduction

The Scrimp FRP Deck - Hardcore Composites fiberglass panels are fabricated using the "cell core" technology in conjunction with SCRIMP (Seeman Composite Resin Infusion Molding Process). The cell core is a foam or plastic form that is wrapped with fiberglass fabric to create an internal lattice structure for the composite deck. The composite deck is comprised of multiple wrapped cells with upper and lower fiberglass fabric skin faces (Figure II.6.1). The multiple wrapped cells form the longitudinal and transverse stiffening webs, create a deck with bi-directional stiffness. The length, effective length (distance between centerlines of supports), width and thickness of all single span and double span deck panels are presented in Table II.6.1. The single span panels are designated as HC1, HC2 and HC3, and the double span panel is designated as HC4 (Table II.6.1). The single and double span panels are loaded as per the steps outlined in section II.2.3.

II.6.3 Specimen HC1 – 2.44 m (8 ft) Panel

The load vs strain curves and load vs deflection curves for loading step 4 are presented for deck panel HC1 in Figures II.6.2 and II.6.3.

The maximum centerline deflection at the applied service load of 58.38 kN/m (4,000 lb/ft) of width, the maximum strain at service load (LL+IM+DL) and maximum strain at dead load (DL) are presented in Table II.6.2. The baseline deflection, allowable deflection as per deflection criteria and allowable strain as per the flexure criteria specified by ODOT are also presented in Table II.6.2.

The ultimate load, maximum deflection at ultimate load, and mode of failure are presented in Table II.6.3. The ultimate load is compared with the required load in Table II.6.3 as per the flexure criteria specified by ODOT. The ultimate load and maximum deflection at ultimate load are also compared with their respective baseline ultimate load and maximum deflection (Table II.6.3).

The load vs deflection plots show that the stiffness of the deck remains constant during the cyclic loading. For the failure load in step 4, the load vs deflection curve (Figure II.6.3) indicates that the deck panel fails at 885,850 N (199,147 lb).

While loading the deck panel, cracking sound resulting from delamination of the fabric is observed starting at a load of 127,929 N (40,000 lb) to failure. At the time of failure, a blast like sound is heard and the deck panel started load shedding, and failure is observed to be sudden. Failure of the deck panel is due to web buckling nearer to quarter span from the support A (Figure II.2.2) followed by delamination of upper face skin from the wrapped cell core. No punching at the loading point is seen on the deck panel. After releasing the load, the deck panel did not return to its original shape. The flexural and shear rigidities (EI and GA_w respectively) for the deck panel are determined by different techniques (Refer chapter II.2.5 for the equations used). The calculated values are presented in Table II.6.4.

II.6.4 Specimen HC2 – 2.74 m (9 ft) Panel

The load vs strain curves and load vs deflection curves for loading step 4 are presented for deck panels HC2 in Figures II.6.4 and II.6.5.

The maximum centerline deflection at the applied service load of 58.38 kN/m (4,000 lb/ft) of width, the maximum strain at service load (LL+IM+DL) and maximum strain at dead load (DL) are presented in Table II.6.2. The baseline deflection, allowable deflection as per deflection criteria and allowable strain as per the flexure criteria specified by ODOT are also presented in Table II.6.2.

The ultimate load, maximum deflection at ultimate load, and mode of failure are presented in Table II.6.3. The ultimate load is compared with the required load in Table II.6.3 as per the flexure criteria specified by ODOT. The ultimate load and maximum deflection at ultimate load are also compared with their respective baseline ultimate load and maximum deflection (Table II.6.3).

The load vs deflection plots show that the stiffness of the deck remains constant during the cyclic loading. For the failure load in step 4, the load vs strain curve (Figure II.6.4) indicates that the deck panel fails at 819,394 N (184,207 lb).

While loading the deck panel, cracking sound resulting from delamination of the fabric is observed starting at a load of 155,688 N (35,000 lb) to failure. At the time of failure, a blast like sound is heard and the deck panel started load shedding, and failure is observed to be sudden. Failure of the deck panel is due to web buckling at quarter span from support B (Figure II.2.2) followed by delamination of fiberglass fabric from the wrapped cell core only at the support B. After releasing the load, the deck panel did not return to its original shape. The flexural and shear rigidities (EI and GA_w respectively) for the deck panel are determined by different techniques (Refer chapter II.2.5 for the equations used). The calculated values are presented in Table II.6.4.

II.6.5 Specimen HC3 – 3.05 m (10 ft) Panel

The load vs strain curves and load vs deflection curves for loading step 4 are presented for deck panels HC3 in Figures II.6.6 and II.6.7.

The maximum centerline deflection at the applied service load of 58.38 kN/m (4,000 lb/ft) of width, the maximum strain at service load (LL+IM+DL) and maximum strain at dead load (DL) are presented in Table II.6.2. The baseline deflection, allowable deflection as per deflection criteria and allowable strain as per the flexure criteria specified by ODOT are also presented in Table II.6.2.

The ultimate load, maximum deflection at ultimate load and mode of failure are presented in Table II.6.3. The ultimate load is compared with the required load in Table II.6.3 as per the flexure criteria specified by ODOT. The ultimate load and maximum deflection at ultimate load are also compared with their respective baseline ultimate load and maximum deflection (Table II.6.3).

The load vs deflection plots show that the stiffness of the deck remains constant during the cyclic loading. For the failure load in step 4, the load vs deflection curve (Figure II.6.7) indicates that the deck panel fails at 762,074 N (171,321 lb).

While loading the deck panel, cracking sound resulting from delamination of the fabric is observed starting at a load of 177,929 N (40,000 lb) to failure. At the time of failure, a blast like sound is heard and the deck panel started load shedding, and failure is observed to be sudden. Failure of the deck panel is due to web buckling nearer to mid span followed by the delamination of lower face skin from the wrapped cell core. A portion of fabric in lower face skin at the loading point squeezed out and is shown in Figure II.6.8. After releasing the load, the deck panel did not return to its original shape. The flexural and shear rigidities (EI and GA_w respectively) for the deck panel are determined by different techniques (Refer chapter II.2.5 for the equations used). The calculated values are presented in Table II.6.4.

II.6.6 Specimen HC4 – Double Span Panel

The load vs strain curves and load vs deflection curves for loading step 4 are presented for deck panels HC4 in Figures II.6.9 and II.6.10.

The maximum centerline deflections at the applied service load of 58.38 kN/m (4,000 lb/ft) of width, the maximum strain at service load (LL+IM+DL) and maximum strain at dead load (DL) are presented in Table II.6.2. The baseline deflection, allowable deflection as per deflection criteria and allowable strain as per the flexure criteria specified by ODOT are also presented in Table II.6.2.

The ultimate load, maximum deflection at ultimate load, and mode of failure are presented in Table II.6.3. The ultimate load is compared with the required load in Table II.6.3 as per the flexure

criteria specified by ODOT. The ultimate load and maximum deflection at ultimate load are also compared with their respective baseline ultimate load and maximum deflection (Table II.6.3).

The load vs deflection plots show that the stiffness of the deck remains constant during the cyclic loading. For the failure load in step 4, the load vs deflection curve (Figure II.6.10) indicates that the deck panel fails at 946,195 N (212,713 lb).

While loading the deck panel cracking sound resulting from delamination of the fabric is observed starting at a load of 222,411 N (50,000 lb) to failure. At the time of failure, a blast like sound is heard and the deck panel started load shedding, and failure is observed to be sudden. Failure of the deck panel is due to web buckling nearer to middle support B (Figure II.2.3) followed by the delamination of lower face skin from the wrapped cell core and is shown in Figure II.6.11. The flexural and shear rigidities (EI and GA_w respectively) for the deck panel are determined by different techniques (Refer chapter II.2.5 for the equations used). The calculated values are presented in Table II.6.4.

Table II.6.1 Scrimp FRP Deck - Hardcore Composites Panels

Specimen Identification	Length (m)	Effective Length[a] (m)	Width (m)	Thickness[b] (m)	Remarks
(1)	(2)	(3)	(4)	(5)	(6)
HC1	2.74	2.44	0.91	0.216	Each specimen possessed some minor deformations (waviness) along the top and bottom surfaces.
HC2	3.35	3.05	0.91	0.229	
HC3	3.96	3.66	0.91	0.241	
HC4 (Double Span)	6.10	2.74 (each span)	0.91	0.203	

[a] Distance between centerline of supports (Figures II.2.2 and II.2.3).

[b] Average thickness.

Note: The effective span is 2.667 m (105 in) for the First Salem Bridge over the Great Miami River in Montgomery County, Ohio.

Table II.6.2 Deflections and Strains for Scrimp FRP Deck - Hardcore Composites Panels

Specimen Identification[a]	Centerline Deflection @ Applied Service Load of 58.38 kN/m of Width (mm)			Maximum Strain @ (LL+IM+DL)		Maximum Strain @ DL	
	Measured[b]	Baseline[c]	Allowable[d]	Measured[e]	Allowable[f]	Measured[e]	Allowable[f]
(1)	(2)	(3)	(4)	(5)	(6)	(7)	(8)
HC1 (2.44 m)	3.353	3.607	3.175	0.001230	0.004100	0.000091	0.002050
HC2 (3.05 m)	4.572	5.029	4.318	0.001188	0.004100	0.000102	0.002050
HC3 (3.66 m)	6.274	6.731	6.096	0.001400	0.004100	0.000156	0.002050
HC4 Span1[g] (2.74 m)	2.515	1.372	4.572	0.001205[h]	0.004100	0.000176[h]	0.002050
HC4 Span2[g] (2.74 m)	2.565	1.499	4.572				

[a] Effective span is shown in parentheses.
[b] The centerline deflections are derived by interpolation from the baseline deflection curves.
[c] The baseline deflection is obtained from tests conducted on the baseline panels (Table II.3.2).
[d] The allowable deflections are provided by the Ohio Department of Transportation.
[e] The centerline strains are derived by interpolation from the baseline strain curves*.
[f] The allowable strain = 20% of maximum strain of the FRP coupon test (Refer Section I, Tables I.8.1 and I.8.2).
[g] Span 1 and span 2 for the two span panel are shown in Figure II.2.5.
[h] The maximum strain is measured along the middle support in the double span panel *.
* The strains are measured at 285.8 mm (11.25 inches) on both sides from the centerline of the panels (Figures II.2.4 and II.2.5).
Note: The effective span for the First Salem Bridge is 2.667 m (105 in).

Table II.6.3 Load at Failure, Maximum Deflection , and Mode of Failure for Scrimp FRP Deck - Hardcore Composites Panels

Specimen Identification[a]	Ultimate Load (N)			Maximum Deflection at Ultimate Load [c] (mm)		Mode of Failure
	Measured	Baseline	Required[b]	Measured	Baseline	
(1)	(2)	(3)	(4)	(5)	(6)	(7)
HC1 (2.44 m)	885,717	189,859	524,552	65.96	29.79	Web buckling and delamination
HC2 (3.05 m)	819,394	197,781	530,575	74.14	33.35	Web buckling and delamination
HC3 (3.66 m)	762,074	181,652	536,758	98.98	41.61	Web buckling and delamination
HC4 Span1 [d] (2.74 m)	946,195	243,380	526,972	50.19	29.19	Web buckling and delamination
HC4 Span2 [d] (2.74 m)	946,195	243,380	526,972	51.74	21.92	

[a] Effective span is shown in parentheses.

[b] Required ultimate load = 2 x 1.3 [1.67(LL+IM)+DL)].

[c] The measured and baseline maximum deflections do not occur under the same load. Refer to columns (2) and (3) of this table for the magnitude of load at failure.

[d] Span 1 and span 2 for the two span panel are shown in Figure II.2.5.

Note: The effective span for the First Salem Bridge is 2.667 m (105 in).

Table II.6.4 Flexural and Shear Rigidities for Scrimp FRP Deck – Hardcore Composites Panels

Specimen Identification	Effective Length (m)	Flexural Rigidity			Shear Rigidity
		EI [1] (N-m^2)	EI [2] (N-m^2)	EI [3] (N-m^2)	GA_w [4] (N)
(1)	(2)	(3)	(4)	(5)	(6)
HC1	2.44	5.613×10^6	6.288×10^6	4.784×10^6	6.530×10^7
HC2	3.05	8.480×10^6	9.278×10^6	6.850×10^6	4.604×10^7
HC3	3.66	9.864×10^6	1.033×10^7	8.687×10^6	6.526×10^7
HC4 (Double Span panel)	2.74 (Span 1)	1.212×10^7	6.021×10^6	3.983×10^6	1.351×10^7
	2.74 (Span 2)	1.101×10^7	7.051×10^6	4.009×10^6	1.437×10^7
	Average of Spans 1 & 2	1.157×10^7 (recommended [5])	6.537×10^6	3.996×10^6	1.394×10^7 (recommended [6])

[1] Flexural rigidity by considering shear deformation (derived from experimental deflection).

[2] Flexural rigidity from moment-curvature relationship (derived from experimental strain).

[3] Flexural rigidity without considering shear deformation (derived from experimental deflection).

[4] Shear rigidity based on first order shear deformation equation (derived from experimental deflection)

[5] This flexural rigidity (EI) is recommended for use in modeling the First Salem Bridge.

[6] This shear rigidity (GA_w)is recommended for use in modeling the First Salem Bridge.

Note: The effective span is 2.667 m (105 in) for the First Salem Bridge over the Great Miami River in Montgomery County, Ohio.

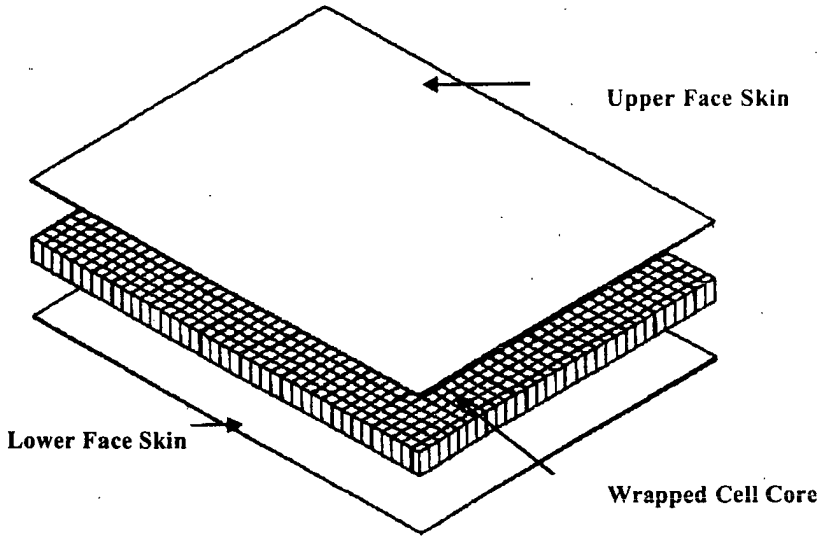

Figure II.6.1 Components of Fiberglass Deck Panel

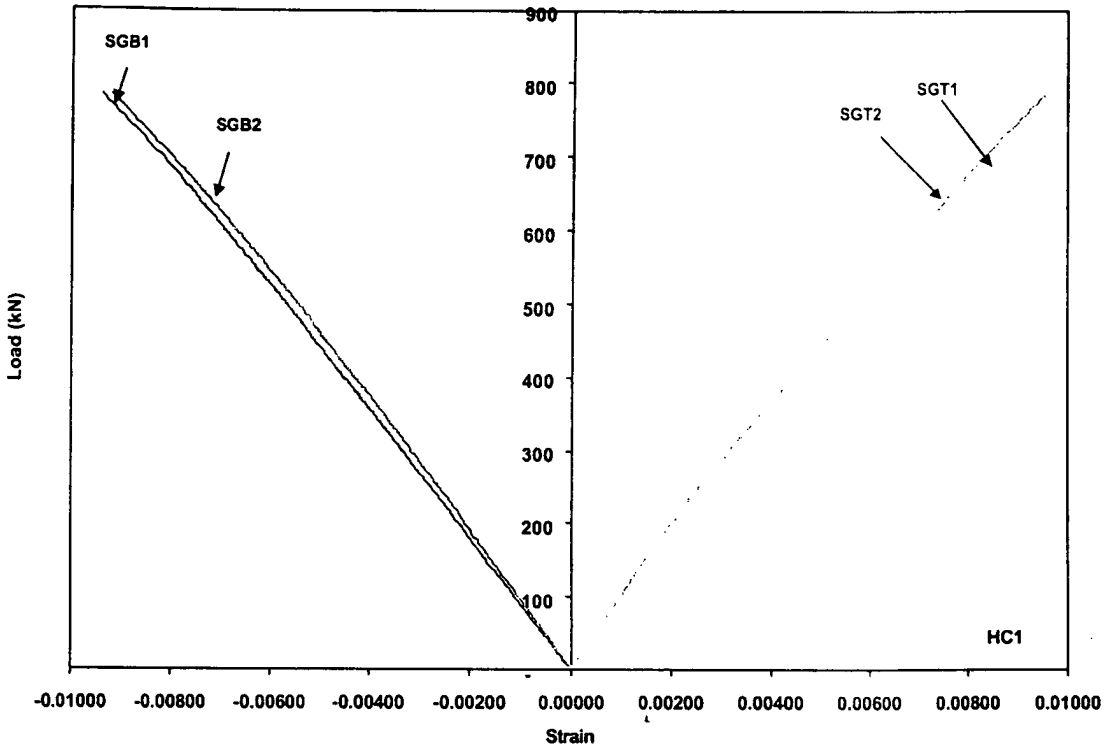

Figure II.6.2 Load vs Strain for Loading to Failure for the Deck Panel HC1
(Refer to Figure II.2.4 for the location of strain gages SGT1 and SGT2, and refer to Table II.6.1 for the properties of the HC1 Panel)

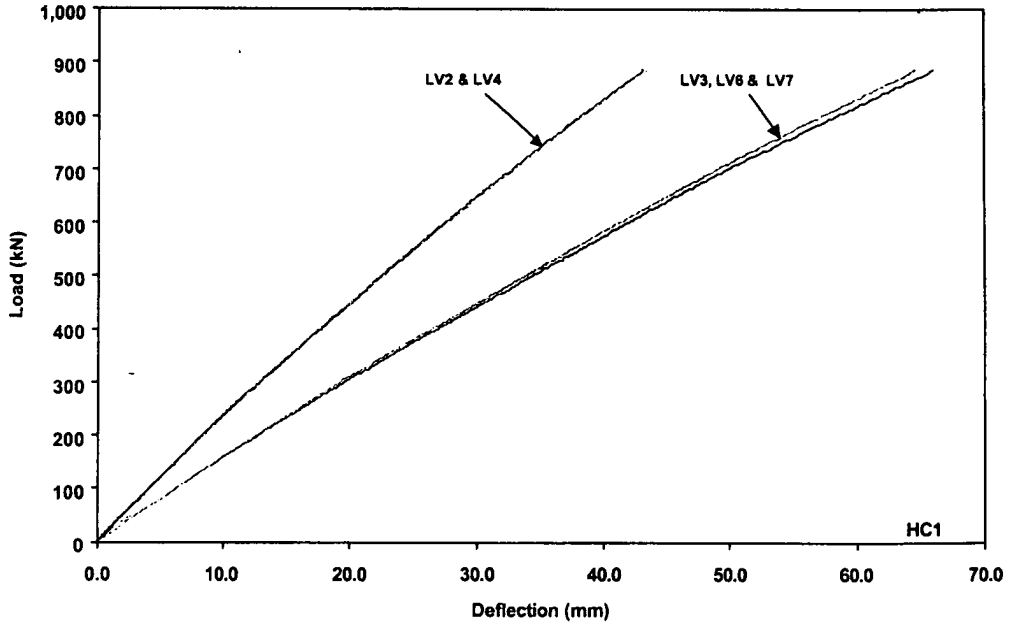

Figure II.6.3 Load vs Deflection for Loading to Failure for the Deck Panel HC1
(Refer to Figure II.2.6 for the location of LVDT's LV2, LV3, LV4, LV6 and LV7, and refer to Table II.6.1 for the properties of the HC1 Panel)

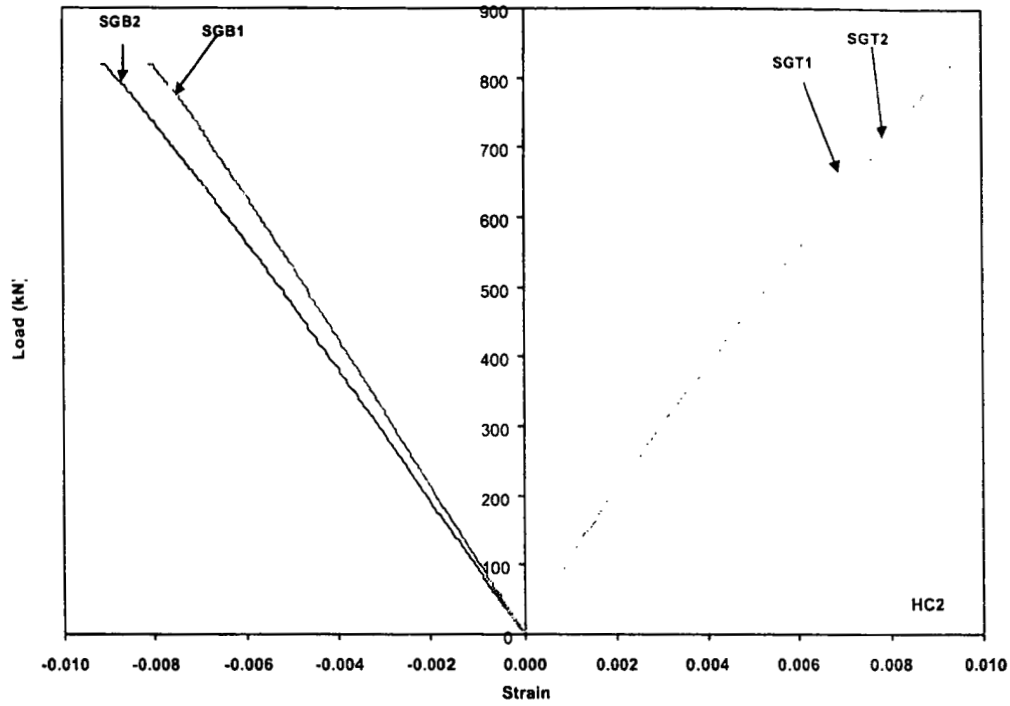

Figure II.6.4 Load vs Strain for Loading to Failure for the Deck Panel HC2
(Refer to Figure II.2.4 for the location of strain gages SGT1 and SGT2, and refer to Table II.6.1 for the properties of the HC2 Panel)

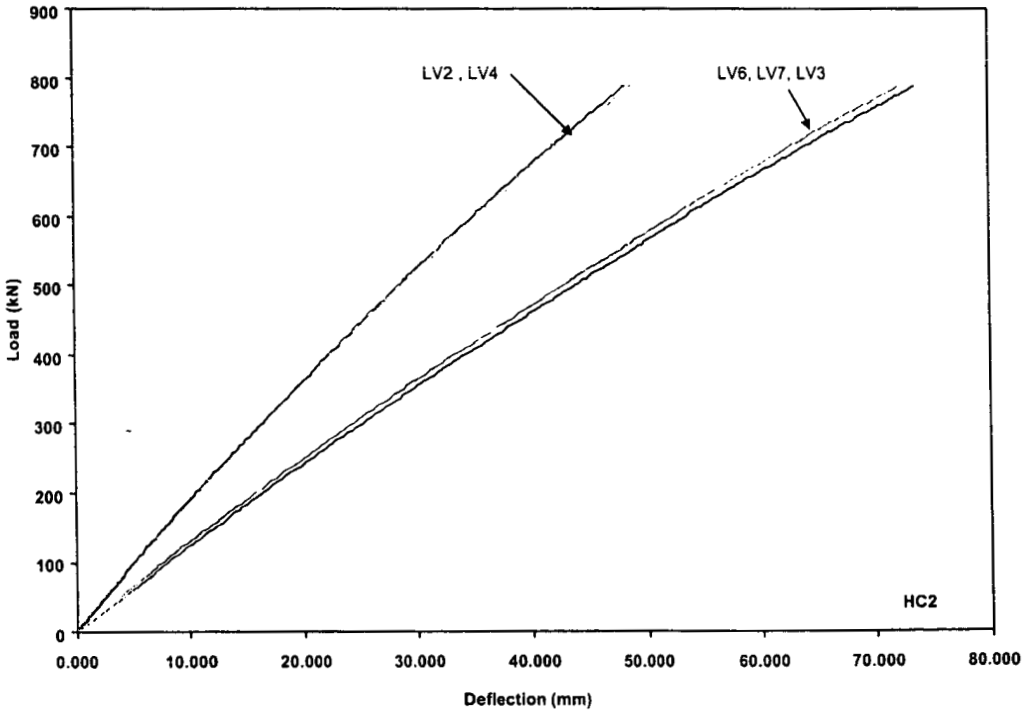

Figure II.6.5 Load vs Deflection for Loading to Failure for the Deck Panel HC2
(Refer to Figure II.2.6 for the location of LVDT's LV2, LV3, LV4, LV6 and LV7, and refer to Table II.6.1 for the properties of the HC2 Panel)

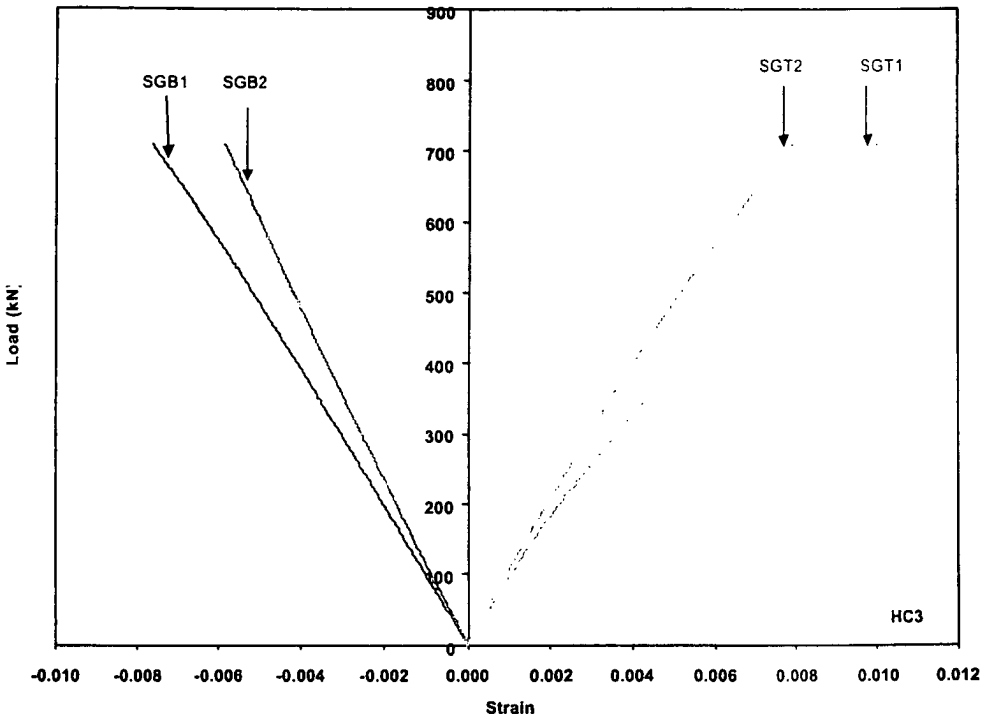

Figure II.6.6 Load vs Strain for Loading to Failure for the Deck Panel HC3
(Refer to Figure II.2.4 for the location of strain gages SGT1 and SGT2, and refer to Table II.6.1 for the properties of the HC3 Panel)

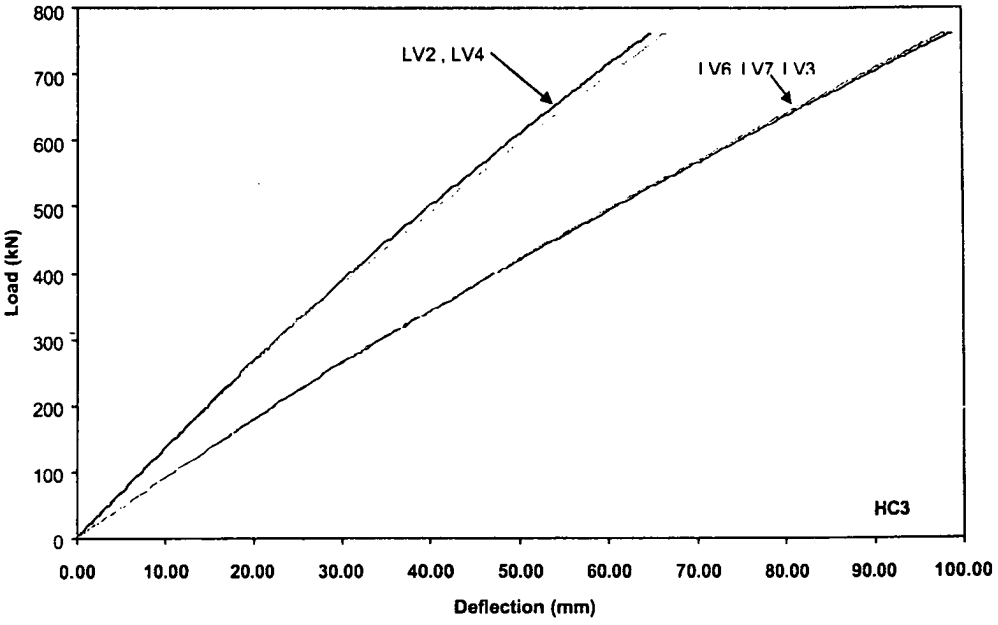

Figure II.6.7 Load vs Deflection for Loading to Failure for the Deck Panel HC3
(Refer to Figure II.2.6 for the location of LVDT's LV2, LV3, LV4, LV6 and LV7, and refer to Table II.6.1 for the properties of the HC3 Panel)

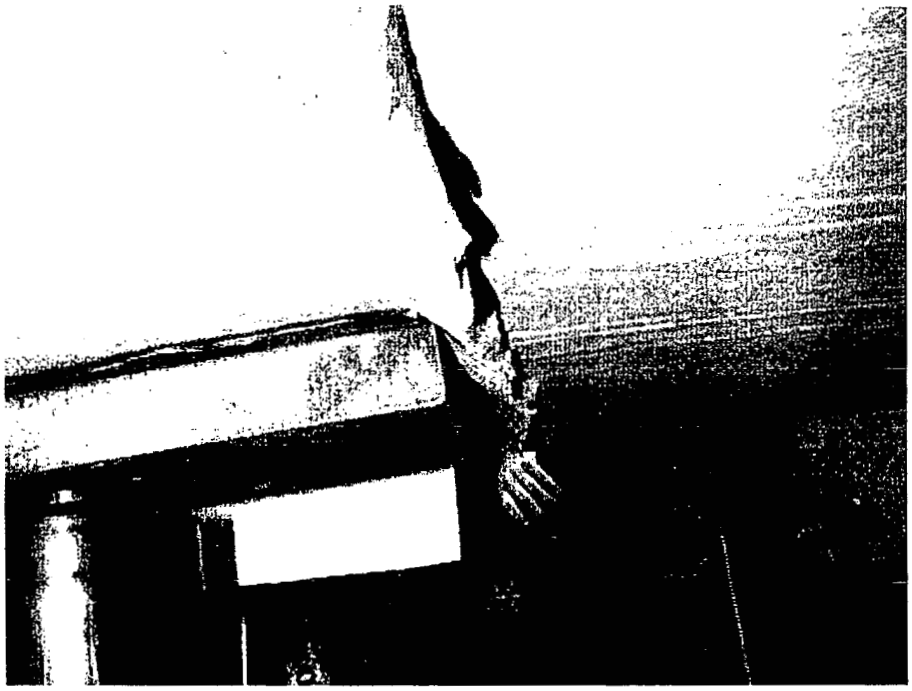

Figure II.6.8 Squeezing of Lower Face Skin in Deck Panel HC3

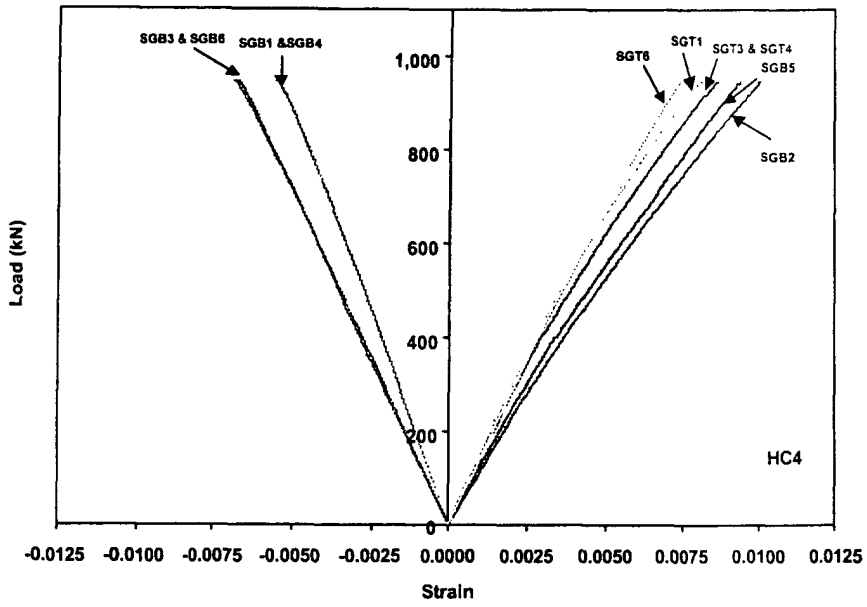

Figure II.6.9 Load vs Strain for Loading to Failure for the Deck Panel HC4
(Refer to Figure II.2.5 for the location of strain gages SGT1 and SGT2, and refer to Table II.6.1 for the properties of the HC4 Panel)

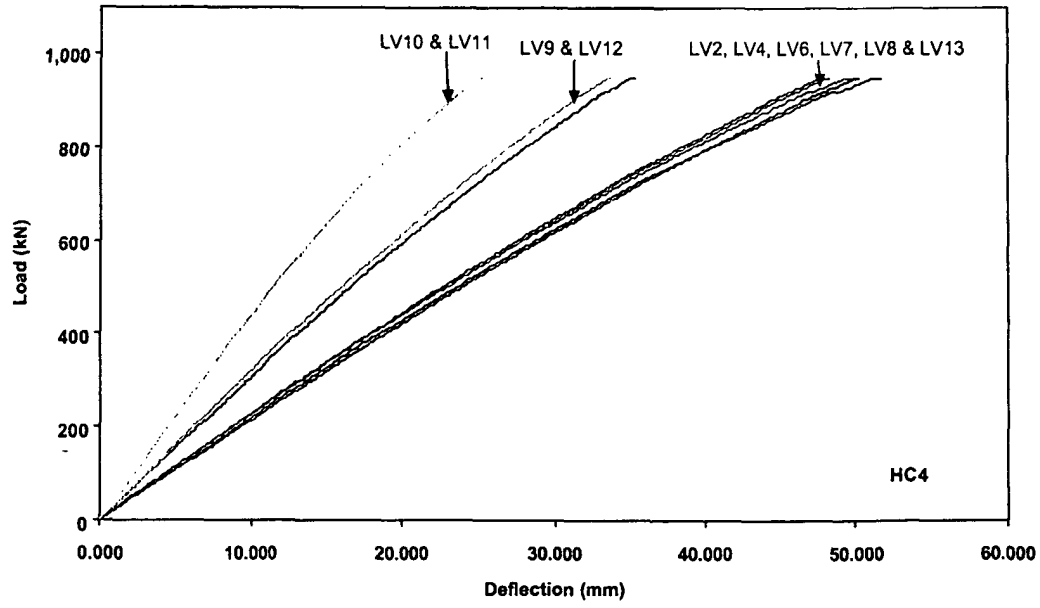

Figure II.6.10 Load vs Deflection for Loading to Failure for the Deck Panel HC4
(Refer to Figure II.2.7 for the location of LVDT's LV2, LV4, LV6, LV7, LV8, LV9, LV10, LV11, LV12 and LV13, and refer to Table II.6.1 for the properties of the HC4 Panel)

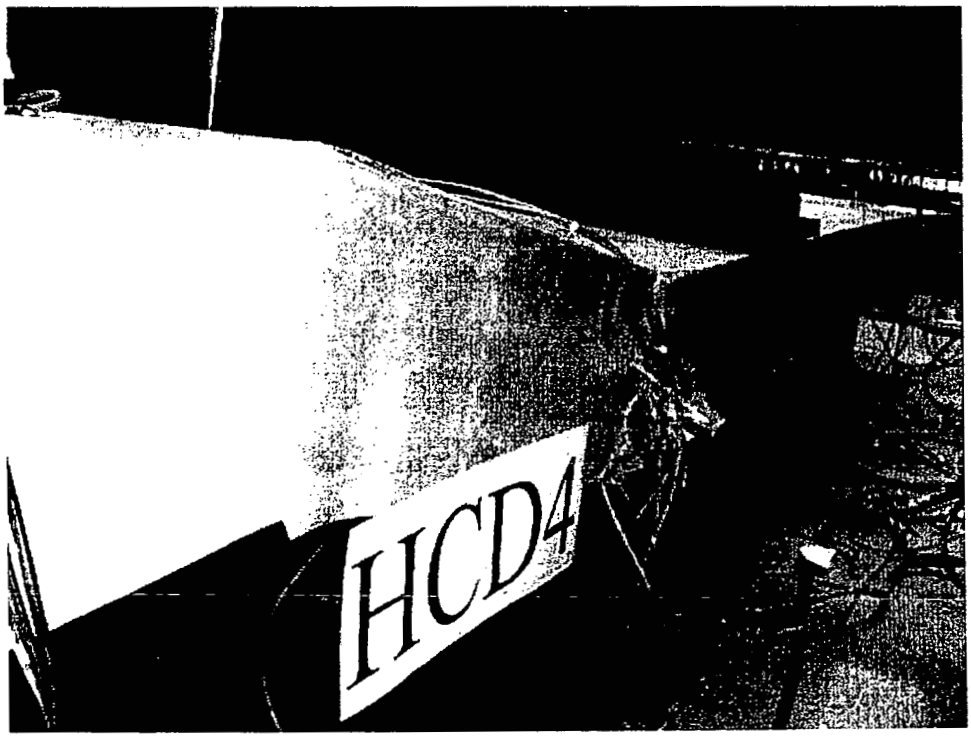

Figure II.6.11 Failure Pattern of the Deck Panel HC4

II.7 CONTACT MOLDING HAND LAY-UP FRP DECK - INFRASTRUCTURE COMPOSITES INTERNATIONAL

II.7.1 Summary

The single span Contact Molding Hand Lay-up FRP deck - Infrastructure Composites International (ICI) panels satisfy the deflection criteria and flexure criteria. The double span deck panel satisfies the deflection criteria and strain limits specified in the flexure criteria but does not satisfy the required ultimate load specified in the flexure criteria (Measured ultimate load = 483,473 N (108,689 lb), required ultimate load = 528,431 N (118,796 lb), Table II.7.3).

The following flexural rigidity (EI) and shear rigidity (GA_w) are recommended for use in modeling the First Salem Bridge: EI = 1.665 x 10^7 N-m^2 (5.802 x 10^9 lb-in^2) and GA_w = 1.809 x 10^7 N (4.066 x 10^6 lb).

II.7.2 Introduction

The Contact Molding Hand Lay-up FRP deck - Infrastructure Composites International (ICI) fiberglass panels consist of the core craft corrugated core sandwich system. The basic system is a single-tier sandwich panel with a standard core configuration (Figure II.7.1). The flats of the core will be in the direction normal to traffic flow. The longitudinal direction of the panels will be perpendicular to the traffic flow (Figure II.7.2). The length, effective length (distance between centerlines of supports), width and thickness of all single span and double span deck panel are presented in Table II.7.1. The single span panels are designated as ICI1, ICI2 and ICI3, and the double span panel is designated as ICI4 (Table II.7.1). The single and double span panels are loaded as per the steps outlined in section II.2.3.

II.7.3 Specimen ICI1 – 2.44 m (8 ft) Panel

The load vs strain curves and load vs deflection curves for loading step 4 are presented for deck panel ICI1 in Figures II.7.3 and II.7.4.

The maximum centerline deflection at the applied service load of 58.38 kN/m (4,000 lb/ft) of width, the maximum strain at service load (LL+IM+DL) and maximum strain at dead load (DL) are presented in Table II.7.2. The baseline deflection, allowable deflection as per deflection criteria and allowable strain as per the flexure criteria specified by ODOT are also presented in Table II.7.2.

The ultimate load, maximum deflection at ultimate load, and mode of failure are presented in Table II.7.3. The ultimate load is compared with the required load in Table II.7.3 as per the flexure criteria specified by ODOT. The ultimate load and maximum deflection at ultimate load are also compared with their respective baseline ultimate load and maximum deflection (Table II.7.3).

The load vs deflection plots show that the stiffness of the deck remains constant during the cyclic loading. For the failure load in step 4, the load vs deflection curve (Figure II.7.4) indicates that the deck panel fails at 593,540 N (133,433 lb).

While loading cracking sound resulting from the delamination of the panel is observed starting at a load of 177,929 N (40,000 lb) to failure. At the time of failure, a blast like sound is heard and the deck panel started load shedding, and failure is observed to be sudden. Failure of the deck panel is due to the delamination on the compression side. After releasing the load, the deck panel returns to its original shape and looks like the original untested specimen. The flexural and shear rigidities (EI and GA_w respectively) for the deck panel are determined by different techniques (Refer chapter II.2.5 for the equations used). The calculated values are presented in Table II.7.4.

II.7.4 Specimen ICI2 – 2.74 m (9 ft) Panel

The load vs strain curves and load vs deflection curves for loading step 4 are presented for deck panel ICI2 in Figures II.7.5 and II.7.6.

The maximum centerline deflection at the applied service load of 58.38 kN/m (4,000 lb/ft) of width, the maximum strain at service load (LL+IM+DL) and maximum strain at dead load (DL) are presented in Table II.7.2. The baseline deflection, allowable deflection as per deflection criteria and allowable strain as per the flexure criteria specified by ODOT are also presented in Table II.7.2.

The ultimate load, maximum deflection at ultimate load, and mode of failure are presented in Table II.7.3. The ultimate load is compared with the required load in Table II.7.3 as per the flexure criteria specified by ODOT. The ultimate load and maximum deflection at ultimate load are also compared with their respective baseline ultimate load and maximum deflection (Table II.7.3).

The load vs deflection plots show that the stiffness of the deck remains constant during the cyclic loading. For the failure load in step 4, the load vs deflection curve (Figure II.7.6) indicates that the deck panel fails at 719,313 N (161,708 lb).

While loading cracking sound resulting from the delamination of the fabric is observed starting at a load of 177,929 N (40,000 lb) to failure. At the time of failure, a blast like sound is heard and the deck panel started load shedding, and failure is observed to be sudden. Failure of the deck panel is due to the delamination on the compression side. After releasing the load, the deck panel returns to its original shape and looks like the original untested specimen. The flexural and shear rigidities (EI and GA_w respectively) for the deck panel are determined by different techniques (Refer chapter II.2.5 for the equations used). The calculated values are presented in Table II.7.4.

II.7.5 Specimen ICI3 – 3.05 m (10 ft) Panel

The load vs strain curves and load vs deflection curves for loading step 4 are presented for deck panel ICI3 in Figures II.7.7 and II.7.8.

The maximum centerline deflection at the applied service load of 58.38 kN/m (4,000 lb/ft) of width, the maximum strain at service load (LL+IM+DL) and maximum strain at dead load (DL) are presented in Table II.7.2. The baseline deflection, allowable deflection as per deflection criteria and allowable strain as per the flexure criteria specified by ODOT are also presented in Table II.7.2.

The ultimate load, maximum deflection at ultimate load, and mode of failure are presented in Table II.7.3. The ultimate load is compared with the required load in Table II.7.3 as per the flexure criteria specified by ODOT. The ultimate load and maximum deflection at ultimate load are also compared with their respective baseline ultimate load and maximum deflection (Table II.7.3).

The load vs deflection plots show that the stiffness of the deck remains constant during the cyclic loading. For the failure load in step 4, the load vs deflection curve (Figure II.7.8) indicates that the deck panel fails at 833,592 N (187,399 lb).

While loading the deck panel, cracking sound resulting from the delamination of the fabric is observed starting at a load of 222,411 N (50,000 lb) to failure. At the time of failure, a blast like sound is heard and the deck panel started load shedding, and failure is observed to be sudden. Failure of the deck panel is due to web buckling and delaminations on the compression and tension sides (Figure II.7.9). After releasing the load, the deck panel did not return to its original shape. The flexural and shear rigidities (EI and GA_w respectively) for the deck panel are determined by different techniques (Refer chapter II.2.5 for the equations used). The calculated values are presented in Table II.7.4.

II.7.6 Specimen ICI4 – Double Span Panel

The load vs strain curves and load vs deflection curves for loading step 4 are presented for deck panel ICI4 in Figures II.7.10 and II.7.11.

The maximum centerline deflections at the applied service load of 58.38 kN/m (4,000 lb/ft) of width, the maximum strain at service load (LL+IM+DL) and maximum strain at dead load (DL) are presented in Table II.7.2. The baseline deflection, allowable deflection as per deflection criteria and allowable strain as per the flexure criteria specified by ODOT are also presented in Table II.7.2.

The ultimate load, maximum deflection at ultimate load, and mode of failure are presented in Table II.7.3. The ultimate load is compared with the required load in Table II.7.3 as per the flexure criteria specified by ODOT. The ultimate load and maximum deflection at ultimate load are also compared with their respective baseline ultimate load and maximum deflection (Table II.7.3).

The load vs deflection plots show that the stiffness of the deck remains constant during the cyclic loading. For the failure load in step 4, the load vs deflection curve (Figure II.7.11) indicates that the deck panel fails at 483,473 N (108,689 lb).

While loading the deck panel, cracking sound resulting from the delamination of the panels is observed starting at a load of 280,238 N (63,000 lb) to failure. At the time of failure, a blast like sound is heard and the deck panel started load shedding, and failure is observed to be sudden. Failure of the deck panel is due to delamination close to the middle support B (Figure II.2.3) and is shown in Figure II.7.12. After releasing the load, the deck panel returns to its original shape and looks like the original untested specimen. The flexural and shear rigidities (EI and GA_w respectively) for the deck panel are determined by different techniques (Refer chapter II.2.5 for the equations used). The calculated values are presented in Table II.7.4.

Table II.7.1 Contact Molding Hand Lay-up FRP Deck Infrastructure Composites International Panels

Specimen Identification	Length (m)	Effective Length[a] (m)	Width (m)	Thickness[b] (m)	Remarks
(1)	(2)	(3)	(4)	(5)	(6)
ICI1	2.74	2.44	0.91	0.211	Each specimen possessed some minor deformations (waviness) along the top and bottom surfaces.
ICI2	3.35	3.05	0.91	0.241	
ICI3	3.96	3.66	0.91	0.249	
ICI4 (Double Span)	6.10	2.74 (each span)	0.91	0.203	

[a] Distance between centerline of supports (Figures II.2.2 and II.2.3).
[b] Average thickness.
Note: The effective span is 2.667 m (105 in) for the First Salem Bridge over the Great Miami River in Montgomery County, Ohio.

Table II.7.2 Deflections and Strains for Contact Molding Hand Lay-up FRP Deck Infrastructure Composites International Panels

Specimen Identification[a]	Centerline Deflection @ Applied Service Load of 58.38 kN/m of Width (mm)			Maximum Strain @ (LL+IM+DL)		Maximum Strain @ DL	
	Measured[b]	Baseline[c]	Allowable[d]	Measured[e]	Allowable[f]	Measured[e]	Allowable[f]
(1)	(2)	(3)	(4)	(5)	(6)	(7)	(8)
ICI1 (2.44 m)	2.311	3.607	3.175	0.000974	0.004200	0.000069	0.002100
ICI2 (3.05 m)	3.277	5.029	4.318	0.001011	0.004200	0.000094	0.002100
ICI3 (3.66 m)	4.394	6.731	6.096	0.001118	0.004200	0.000118	0.002100
ICI4 Span1[g] (2.74 m)	1.854[g]	1.372	4.572	0.000932[h]	0.004200	0.000130[h]	0.002100
ICI4 Span2[g] (2.74 m)	1.905[g]	1.499	4.572				

[a] Effective span is shown in parentheses.
[b] The centerline deflections are derived by interpolation from the baseline deflection curves.
[c] The baseline deflection is obtained from tests conducted on the baseline panels (Table II.3.2).
[d] The allowable deflections are provided by the Ohio Department of Transportation.
[e] The centerline strains are derived by interpolation from the baseline strain curves*.
[f] The allowable strain = 20% of maximum strain of the FRP coupon test (Refer Section I, Tables I.8.1 and I.8.2).
[g] Span 1 and span 2 for the two span panel are shown in Figure II.2.5.
[h] The maximum strain is measured along the middle support in the double span panel *.
* The strains are measured at 285.8 mm (11.25 inches) on both sides from the centerline of the panels (Figures II.2.4 and II.2.5).
Note: The effective span for the First Salem Bridge is 2.667 m (105 in).

Table II.7.3 Load at Failure, Maximum Deflection, and Mode of Failure for Contact Molding Hand Lay-up FRP Deck – Infrastructure Composites International Panels

Specimen Identification[a]	Ultimate Load (N)			Maximum Deflection at Ultimate Load [c] (mm)		Mode of Failure
	Measured	Baseline	Required[b]	Measured	Baseline	
(1)	(2)	(3)	(4)	(5)	(6)	(7)
ICI1 (2.44 m)	593,540	189,859	525,762	26.65	29.79	Delamination
ICI2 (3.05 m)	719,313	197,781	532,915	49.28	33.35	Delamination
ICI3 (3.66 m)	833,592	181,652	539,436	76.36	41.61	Web-buckling and delamination
ICI4 Span1 [d] (2.74 m)	483,473	243,380	528,431	17.60	29.19	Delamination
ICI4 Span2 [d] (2.74 m)	483,473	243,380	528,431	17.50	21.92	

[a] Effective span is shown in parentheses.

[b] Required ultimate load = 2 x 1.3 [1.67(LL+IM)+DL)].

[c] The measured and baseline maximum deflections do not occur under the same load. Refer to columns (2) and (3) of this table for the magnitude of load at failure.

[d] Span 1 and span 2 for the two span panel are shown in Figure II.2.5.

Note: The effective span for the First Salem Bridge is 2.667 m (105 in).

Table II.7.4 Flexural and Shear Rigidities for Contact Molding Hand Lay-up FRP Deck - Infrastructure Composites International Panels

Specimen Identification	Effective Length (m)	Flexural Rigidity			Shear Rigidity
		EI [1] ($N\text{-}m^2$)	EI [2] ($N\text{-}m^2$)	EI [3] ($N\text{-}m^2$)	GA [4] (N)
(1)	(2)	(3)	(4)	(5)	(6)
ICI1	2.44	9.404×10^6	9.657×10^6	6.962×10^6	5.409×10^7
ICI2	3.05	1.068×10^7	1.190×10^7	9.611×10^6	1.237×10^8
ICI3	3.66	1.430×10^7	1.334×10^7	1.241×10^7	8.456×10^7
ICI4 (Double Span Panel)	2.74 (Span 1)	1.586×10^7	9.307×10^6	5.444×10^6	1.888×10^7
	2.74 (Span 2)	1.744×10^7	8.934×10^6	5.289×10^6	1.729×10^7
	Average of Spans 1 & 2	1.665×10^7 (recommended [5])	9.120×10^6	5.367×10^6	1.809×10^7 (recommended [6])

[1] Flexural rigidity by considering shear deformation (derived from experimental deflection).

[2] Flexural rigidity from moment-curvature relationship (derived from experimental strain).

[3] Flexural rigidity without considering shear deformation (derived from experimental deflection).

[4] Shear rigidity based on first order shear deformation equation (derived from experimental deflection)

[5] This flexural rigidity (EI) is recommended for use in modeling the First Salem Bridge.

[6] This shear rigidity (GA_w)is recommended for use in modeling the First Salem Bridge.

Note: The effective span is 2.667 m (105 in) for the First Salem Bridge over the Great Miami River in Montgomery County, Ohio.

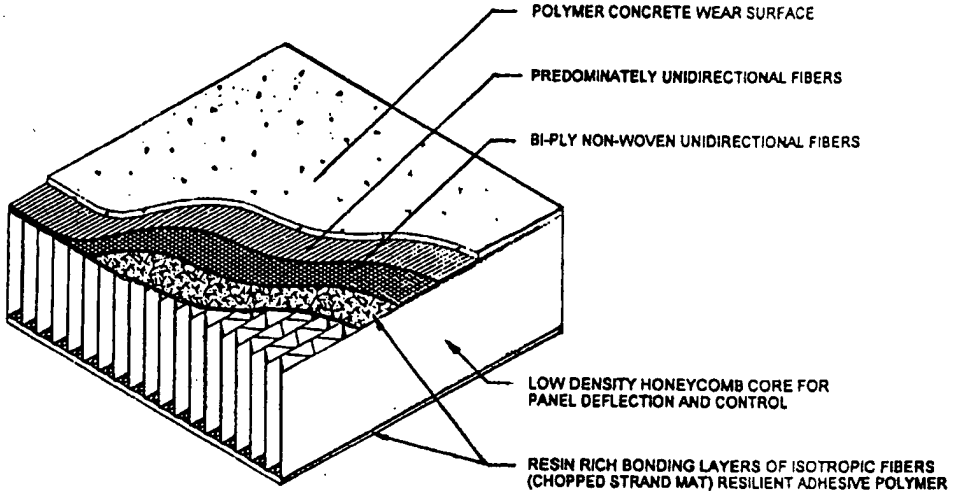

Figure II.7.1 Basic ICI Deck panel Configuration

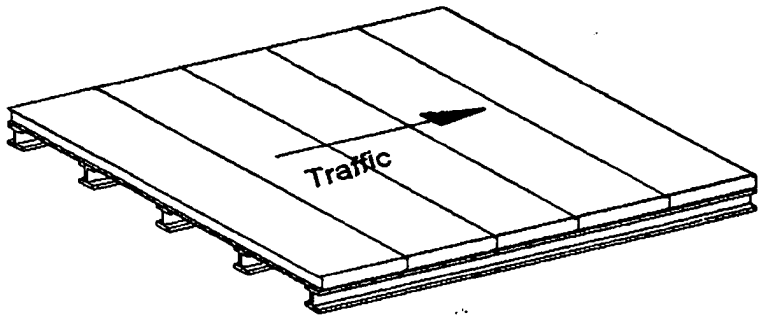

Figure II.7.2 Arrangement of Deck Panels in Bridge Structure

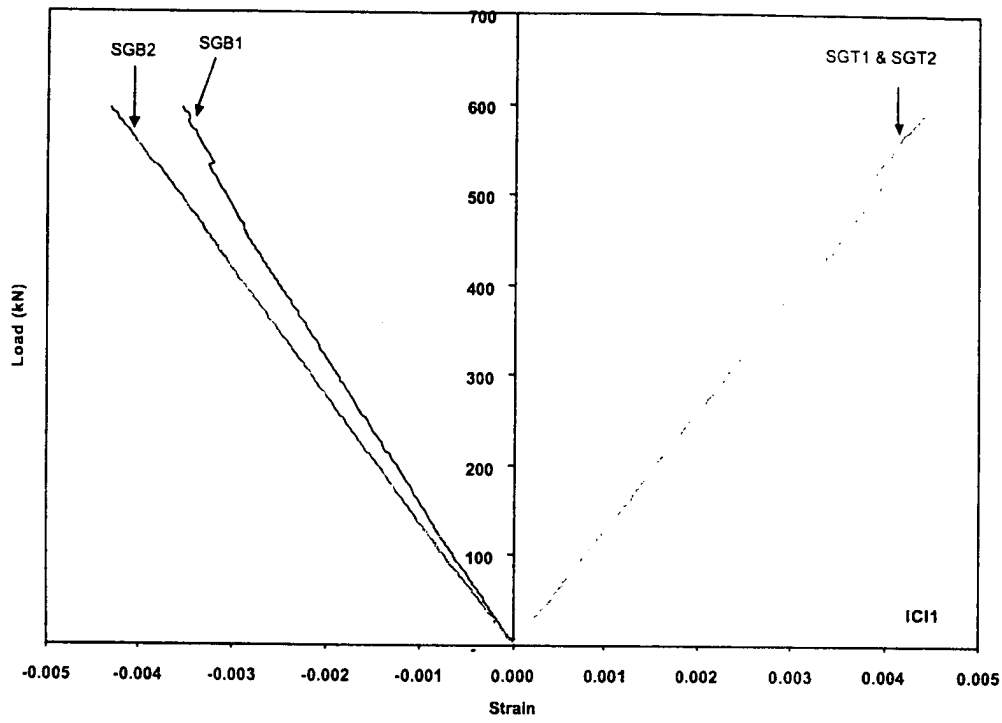

Figure II.7.3 Load vs Strain for Loading to Failure for the Deck panel ICI1
(Refer to Figure II.2.4 for the location of strain gages SGT1 and SGT2, and refer to Table II.7.1 for the properties of the ICI1 Panel)

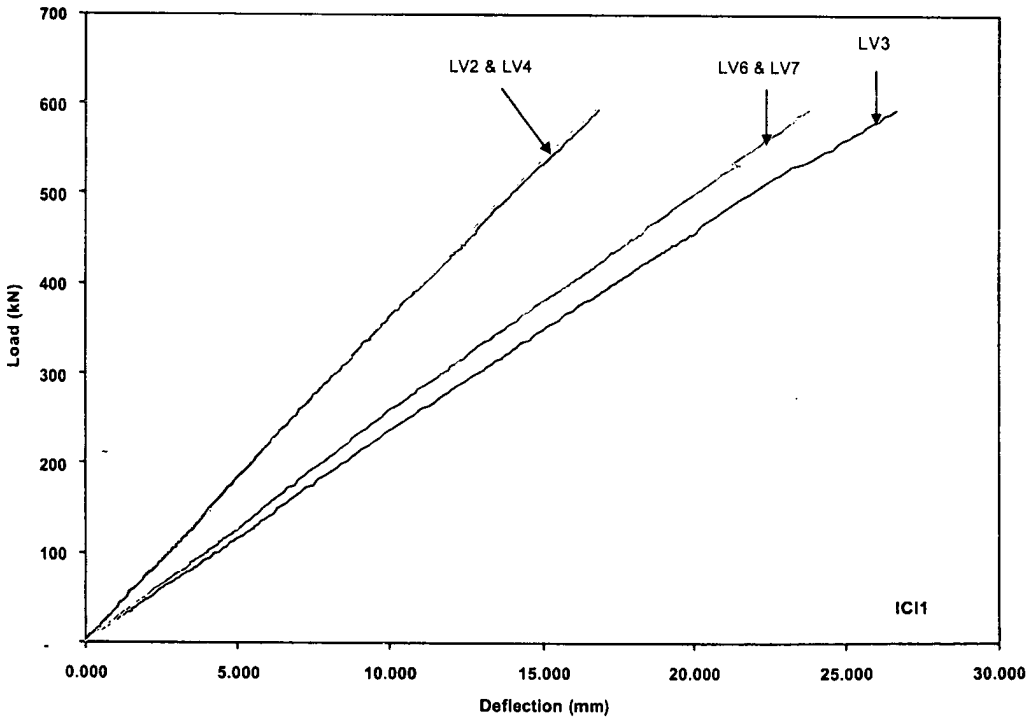

Figure II.7.4 Load vs Deflection for Loading to Failure for the Deck panel ICI1
(Refer to Figure II.2.6 for the location of LVDT's LV2, LV3, LV4, LV6 and LV7, and refer to Table II.7.1 for the properties of the ICI1 Panel)

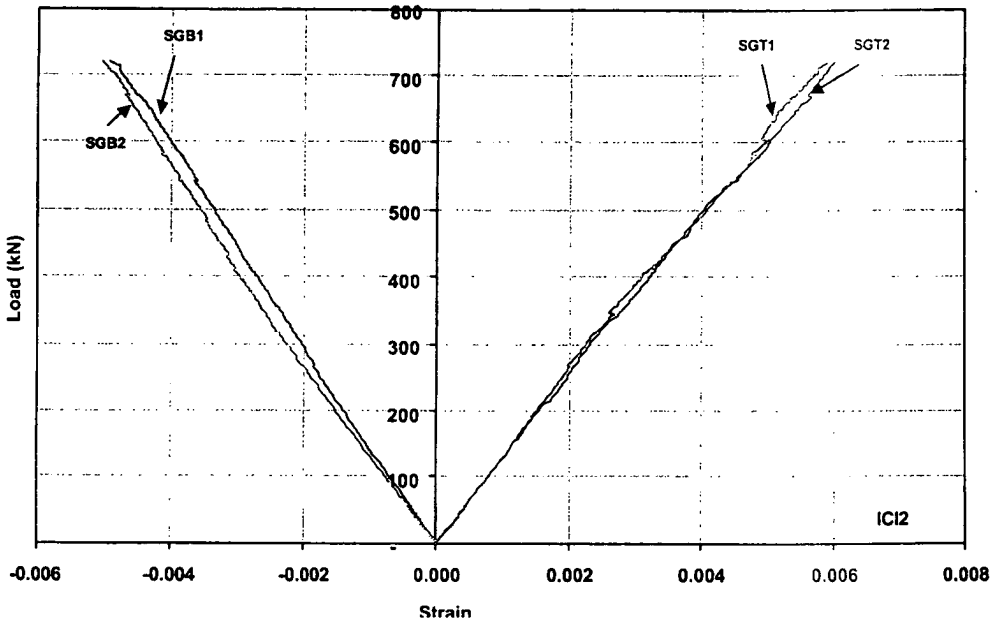

Figure II.7.5 Load vs Strain for Loading to Failure for the Deck Panel ICI2
(Refer to Figure II.2.4 for the location of strain gages SGT1 and SGT2, and refer to Table II.7.1 for the properties of the ICI2 Panel)

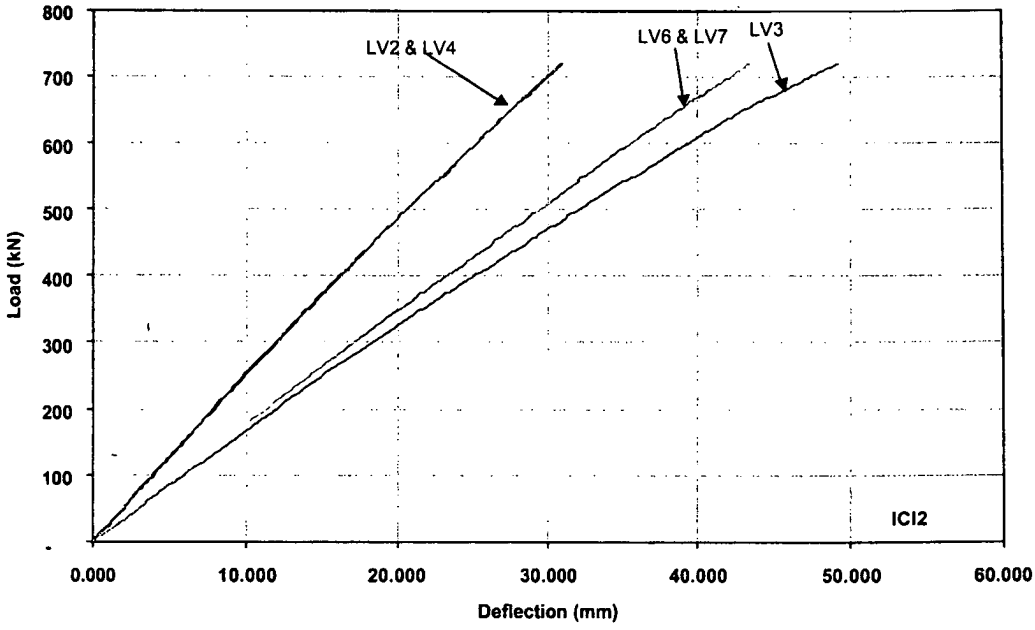

Figure II.7.6 Load vs Deflection for Loading to Failure for the Deck Panel ICI2
(Refer to Figure II.2.6 for the location of LVDT's LV2, LV3, LV4, LV6 and LV7, and refer to Table II.7.1 for the properties of the ICI2 Panel)

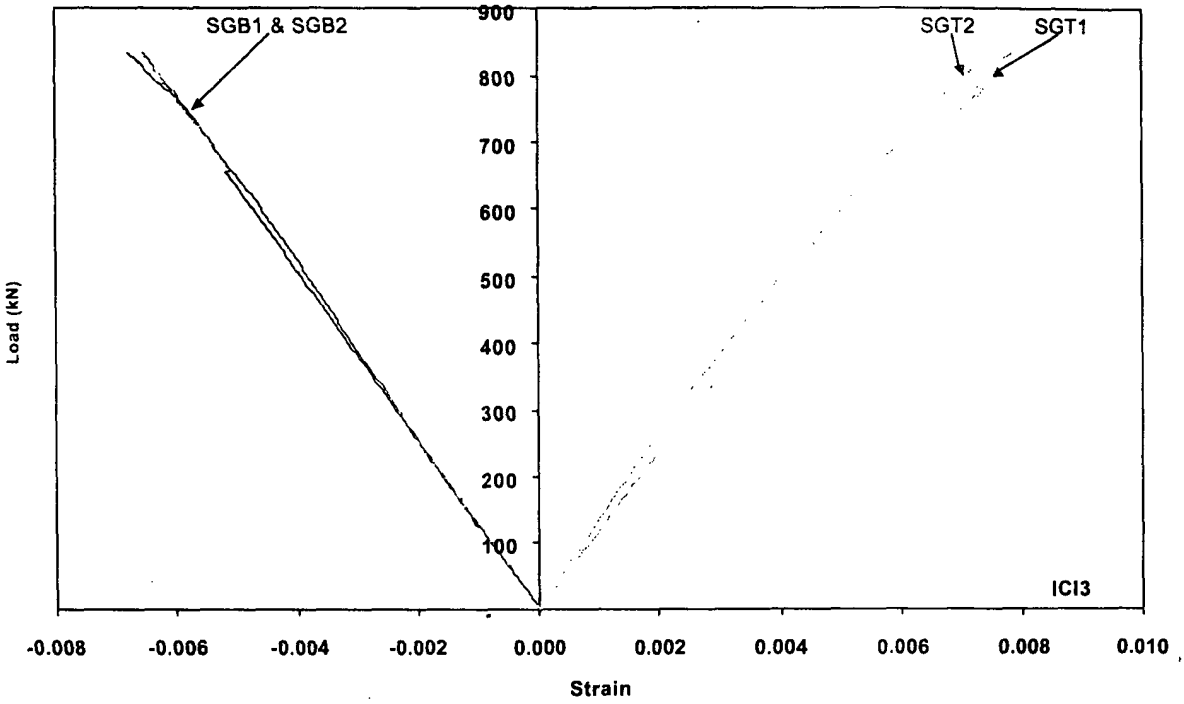

Figure II.7.7 Load vs Strain for Loading to Failure for the Deck Panel ICI3
(Refer to Figure II.2.4 for the location of strain gages SGT1 and SGT2, and refer to Table II.7.1 for the properties of the ICI3 Panel)

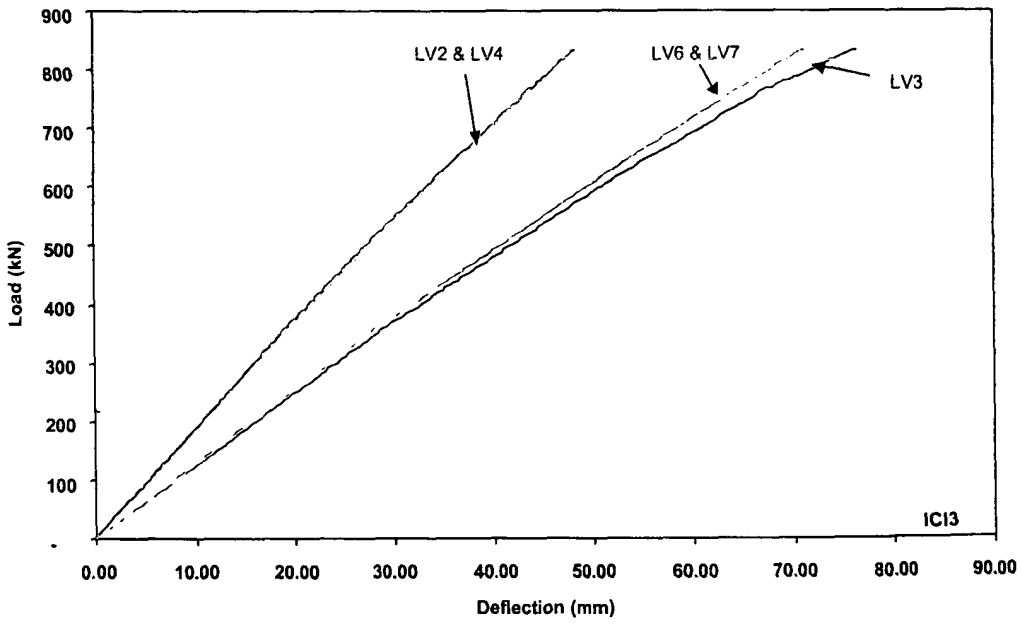

Figure II.7.8 Load vs Deflection for Loading to Failure for the Deck Panel ICI3
(Refer to Figure II.2.6 for the location of LVDT's LV2, LV3, LV4, LV6 and LV7, and refer to Table II.7.1 for the properties of the ICI3 Panel)

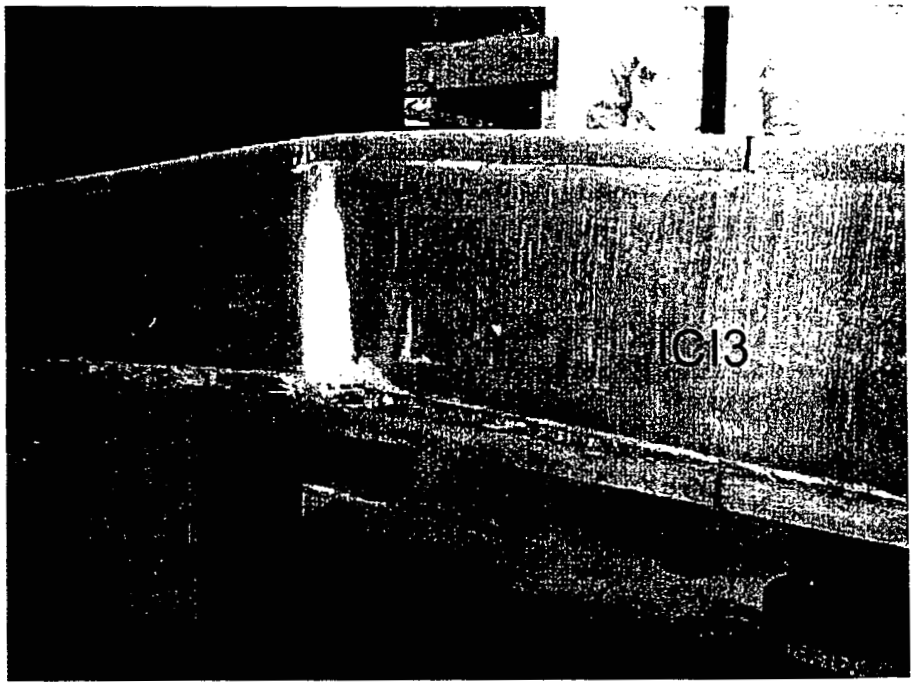

Figure II.7.9 Failure Pattern of the Deck Panel ICI3

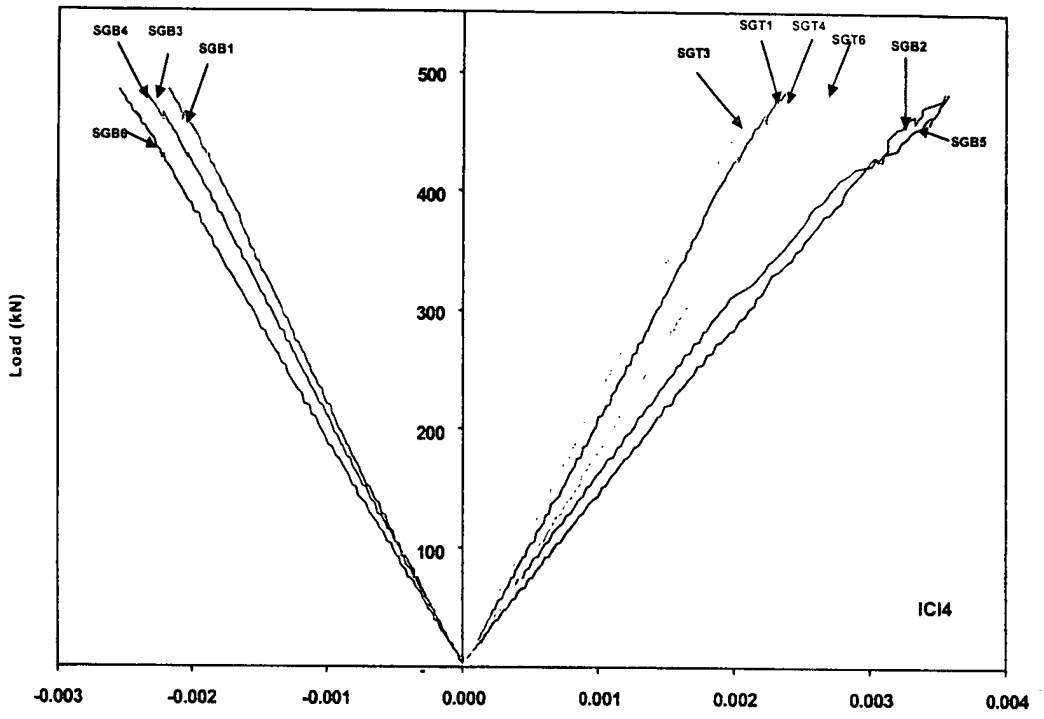

Figure II.7.10 Load vs Strain for Loading to Failure for the Deck Panel ICI4
(Refer to Figure II.2.5 for the location of strain gages SGT1 and SGT2, and refer to Table II.7.1 for the properties of the ICI4 Panel)

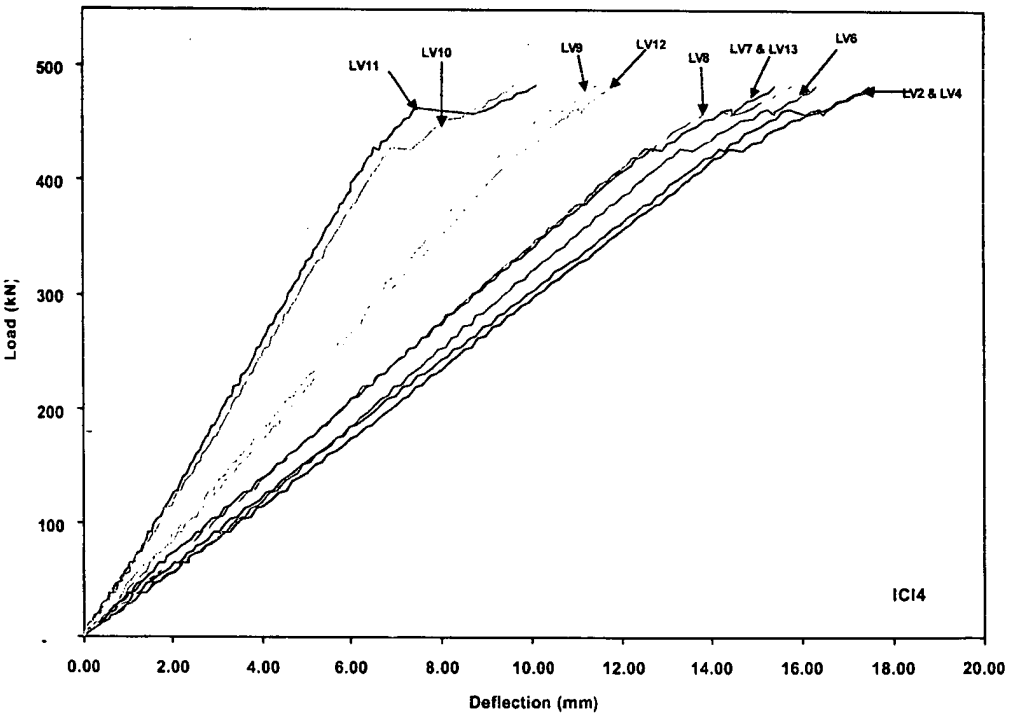

Figure II.7.11 Load vs Deflection for Loading to Failure for the Deck Panel ICI4
(Refer to Figure II.2.7 for the location of LVDT's LV2, LV4, LV6, LV7, LV8, LV9, LV10, LV11, LV12 and LV13, and refer to Table II.7.1 for the properties of the ICI4 Panel)

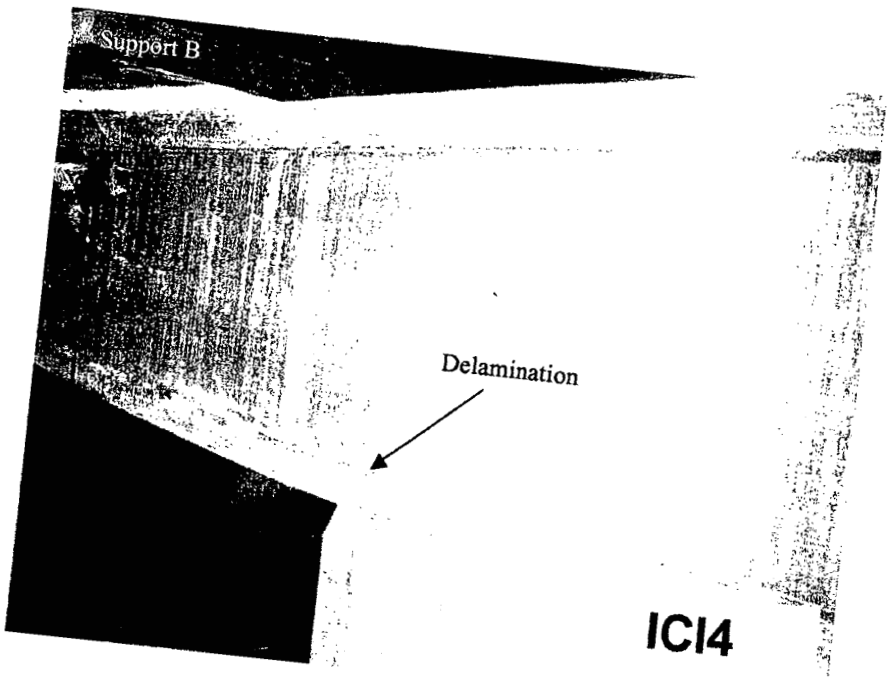

Figure II.7.12 Failure Pattern of the Deck Panel ICI4

II.8 CONCLUSIONS AND COMMENDATIONS

Tests are conducted up to failure on sixteen FRP deck panels supplied by the following manufacturers: Creative Pultrusions (CP), Composite Deck Solutions (CDS), Hardcore Composites (HP) and Infrastructure Composites International (ICI). Five additional reinforced concrete (RC) conventional deck panels are tested, and are used as "baseline" panels. The test panels are instrumented with Linear Variable Deflection Transducers (LVDT) and strain gages to measure the out-of-plane deflections and strains. The panels are subjected to four loading steps in order to establish the baseline curve, to predict the responses under cyclic loading of 53.4 kN (12 kips) and 115.7 kN (26 kips), and to study the behavior up to failure. The test results of FRP deck panels are compared with the deflection criteria, flexure criteria and shear criteria specified by the Ohio Department of Transportation (ODOT), and with the test results from the reinforced concrete (RC) conventional deck panels. The flexural rigidities (EI) and shear rigidities (GA_w) of FRP deck panels are determined using the first-order shear deformation beam equations, and by conducting a linear regression analysis on the load vs deflection relationship for the baseline curve. The flexural rigidity (EI) is also calculated using (i) the first order beam equation without considering the shear deformation, and (ii) the moment-curvature relationship on the load vs deflection relationship for the baseline curve.

The following conclusions are drawn based upon the static testing, and without any account for the " knock down" factors. The double span deck panels are assumed to be representative of the panels placed on the First Salem Bridge.

(i) None of the panels supplied by the FRP manufacturers failed in shear, and all panels satisfied the shear criteria.

(ii) The single and double span Pultruded FRP Deck - Creative Pultrusions (CP) panels satisfy the deflection criteria and flexure criteria.

(iii) The single and double span Hybrid FRP - Concrete Deck - Composite Deck Solutions (CDS) panels satisfy the deflection criteria and flexure criteria.

(iv) The single span Scrimp FRP Deck - Hardcore Composites (HC) panels satisfy the flexure-strain criteria but do not satisfy the deflection criteria (Measured deflection/allowable deflection = 1.029 to 1.059, Table II.6.2). The double span deck panel satisfies the deflection criteria and flexure criteria.

(v) The single span Contact Molding Hand Lay-up FRP deck - Infrastructure Composites International (ICI) panels satisfy the deflection criteria and flexure criteria. The double span deck panel satisfies the deflection criteria and strain limits specified in the flexure criteria but does not satisfy the required ultimate load specified in the flexure criteria (Measured ultimate load = 483,473 N (108,689 lb), required ultimate load = 528,431 N (118,796 lb), Table II.7.3).

The following flexural rigidities (EI) and shear rigidities (GA_w) are recommended for use in modeling the First Salem Bridge.

Creative Pultrusions panels (CP): $EI = 2.428 \times 10^7$ N-m^2 (8.461×10^9 lb-in^2) and $GA_w = 1.120 \times 10^7$ N (2.518×10^6 lb.)

Composite Deck Solutions panels (CDS): $EI = 1.588 \times 10^7$ N-m^2 (5.532×10^9 lb-in^2) and $GA_w = 3.358 \times 10^7$ N (7.550×10^6 lb.)

Hardcore Composites panels (HC): $EI = 1.157 \times 10^7$ N-m^2 (4.031×10^9 lb-in^2) and $GA_w = 1.394 \times 10^7$ N (3.134×10^6 lb.)

Infrastructure Composites International panels (ICI): $EI = 1.665 \times 10^7$ N-m^2 (5.802×10^9 lb-in^2) and $GA_w = 1.809 \times 10^7$ N (4.066×10^6 lb.)

These rigidities are obtained by calculating the average values of the rigidities in span 1 and span 2 for the double span panels. They are based on first-order shear deformation beam equations, and are derived by conducting a linear regression analysis on the load vs deflection relationship for the baseline curve.

II.9 FERENCES

American Association of State Highway and Transportation officials, LRFD Bridge Design Specifications, Washington, DC, (1998).

American Association of State Highway and Transportation officials, Standard Specifications for Highway Bridges, Washington, DC, (1996).

D.R. Mertz and J.M. Kulicki. "The Application of the AASHTO LRFD Bridge Design Specifications to Composite-Material Bridges". Symposium on Advanced Rehabilitation, Durable Materials, Non-Destructive Evaluation and Management, Eds. U. Meier and Betti, Zurich, CH, 178-184 (1997).

11.10 ACKNOWLEDGEMENTS

The authors would like to acknowledge the following individuals who assisted during the conduct of this research: Anthony Kordenbrock, Dr. Chelliah Madasamy, Chris Hill, Dan Eaton, David Ritchie, Everett Wilson, Joshua Johnson, Louis Mattingly, Mario Johnson, Sean Anderson, Tim Taylor, Dr. Vasudevan Krishnappa Naidu and Dr. Vijay Gupta.

Section III

FATIGUE EVALUATION OF FRP BRIDGE DECKS ON STEEL GIRDERS UNDER EXTREME TEMPERATURE CONDITIONS FOR SINGLE AASHTO HS20 DESIGN WHEEL LOAD

Piyush Dutta[1] and Roberto Lopez-Anido[2]

Abstract

The fatigue performance evaluation at extreme temperature of two-span continuous fiber-reinforced polymer (FRP) deck prototypes built on three W-section steel girders is presented. The deck-girder system was subjected to an eccentric cyclic load that simulates an AASHTO HS20 design truck wheel load with impact. Initially, one million load cycles were applied at a controlled high temperature (49°C), and then another million load cycles were applied at a controlled low temperature (–30°C). Quasi-static load tests were conducted at specific intervals during fatigue cycling to evaluate the load-deflection and load-strain response at several deck locations. A reinforced-concrete conventional (RCC) deck designed by the Ohio Department of Transportation was fabricated and tested under the same load and temperature regime. The RCC deck was utilized to establish the "current practice" baseline response. The FRP deck performance was compared with the RCC deck. The fatigue tests of the FRP and RCC decks were conducted at the U.S. Army Cold Regions Research and Engineering Laboratory in

[1] Research Engineer, Cold Regions Research and Engineering Laboratory (CRREL), ERDC, U.S. Army Corps of Engineers, Hanover, NH.

[2] Assistant Professor, Department of Civil and Environmental Engineering, Advanced Engineered Wood Composites Center, University of Maine, Orono, ME.

Hanover, NH. The fatigue-temperature performance was assessed based on two damage indicators by establishing if the FRP deck apparent bending stiffness in the x and y directions degrades with number of load cycles and temperature changes.

Table of Contents

List of Tables

List of Figures

III.1 Fatigue Response of Reinforced-Concrete Bridge Deck under Extreme Temperature Conditions

III.1.1 Abstract

The fatigue performance evaluation at extreme temperatures of a reinforced-concrete conventional (RCC) deck over steel W-section girders is presented. The reinforced-concrete conventional deck was considered in this study to establish the benchmark fatigue response of a set of fiber-reinforced polymer (FRP) bridge decks.

II.1.2 Introduction

The fatigue performance evaluation of a reinforced-concrete conventional (RCC) deck over steel W-section girders is presented. An RCC deck was designed by the Ohio Department of Transportation and considered in this study for the benchmark response of a set of fiber-reinforced polymer (FRP) bridge decks.

The deck-girder system was subjected to an eccentric cyclic load that simulates an AASHTO HS20 design truck wheel load with impact. Initially, one million load cycles were applied at a controlled high temperature, 49°C (120°F), and then another million load cycles were applied at a controlled low temperature, –30°C (–22°F). Quasi-static load tests were conducted at specific intervals during fatigue cycling to evaluate the load-deflection and load-strain response at several deck locations. The performance of all FRP decks was compared with this RCC deck. The fatigue tests of the decks were conducted at the U.S. Army Cold Regions Research and Engineering Laboratory (CRREL) in Hanover, N.H.

The fatigue-temperature performance was assessed based on two damage indicators by

1. Establishing if the reinforced-concrete deck apparent bending stiffness in the x-direction degrades with number of load cycles and temperature changes. The apparent bending stiffness in the x-direction is associated with and is measured by the corrected maximum deflections.
2. Establishing if the reinforced-concrete deck apparent bending stiffness in the y-direction degrades with number of load cycles and temperature changes. The apparent bending stiffness in the y-direction is associated with and is measured by the change in slope angle in the transverse direction of the deck under maximum loading conditions.

III.1.3 Description of the Deck System

The reinforced-concrete deck test specimen had dimensions of 1.828 m (72 in.) in width and 6.100 m (240 in.) in length, as shown in Figure III.1.1. The deck is connected to the supporting steel girders using shear studs.

III.1.4 Test Protocol

There are no specifications available for FRP bridge decks on the number of load cycles required for fatigue performance evaluation. A fatigue performance evaluation procedure was initially developed and applied to qualify FRP decks panels fabricated by pultrusion and vacuum-assisted resin transfer molding (VARTM) (Lopez-Anido et al. 1998).

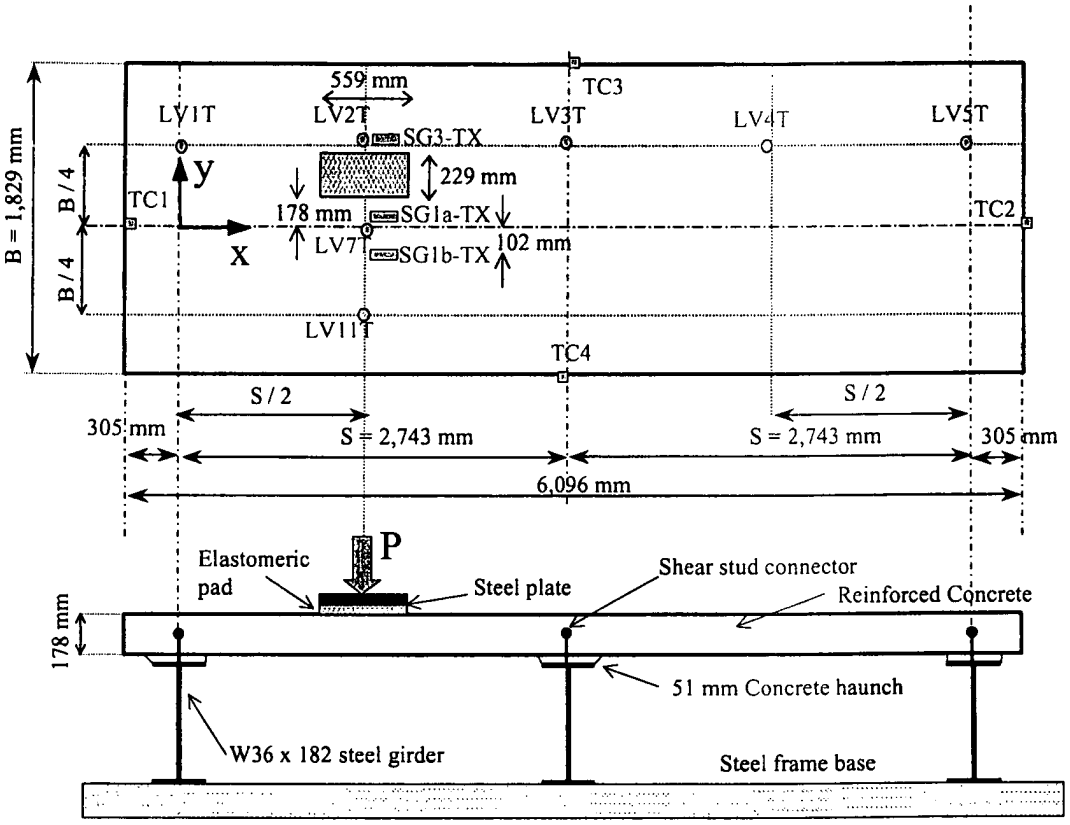

Figure III.1.1 - Test Setup

The proposed fatigue evaluation procedure consisted of applying two million simulated wheel load cycles at two controlled extreme temperatures on both the FRP panels and the reinforced-concrete benchmark panel attached to steel girders, i.e., one million cycles at 49°C (120°F) and one million cycles at –30°C (–22°F). The fatigue performance of the FRP decks was compared with the benchmark response of the conventional reinforced-concrete deck. The experimental setup consisted of a two-span continuously supported deck subjected to a simulated AASHTO HS20-44 design truck wheel load (Figure III.1.2). A girder spacing of 2.74 m (108 in.) was selected, as shown in Figure III.1.1.

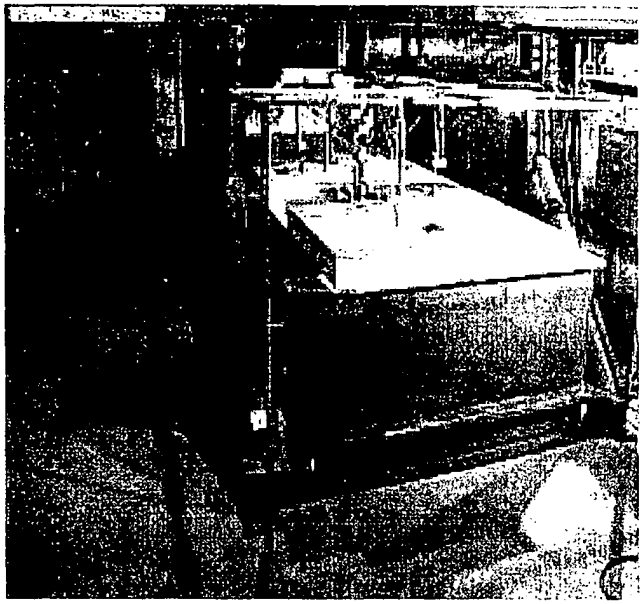

Figure III.1.2 Reinforced-Concrete Deck Supported by Steel Beams during Fatigue Testing

The maximum load to be applied was computed based on an AASHTO HS20-44 design truck wheel load with a dynamic load allowance (impact factor). The design truck wheel load is one half of the axle load. The impact factor adopted was 30%. Thus, the maximum applied load resulted in P_{max} = 71.2 kN (16,000 lb.) × 1.3 = 92.5 kN (20,800 lb). The applied load frequency ranged between 2.4 and 3 Hz. Based on these applied load frequencies and the flexibility of the FRP deck, the actual maximum applied fatigue load attained was P_{max} = 89.0 kN (20,000 lb). The minimum applied load was P_{min} = 8.9 kN (2,000 lb). Therefore, the fatigue stress ratio was approximately R = 0.1.

The fatigue test specimens were not anticipated to fail during the two-million-cycle duration, so the fatigue analysis was focused on assessing the structural degradation associated with the cyclic loading. Fatigue damage accumulation can induce stiffness degradation of the FRP and concrete deck panels. Besides, fatigue damage can lead to

residual damage in the deck-steel girder haunch connection. To assess fatigue damage, quasistatic tests were conducted prior to the application of load cycling and at specified increments of fatigue cycling, as shown in Figure III.1.3.

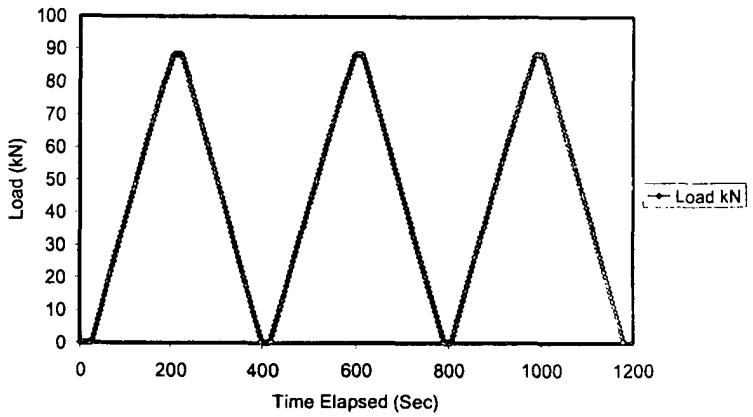

Figure III.1.3 Typical Quasi-Static Load Tests

First, at ambient temperature, 24°C (75°F), a set of quasi-static tests was conducted to obtain baseline load-deflection and load-strain values. Then, the test room was warmed up to 49°C (120°F). The deck prototypes temperature was monitored until it reached the room temperature. Then, a second set of quasi-static test, but now at high temperature, was conducted. After this evaluation, one million load cycles were applied. Quasi-static tests were conducted at 100,000, 500,000 and 1,000,000 load cycles. For low-temperature tests, the room was cool down to –30°C (–22°F), and the fatigue test with the corresponding quasi-static tests were repeated for the second million load cycles.

III.1.5 Test Setup

The deck prototype dimensions were specified to model a typical slab-on-steel girder highway bridge, as shown in Figure III.1.1. A fatigue-testing frame was designed

to accommodate the deck system prototype with the three connected steel girders. The deck prototype was instrumented with strain gauges, thermocouples, and Linear Voltage Differential Transducers (LVDTs) to measure vertical deflection (Figure III.1.1).

The fatigue tests were performed in CRREL's Material Evaluation Facility (MEF). This is a well-insulated room with interior dimensions of approximately 7.92 m (26 ft) wide by 12.80 m (42 ft) long and 3.66 m (12 ft) high. A set of double doors 3.35 m (11 ft) wide by 3.35 m (11 ft) tall allows the large fatigue test frame and the bridge deck prototypes to be moved in and out of the MEF facility. A self-reacting steel test frame was designed and built at CRREL for a maximum load capacity of 266.9 kN (60,000 lb.). One 97.9-kN- (22,000-lb-) capacity hydraulic actuator was mounted on the steel reaction frame to apply cyclic loading on the deck. The bridge deck specimens were attached to three steel girders W36x182, resulting in a continuous two-span bridge structure (Figure III.1.2). The actuator applied the load on a rectangular steel plate of 229 × 559 mm (9 × 22 in.) that simulates a wheel load contact area (AASHTO 1996). An elastomeric pad was placed between the steel plate and the top deck surface to provide uniform pressure. The load was applied eccentrically with respect to the traffic flow direction to study the load distribution in the y-direction, as shown in Figure III.1.1.

Load, deflection, strain, and temperature were the general parameters of measurement in this test program. The reinforced-concrete deck specimen was instrumented with strain gauges, LVDTs, and thermocouples. Seven LVDTs supported by an independent frame were used to measure deflections on the top surface of the deck. Four thermocouples were placed on four sides of the deck top surface, and one thermocouple was used for air temperature. The thermocouples were used to verify that

the deck prototype reaches equilibrium with room temperature. The locations of the LVDTs, strain gauges, and thermocouples on the top of the deck are shown in Figure III.1.1. The location of the strain gauges bonded to the bottom deck surface (BX) was symmetrical with respect to the numerically matching strain gauges bonded to the top surface (TX).

The test setup induced a positive bending moment under the applied load ($x = S/2$) and negative bending moment on the central support ($x = S$) and the adjacent span. An uplifting force resulted on the end girder support ($x = 2 \times S$). This uplifting force was partially counteracted by the weight of the deck and steel beams.

As mentioned before, the deck prototype was evaluated for approximately 2,000,000 load cycles with controlled temperature. The first million load cycles were conducted at 49°C (120°F), while the second million cycles were performed at about –30°C (–22°F). The first quasi-static test was at room temperature, about 24°C (75°F), before the fatigue cycles began, and it served as the control baseline. In the quasi-static tests the load was applied at a rate of 1 mm/min (0.04 in./min), and sensor measurements were recorded every 3 s. Each quasi-static test consisted of a loading and unloading cycle. The quasi-static test was repeated three times, resulting in three peak loads and six varying load intervals for data analysis (Figure III.1.3).

III.1.6 Experimental Results

The raw data were analyzed to produce load-deflection curves for each deck test. Typical load-deflection curves for room temperature, 24°C (75°F), at five deck locations corresponding to LVDTs mounted on the top of the panel and aligned in the x-direction, are shown in Figure III.1.4. Similarly, high-temperature load-deflection curves at the five

locations after one million high-temperature load cycling is shown in Figure III.1.5. Figure III.1.6 shows the low-temperature load-deflection curves for the same locations after one million hot plus one million cold fatigue cycles. Figure III.1.7 compares the maximum deflection data for the room-temperature baseline, after one million cycles at high temperature, and after an additional one million cycles at low temperature. From these load-deflection curves we observe that the low-temperature stiffness after an accumulated two million load cycles is higher than the initial stiffness at room temperature. This observation implies that the panel stiffness is controlled mainly by temperature and not by the number of load cycles.

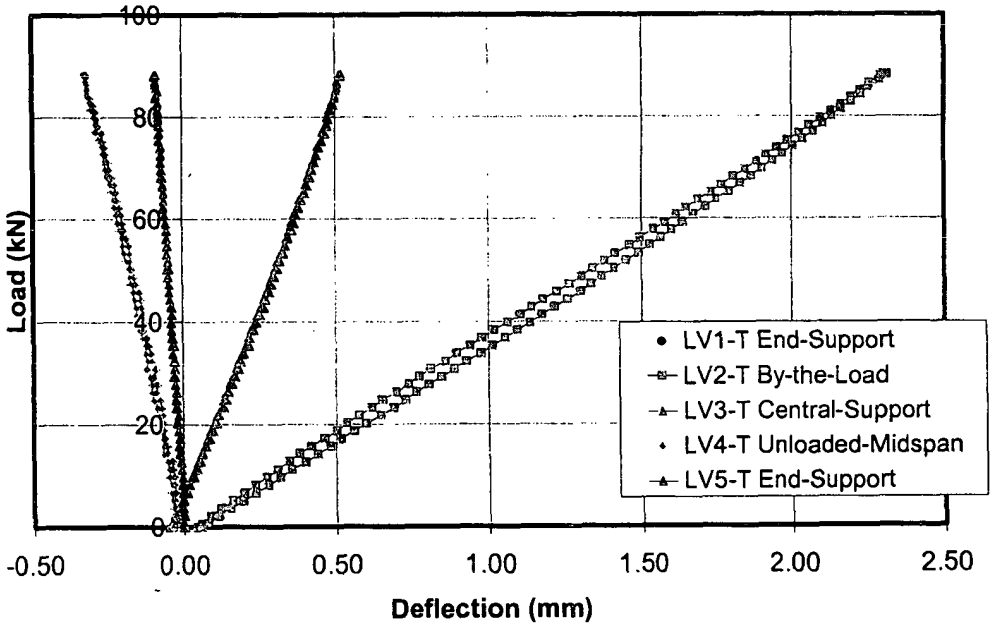

Figure III.1.4 Room-Temperature Load-Deflection Curves for Top LVDTs aligned in x-Direction prior to Fatigue Cycling

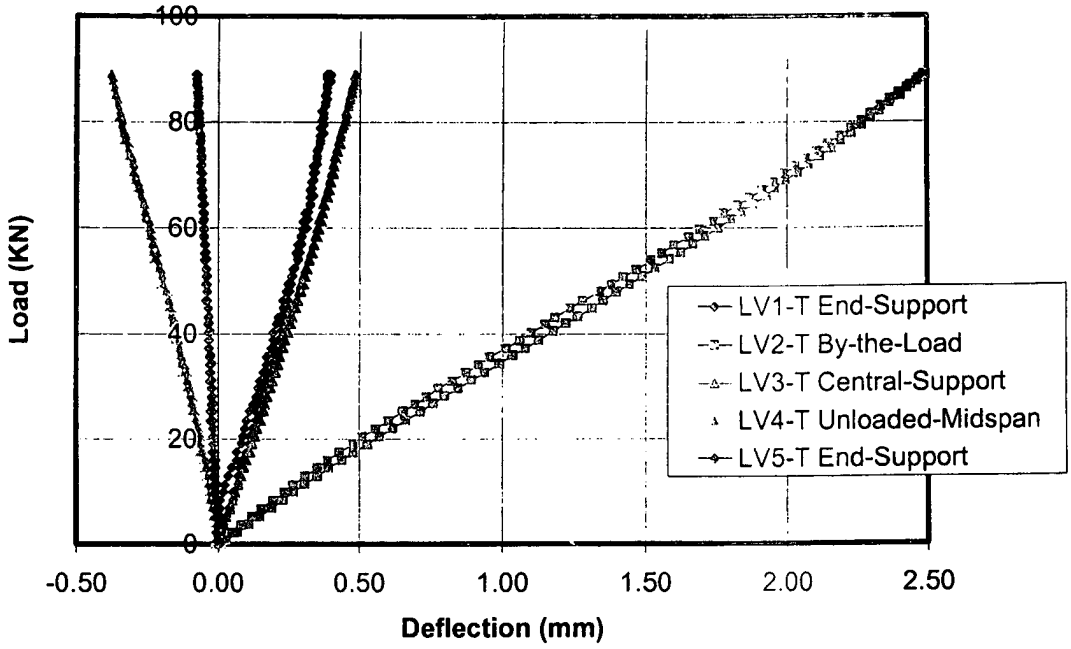

Figure III.1.5 High-Temperature Load-Deflection Curves for Top LVDTs aligned in x-Direction after One Million Hot Fatigue Cycles

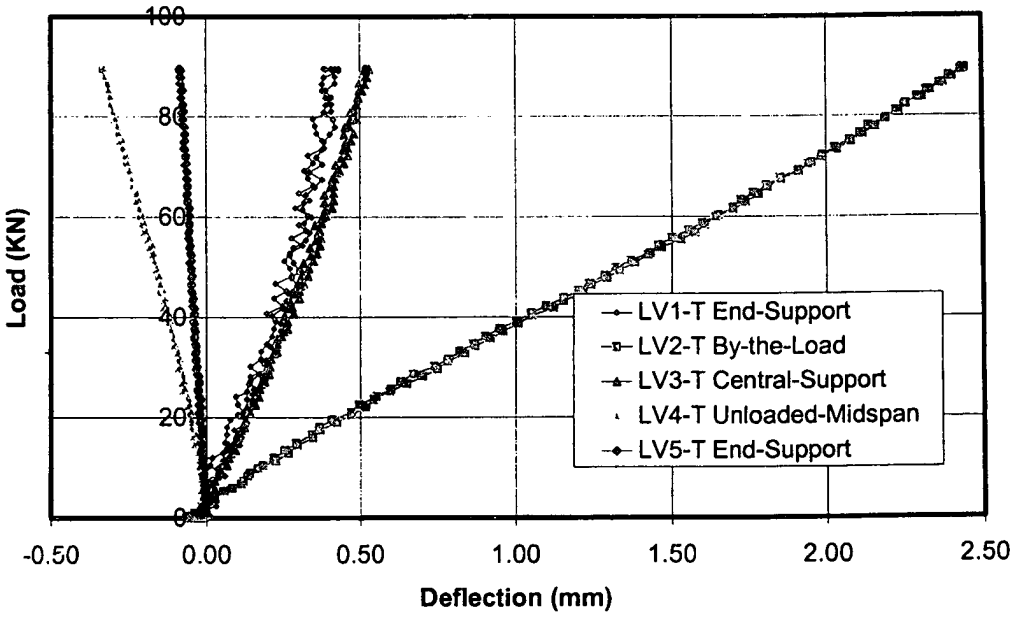

Figure III.1.6 Low-Temperature Load-Deflection Curves for Top LVDTs aligned in x-Direction after One Million Hot plus One Million Cold Fatigue Cycles

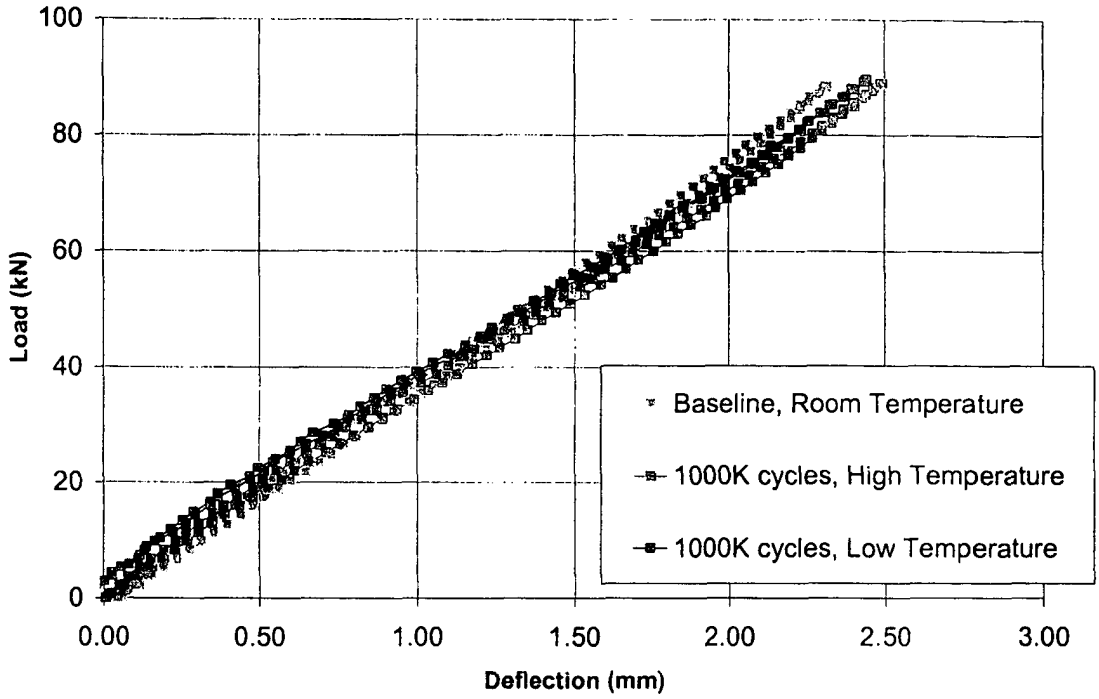

Figure III.1.7 Maximum Deflections for Three Test Conditions (Measured by LV2-T)

The maximum total deflections measured with the top LVDTs (LV1T, LV2T, LV3T, LV4T, and LV5T) aligned the x-direction are shown in Figure III.1.8 for room temperature (RT) baseline, high temperature (HT), and low temperature (LT), the last two after one million cycles at each temperature. These total deflections include both deck deflections and support deflections measured during the quasi-static tests. No deck uplifting was observed over the end girder. The maximum deflections measured with the top LVDTs (LV2T, LV7T, and LV11T) aligned along the y-direction during the quasi-static tests are shown in Figure III.1.9.

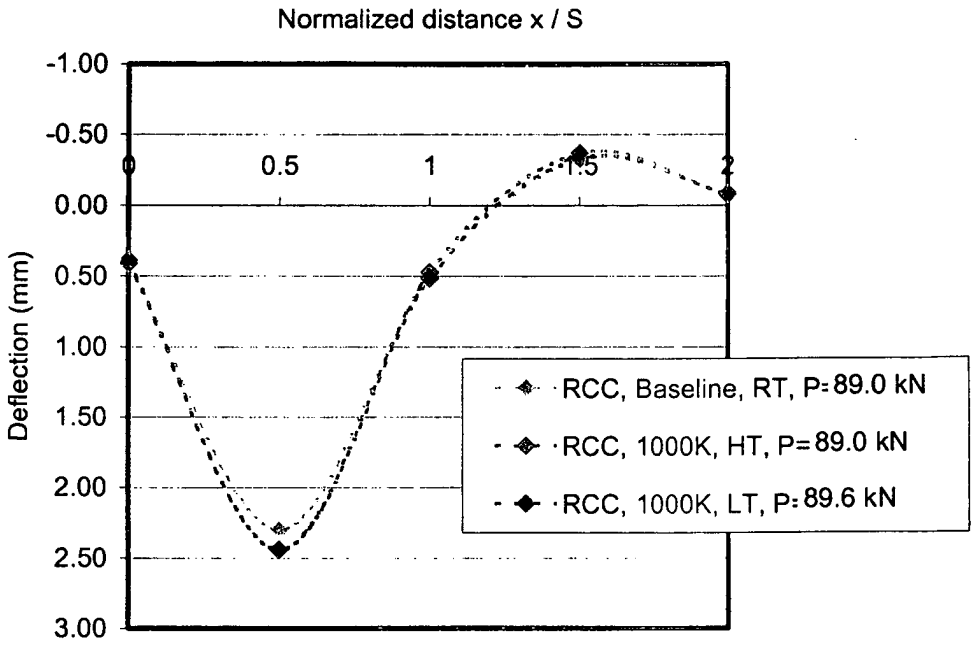

Figure III.1.8 Top Deflection Variation along the x-Direction for Maximum Load: LV1-T, LV2-T, LV3-T, LV4-T, LV5-T

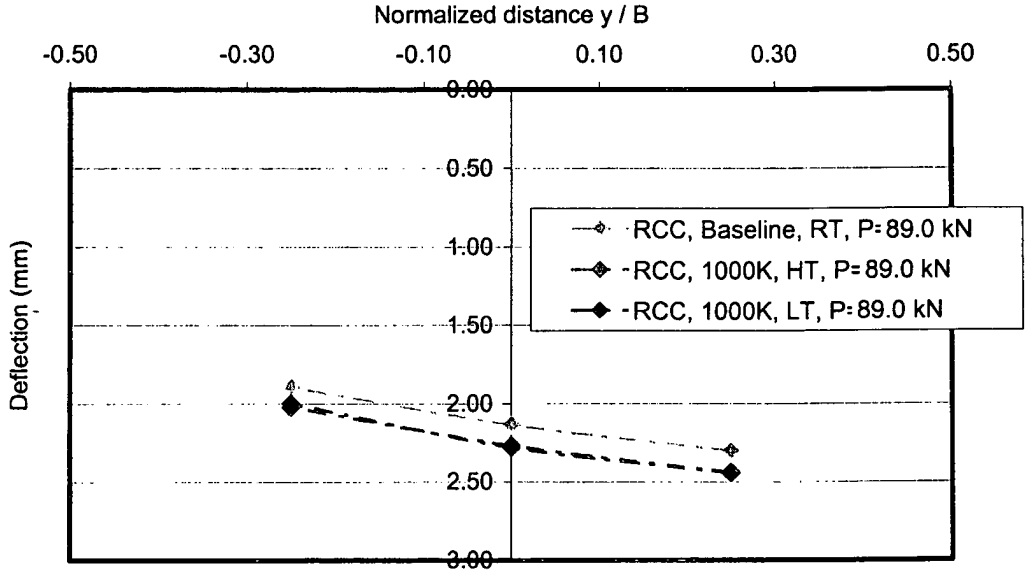

Figure III.1.9 Top Deflection Variation along the y-Direction for Maximum Load: LV2-T, LV7-T, LV11-T

Compressive strains on the top of the deck in the x-direction measured at room temperature prior to fatigue cycling are shown in Figure III.1.10. All the curves are approximately linear within the loading range. Compressive strain curves were obtained at high temperature after one million load cycles (Figure III.1.11). In the same way, compressive strain curves were plotted at low temperature after an additional million of load cycles (Figure III.1.12). From these curves we observed that the load-compressive strain response exhibit a degree of nonlinearity after two million load cycles.

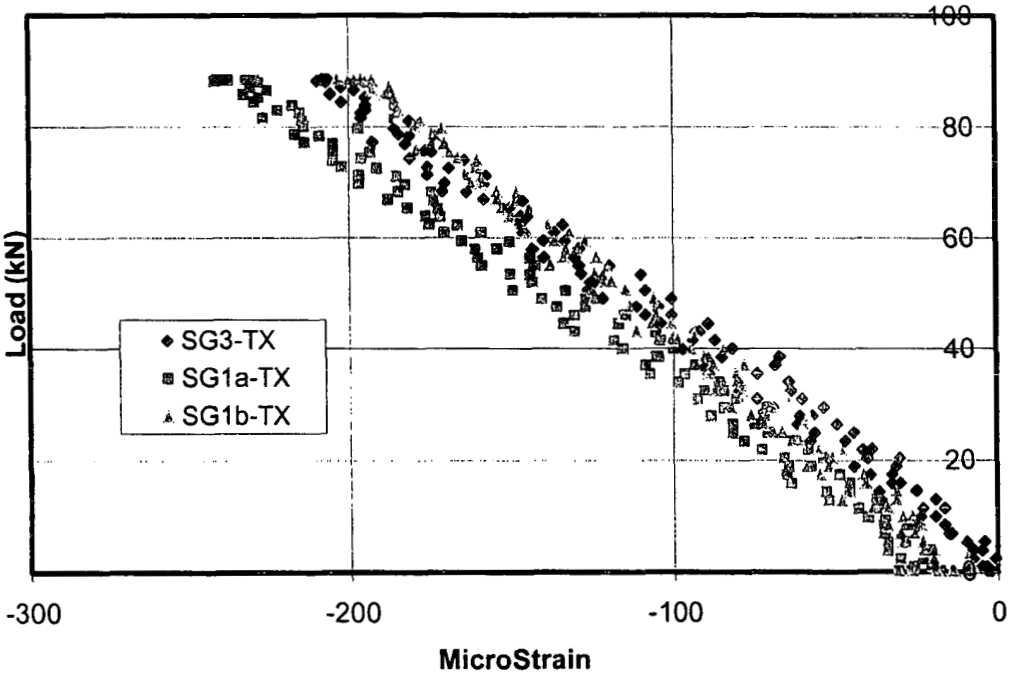

Figure III.1.10 Room-Temperature Strain (x-Direction) Curves Prior to Fatigue Cycling for Top Gauges (Loaded Span): SG1a-TX, SG1b-TX, SG3-TX

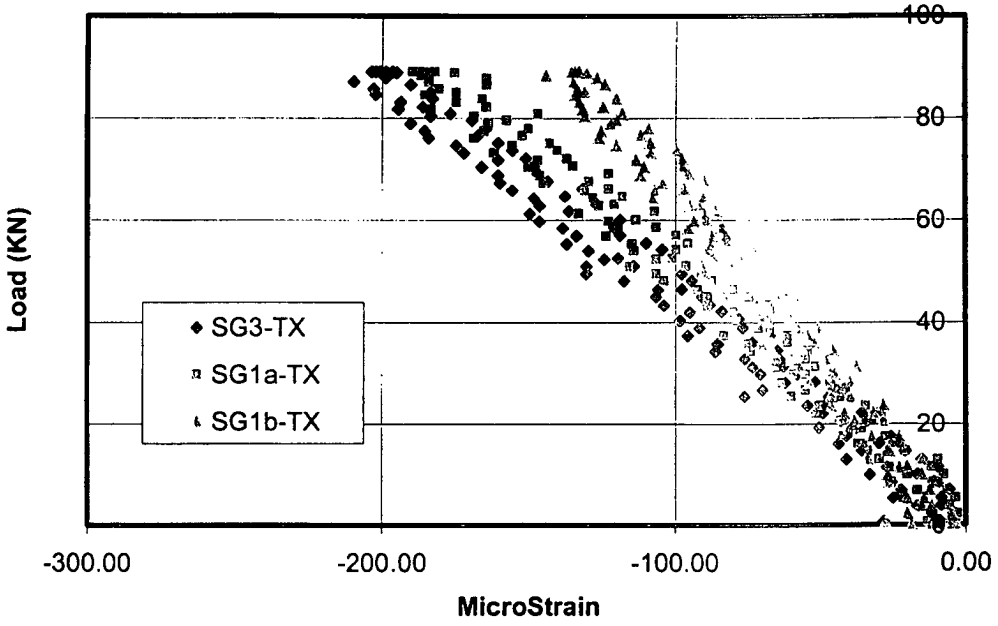

Figure III.1.11 High-Temperature Strain (x-Direction) Curves after One Million Hot Cycles for Top Gauges (Loaded Span): SG1a-TX, SG1b-TX, SG3-TX

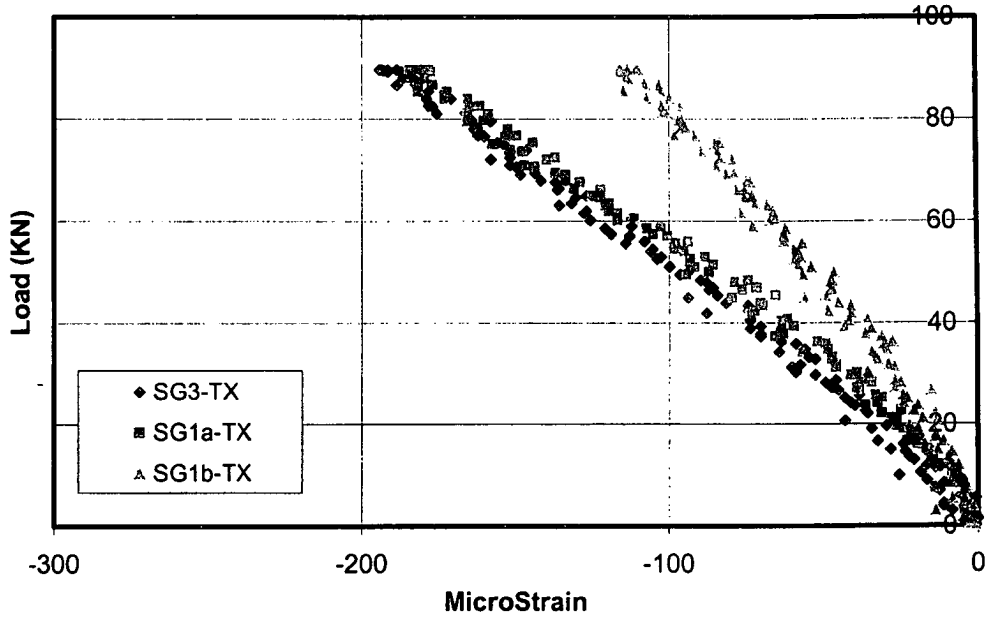

Figure III.1.12 Low-Temperature Strain (x-Direction) Curves (after One Million Hot plus One Million Cold Cycles) for Top Gauges (Loaded Span): SG1a-TX, SG1b-TX, SG3-TX

III.1.7 Data Analysis

To evaluate the deck prototype response with temperature and number of load cycles, two stiffness indicators are defined:

1) Stiffness indicator in the x-direction is computed based on corrected maximum deflections along a longitudinal line (LV1T, LV2T, LV3T); and
2) Stiffness indicator in the y-direction is computed based on maximum deflections across a transverse line (LV2T, LV7T, LV11T).

III.1.7.1 Retained Stiffness in the x-Direction

The maximum deflection, δ_c, was corrected to account for support deflection according to (III.1.1)

$$\delta_c = (LV2T) - \tfrac{1}{2}(LV1T + LV3T) \qquad \text{(III.1.1)}$$

where LV1T, LV2T, and LV3T are defined as deflection at the points given in Figure III.1.1. For each quasi-static test corresponding to the number of applied load cycles, *n*, the six segments of the load-deflection curves (see the loading and unloading segments in Figure III.1.3) for varying load intervals were plotted. A linear response was observed in all cases and approximated with a linear least-squares regression line to compute the load-deflection ratio $\left(P/\delta_c\right)_n$. These load-deflection ratios are related to the stiffness of the deck in the x-direction. The resulting load-deflection ratios are given in Table III.1.1.

An indicator of retained stiffness in the x-direction, $R_{x,n}$, is defined as the mean residual load-deflection ratio after *n* load cycles with controlled temperature with respect to the mean initial load-deflection ratio, as shown in equation III.1.2:

$$R_{x,n} = \frac{(P/\delta_c)_n}{(P/\delta_c)_o} \qquad \text{(III.1.2)}$$

Then $R_{x,n} < 1$ implies a reduction in deck stiffness, while $R_{x,n} > 1$ implies an increase in deck stiffness. The resulting retained stiffness indicators are given in Table III.1.2.

Table III.1.1 Reinforced-Concrete Deck x-Direction Load-Deflection Ratio

	Temperature (°C)					
	24		49		–30	
Load Cycles	Mean (kN/mm)	COV (%)	Mean (kN/mm)	COV (%)	Mean (kN/mm)	COV (%)
0	49.1	0.54	46.4	4.86		
100000			43.5	0.40		
500000			43.0	0.68		
1000000			42.0	0.36	44.4	0.49
1000000 + 100000					43.3	1.04
1000000 + 500000					43.0	0.77
1000000 + 1000000					43.0	1.34

Note: 1 kN/mm = 5.71 kip/in.

Table III.1.2 Reinforced-Concrete Deck x-Direction Stiffness Indicator

	Temperature (°C)					
	24		49		–30	
Load Cycles	Statistical Level	$R_{x,n}$	Statistical Level	$R_{x,n}$	Statistical Level	$R_{x,n}$
0	A	1.000	B	0.946		
100000			C	0.886		
500000			C	0.876		
1000000			C	0.855	D	0.903
1000000 + 100000					C	0.881
1000000 + 500000					C	0.876
1000000 + 1000000					C	0.876

•The same letter indicates the same stiffness ratio with 95% confidence.

III.1.7.2 Retained Stiffness in the y-Direction

Deflections were measured at three points aligned across the FRP deck (LV2-T, LV7-T, and LV11-T), as shown in Figure III.1.1. Load-deflection curves were plotted for the six load-varying intervals of each quasi-static test. These load-deflection curves followed a linear trend and were fitted using linear least-squares regression analysis. The trend lines were then used to calculate the deflection corresponding to P = 89 kN (20,000 lb) for the six segments of the load-deflection curves. The resulting deflections were used to compute the secant slopes at both sides of the longitudinal joint in the FRP decks (i.e., $y > 0$ and $y < 0$), as shown in equation III.1.3:

$$\tan\theta_{Y+} = \frac{LV2T - LV7T}{B/4}$$
$$\tan\theta_{Y-} = \frac{LV7T - LV11T}{B/4} \quad \text{(III.1.3)}$$

Then, the change in the slope angle at the longitudinal joint location is computed as shown in equation III.1.4:

$$\Delta\theta_n = \theta_{Y+} - \theta_{Y-} \quad \text{(III.1.4)}$$

If $\Delta\theta_n > 0$, then the deck curves transversely concave down, and if $\Delta\theta_n < 0$, it curves concave up. The resulting changes in slope angles are given in Table III.1.3.

Table III.1.3 Reinforced-Concrete Deck y-Direction Slope Change

	Temperature (°C)					
	24		49		–30	
Load Cycles	Mean (rad)	COV (%)	Mean (rad)	COV (%)	Mean (rad)	COV (%)
0	–1.65E-04	3.56	–1.65E-04	4.40		
100000			–1.53E-04	2.02		
500000			–1.69E-04	1.27		
1000000			–1.58E-04	2.44	–2.67E-04	3.74
1000000 + 100000					–2.68E-04	4.16
1000000 + 500000					–3.56E-04	3.80
1000000 + 1000000					–2.33E-04	4.74

An indicator of retained deck and joint stiffness in the y-direction, $R_{y,n}$, is defined as the mean change in slope angle after n load cycles with controlled temperature with respect to the mean initial change in slope angle, as shown in equation III.1.5:

$$R_{y,n} = \frac{\Delta\theta_o}{\Delta\theta_n}. \qquad \text{(III.1.5)}$$

If $R_{y,n} > 0$, then the deck does not change the curvature orientation. In particular, if $0 < R_{y,n} < 1$, the change in slope angle is more pronounced, and if $R_{y,n} > 1$, the change in slope angle is less pronounced than the baseline quasi-static test. On the other hand, if $R_{y,n} < 0$, the deck changes the curvature orientation (e.g., from concave up to concave down, or vice versa). The resulting retained stiffness indicators are given in Table III.1.4.

Table III.1.4 Reinforced-Concrete Deck y-Direction Stiffness Indicator

	Temperature (°C)					
	24		49		-30	
Load Cycles	Statistical Level	$R_{y,n}$	Statistical Level	$R_{y,n}$	Statistical Level	$R_{y,n}$
0	A	1.000	A	1.004		
100000			B	1.085		
500000			A	0.979		
1000000			A, B	1.050	C	0.620
1000000 + 100000					C	0.617
1000000 + 500000					D	0.465
1000000 + 1000000					E	0.710

*The same letter indicates the same curvature with 95% confidence.

The longitudinal panel joint, which is located in the FRP deck panels tested between LV2-T and LV11-T, incorporates additional shear and bending flexibility that affects the change in the slope angle. Therefore, the change in the slope angle does not only measure the bending and shear stiffness of the panels, but it also can account for the discrete bending and shear stiffness of the joint. The reason for adopting the slope angle method of measuring the stiffness response in the transverse direction instead of a more conventional quadratic fit of deflections, which is more applicable to reinforced-concrete decks, is to model the articulated nature of FRP panels.

III.1.7.3 Statistical Analysis

Statistical analysis of the load-deflection ratio and the change in slope angle for the deck system was performed using one-way analyses of variance (ANOVA) for each number of cycles and temperature condition. The analysis was conducted using the SYSTAT software package. The ANOVA analysis determined if the response of the deck system was a function of number of cycles or temperature. The model for a one-way ANOVA is represented symbolically as follows:

$$Y_n = B_o + B_1 \cdot X_n + \varepsilon_n \qquad \text{(III.1.6)}$$

where Y_n = observed mechanical property (load-deflection ratio or change in slope angle) for the number of cycles n under controlled temperature

B_o, B_1 = coefficients of the model

X_n = code associated with the variable under study (e.g., temperature or cumulative load cycles)

ε_n = random unit variation within the block of data.

The null hypothesis and alternative hypothesis are given in equation III.1.7:

$$H_0 : B_1 = 0$$
$$H_A : B_1 \neq 0 \qquad \text{(III.1.7)}$$

Post hoc analysis of type Bonferroni was used for pair-wise comparisons with a confidence level of 95% (α = 0.05). Four one-way ANOVA tests were performed for each mechanical property (i.e., load-deflection slope and change in slope angle) of the FRP deck system. The first two compared the mechanical property as the dependent variable with the temperature as the factor and the number of cycles held constant (0 and 1,000,000 cycles, respectively). The second two used the mechanical property as the dependent variable with the number of cycles as the factor, holding the temperature constant, 49°C (120°F) and –30°C (–22°F), respectively. Additional tests were done only if the stiffness ratio was close between two or more cycles across temperatures and compared only those specific tests. This was equivalent to performing paired t-tests.

The reinforced-concrete deck degraded about the same amount for the two factors in the x-direction: cycles and temperature. Of the cycle degradation the majority occurred within the first 100,000 cycles at each temperature (Figure III.1.13). The temperature did not significantly change the stiffness in the x-direction.

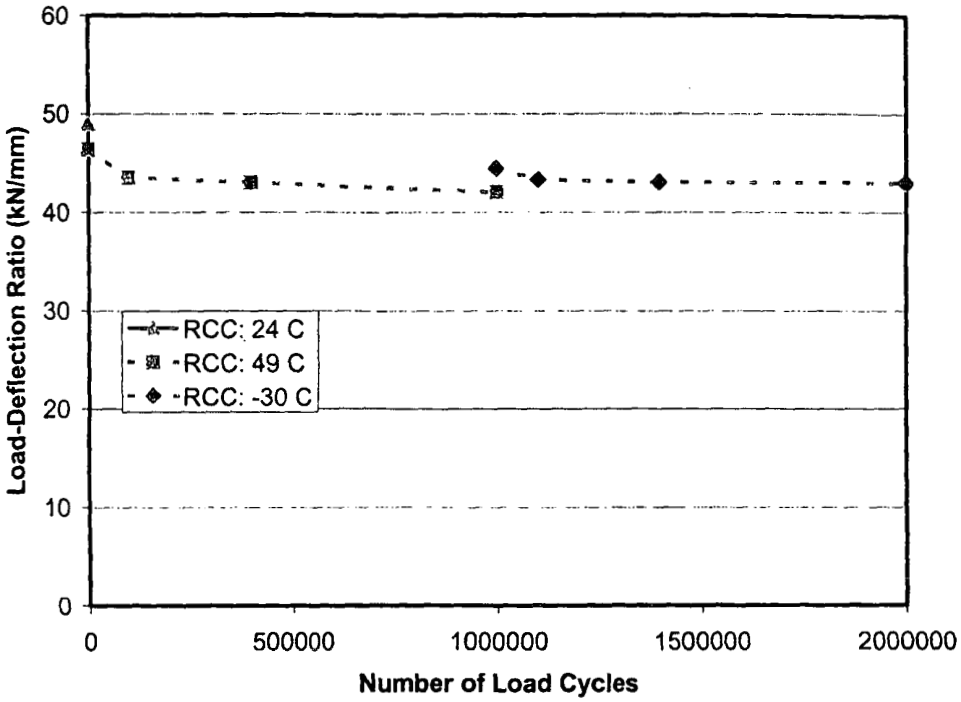

Figure III.1.13 – Load-Deflection Ratio History

Stiffness in the y-direction analysis proved less helpful in measuring the degradation of the decks than that of the x-direction stiffness. For all decks the data had more spread than that of the stiffness in the x-direction test. This indicates that the test is more sensitive to outside factors such as details in the way the quasi-static test was run and the exact conditions at the time of the quasi-static test. This deck had statistically almost no change in the y-direction stiffness indicator for the first one million load cycles

at high temperatures. However, there is a statistically significant reduction in the y-

at high temperatures. However, there is a statistically significant reduction in the y-direction stiffness indicator during the second million load cycles at low temperature.

The micro-strains per unit load in the x-direction on the top surface showed an initial increase with temperature. However, they remained mainly unchanged with the number of load cycles as illustrated in Figure III.1.14.

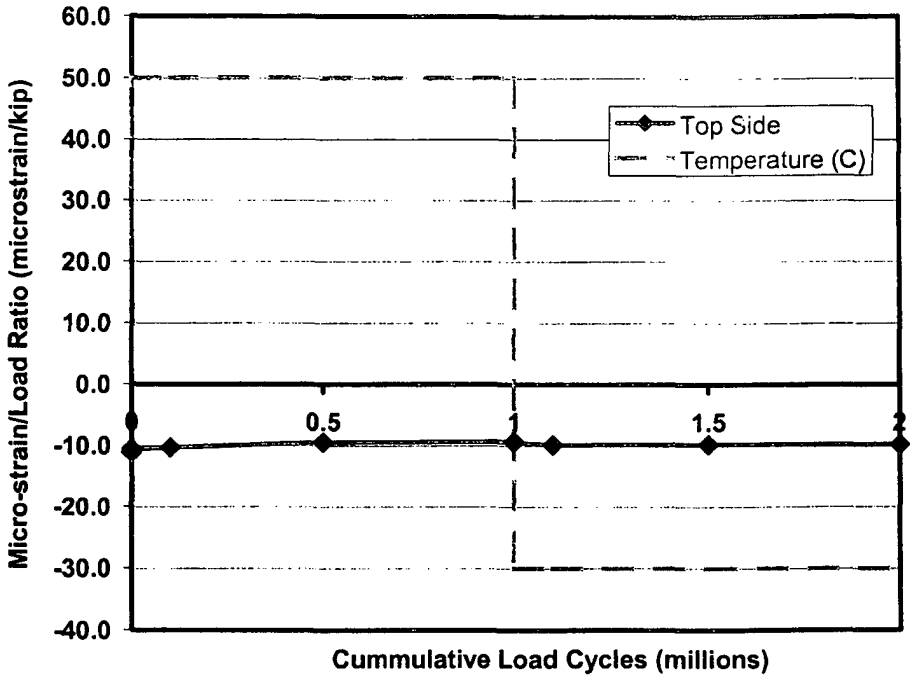

Figure III.1.14 Micro-strain per 4.45 kN (1000 lb) Load during Fatigue Cycling

III.1.9 Conclusions

The analysis done on the deck is a useful measure of stiffness in the x-direction and a useful indicator of stiffness in the y-direction. The x-direction load-deflection analysis takes into account support deflections and is conducted over a continuous span. Both of these factors combine to provide a useful measure for the amount of deflection expected with applied load.

The y-direction analysis is less useful because of the many uncertainties incorporated into one number, the change in slope angle, by the analysis. Unlike the x-direction analysis, the y-direction analysis did not take into account the support deflections and was not conducted over a continuous span.

The statistical analysis performed was adequate for the desired information. The one-way ANOVA was proven to be an efficient analysis tool for determining significant changes in load-deflection ratios and change in slope angle between quasi-static tests.

Overall, the reinforced-concrete conventional deck in the x-direction degraded about the same amount for temperature changes and load cycles. This amounted to about a 6% change with temperature change and another 6% change with the first 100,000 load cycles at each temperature.

III.2 Fatigue Response of Hybrid FRP-Concrete Bridge Deck under Extreme Temperature Conditions

III.2.1 Abstract

The fatigue performance evaluation at extreme temperature of a two-span fiber-reinforced polymer (FRP) concrete hybrid prototype deck prototype built on three W-section steel girders is presented. The FRP material was fabricated by the pultrusion process by Diversified Fabricators Inc. (DFI). The hybrid FRP-concrete deck system was designed by Composites Deck Solutions (CDS). A reinforced-concrete conventional (RCC) deck was considered for the benchmark response.

II.2.2 Introduction

The fatigue performance evaluation at extreme temperature of a two-span continuous fiber-reinforced polymer (FRP) concrete deck prototype built on three W-section steel girders is presented. The structural system studied is a hybrid FRP-concrete deck. The FRP material was fabricated by the pultrusion process by Diversified Fabricators Inc. (DFI), Erlanger, KY. The hybrid FRP-concrete deck system is commercialized by Composites Deck Solutions (CDS). A reinforced-concrete conventional (RCC) deck was considered for the benchmark response.

The deck-girder system was subjected to an eccentric cyclic load that simulates an AASHTO HS20 design truck wheel load with impact. Initially, one million load cycles were applied at a controlled high temperature, 49°C (120°F), and then another million load cycles were applied at a controlled low temperature, –30°C (–22°F). Quasi-static load tests were conducted at specific intervals during fatigue cycling to evaluate the load-

deflection and load-strain response at several deck locations. A reinforced-concrete conventional (RCC) deck designed by the Ohio Department of Transportation was fabricated and tested under the same load and temperature regime (See Chapter III.1). The RCC deck was utilized to establish the "current practice" benchmark response. The FRP deck performance was compared with the RCC deck. The fatigue tests of the FRP and RCC decks were conducted at the U.S. Army Cold Regions Research and Engineering Laboratory in Hanover (CRREL), N.H.

The fatigue-temperature performance was assessed based on two damage indicators by

1. Establishing if the FRP deck apparent bending stiffness in the x-direction degrades with number of load cycles and temperature changes. The apparent bending stiffness in the x-direction is associated with and is measured by the corrected maximum deflections.
2. Establishing if the FRP deck apparent bending stiffness in the y-direction degrades with number of load cycles and temperature changes. The apparent bending stiffness in the y-direction is associated with and is measured by the change in slope angle in the transverse direction of the deck under maximum loading conditions.

III.2.3 Description of the Deck System

FRP pultruded panels are used for stay-in-place formwork that also serves as concrete reinforcement. The pultruded panels have a width of 457 mm (18 in.) and two stiffening tubular cells with a height of 76 mm (3 in.). The pultruded material is reinforced with E-glass roving and directional bias fabric in a polyester-vinyl ester resin

blend. The panels are placed perpendicularly to the traffic direction and have a 25-mm (1-in.) lip and tongue overlapping joint. Epoxy coating is applied on the top surface, and sand is sprayed to provide a mechanical interlock with the concrete. Concrete is cast on the FRP panels to attain a specified slab depth of 203 mm (8 in.). Top reinforcement in both directions is provided by non-corrosive E-glass rebar with deformations to improve the bond with the concrete. The deck is connected to the supporting steel girders using shear studs. Holes are predrilled in the pultruded panel between the tubular cells. After placing the pultruded panels on the steel girders, the shear studs are welded. The stud welding process attaches the shear stud to the steel girder surface in a very rapid operation, and it forms a bond that is actually stronger than the surrounding metal. This type of deck-connection has the advantage of providing monolithic or "composite" action between the deck and the supporting beam. A concrete haunch is placed between the FRP deck panels and the steel girders, as shown in Figure III.2.1.

III.2.4 Test Protocol

There are no specifications available for FRP bridge decks on the number of load cycles required for fatigue performance evaluation. A fatigue performance evaluation procedure was initially developed and applied to qualify FRP decks panels fabricated by pultrusion and vacuum assisted resin transfer molding (VARTM) (Lopez-Anido et al. 1998). The present evaluation consisted of applying two million simulated wheel load cycles at two controlled extreme temperatures, 49°C (120°F) and –30°C (–22°F), on the FRP-concrete panels attached to steel girders, i.e., one million cycles at 49°C (120°F) and one million cycles at –30°C (–22°F). The two-span continuously supported hybrid FRP concrete deck was subjected to a simulated AASHTO HS20-44 design truck wheel load

(Figure III.2.2). A girder spacing of 2.74 m (108 in) was selected, as shown in Figure III.2.1.

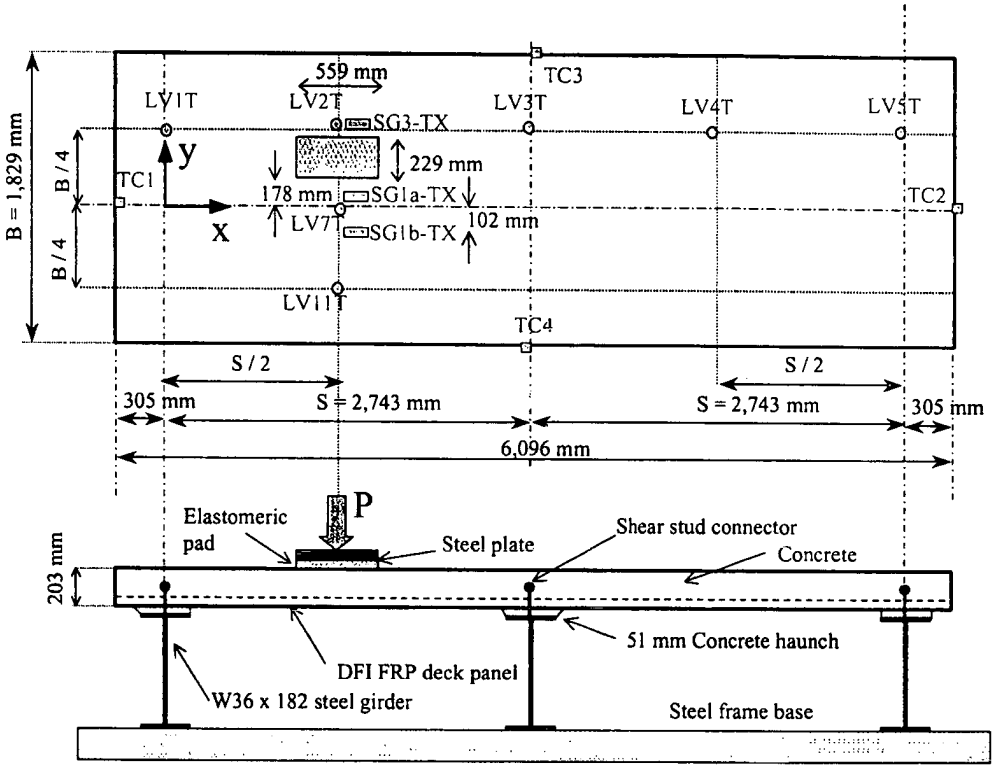

Figure III.2.1 Test Setup

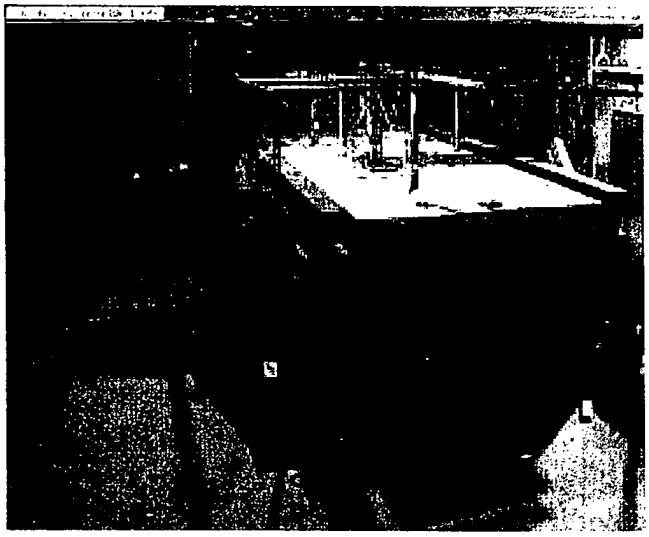

Figure III.2.2 FRP Panel Supported by Steel Beams during Fatigue Testing

The maximum load to be applied was computed based on an AASHTO HS20-44 design truck wheel load with a dynamic load allowance (impact factor). The design truck wheel load is one half of the axle load. The impact factor adopted was 30%. Then, the maximum computed fatigue load resulted in P_{max} = 71.2 kN (16,000 lb) × 1.3 = 92.5 kN (20,800 lb). The applied load frequency ranged between 2.4 and 3 Hz. Based on these applied load frequencies and the flexibility of the FRP deck, the actual maximum applied fatigue load attained was P_{max} = 89.0 kN (20,000 lb). The minimum applied load was P_{min} = 8.9 kN (2,000 lb). Therefore, the fatigue stress ratio was approximately R = 0.1.

The fatigue test specimens were not anticipated to fail during the two-million-cycle duration, so the fatigue analysis was focused on assessing the structural degradation associated with the cyclic loading. Fatigue damage accumulation can induce stiffness degradation of the deck panels and in the panel-to-panel longitudinal joints of the FRP pultruded profiles in the bottom reinforcement. Besides, fatigue damage can lead to residual damage in the FRP-concrete deck to steel girder haunch connection. To assess fatigue damage, quasi-static tests were conducted prior to the application of load cycling and at specified increments of fatigue cycling, as shown in Figure III.2.3.

First, at ambient temperature, 24°C (75°F), a set of quasi-static tests was conducted to obtain baseline load-deflection and load-strain values. Then, the test room was warmed up to 49°C (120°F). The hybrid FRP-concrete deck temperature was monitored until it reached the room temperature. Then, a second set of quasi-static test, but now at high temperature, was conducted. After this evaluation, one million load cycles were applied. Quasi-static tests were conducted at 100,000, 500,000, and

1,000,000 load cycles. For the low-temperature tests, the room was cooled to –30°C (–22°F), and the fatigue test with the corresponding quasi-static tests was repeated for the second million of load cycles.

III.2.5 Test Setup

The hybrid FRP concrete deck dimensions were specified to model a typical slab-on-steel girder highway bridge, as shown in Figure III-2-1. A fatigue-testing frame was designed to accommodate the deck system prototype with the three connected steel girders. The deck prototype was instrumented with strain gauges, thermocouples, and Linear Voltage Differential Transducers (LVDTs) to measure vertical deflection (Figure III.2.1). As discussed before, the applied load represents an AASHTO HS20-44 design truck wheel load with a dynamic load allowance (impact factor). The impact factor adopted was 30%. Thus, the maximum applied load resulted in P_{max} = 71.2 kN (16,000 lb) × 1.3 = 92.5 kN (20,800 lb).

The fatigue tests were performed in CRREL's Material Evaluation Facility (MEF). This is a well-insulated room with interior dimensions of approximately 7.92 m (26 ft) wide by 12.80 m (42 ft) long and 3.66 m (12 ft) high. A set of double doors 3.35 m (11 ft) wide by 3.35 m (11 ft) tall allows the large fatigue test frame and the hybrid FRP concrete bridge deck prototypes to be moved in and out of the MEF facility. A self-reacting steel test frame was designed and built at CRREL for a maximum load capacity of 266.9 kN (60,000 lb). One 97.9-kN- (22,000-lb-) capacity hydraulic actuator was mounted on the steel reaction frame to apply cyclic loading on the deck. The hybrid FRP concrete deck specimen was attached to three steel girders W36x182, resulting in a continuous two-span bridge structure (Figure III.2.2). The actuator applied the load on a

rectangular steel plate of 229 × 559 mm (9 × 22 in.) that simulates a wheel load contact area (AASHTO 1996). An elastomeric pad was placed between the steel plate and the hybrid FRP concrete deck surface to provide uniform pressure. The load was applied eccentrically with respect to the traffic flow direction to study the load distribution in the y-direction, as shown in Figure III.2.1.

Load, deflection, strain, and temperature were the general parameters of measurement in this test program. The hybrid FRP-concrete deck specimen was instrumented with strain gauges, LVDTs, and thermocouples. Seven LVDTs supported by an independent frame were used to measure deflections on the top surface of the deck. Four thermocouples were placed on four sides of the deck surface, and one thermocouple was used for air temperature. The thermocouples were used to verify that the deck panel reached equilibrium with room temperature. The locations of the LVDTs, strain gauges, and thermocouples on the top of the deck are shown in Figure III.2.1. The location of the strain gauges bonded to the bottom deck surface (BX) was symmetrical with respect to the numerically matching strain gauges bonded to the top surface (TX).

The test setup induced a positive bending moment under the applied load (x = S/2) and a negative bending moment on the central support (x = S) and the adjacent span. An uplifting force resulted on the end girder support (x = 2 × S). This uplifting force was partially counteracted by the weight of the deck and steel beams.

As mentioned before, the hybrid FRP-concrete deck was evaluated for approximately 2,000,000 load cycles with controlled temperature. The first million load cycles were conducted at 49°C (120°F), while the second million cycles were performed at about –30°C (–22°F). The first quasi-static test was at room temperature, about 24°C

(75°F), before the fatigue cycles began and served as the control baseline. In the quasi-static tests, the load was applied at a rate of 1 mm/min (0.04 in./min), and sensor measurements were recorded every 3 s. Each quasi-static test consisted of a loading and unloading cycle. The quasi-static test was repeated three times, resulting in three peak loads and six varying load intervals for data analysis (Figure III.2.3).

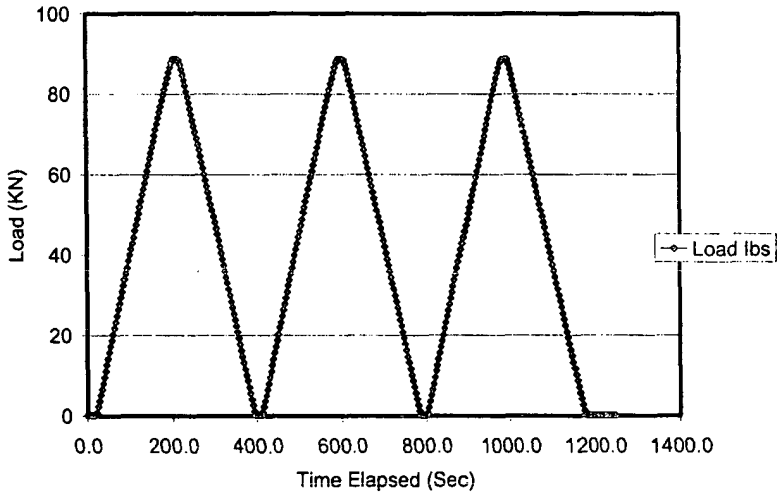

Figure III.2.3 Typical Quasi-Static Load Tests

III.2.6 Experimental Results

The raw data were analyzed to produce load-deflection curves for each deck test. Typical load-deflection curves for room temperature, 24°C (75°F), at five deck locations corresponding to LVDTs mounted on the top of the panel and aligned in the x-direction, are shown in Figure III.2.4. Similarly, high-temperature load-deflection curves at the five locations after one million high-temperature load cycling are shown in Figure III.2.5. Figure III.2.6 shows the low-temperature load-deflection curves for the same locations after one million hot plus one million cold fatigue cycles. Figure III.2.7 compares the

maximum deflection data for the room-temperature baseline, after one million cycle at high-temperature, and after an additional one million cycles at low temperature. From these load-deflection curves we observe that the low-temperature stiffness after an accumulated two million load cycles is lower than the initial stiffness at room temperature. This observation implies that in this case the panel stiffness is controlled not by temperature but by the number of load cycles.

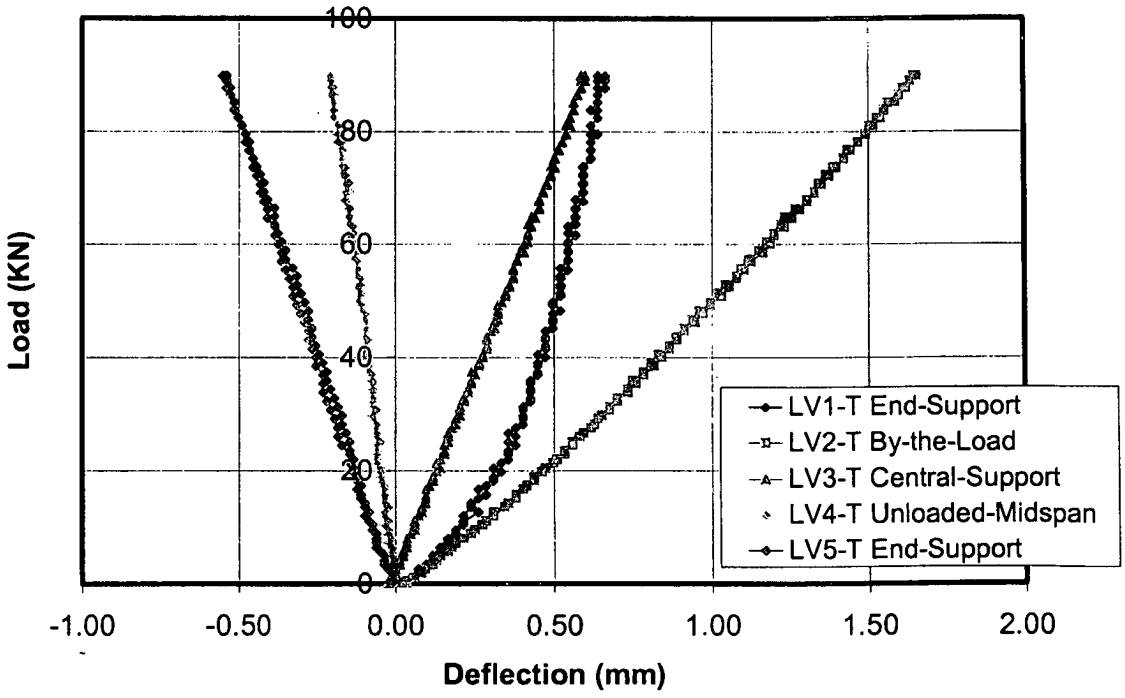

Figure III.2.4 Room-Temperature Load-Deflection Curves for Top LVDTs Aligned in x-Direction prior to Fatigue Cycling

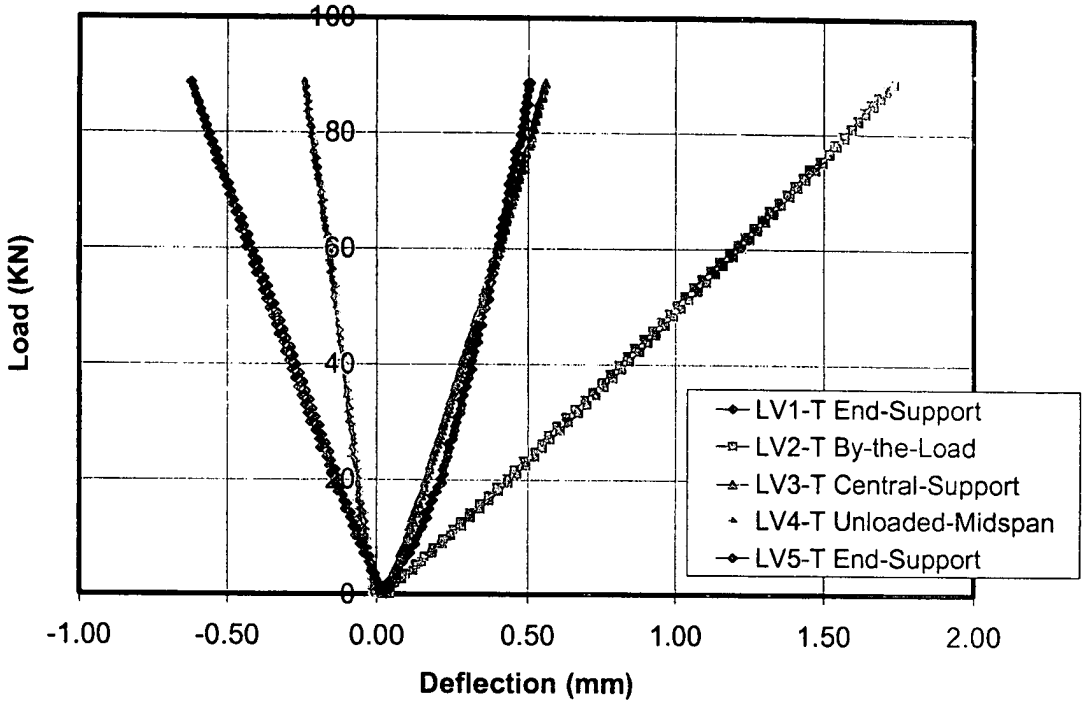

Figure III.2.5 High-Temperature Load-Deflection Curves for Top LVDTs aligned in x-Direction after One Million Hot Fatigue Cycles

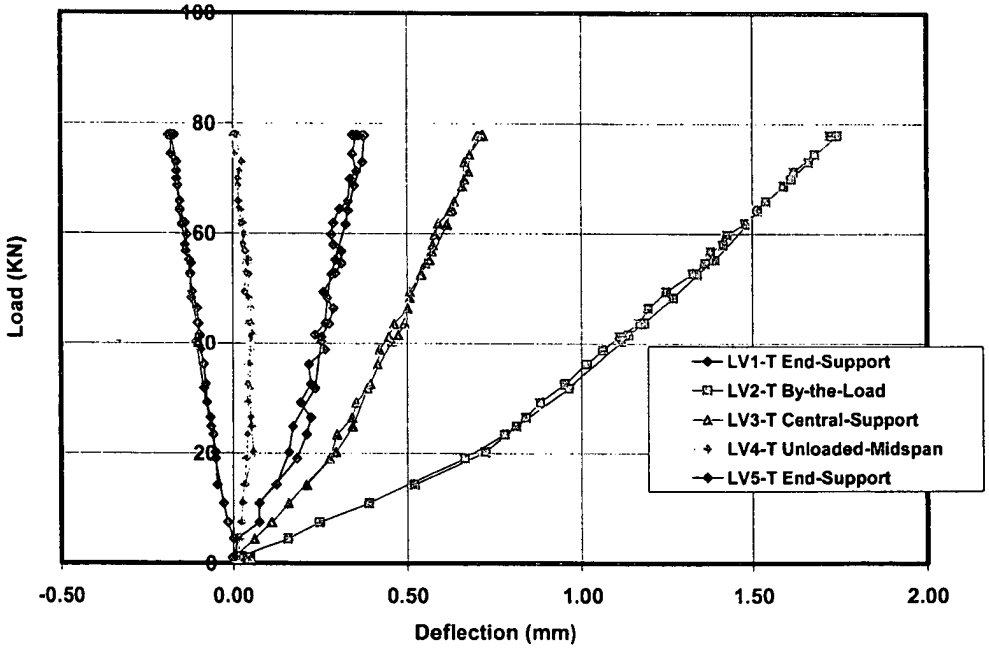

Figure III.2.6 Low-Temperature Load-Deflection Curves for Top LVDTs Aligned in x-Direction after One Million Hot plus One Million Cold Fatigue Cycles

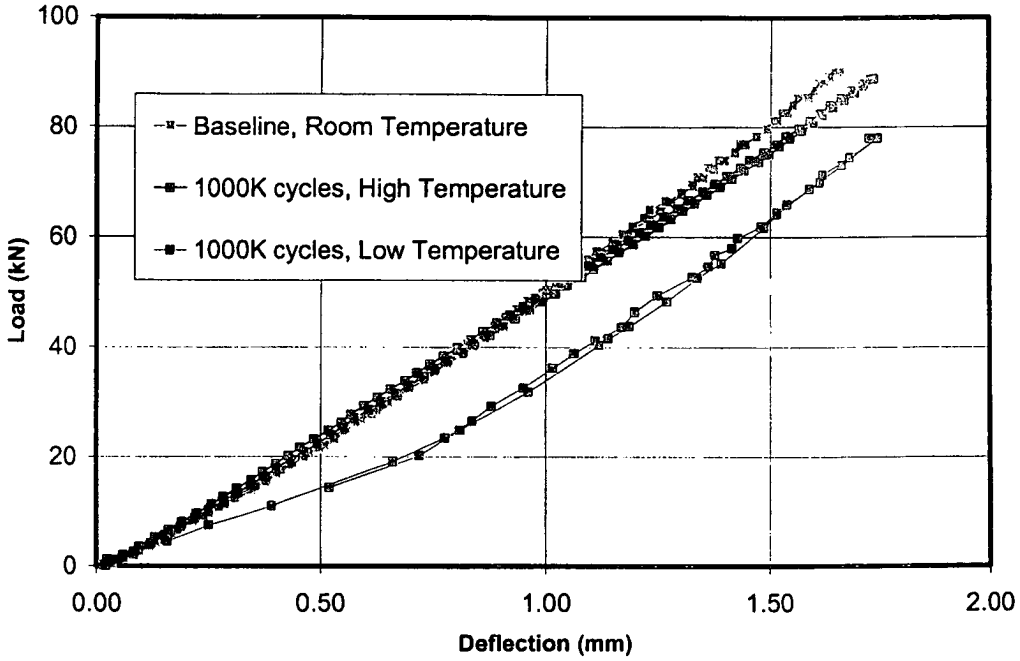

Figure III.2.7 Maximum Deflections for Three Test Conditions (Measured by LV2-T)

The maximum total deflections measured with the top LVDTs (LV1T, LV2T, LV3T, LV4T, and LV5T) aligned the x-direction are shown in Figure III.2.8 for room-temperature (RT) baseline, high temperature (HT) and low temperature (LT), the last two after one million cycles at each temperature. These total deflections include both deck deflections and support deflections measured during the quasi-static tests. A deck uplifting was observed over the end girder. These deflection curves confirm that the decrease in temperature increased the panel stiffness only slightly after a two million load cycles.

The maximum deflections measured with the top LVDTs (LV2T, LV7T, and LV11T) aligned along the y-direction during the quasi-static tests are shown in Figure III.2.9. From this figure we observe that the panel longitudinal joint is able to transfer the shear force in the y-direction without any noticeable joint vertical slip.

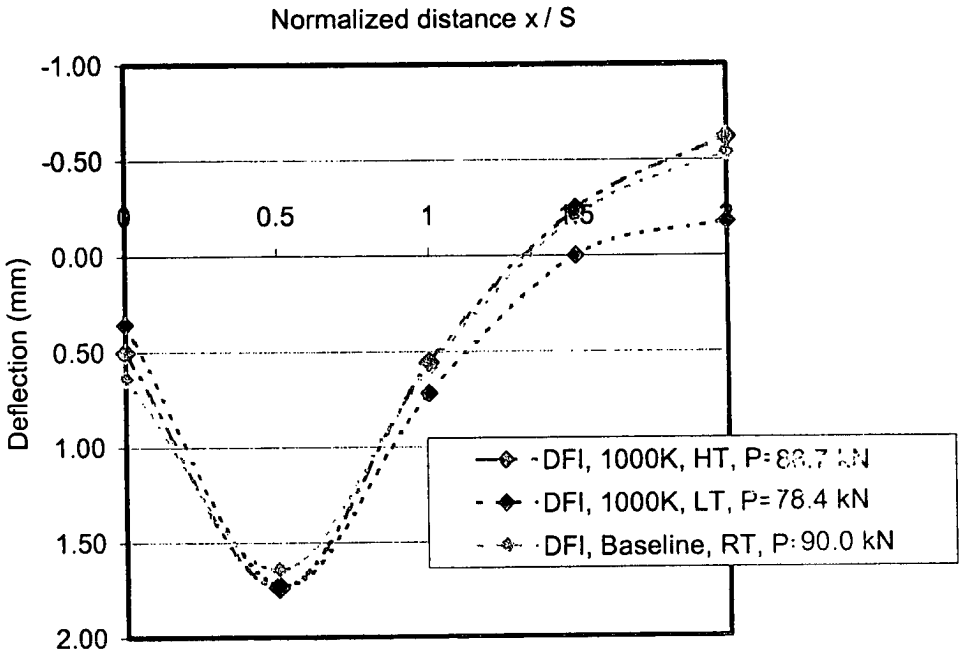

Figure III.2.8 Top Deflection Variation along the x-Direction for Maximum Load: LV1-T, LV2-T, LV3-T, LV4-T, LV5-T

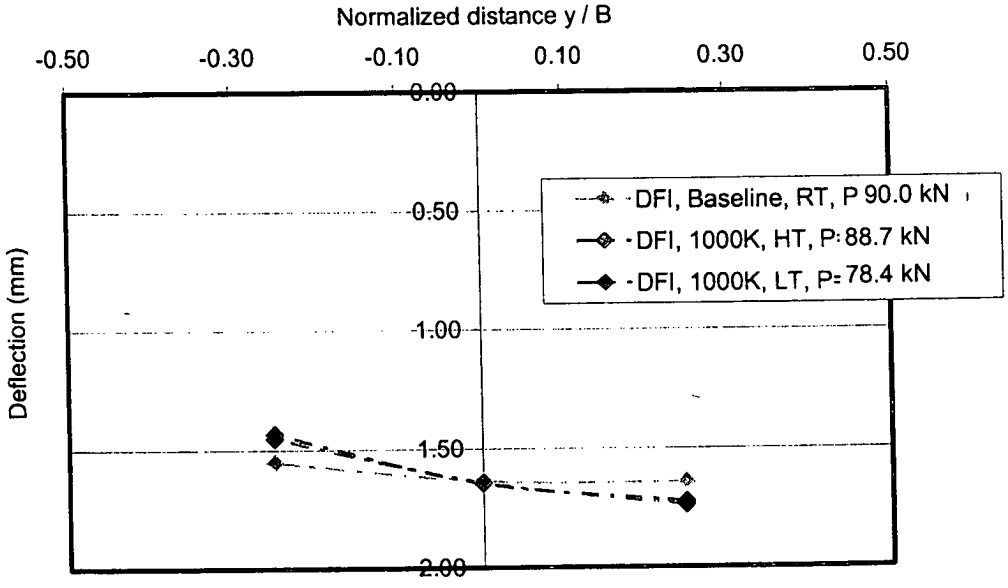

Figure III.2.9 Top Deflection Variation along the y-Direction for Maximum Load: LV2-T, LV7-T, LV11-T

Compressive strains on the top of the deck in the x-direction measured at room temperature prior to fatigue cycling are shown in Figure III.2.10. Similarly, tensile strains at symmetrical locations on the bottom surface are shown in Figure III.2.11. All the curves are linear within the loading range. Compressive strains on the top surface are slightly smaller than the corresponding tensile strains on the bottom surface. Possibly the FRP at the bottom layer deformed more than the concrete for a given load. Linear strain curves were obtained at high temperature after one million load cycles (Figure III.2.12 and Figure III.2.13).

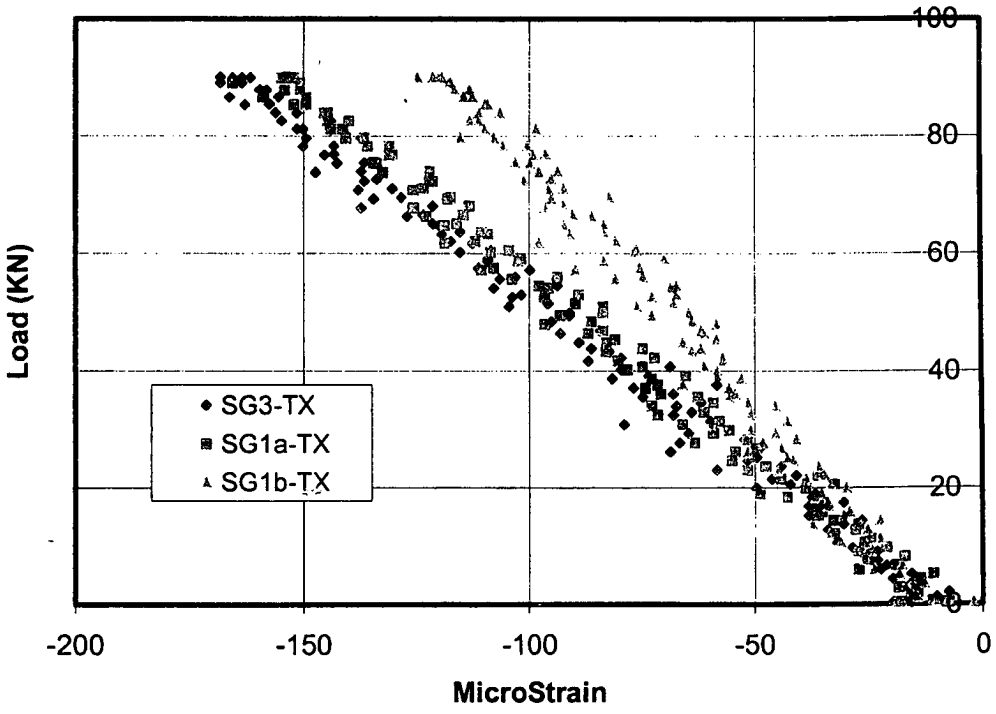

Figure III.2.10 Room-Temperature Strain (x-Direction) Curves Prior to Fatigue Cycling for Top Gauges (Loaded Span): SG1a-TX, SG1b-TX, SG3-TX

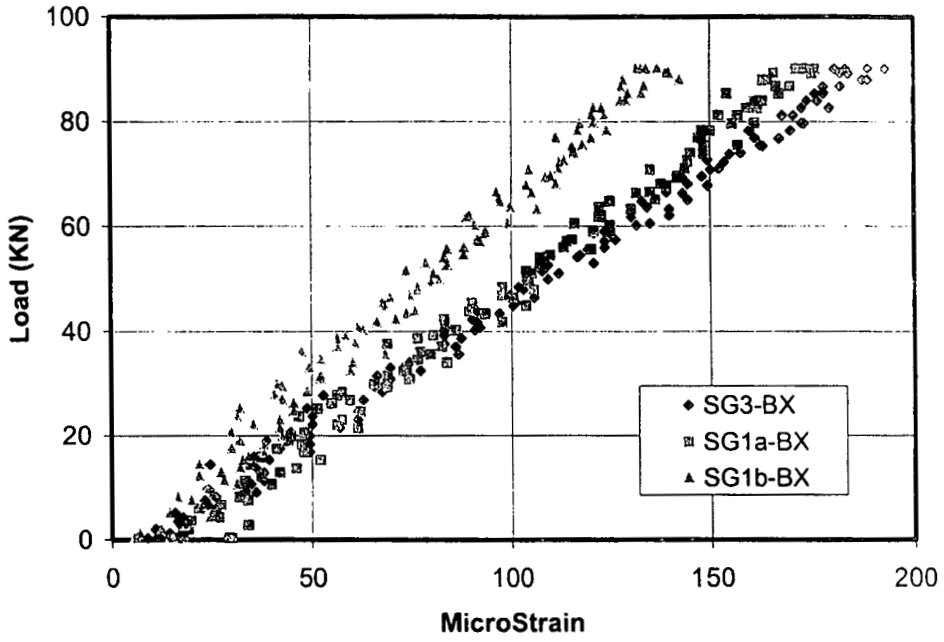

Figure III.2.11 Room-Temperature Strain (x-Direction) Curves Prior to Fatigue Cycling for Bottom Gauges (Loaded Span): SG1a-BX, SG1b-BX, SG3-BX

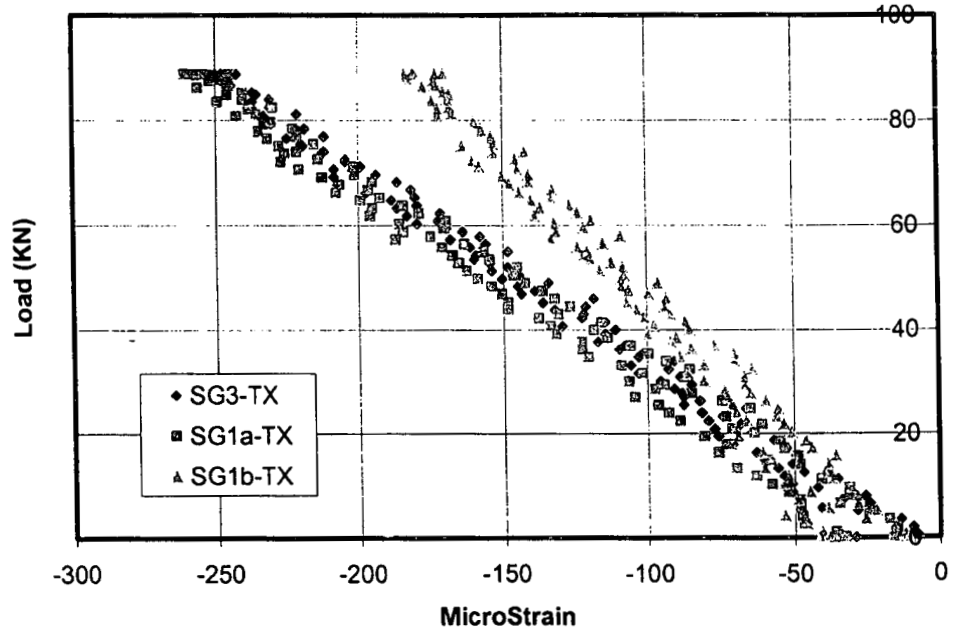

Figure III.2.12 High-Temperature Strain (x-Direction) Curves After One Million Hot Cycles for Top Gauges (Loaded Span): SG1a-TX, SG1b-TX, SG3-TX

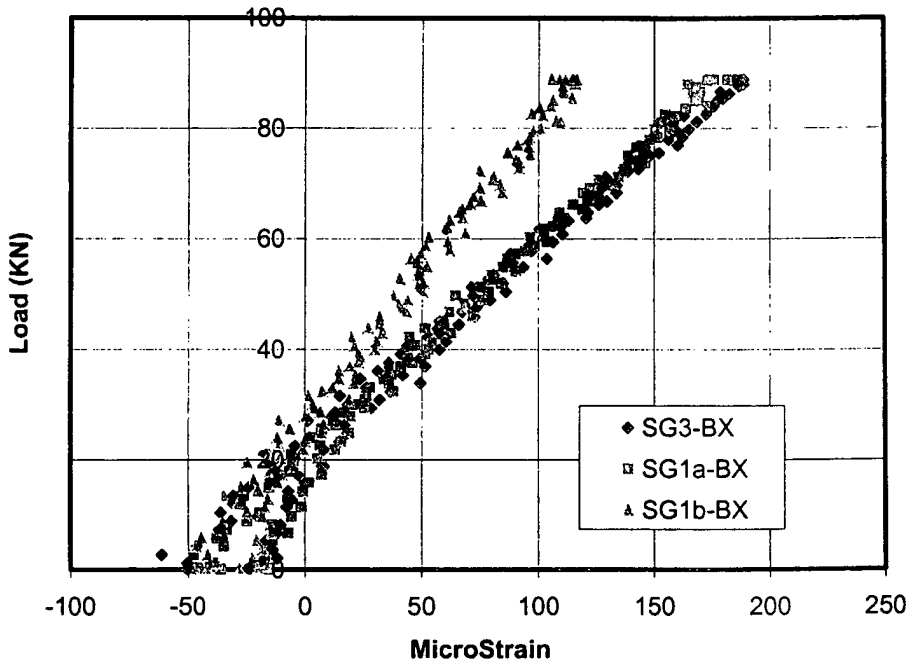

Figure III.2.13 High-Temperature Strain (x-Direction) Curves After One Million Hot Cycles for Bottom Gauges (Loaded Span): SG1a-BX, SG1b-BX, SG3-BX

The FRP deck was inspected visually for signs of distress such as cracks and damage at connections after fatigue cycling. Hairline concrete cracks in the tension region over the central support were observed. After 1,000,000 cycles an increase in the central support deformation, as well as uplifting of the end support, was observed.

III.2.7 Data Analysis

To evaluate the hybrid FRP-concrete deck response with temperature and number of load cycles, two stiffness indicators are defined:

1) Stiffness indicator in the x-direction is computed based on corrected maximum deflections along a longitudinal line (LV1T, LV2T, LV3T); and
2) Stiffness indicator in the y-direction is computed based on maximum deflections across a transverse line (LV2T, LV7T, LV11T).

III.2.7.1 Retained Stiffness in the x-Direction

The maximum deflection, δ_c, was corrected to account for support deflection according to equation III.2.1:

$$\delta_c = (LV2T) - \tfrac{1}{2}(LV1T + LV3T) \qquad \text{(III.2.1)}$$

where LV1T, LV2T, and LV3T are defined as deflection at the points given in Figure III.2.1. For each quasi-static test corresponding to number of applied load cycles, n, the six segments of the load-deflection curves (see the loading and unloading segments in Figure III.2.3) for varying load intervals were plotted. A linear response was observed in all cases and approximated with a linear least-squares regression line to compute the load-deflection ratio $\left(P/\delta_c\right)_n$. These load-deflection ratios are related to the stiffness of the deck in the x-direction. The resulting load-deflection ratios are given in Table III.2.1.

Table III.2.1 Hybrid FRP-Concrete Deck x-Direction Load-Deflection Ratio

	Temperature (°C)					
	24		49		-30	
Load Cycles	Mean (kN/mm)	COV (%)	Mean (kN/mm)	COV (%)	Mean (kN/mm)	COV (%)
0	89.1	0.51	77.7	1.04		
100000			72.7	0.52		
500000			71.9	0.38		
1000000			72.3	0.55	83.8	0.39
1000000 + 100000					80.9	1.00
1000000 + 500000					71.8	5.44
1000000 + 1000000					70.8	7.95

Note: 1 kN/mm = 5.71 kip/in.

An indicator of retained stiffness in the x-direction, $R_{x,n}$, is defined as the mean residual load-deflection ratio after n load cycles with controlled temperature with respect to the mean initial load-deflection ratio, as shown in equation III.2.2:

$$R_{x,n} = \frac{(P/\delta_c)_n}{(P/\delta_c)_o} \quad \text{(III.2.2)}$$

Then $R_{x,n} < 1$ implies a reduction in deck stiffness, while $R_{x,n} > 1$ implies an increase in deck stiffness. The resulting retained stiffness indicators are given in Table III.2.2.

Table III.2.2 Hybrid FRP-Concrete Deck x-Direction Stiffness Indicator

	Temperature (°C)					
	24		49		–30	
Load Cycles	Statistical Level	$R_{x,n}$	Statistical Level	$R_{x,n}$	Statistical Level	$R_{x,n}$
0	A, E	1.000	B	0.871		
100000			C	0.816		
500000			C	0.807		
1000000			C	0.811	D, E	0.940
1000000 + 100000					D	0.908
1000000 + 500000					C	0.805
1000000 + 1000000					C	0.794

*The same letter indicates the same stiffness ratio with 95% confidence

III.2.7.2 Retained Stiffness in the y-Direction

Deflections were measured at three points aligned across the hybrid FRP-concrete deck (LV2-T, LV7-T, and LV11-T), as shown in Figure III.2.1. Load-deflection curves were plotted for the six load-varying intervals of each quasi-static test. These load-deflection curves followed a linear trend and were fitted using linear least-squares regression analysis. The trend lines were then used to calculate the deflection corresponding to P = 89 kN (20,000 lb) for the six segments of the load-deflection curves. The resulting deflections were used to compute the secant slopes at both sides of the longitudinal FRP joint (i.e., $y > 0$ and $y < 0$), as shown in equation III.2.3:

$$\tan\theta_{Y+} = \frac{LV2T - LV7T}{B/4}$$
$$\tan\theta_{Y-} = \frac{LV7T - LV11T}{B/4} \quad \text{(III.2.3)}$$

Then, the change in the slope angle at the longitudinal joint location is computed as shown in equation III.2.4:

$$\Delta\theta_n = \theta_{Y+} - \theta_{Y-} \quad \text{(III.2.4)}$$

If $\Delta\theta_n > 0$, then the deck curves transversely concave down, and if $\Delta\theta_n < 0$, it curves concave up. The resulting changes in slope angles are given in Table III.2.3.

Table III.2.3 Hybrid FRP-Concrete Deck y-Direction Slope Change

	Temperature (°C)					
	24		49		–30	
Load Cycles	Mean (rad)	COV (%)	Mean (rad)	COV (%)	Mean (rad)	COV (%)
0	–1.69E-04	3.59	–2.70E-04	7.30		
100000			–2.04E-04	2.15		
500000			–2.04E-04	2.40		
1000000			–2.18E-04	2.87	–2.71E-04	8.30
1000000 + 100000					–2.02E-04	6.60
1000000 + 500000					–2.08E-04	1.69
1000000 + 1000000					–2.79E-04	8.29

An indicator of retained deck and joint stiffness in the y-direction, $R_{y,n}$, is defined as the mean change in slope angle after n load cycles with controlled temperature with respect to the mean initial change in slope angle, as shown in equation III.2.5:

$$R_{y,n} = \frac{\Delta\theta_o}{\Delta\theta_n} \quad \text{(III.2.5)}$$

If $R_{y,n} > 0$, then the deck does not change the curvature orientation. In particular, if $0 < R_{y,n} < 1$, the change in slope angle is more pronounced, and if $R_{y,n} > 1$, the change in

slope angle is less pronounced than the baseline quasi-static test. On the other hand, if $R_{y,n} < 0$, the deck changes the curvature orientation (e.g., from concave up to concave down, or vice versa). The resulting retained stiffness indicators are given in Table III.2.4.

Table III.2.4 Hybrid FRP-Concrete Deck y-Direction Stiffness Indicator

	Temperature (°C)					
	24		49		-30	
Load Cycles	Statistical Level	$R_{y,n}$	Statistical Level	$R_{y,n}$	Statistical Level	$R_{y,n}$
0	A	1.000	B	0.628		
100000			C	0.831		
500000			C	0.831		
1000000			C	0.778	B	0.625
1000000 + 100000					C	0.837
1000000 + 500000					C	0.816
1000000 + 1000000					B	0.607

*The same letter indicates the same curvature with 95% confidence

The longitudinal panel joint, which is located between LV2-T and LV11-T, incorporates additional shear and bending flexibility that affects the change in the slope angle. Therefore, the change in the slope angle not only measures the bending and shear stiffness of the panels, but it also accounts for the discrete bending and shear stiffness of the joint. The reason for adopting the slope angle method of measuring the stiffness response in the transverse direction instead of a more conventional quadratic fit of deflections, which is more applicable to reinforced-concrete decks, is to model the articulated nature of the hybrid FRP-concrete panels.

Statistical Analysis

Statistical analysis of the load-deflection ratio and the change in slope angle for the hybrid FRP-concrete deck system was performed using one-way analyses of variance

(ANOVA) for each number of cycles and temperature condition. The analysis was conducted using the SYSTAT software package. The ANOVA analysis determined if the response of the deck system was a function of number of cycles or temperature. The model for a one-way ANOVA is represented symbolically as follows:

$$Y_n = B_o + B_1 \cdot X_n + \varepsilon_n \tag{III.2.6}$$

where Y_n = observed mechanical property (load-deflection ratio or change in slope angle) for the number of cycles n under controlled temperature

B_o, B_1 = coefficients of the model

X_n = code associated with the variable under study (e.g., temperature or cumulative load cycles)

ε_n = random unit variation within the block of data.

The null hypothesis and alternative hypothesis are given in equation III.2.7:

$$H_0 : B_1 = 0$$
$$H_A : B_1 \neq 0 \tag{III.2.7}$$

Post hoc analysis of type Bonferroni was used for pair-wise comparisons with a confidence level of 95% (α = 0.05). Four one-way ANOVA tests were performed for each mechanical property (i.e., load-deflection slope and change in slope angle) of the FRP deck system. The first two compared the mechanical property as the dependent variable with the temperature as the factor and the number of cycles held constant (0 and 1,000,000 cycles, respectively). The second two used the mechanical property as the dependent variable with the number of cycles as the factor, holding the temperature constant, 49°C (120°F) and –30°C (–22°F), respectively. Additional tests were done only

if the stiffness ratio was close between two or more cycles across temperatures and compared only those specific tests. This was equivalent to performing paired t-tests.

III.2.8 Discussion

The FRP-concrete deck has initially more stiffness in the x-direction than that of reinforced-concrete conventional (RCC) deck, as shown in Figure III.2.14. The fact that FRP is used only for tension reinforcement is apparent based on the change in stiffness with temperature. This change in stiffness in the x-direction, 13%, is almost the same change that both temperature and cycle caused in the RCC deck. Additionally, cycles induced degradation, most likely in the concrete because of the similarity in the pattern of damage accumulation (i.e., concrete cracking).

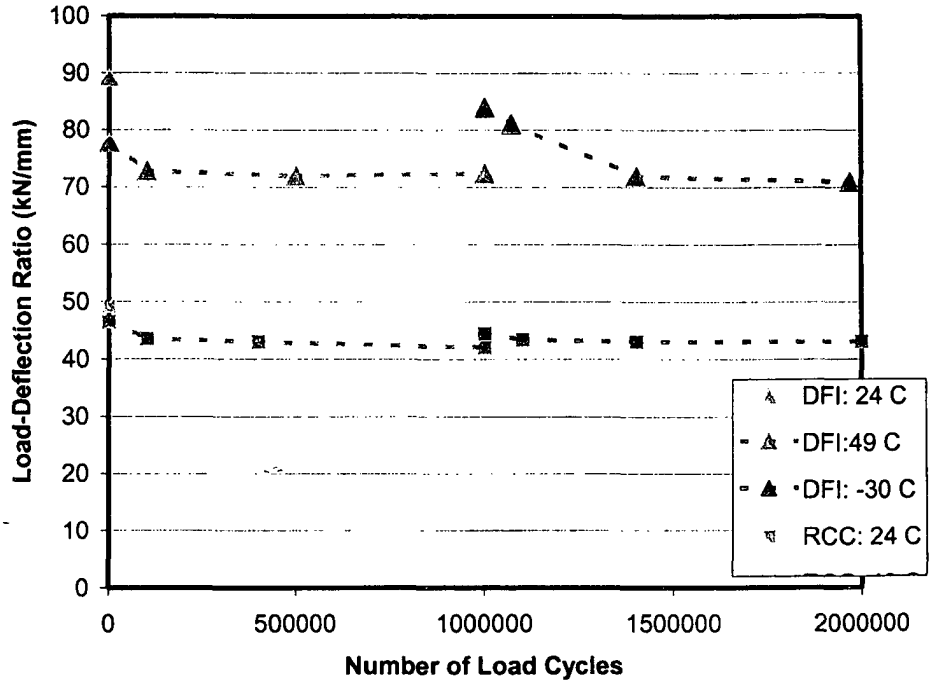

Figure III.2.14 Load-Deflection Ratio History Comparison

Degradation of stiffness in the y-direction is characterized by large coefficients of variation and a large initial reduction with the change from room to high temperature, followed by statistically little degradation with number of cycles. This varies from the RCC deck, which showed almost no degradation until the temperature changed from high to low. However, the amount of stiffness change in the y-direction is approximately the same.

The variation of strains in the x-direction with temperature and number of load cycles is illustrated in Figure III.2.15. The strain curves measured on the top face (bonded to concrete) show a reduction in micro-strains per unit load with the decrease in temperature. Because of strain gauge failure, data are not available for the bottom surface strain gauge after one million load cycles.

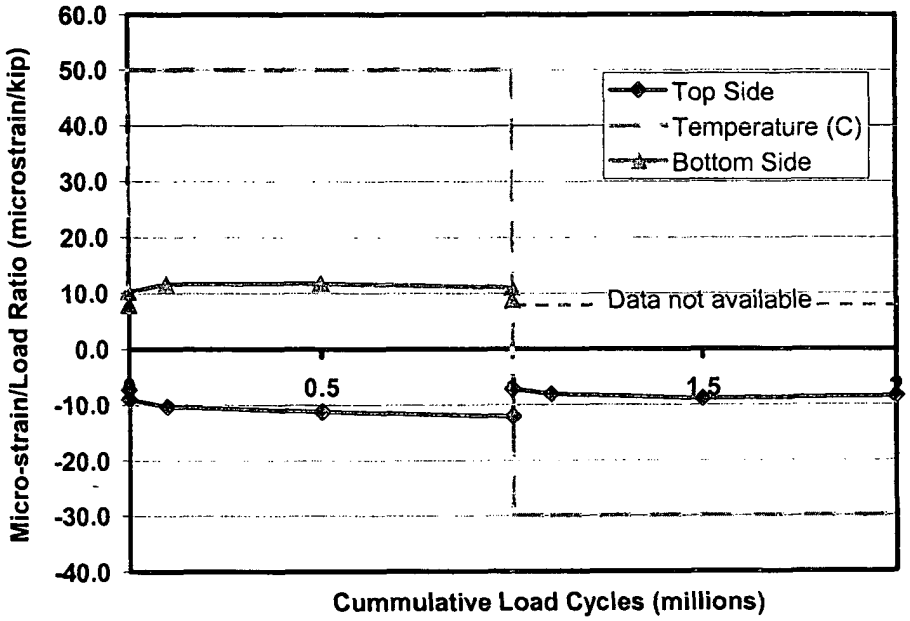

Figure III.2.15 Micro-strain per 4.45 kN (1000 lb) Load during Fatigue Cycling

III.2.9 Conclusions

The analysis done on the deck is a useful measure of stiffness in the x-direction and a useful indicator of stiffness in the y-direction. The x-direction load-deflection analysis takes into account support deflections and is conducted over a continuous span. Both of these factors combine to provide a useful measure for the amount of deflection expected with applied load.

The y-direction analysis is less useful because of the many uncertainties incorporated into one number, the change in slope angle, by the analysis. Unlike the x-direction analysis, the y-direction analysis did not take into account the support deflections and was not conducted over a continuous span.

The statistical analysis performed was adequate for the desired information. The one-way ANOVA was proven to be an efficient analysis tool for determining significant changes in load-deflection ratios and change in slope angle between quasi-static tests.

Overall, the hybrid FRP-concrete deck exhibited more variation in stiffness throughout temperature changes and fatigue cycles than did the RCC benchmark deck. However, the x-direction stiffness was initially considerably higher than that of the RCC deck. Both types of constituent materials contribute to the hybrid deck performance, with the FRP material exhibiting a change in stiffness (viscoelastic response) with temperature and the concrete showing degradation in stiffness (microcracking) with load cycles.

III.3 Fatigue Response of FRP Bridge Deck Fabricated by VARTM under Extreme Temperature Conditions

III.3.1 Abstract

The fatigue performance evaluation at extreme temperature of a two-span continuous fiber-reinforced polymer (FRP) deck prototype built on three W-section steel girders are presented. The FRP deck was fabricated by the vacuum-assisted resin transfer molding (VARTM) process.

II.3.2 Introduction

The fatigue performance evaluation at extreme temperature of a two-span continuous fiber-reinforced polymer (FRP) deck prototype built on three W-section steel girders are presented. The FRP deck was fabricated by the vacuum-assisted resin transfer molding (VARTM) process and supplied by HardCore Composites (HCC) from New Castle, DE.

A transverse joint was also constructed on one of the end supporting beams. The joints have bonded splice plates. The panels were recessed to allow for the splice plate thickness. The deck-girder system was subjected to an eccentric cyclic load that simulates an AASHTO-HS20 design truck wheel load with impact. Initially, one million load cycles were applied at a controlled high temperature, 49°C (120°F), and then another million load cycles were applied at a controlled low temperature, –30°C (–22°F). Quasi-static load tests were conducted at specific intervals during fatigue cycling to evaluate the load-deflection and load-strain responses at several deck locations. A reinforced-concrete

conventional (RCC) deck, designed by the Ohio Department of Transportation, was fabricated and tested under the same load and temperature regime (See Chapter III.1). The RCC deck was utilized to establish the "current practice" benchmark response. The VARTM deck performance was compared with the RCC deck. The fatigue tests of the VARTM and RCC decks were conducted at the U.S. Army Cold Regions Research and Engineering Laboratory in Hanover (CRREL), N.H.

The fatigue-temperature performance was assessed based on two damage indicators by

1. Establishing if the FRP deck apparent bending stiffness in the x-direction degrades with number of load cycles and temperature changes. The apparent bending stiffness in the x-direction is associated with and is measured by the corrected maximum deflections.
2. Establishing if the FRP deck apparent bending stiffness in the y-direction degrades with number of load cycles and temperature changes. The apparent bending stiffness in the y-direction is associated with and is measured by the change in slope angle in the transverse direction of the deck under maximum loading conditions.

III.3.3 Description of the Deck System

The VARTM panels were made of vertical foam-filled cells of square section with skin face sheets. Two panels of 0.914 m (36 in.) in width and 6.10 m (240 in.) in length were connected with a longitudinal joint to form the deck test specimen, as shown in Figure III.3.1. At the joint the panels were recessed, both on the top and bottom surface, and then covered with adhesively bonded FRP splice plates to provide a smooth

surface. The VARTM deck was attached to the steel girders with Z-type steel clip connectors supplied by the deck fabricator. One connector per panel was bolted to the FRP deck and the steel girder. A concrete haunch with a thickness of 44 mm (1.75 in.) was cast on the steel girder flanges. An elastomeric bearing pad with a thickness of 19 mm (0.75 in.) was placed between the haunch and the FRP panel. A general observation was that the top surface of the VARTM deck was not as level as other FRP decks evaluated.

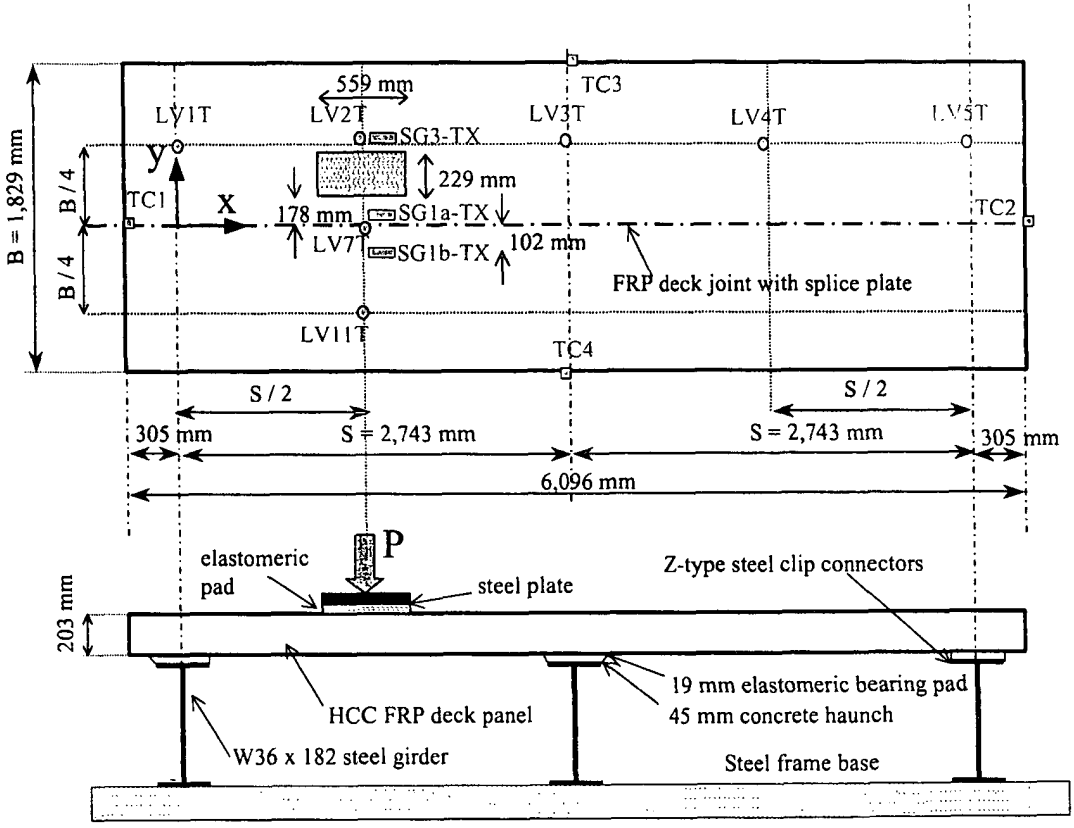

Figure III.3.1 Test Setup

III.3.4 Test Protocol

There are no specifications available for FRP bridge decks on the number of load cycles required for fatigue performance evaluation. A fatigue performance evaluation procedure was initially developed and applied to qualify FRP decks panels fabricated by pultrusion and vacuum-assisted resin transfer molding (VARTM) (Lopez-Anido et al. 1998). The present evaluation procedure consisted of applying two million simulated wheel load cycles at two controlled extreme temperatures on FRP panels attached to steel girders, i.e., one million cycles at 49°C (120°F) and one million cycles at –30°C (–22°F). The two-span continuously supported FRP deck was subjected to a simulated AASHTO HS20-44 design truck wheel load (Figure III.3.2). A girder spacing of 2.74 m (108 in.) was selected, as shown in Figure III.3.1.

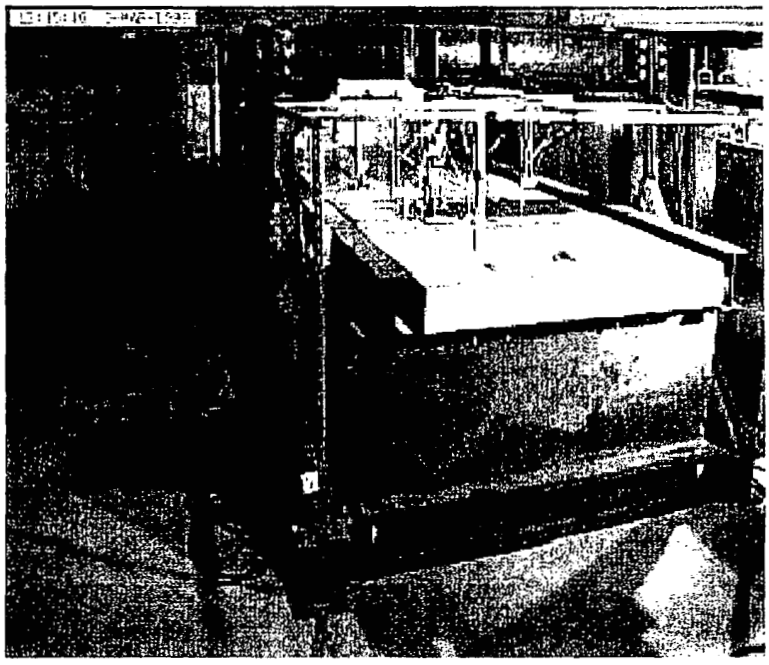

Figure III.3.2 VARTM Panel Supported by Steel Beams during Fatigue Testing

The maximum load to be applied was computed based on an AASHTO HS20-44 design truck wheel load with a dynamic load allowance (impact factor). The design truck wheel load is one half of the axle load. The impact factor adopted was 30%. Then, the maximum computed fatigue load resulted in P_{max} = 71.2 kN (16,000 lb) × 1.3 = 92.5 kN (20,800 lb).

The applied load frequency ranged between 2.4 and 3 Hz. Based on these applied load frequencies and the flexibility of the FRP deck, the actual maximum applied fatigue load attained was P_{max} = 89.0 kN (20,000 lb). The minimum applied load was P_{min} = 8.9 kN (2,000 lb). Therefore, the fatigue stress ratio was approximately R = 0.1.

The fatigue test specimens were not anticipated to fail during the two-million-cycle duration, so the fatigue analysis was focused on assessing the structural degradation associated with the cyclic loading. Fatigue damage accumulation can induce stiffness degradation of the FRP deck panels and in the panel-to-panel longitudinal joint. Besides, fatigue damage can lead to residual damage in the FRP deck-steel girder haunch connection. To assess fatigue damage, quasi-static tests were conducted prior to the application of load cycling and at specified increments of fatigue cycling, as shown in Figure III.3.3.

First, at ambient temperature, 24°C (75°F), a set of quasi-static tests was conducted to obtain baseline load-deflection and load-strain values. Then, the test room was warmed to 49°C (120°F). The FRP deck temperature was monitored until it reached the room temperature. Then, a second set of quasi-static test, but now at high temperature, was conducted. After this evaluation, one million load cycles were applied. Quasi-static tests were conducted at 100,000, 500,000 and 1,000,000 load cycles. For the

low-temperature tests, the room was cooled to –30°C (–22°F), and the fatigue test with the corresponding quasi-static tests were repeated for the second million load cycles.

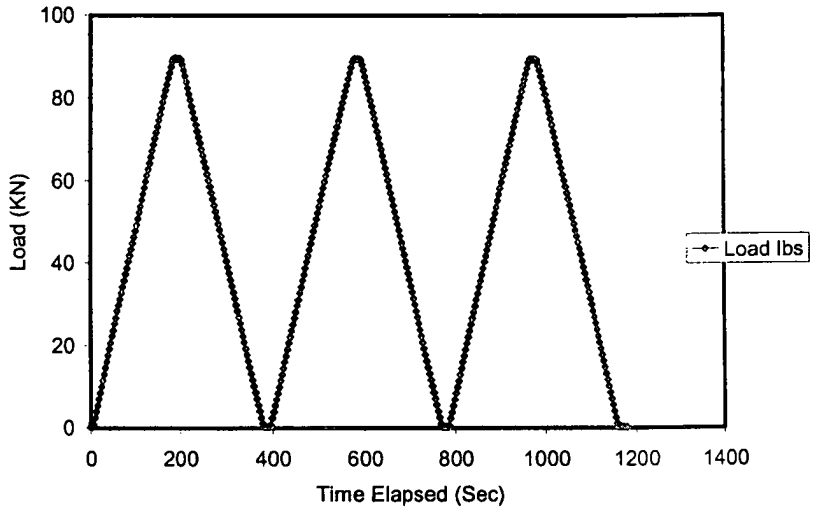

Figure III.3.3 Typical Quasi-Static Load Tests

III.3.5 Test Setup

The FRP deck dimensions were specified to model a typical slab-on-steel girder highway bridge, as shown in Figure III.3.1. A fatigue-testing frame was designed to accommodate the deck system prototype with the three connected steel girders. The deck prototype was instrumented with strain gauges, thermocouples, and Linear Voltage Differential Transducers (LVDTs) to measure vertical deflection (Figure III.3.1).

The fatigue tests were performed in CRREL's Material Evaluation Facility (MEF). This is a well-insulated room with interior dimensions of approximately 7.92 m (26 ft) wide by 12.80 m (42 ft) long and 3.66 m (12 ft) high. A set of double doors 3.35 m (11 ft) wide by 3.35 m (11 ft) tall allows the large fatigue test frame and the FRP bridge deck prototypes to be moved in and out of the MEF facility. A self-reacting steel

test frame was designed and built at CRREL for a maximum load capacity of 266.9 kN (60,000 lb). One 97.9-kN- (22,000-lb-) capacity hydraulic actuator was mounted on the steel reaction frame to apply cyclic loading on the deck. The FRP deck specimen was attached to three steel girders W36x182, resulting in a continuous two-span bridge structure (Figure III.3.2). The actuator applied the load on a rectangular steel plate of 229 × 559 mm (9 × 22 in.) that simulates a wheel load contact area (AASHTO 1996). An elastomeric pad was placed between the steel plate and the FRP deck surface to provide uniform pressure. The load was applied eccentrically with respect to the traffic flow direction to study the load distribution in the y-direction, as shown in Figure III.3.1.

Load, deflection, strain, and temperature were the general parameters of measurement in this test program. The FRP deck specimen was instrumented with strain gauges, LVDTs, and thermocouples. Seven LVDTs supported by an independent frame were used to measure deflections on the top surface of the deck. Four thermocouples were placed on four sides of the top FRP deck surface and one thermocouple was used for air temperature. The thermocouples were used to verify that the FRP deck panel reached equilibrium with room temperature. The locations of the LVDTs, strain gauges, and thermocouples on the top of the deck are shown in Figure III.3.1. The location of the strain gauges bonded to the bottom deck surface (BX) was symmetrical with respect to the numerically matching strain gauges bonded to the top surface (TX).

The test setup induced a positive bending moment under the applied load ($x = S/2$) and a negative bending moment on the central support ($x = S$) and the adjacent span. An uplifting force resulted on the end girder support ($x = 2 \times S$). This uplifting force was partially counteracted by the weight of the deck and steel beams.

As mentioned before, the FRP deck was evaluated for approximately 2,000,000 load cycles with controlled temperature. The first million load cycles were conducted at 49°C (120°F), while the second million cycles were performed at about –30°C (–22°F). The first quasi-static test was at room temperature, about 24°C (75°F), before the fatigue cycles began and served as the control baseline. In the quasi-static tests, the load was applied at a rate of 1 mm/min (0.04 in/min), and sensor measurements were recorded every 3 s. Each quasi-static test consisted of a loading and unloading cycle. The quasi-static test was repeated three times, resulting in three peak loads and six varying load intervals for data analysis (Figure III.3.3).

III.3.6 Experimental Results

The raw data were analyzed to produce load-deflection curves for each deck test. Typical load-deflection curves for room temperature, 24°C (75°F), at five deck locations corresponding to LVDTs mounted on the top of the panel and aligned in the x-direction, are shown in Figure III.3.4. Similarly, high-temperature load-deflection curves at the five locations after one million high-temperature load cycling is shown in Figure III.3.5. Figure III.3.6 shows the low-temperature load-deflection curves for the same locations after one million hot plus one million cold fatigue cycles. Figure III.3.7 compares the maximum deflection data for the room temperature baseline, after one million cycle at high-temperature, and after an additional one million cycles at low temperature. From these load-deflection curves we observe that the low-temperature stiffness after an accumulated two million load cycles is only slightly higher than the initial stiffness at room temperature. This observation implies that the panel stiffness is controlled mainly by temperature and not by the number of load cycles.

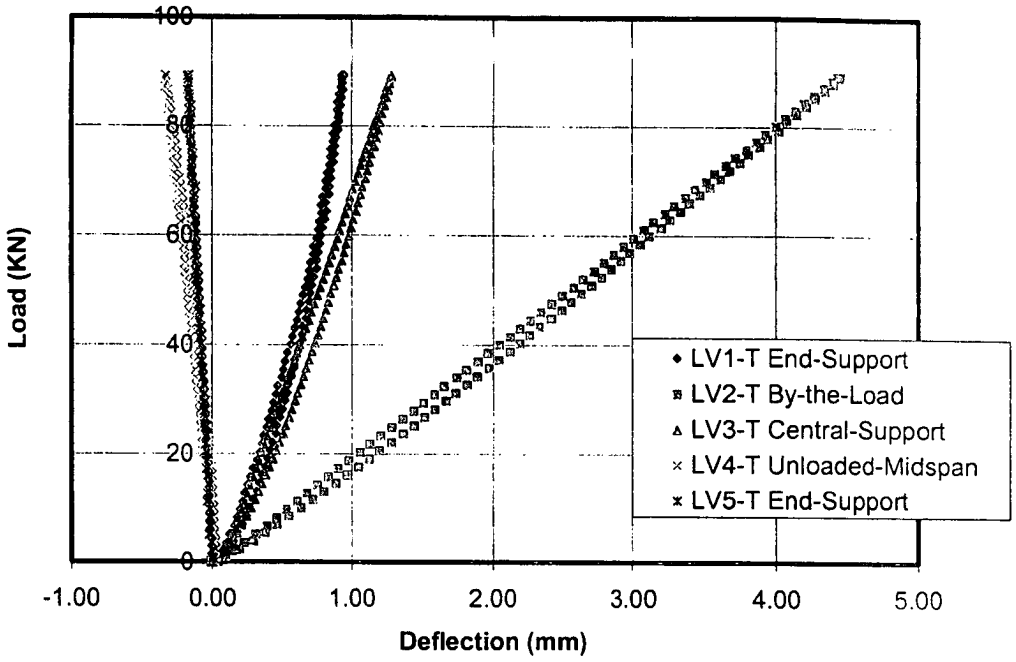

Figure III.3.4 Room-Temperature Load-Deflection Curves for Top LVDTs aligned in x-Direction prior to Fatigue Cycling

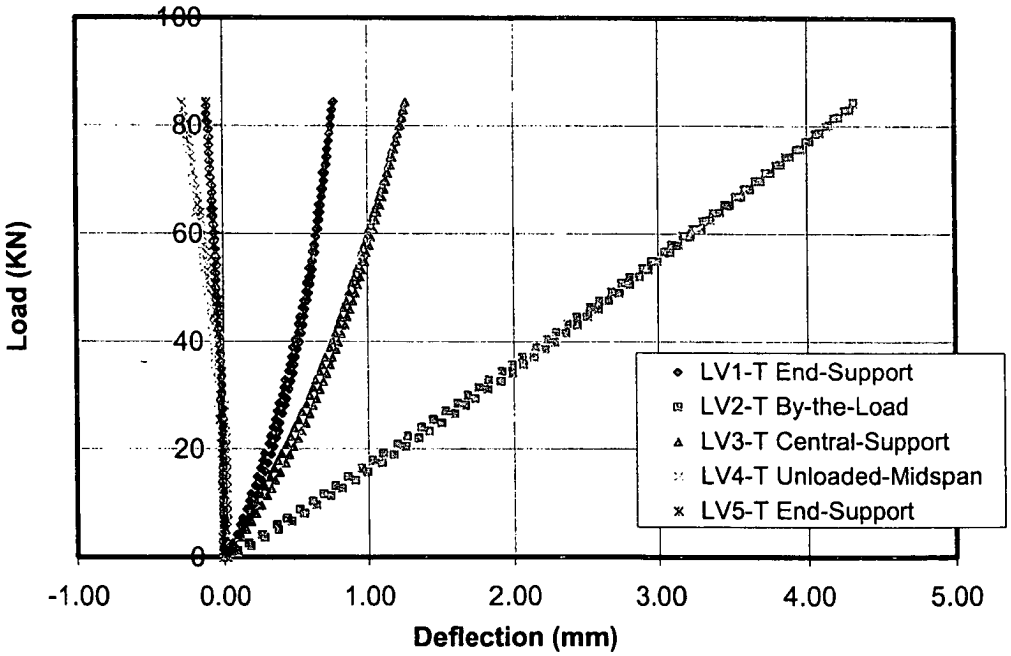

Figure III.3.5 High-Temperature Load-Deflection Curves for Top LVDTs aligned in x-Direction after One Million Hot Fatigue Cycles

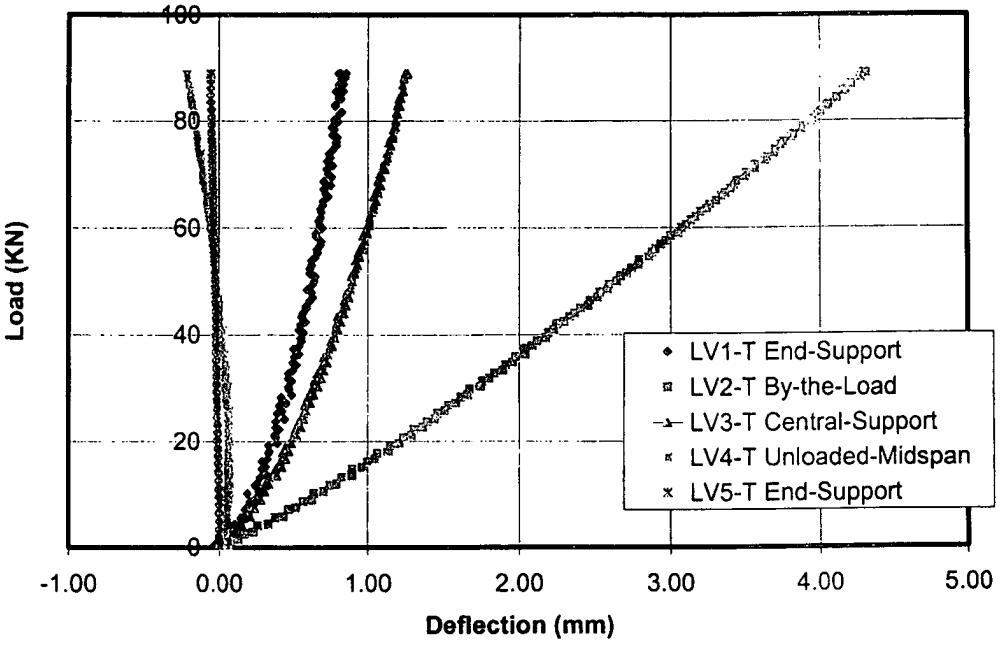

Figure III.3.6 Low-Temperature Load-Deflection Curves for Top LVDTs aligned in x-Direction after One Million Hot plus One Million Cold) Fatigue Cycles

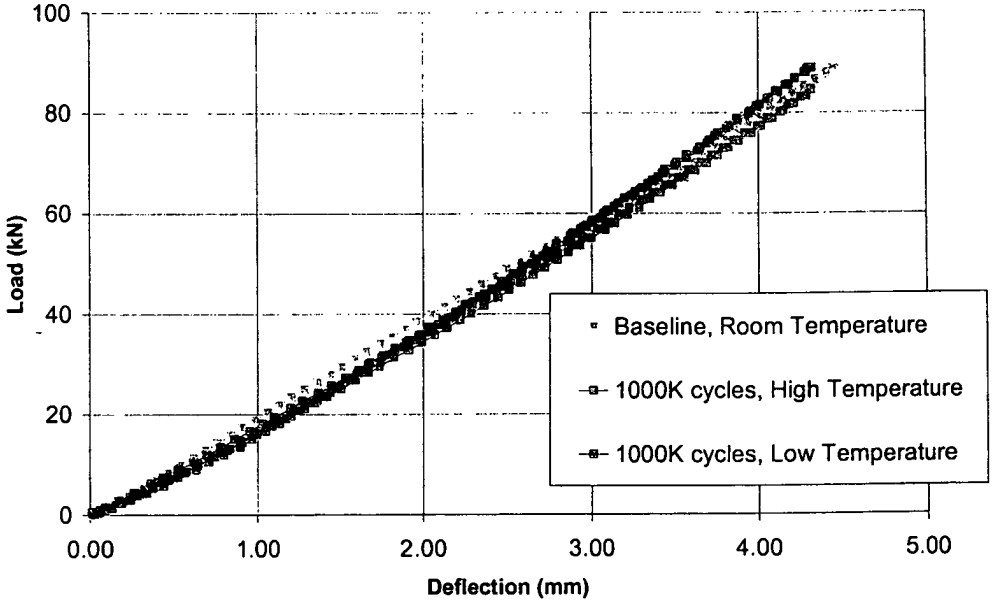

Figure III.3.7 Maximum Deflections for Three Test Conditions (Measured by LV2-T)

The maximum total deflections measured with the top LVDTs (LV1T, LV2T, LV3T, LV4T, and LV5T) aligned in the x-direction are shown in Figure III.3.8 for room-temperature (RT) baseline, high temperature (HT), and low temperature (LT), the last two after one million cycles at each temperature. These total deflections include both deck deflections and support deflections measured during the quasi-static tests. No deck uplifting was observed over the end girder. These deflection curves confirm the previous observation that the decrease in temperature increases the panel stiffness, although by a small magnitude, even after higher number of accumulated load cycles.

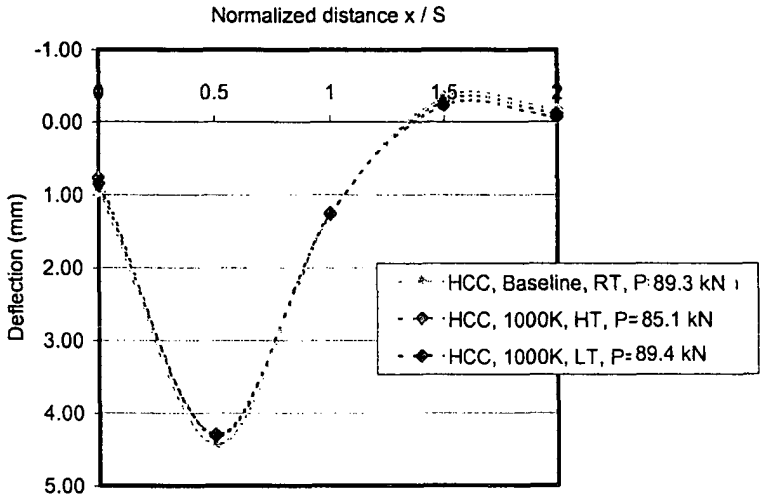

Figure III.3.8 - Top Deflection Variation along the x-Direction for Maximum Load: LV1-T, LV2-T, LV3-T, LV4-T, LV5-T

The maximum deflections measured with the top LVDTs (LV2T, LV7T, and LV11T) aligned along the y-direction during the quasi-static tests are shown in Figure III.3.9. From this figure we observe that the panel longitudinal joint is able to transfer the shear force in the y-direction without any noticeable joint vertical slip.

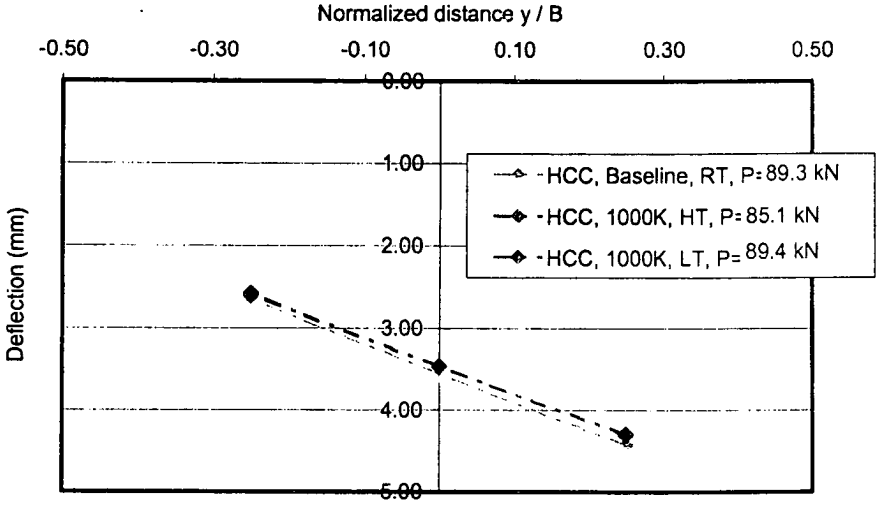

Figure III.3.9 - Top Deflection Variation along the y-Direction for Maximum Load: LV2-T, LV7-T, LV11-T

Compressive strains on the top of the deck in the x-direction measured at room temperature prior to fatigue cycling are shown in Figure III.3.10. Similarly, tensile strains at symmetric locations on the bottom surface are shown in Figure III.3.11. All the curves are linear within the loading range. Compressive strains on the top surface are slightly larger than the corresponding tensile strains on the bottom surface. Linear strain curves were obtained at high temperature after one million load cycles (Figure III.3.12 and Figure III.3.13). In the same way, strain curves were plotted at low temperature after an additional million of load cycles (Figure III.3.14 and Figure III.3.15). From these curves we observed that temperature reduction results in lower strains, which can be explained by the higher stiffness as we observed in the load-deflection curves (Figure III.3.7).

The FRP deck was inspected visually for signs of distress such as cracks and damage at connections after fatigue cycling. No visible damage was observed in the FRP deck and in the deck-beam connection.

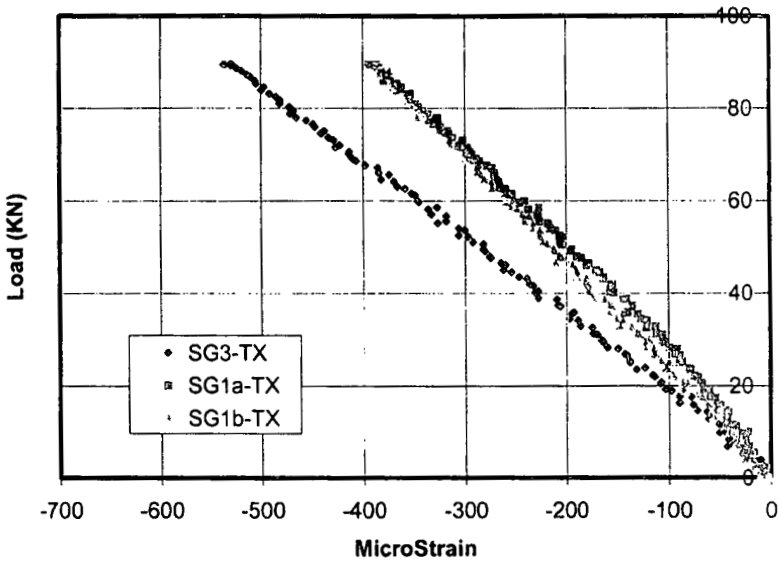

Figure III.3.10 Room-Temperature Strain (x-Direction) Curves Prior to Fatigue Cycling for Top Gauges (Loaded Span): SG1a-TX, SG1b-TX, SG3-TX

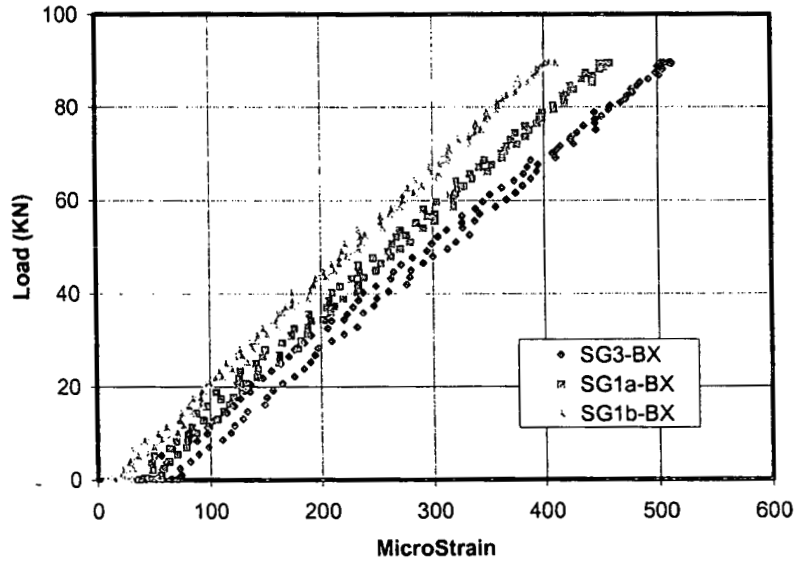

Figure III.3.11 Room-Temperature Strain (x-Direction) Curves Prior to Fatigue Cycling for Bottom Gauges (Loaded Span): SG1a-BX, SG1b-BX, SG3-BX

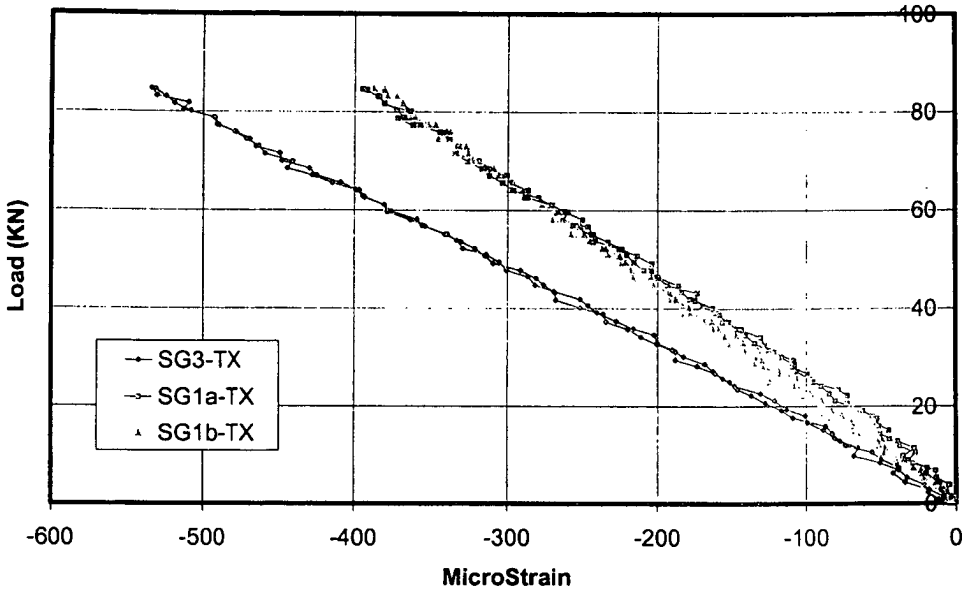

Figure III.3.12 High-Temperature Strain (x-Direction) Curves after One Million Hot Cycles) for Top Gauges (Loaded Span): SG1a-TX, SG1b-TX, SG3-TX

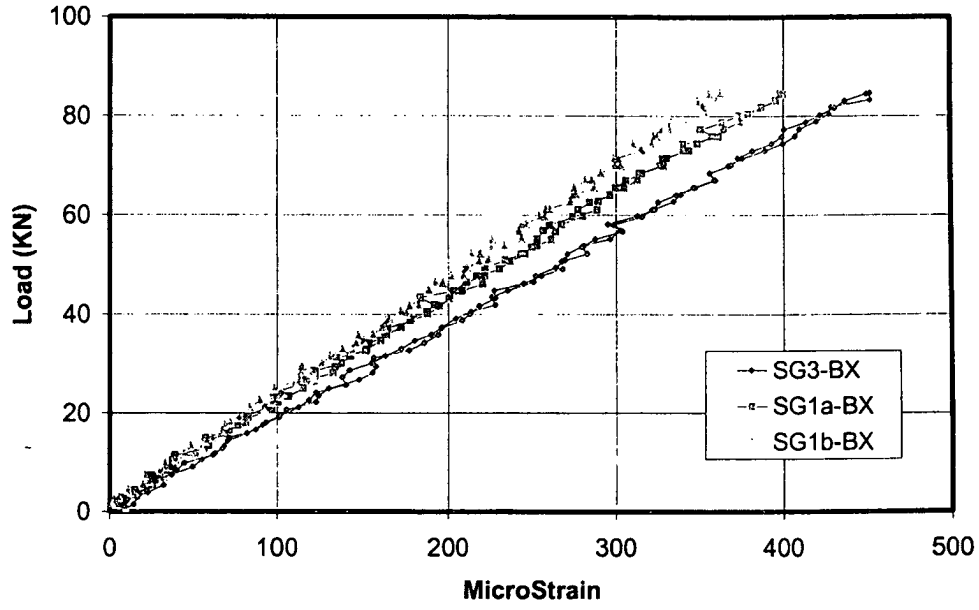

Figure III.3.13 High-Temperature Strain (x-Direction) Curves after One Million Hot Cycles for Bottom Gauges (Loaded Span): SG1a-BX, SG1b-BX, SG3-BX

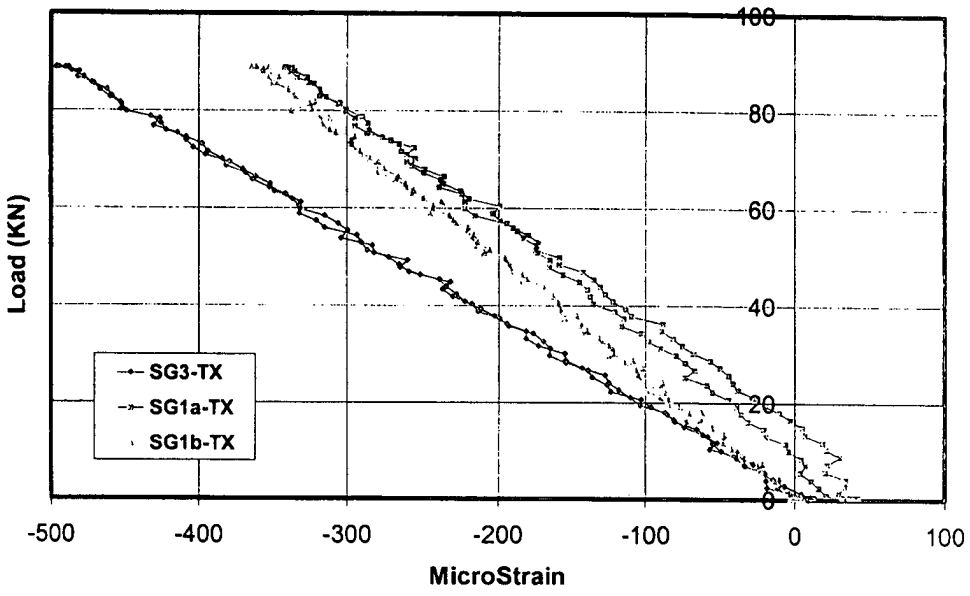

Figure III.3.14 Low-Temperature Strain (x-Direction) Curves after One Million Hot plus One Million Cold Cycles) for Top Gauges (Loaded Span): SG1a-TX, SG1b-TX, SG3-TX

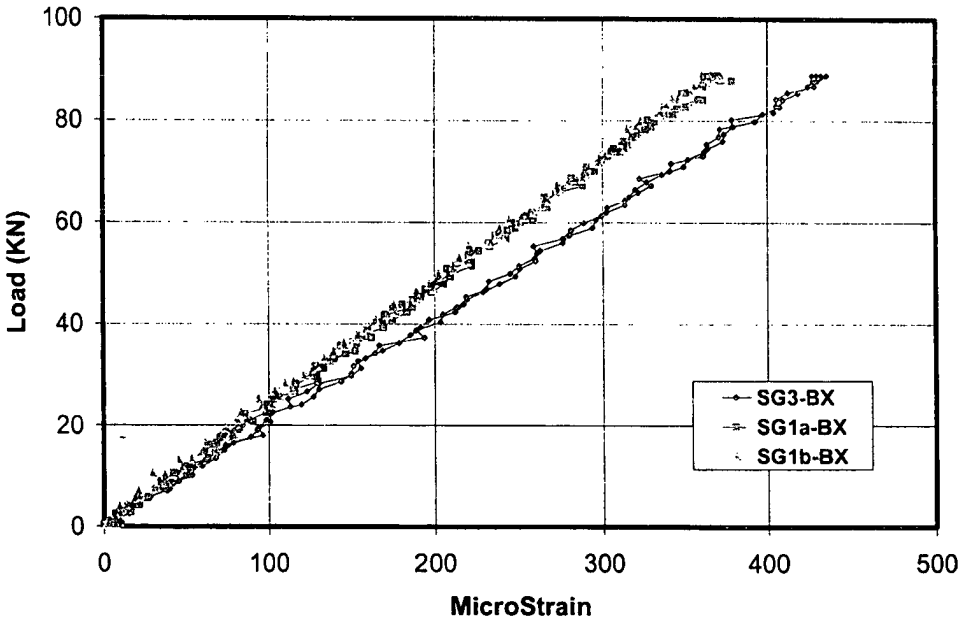

Figure III.3.15 Low-Temperature Strain (x-Direction) Curves after One Million Hot plus One Million Cold Cycles) for Bottom Gauges (Loaded Span): SG1a-BX, SG1b-BX, SG3-BX

III.3.7 Data Analysis

To evaluate the FRP deck response with temperature and number of load cycles, two stiffness indicators are defined:

1) Stiffness indicator in the x-direction is computed based on corrected maximum deflections along a longitudinal line (LV1T, LV2T, LV3T); and
2) Stiffness indicator in the y-direction is computed based on maximum deflections across a transverse line (LV2T, LV7T, LV11T).

III.3.7.1 Retained Stiffness in the x-Direction

The maximum deflection, δ_c, was corrected to account for support deflection according to equation III.3.1

$$\delta_c = (LV2T) - \tfrac{1}{2}(LV1T + LV3T) \qquad \text{(III.3.1)}$$

where LV1T, LV2T, and LV3T are defined as deflection at the points given in Figure III.3.1. For each quasi-static test corresponding to number of applied load cycles, n, the six segments of the load-deflection curves (see the loading and unloading segments in Figure III.3.3) for varying load intervals were plotted. A linear response was observed in all cases and approximated with a linear least-squares regression line to compute the load-deflection ratio $\left(P/\delta_c\right)_n$. These load-deflection ratios are related to the stiffness of the deck in the x-direction. The resulting load-deflection ratios are given in Table III.3.1.

An indicator of retained stiffness in the x-direction, $R_{x,n}$, is defined as the mean residual load-deflection ratio after n load cycles with controlled temperature with respect to the mean initial load-deflection ratio, as shown in equation III.3.2:

$$R_{x,n} = \frac{(P/\delta_c)_n}{(P/\delta_c)_o} \qquad \text{(III.3.2)}$$

Then $R_{x,n} < 1$ implies a reduction in deck stiffness, while $R_{x,n} > 1$ implies an increase in deck stiffness. The resulting retained stiffness indicators are given in Table III.3.2.

Table III.3.1 - VARTM Deck x-Direction Load-Deflection Ratio

	Temperature (°C)					
	24		49		–30	
Load Cycles	Mean (kN/mm)	COV (%)	Mean (kN/mm)	COV (%)	Mean (kN/mm)	COV (%)
0	26.6	0.18	26.0	0.29		
100000			26.3	0.22		
500000			26.0	0.17		
1000000			25.9	1.36	27.1	0.45
1000000 + 100000					27.4	0.71
1000000 + 500000					27.8	2.98
1000000 + 1000000					27.4	0.38

Note: 1 kN/mm = 5.71 kip/in.

Table III.3.2 - VARTM Deck x-Direction Stiffness Indicator

	Temperature (°C)					
	24		49		-30	
Load Cycles	Statistical Level	$R_{x,n}$	Statistical Level	$R_{x,n}$	Statistical Level	$R_{x,n}$
0	A	1.000	B, C	0.980		
100000			B	0.989		
500000			B, C	0.977		
1000000			C	0.975	D	1.021
1000000 + 100000					D	1.033
1000000 + 500000					D	1.047
1000000 + 1000000					D	1.030

*The same letter indicates the same stiffness ratio with 95% confidence

III.3.7.2 Retained Stiffness in the y-Direction

Deflections were measured at three points aligned across the FRP deck (LV2-T, LV7-T, and LV11-T), as shown in Figure III.3.1. Load-deflection curves were plotted for the six load-varying intervals of each quasi-static test. These load-deflection curves followed a linear trend and were fitted using linear least-squares regression analysis. The trend lines were then used to calculate the deflection corresponding to P = 89 kN (20,000 lb) for the six segments of the load-deflection curves. The resulting deflections were used to compute the secant slopes at both sides of the longitudinal FRP joint (i.e., y > 0 and y < 0), as shown in equation III.3.3:

$$\tan\theta_{Y+} = \frac{LV2T - LV7T}{B/4}$$
$$\tan\theta_{Y-} = \frac{LV7T - LV11T}{B/4} \quad \text{(III.3.3)}$$

Then, the change in the slope angle at the longitudinal joint location is computed as shown in equation III.3.4:

$$\Delta\theta_n = \theta_{Y+} - \theta_{Y-} \quad \text{(III.3.4)}$$

If $\Delta\theta_n > 0$, then the deck curves transversely concave down, and if $\Delta\theta_n < 0$, it curves concave up. The resulting changes in slope angles are given in Table III.3.3.

An indicator of retained deck and joint stiffness in the y-direction, $R_{y,n}$, is defined as the mean change in slope angle after n load cycles with controlled temperature with respect to the mean initial change in slope angle, as shown in equation III.3.5:

$$R_{y,n} = \frac{\Delta\theta_o}{\Delta\theta_n} \quad \text{(III.3.5)}$$

If $R_{y,n} > 0$, then the deck does not change the curvature orientation. In particular, if $0 < R_{y,n} < 1$, the change in slope angle is more pronounced, and if $R_{y,n} > 1$, the change in slope angle is less pronounced than the baseline quasi-static test. On the other hand, if $R_{y,n} < 0$, the deck changes the curvature orientation (e.g., from concave up to concave down, or vice versa). The resulting retained stiffness indicators are given in Table III.3.4.

Table III.3.3 - VARTM Deck y-Direction Slope Change

	Temperature (°C)					
	24		49		–30	
Load Cycles	Mean (rad)	COV (%)	Mean (rad)	COV (%)	Mean (rad)	COV (%)
0	–7.29E-05	–4.79	–8.41E-05	9.21		
100000			–8.90E-05	7.21		
500000			–5.42E-05	7.08		
1000000			N.A.	- - -	–1.18E-04	8.50
1000000 + 100000					–6.23E-05	23.06
1000000 + 500000					–4.10E-05	9.18
1000000 + 1000000					–9.65E-05	12.45

Table III.3.4 - VARTM Deck y-Direction Stiffness Indicator

	Temperature (°C)					
	24		49		–30	
Load Cycles	Statistical Level	$R_{y,n}$	Statistical Level	$R_{y,n}$	Statistical Level	$R_{y,n}$
0	A	1.000	B	0.867		
100000			B	0.818		
500000			B	1.343		
1000000			B	0.817	B	0.619
1000000 + 100000					B	1.169
1000000 + 500000					C	1.778
1000000 + 1000000					B	0.755

*The same letter indicates the same curvature with 95% confidence

The longitudinal panel joint, which is located between LV2-T and LV11-T, incorporates additional shear and bending flexibility that affects the change in the slope angle. Therefore, the change in the slope angle not only measures the bending and shear stiffness of the panels, but it also accounts for the discrete bending and shear stiffness of the joint. The reason for adopting the slope angle method of measuring the stiffness response in the transverse direction instead of a more conventional quadratic fit of deflections, which is more applicable to reinforced-concrete decks, is to model the articulated nature of the VARTM panels.

III.3.7.3 Statistical Analysis

Statistical analysis of the load-deflection ratio and the change in slope angle for the FRP deck system was performed using one-way analyses of variance (ANOVA) for each number of cycles and temperature condition. The analysis was conducted using the SYSTAT software package. The ANOVA analysis determined if the response of the deck system was a function of number of cycles or temperature. The model for a one-way ANOVA is represented symbolically as follows:

$$Y_n = B_o + B_1 \cdot X_n + \varepsilon_n \qquad \text{(III.3.6)}$$

where Y_n = observed mechanical property (load-deflection ratio or change in slope angle) for the number of cycles n under controlled temperature

B_o, B_1 = coefficients of the model

X_n = code associated with the variable under study (e.g., temperature or cumulative load cycles)

ε_n = random unit variation within the block of data.

The null hypothesis and alternative hypothesis are given in equation III.3.7:

$$H_0 : B_1 = 0$$
$$H_A : B_1 \neq 0 \quad \text{(III.3.7)}$$

Post hoc analysis of type Bonferroni was used for pair-wise comparisons with a confidence level of 95% (α = 0.05). Four one-way ANOVA tests were performed for each mechanical property (i.e., load-deflection slope and change in slope angle) of the FRP deck system. The first two compared the mechanical property as the dependent variable with the temperature as the factor and the number of cycles held constant (0 and 1,000,000 cycles, respectively). The second two used the mechanical property as the dependent variable with the number of cycles as the factor, holding the temperature constant, 49°C (120°F) and –30°C (–22°F), respectively. Additional tests were done only if the stiffness ratio was close between two or more cycles across temperatures and compared only those specific tests. This was equivalent to performing paired t-tests.

III.3.8 Discussion

In the x-direction the load-deflection ratios are lower than those of RCC, as shown in Figure III.3.16. However, there is only a minor variation in the load-deflection factors throughout the test in Table III.3.1. In the x-direction the load-deflection factor did not vary more than 5% from initial values through both fatigue cycles and temperature changes (Table III.3.2). In the y-direction the deck also is consistent throughout the test, as shown in Table III.3.3. However, the coefficients of variance for these values are relatively high, indicating high sensitivity to the loading and unloading segments of each quasi-static test. In the statistical analysis the indicator of retained deck and joint stiffness in the y-direction exhibits an initial degradation of approximately 20% and presents only one outlier during the load history (Table III.3.4). This is considerably

less than that of reinforced concrete, which had an approximately 40% drop with low temperature.

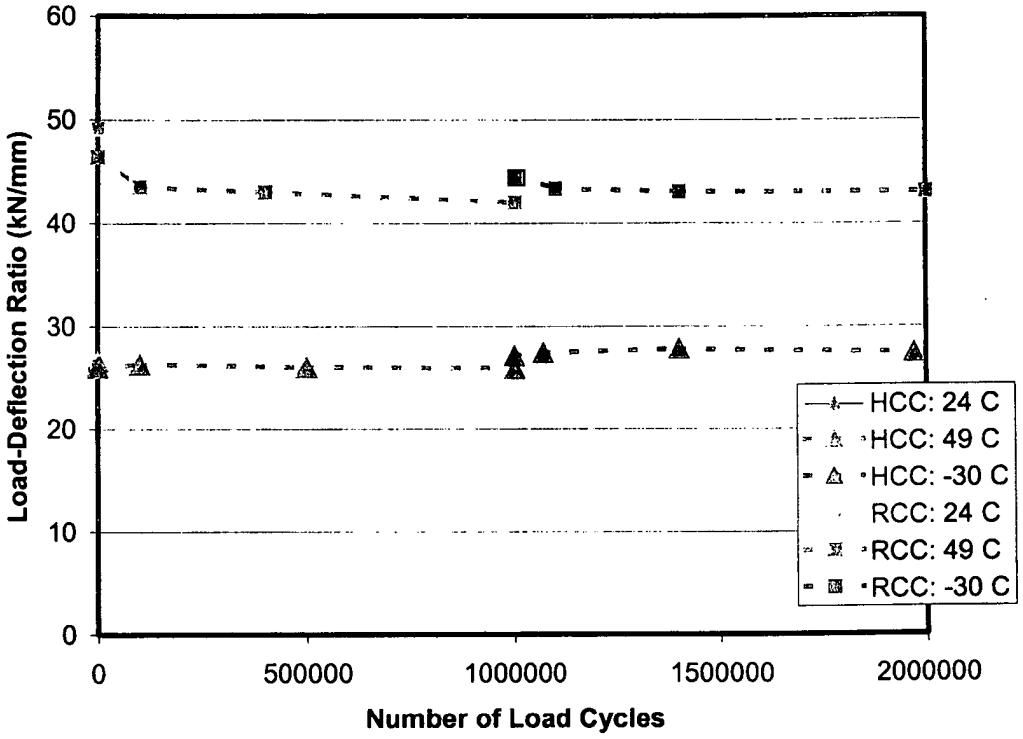

Figure III.3.16 Load-Deflection Ratio History Comparison

The variation of strains in the x-direction with temperature and number of load cycles is illustrated in Figure III.3.17. Both the top and bottom strain curves have shown a reduction in micro-strains per unit load with the decrease in temperature.

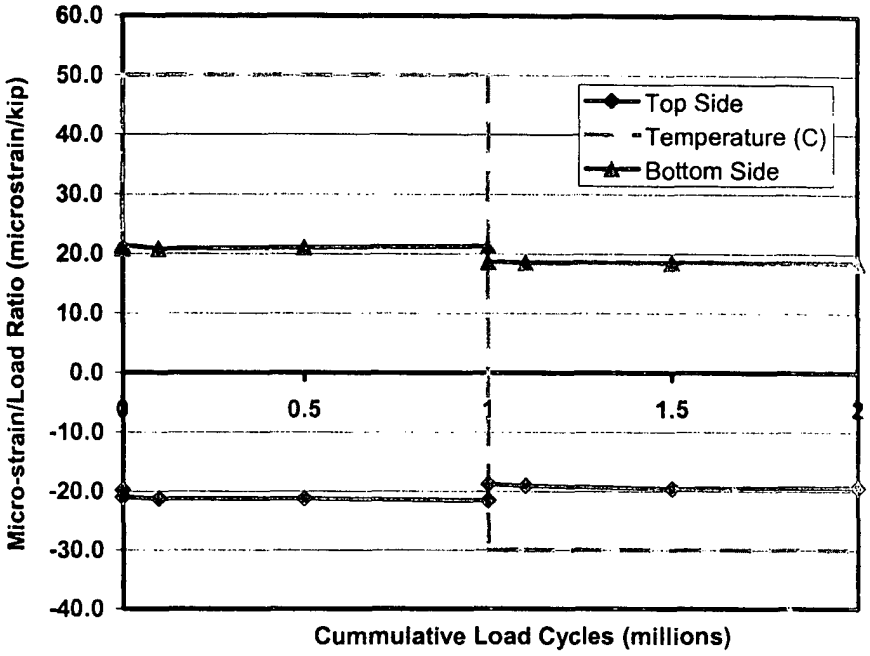

Figure III.3.17 Micro-strain per 4.45 kN (1000 lb) Load during Fatigue Cycling

III.3.9 Conclusions

The analysis done on the deck is a useful measure of stiffness in the x-direction and a useful indicator of stiffness in the y-direction. The x-direction load-deflection analysis takes into account support deflections and is conducted over a continuous span. Both of these factors combine to provide a useful measure for the amount of deflection expected with applied load. The y-direction analysis is less useful because of the many uncertainties incorporated into one number, the change in slope angle, by the analysis. Unlike the x-direction analysis, the y-direction analysis did not take into account the support deflections and was not conducted over a continuous span.

The statistical analysis performed was adequate for the desired information. The one-way ANOVA was proven to be an efficient analysis tool for determining significant changes in load-deflection ratios and change in slope angle between quasi-static tests.

Overall, the VARTM deck performed very consistently throughout both temperature changes and load cycling. In the x-direction the indicator of retained stiffness exhibited less than 5% change, while in the y-direction the indicator of retained stiffness did not exhibit statistically significant variations throughout the test. The VARTM deck stiffness, although initially lower than that of the benchmark reinforced concrete, was more efficient in retaining stiffness during the fatigue cycling. The VARTM deck did not experience the extent of stiffness degradation due to temperature and fatigue cycles observed in the reinforced-concrete deck.

III.4 Fatigue Response of FRP Bridge Deck Fabricated by Pultrusion under Extreme Temperature Conditions

III.4.1 Abstract

The fatigue performance evaluation at extreme temperature of a two-span continuous fiber-reinforced polymer (FRP) deck prototype built on three W-section steel girders is presented. The FRP deck is made of interlocked and bonded profiles fabricated by the pultrusion process.

II.4.2 Introduction

The fatigue performance evaluation at extreme temperature of a two-span continuous fiber-reinforced polymer (FRP) deck prototype built on three W-section steel girders is presented. The FRP deck is made of interlocked and bonded profiles fabricated by the pultrusion process and identified as CPI.

The deck-girder system was subjected to an eccentric cyclic load that simulates an AASHTO HS20 design truck wheel load with impact. Initially, one million load cycles were applied at a controlled high temperature, 49°C (120°F), and then another million load cycles were applied at a controlled low temperature, –30°C (–22°F). Quasi-static load tests were conducted at specific intervals during fatigue cycling to evaluate the load-deflection and load-strain response at several deck locations. A reinforced-concrete conventional (RCC) deck designed by the Ohio Department of Transportation was fabricated and tested under the same load and temperature regime (See Chapter III.1). The RCC deck was utilized to establish the "current practice" baseline response. The FRP deck performance was compared with the RCC deck. The fatigue tests of the FRP

and RCC decks were conducted at the U.S. Army Cold Regions Research and Engineering Laboratory in Hanover (CRREL), N.H.

The fatigue-temperature performance was assessed based on two damage indicators by

1. Establishing if the FRP deck apparent bending stiffness in the x-direction degrades with number of load cycles and temperature changes. The apparent bending stiffness in the x-direction is associated with and is measured by the corrected maximum deflections.
2. Establishing if the FRP deck apparent bending stiffness in the y-direction degrades with number of load cycles and temperature changes. The apparent bending stiffness in the y-direction is associated with and is measured by the change in slope angle in the transverse direction of the deck under maximum loading conditions.

III.4.3 Description of the Deck System

FRP deck panels were made of interlocking and adhesively bonded pultruded profiles. Then, two panels of 0.914 m (36 in.) in width and 6.100 m (240 in.) in length were connected with a longitudinal joint to form the deck test specimen, as shown in Figure III.4.1.

The FRP deck was attached to the steel girders with continuous steel angles. Two angles forming a Z-type connection were bolted to each other, to the steel girder, and to the FRP panel. The angles serve also as a side form for the concrete haunch (blocking).

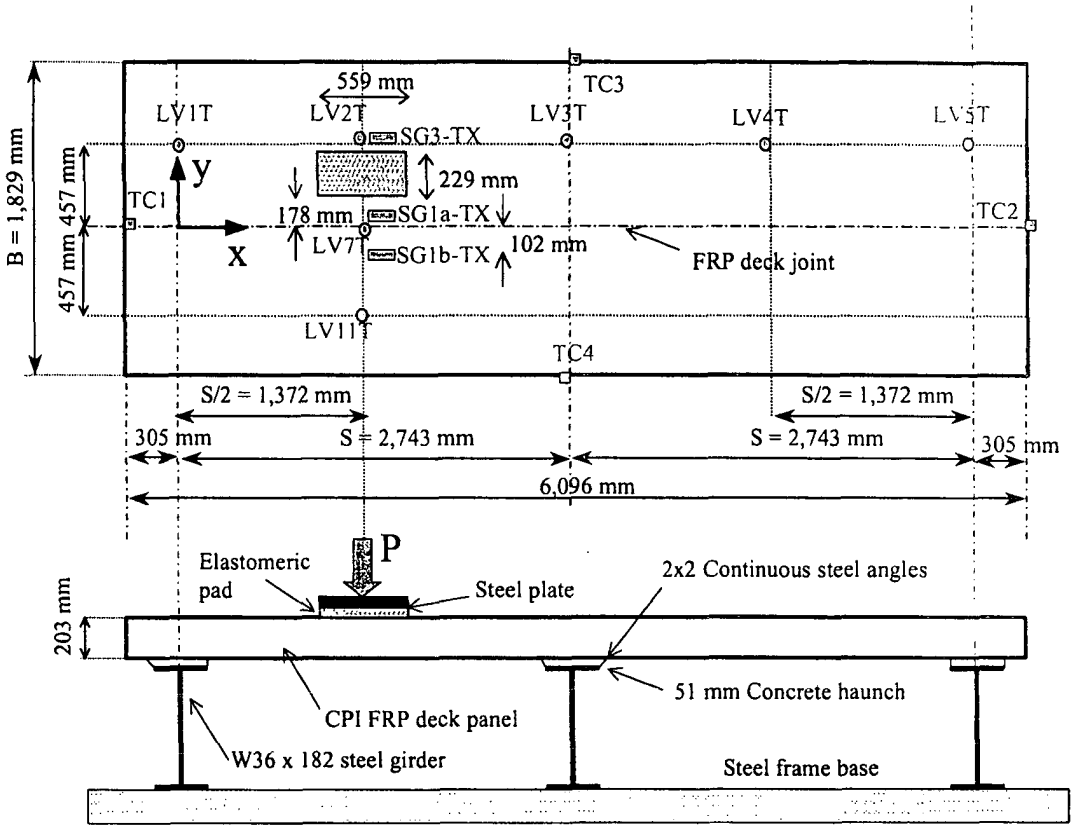

Figure III.4.1 Test Setup

III.4.4 Test Protocol

There are no specifications available for FRP bridge decks on the number of load cycles required for fatigue performance evaluation. A fatigue performance evaluation procedure was initially developed and applied to qualify FRP decks panels fabricated by pultrusion and vacuum-assisted resin transfer molding (VARTM) (Lopez-Anido et al. 1998).

The proposed performance evaluation consisted of applying two million simulated wheel load cycles at two controlled extreme temperatures on FRP panels attached to steel girders, i.e., one million cycles at 49°C (120°F) and one million cycles at –30°C (–22°F). A two-span continuously supported FRP deck was subjected to a

simulated AASHTO HS20-44 design truck wheel load (Figure III.4.2). A girder spacing of 2.74 m (108 in.) was selected, as shown in Figure III.4.1.

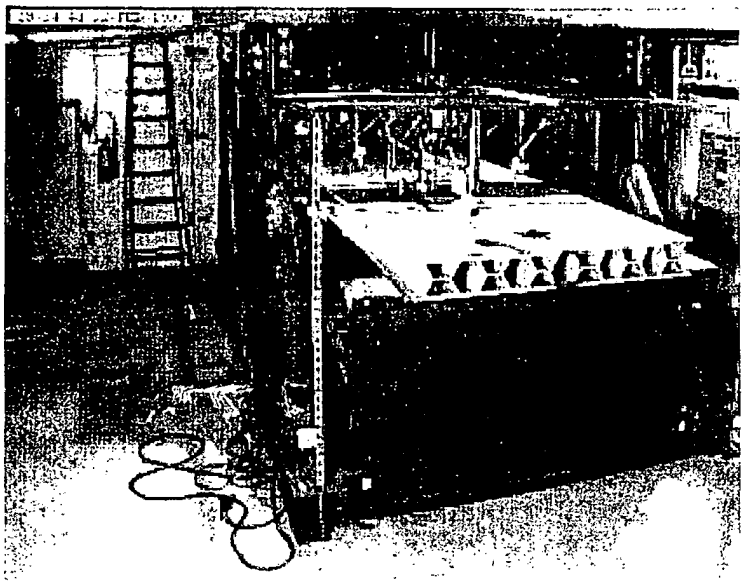

Figure III.4.2 FRP Panel Supported by Steel Beams during Fatigue Testing

The maximum load to be applied was computed based on an AASHTO HS20-44 design truck wheel load with a dynamic load allowance (impact factor). The design truck wheel load is one half of the axle load. The impact factor adopted was 30%. Then, the maximum computed fatigue load resulted in P_{max} = 71.2 kN (16,000 lb) × 1.3 = 92.5 kN (20,800 lb). The applied load frequency ranged between 2.4 and 3 Hz. Based on these applied load frequencies and the flexibility of the FRP deck, the actual maximum applied fatigue load attained was P_{max} = 89.0 kN (20,000 lb). The minimum applied load was P_{min} = 8.9 kN (2,000 lb). Therefore, the fatigue stress ratio was approximately R = 0.1.

The fatigue test specimens were not anticipated to fail during the two-million-cycle duration, so the fatigue analysis was focused on assessing the structural degradation associated with the cyclic loading. Fatigue damage accumulation can induce stiffness degradation of the FRP deck panels and in the panel-to-panel longitudinal joint. Besides,

fatigue damage can lead to residual damage in the FRP deck-steel girder haunch connection. To assess fatigue damage, quasi-static tests were conducted prior to the application of load-cycling and at specified increments of fatigue cycling, as shown in Figure III.4.3.

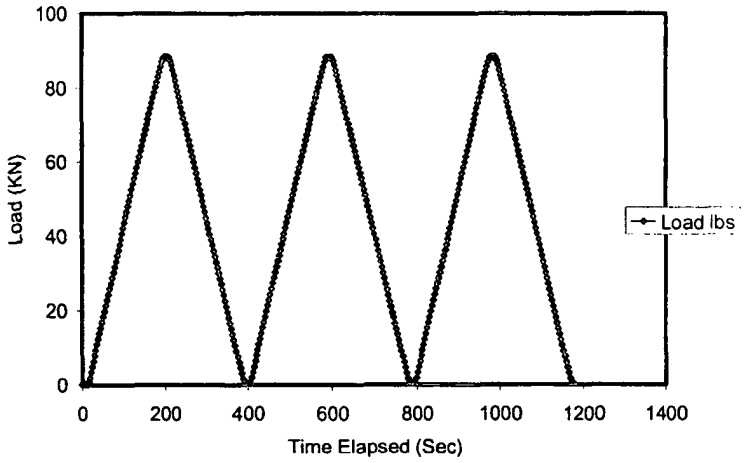

Figure III.4.3 Typical Quasi-Static Load Tests

First, at ambient temperature, 24°C (75°F), a set of quasi-static tests was conducted to obtain baseline load-deflection and load-strain values. Then, the test room was warmed up to 49°C (120°F). The FRP deck temperature was monitored until it reached the room temperature. Then, a second set of quasi-static test, but now at high temperature, was conducted. After this evaluation, one million load cycles were applied. Quasi-static tests were conducted at 100,000, 500,000, and 1,000,000 load cycles. For the low-temperature tests, the room was cooled to –30°C (–22°F), and the fatigue test with the corresponding quasi-static tests was repeated for the second million of load cycles.

III.4.5 Test Setup

The FRP deck dimensions were specified to model a typical slab-on-steel girder highway bridge, as shown in Figure III.4.1. A fatigue-testing frame was designed to accommodate the deck system prototype with the three connected steel girders. The deck prototype was instrumented with strain guages, thermocouples, and Linear Voltage Differential Transducers (LVDTs) (Figure III.4.1).

The fatigue tests were performed in CRREL's Material Evaluation Facility (MEF). This is a well-insulated room with interior dimensions of approximately 7.92 m (26 ft) wide by 12.80 m (42 ft) long and 3.66 m (12 ft) high. A set of double doors 3.35 m (11 ft) wide by 3.35 m (11 ft) tall allows the large fatigue test frame and the FRP bridge deck prototypes to be moved in and out of the MEF facility. A self-reacting steel test frame was designed and built at CRREL for a maximum load capacity of 266.9 kN (60,000 lb). One 97.9-kN- (22,000-lb-) capacity hydraulic actuator was mounted on the steel reaction frame to apply cyclic loading on the deck. The FRP deck specimen was attached to three steel girders W36x182, resulting in a continuous two-span bridge structure (Figure III.4.2). The actuator applied the load on a rectangular steel plate of 229 × 559 mm (9 × 22 in.) that simulates a wheel load contact area (AASHTO 1996). An elastomeric pad was placed between the steel plate and the FRP deck surface to provide uniform pressure. The load was applied eccentrically with respect to the traffic flow direction to study the load distribution in the y-direction, as shown in Figure III.4.1.

Load, deflection, strain, and temperature were the general parameters of measurement in this test program. The FRP deck specimen was instrumented with strain gauges, LVDTs, and thermocouples. Seven LVDTs supported by an independent frame

were used to measure deflections on the top surface of the deck. Four thermocouples were placed on four sides of the top FRP deck surface, and one thermocouple was used for air temperature. The thermocouples were used to verify that the FRP deck panel reached equilibrium with room temperature. The locations of the LVDTs, strain gauges, and thermocouples on the top of the deck are shown in Figure III.4.1. The location of the strain gauges bonded to the bottom deck surface (BX) was symmetrical with respect to the numerically matching strain gauges bonded to the top surface (TX).

The test setup induced a positive bending moment under the applied load (x = S/2) and a negative bending moment on the central support (x = S) and the adjacent span. An uplifting force resulted on the end girder support (x = 2 × S). This uplifting force was partially counteracted by the weight of the deck and steel beams.

As mentioned before, the FRP deck was evaluated for approximately 2,000,000 load cycles with controlled temperature. The first-million-load cycles were conducted at 49°C (120°F), while the second million cycles were performed at about –30°C (–22°F). The first quasi-static test was at room temperature, about 24°C (75°F), before the fatigue cycles began and served as the control baseline. In the quasi-static tests the load was applied at a rate of 1 mm/min (0.04 in./min), and sensor measurements were recorded every 3 s. Each quasi-static test consisted of a loading and unloading cycle. The quasi-static test was repeated three times, resulting in three peak loads and six varying load intervals for data analysis (Figure III.4.3).

III.4.6 Experimental Results

The raw data were analyzed to produce load-deflection curves for each deck test. Typical load-deflection curves for room temperature, 24°C (75°F), at five deck locations

corresponding to LVDTs mounted on the top of the panel and aligned in the x-direction, are shown in Figure III.4.4. Similarly, high-temperature load-deflection curves at the five locations after one million high-temperature load cycling is shown in Figure III.4.5. Figure III.4.6 shows the low-temperature load-deflection curves for the same locations after one million hot plus one million cold fatigue cycles. Figure III.4.7 compares the maximum deflection data for the room temperature baseline, after one million cycle at high-temperature, and after an additional one million cycles at low temperature. From these load-deflection curves we observe that the low-temperature stiffness after an accumulated two million load cycles is higher than the initial stiffness at room temperature. This observation implies that the panel stiffness is controlled mainly by temperature and not by the number of load cycles.

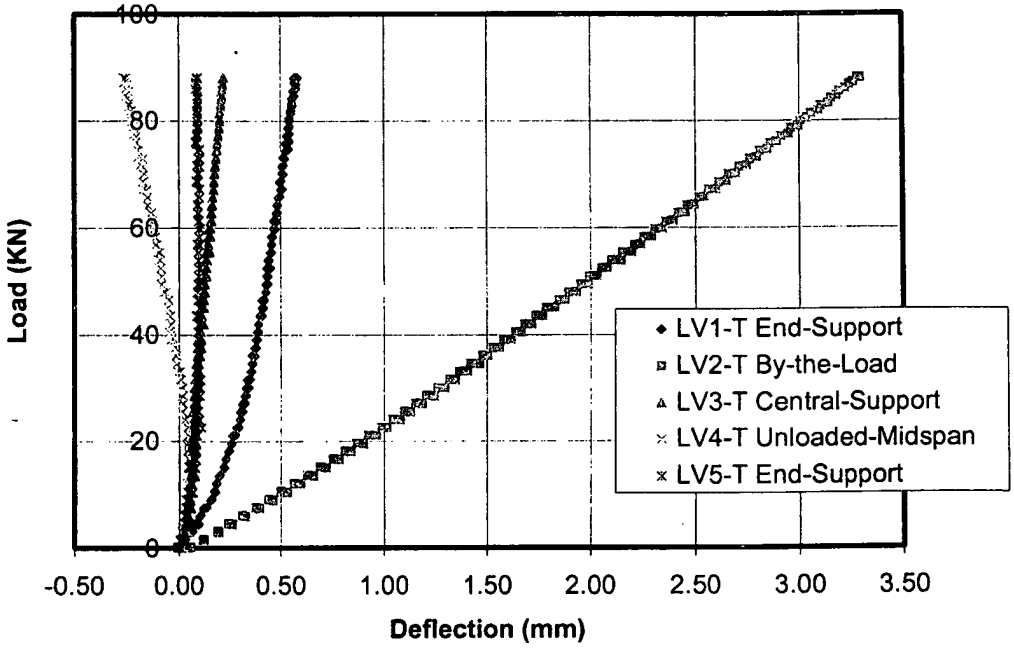

Figure III.4.4 Room-Temperature Load-Deflection Curves for Top LVDTs aligned in x-Direction prior to Fatigue Cycling

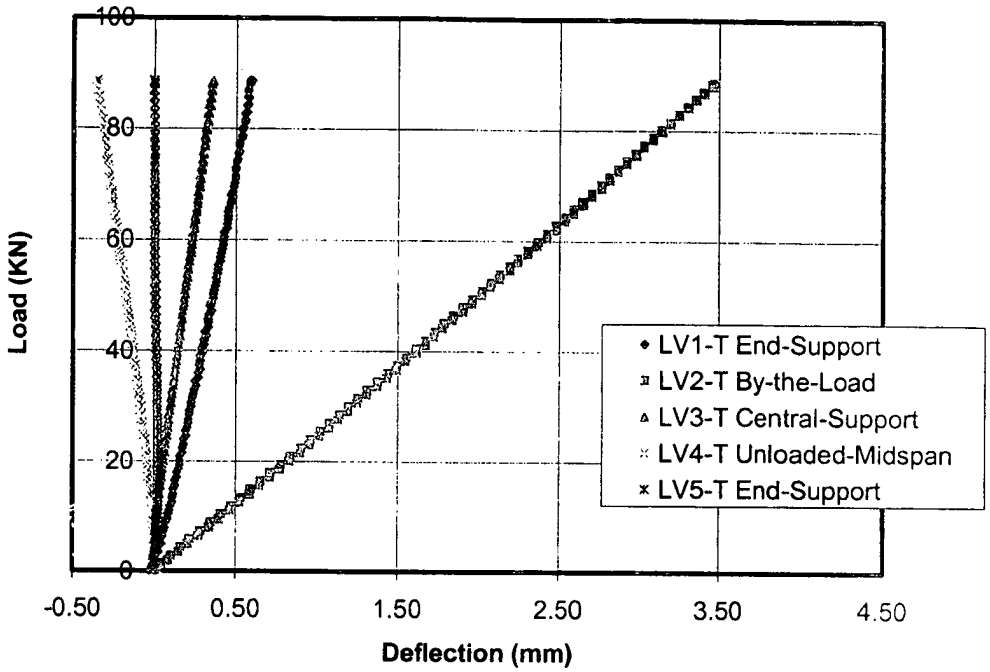

Figure III.4.5 High-Temperature Load-Deflection Curves for Top LVDTs aligned in x-Direction after One Million Hot Fatigue Cycles

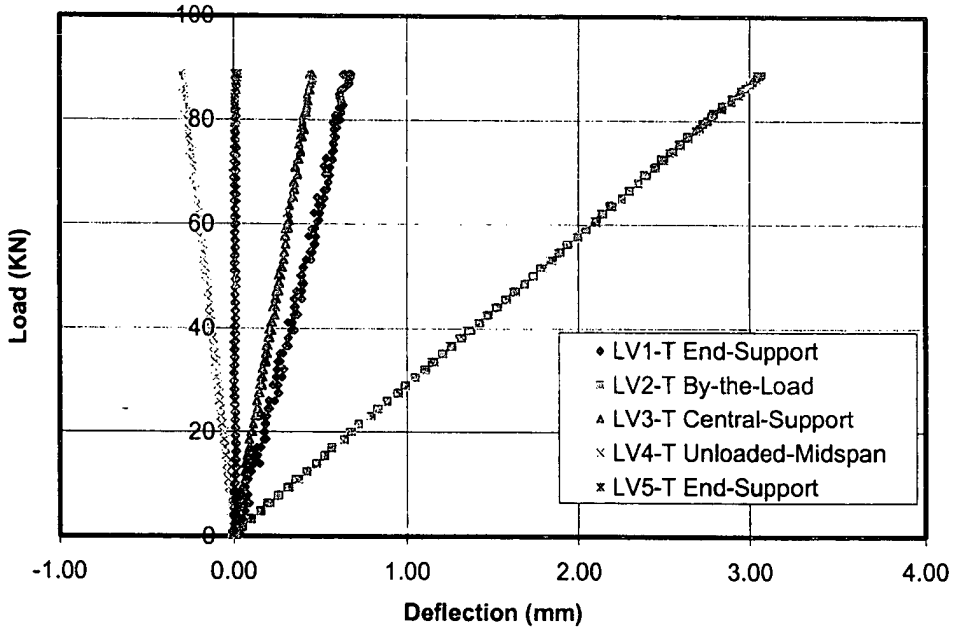

Figure III.4.6 Low-Temperature Load-Deflection Curves for Top LVDTs aligned in x-Direction after One Million Hot plus One Million Cold Fatigue Cycles

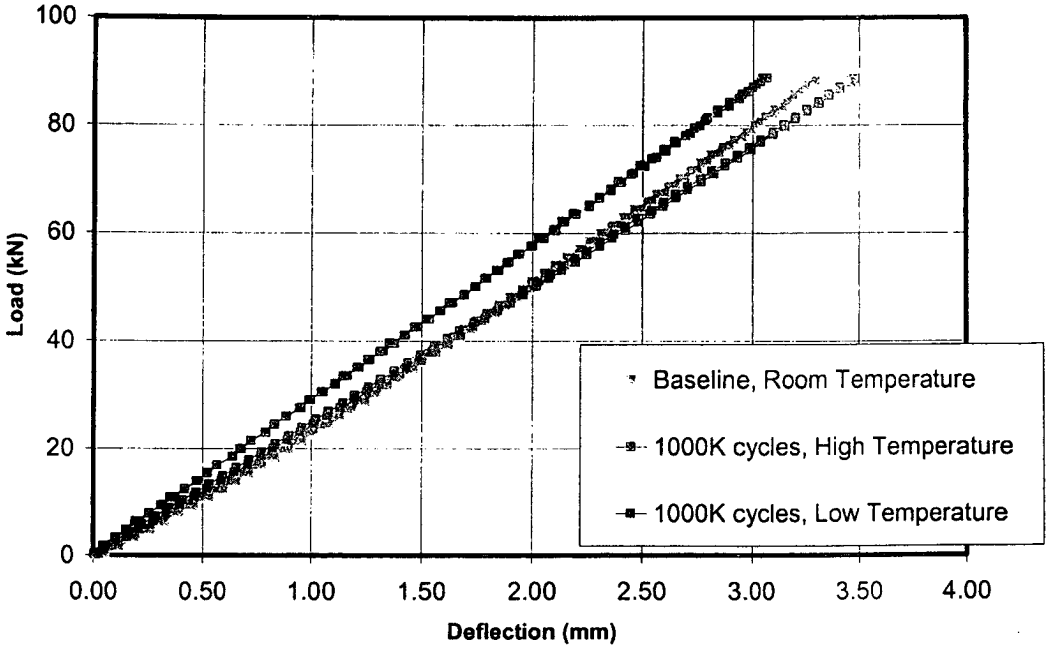

Figure III.4.7 Maximum Deflections for Three Test Conditions (Measured by LV2-T)

The maximum total deflections measured with the top LVDTs (LV1T, LV2T, LV3T, LV4T, and LV5T) aligned in the x-direction are shown in Figure III.4.8 for room-temperature (RT) baseline, high temperature (HT), and low temperature (LT), the last two after one million cycles at each temperature. These total deflections include both deck deflections and support deflections measured during the quasi-static tests. No deck uplifting was observed over the end girder. These deflection curves confirm the previous observation that the decrease in temperature increases the panel stiffness, even after higher number of accumulated load cycles.

The maximum deflections measured with the top LVDTs (LV2T, LV7T, and LV11T) aligned along the y-direction during the quasi-static tests are shown in Figure III.4.9. From this figure we observe that the panel longitudinal joint is able to transfer the shear force in the y-direction without any noticeable joint vertical slip.

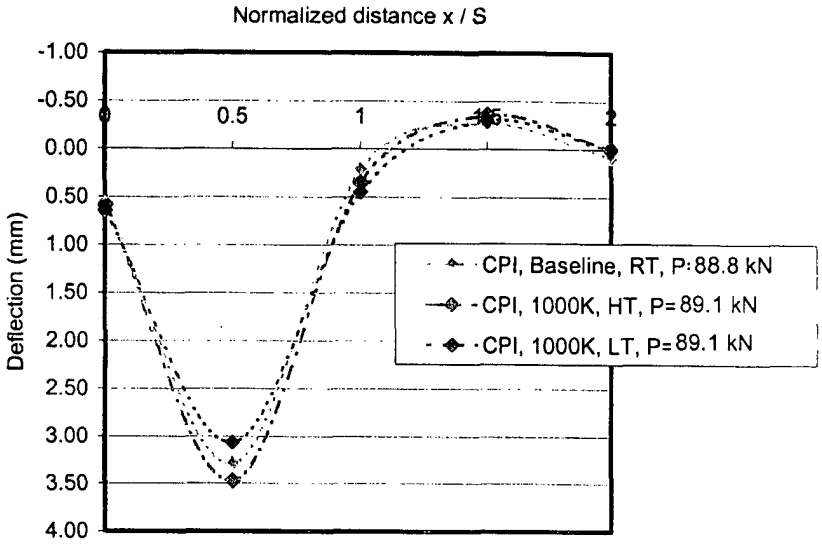

Figure III.4.8 Top Deflection Variation along the x-Direction for Maximum Load: LV1-T, LV2-T, LV3-T, LV4-T, LV5-T

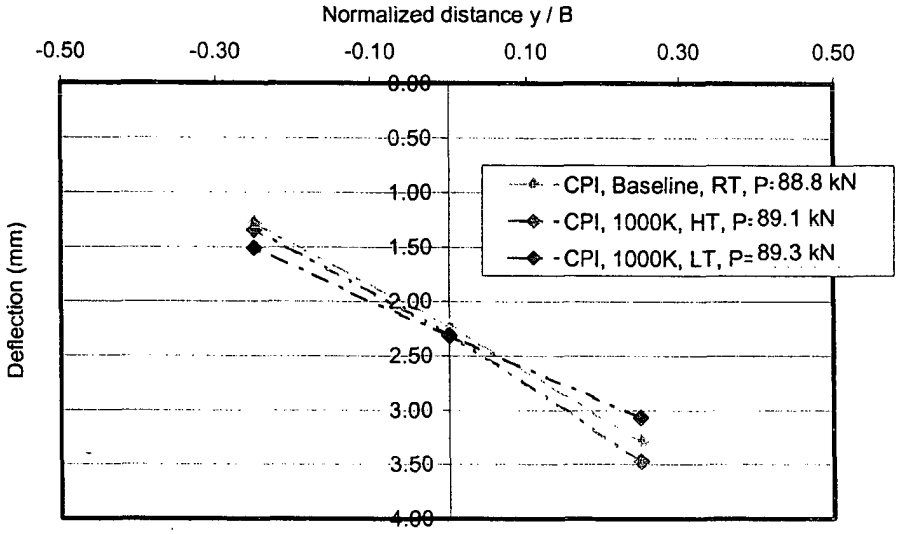

Figure III.4.9 Top Deflection Variation along the y-Direction for Maximum Load: LV2-T, LV7-T, LV11-T

Compressive strains on the top of the deck in the x-direction measured at room temperature prior to fatigue cycling are shown in Figure III.4.10. Similarly, tensile strains at symmetric locations on the bottom surface are shown in Figure III.4.11. All the curves

are linear within the loading range. Compressive strains on the top surface are slightly larger than the corresponding tensile strains on the bottom surface. Linear strain curves were obtained at high temperature after one million load cycles (Figure III.4.12 and Figure III.4.13). In the same way, strain curves were plotted at low temperature after an additional million of load cycles (Figure III.4.14 and Figure III.4.15). From these curves we observe that temperature reduction results in lower strains, which can be explained by the higher stiffness as we observed in the load-deflection curves (Figure III.4.7).

The FRP deck was inspected visually for signs of distress such as cracks and damage at connections after fatigue cycling. No visible damage was observed in the FRP deck and in the deck-beam connection.

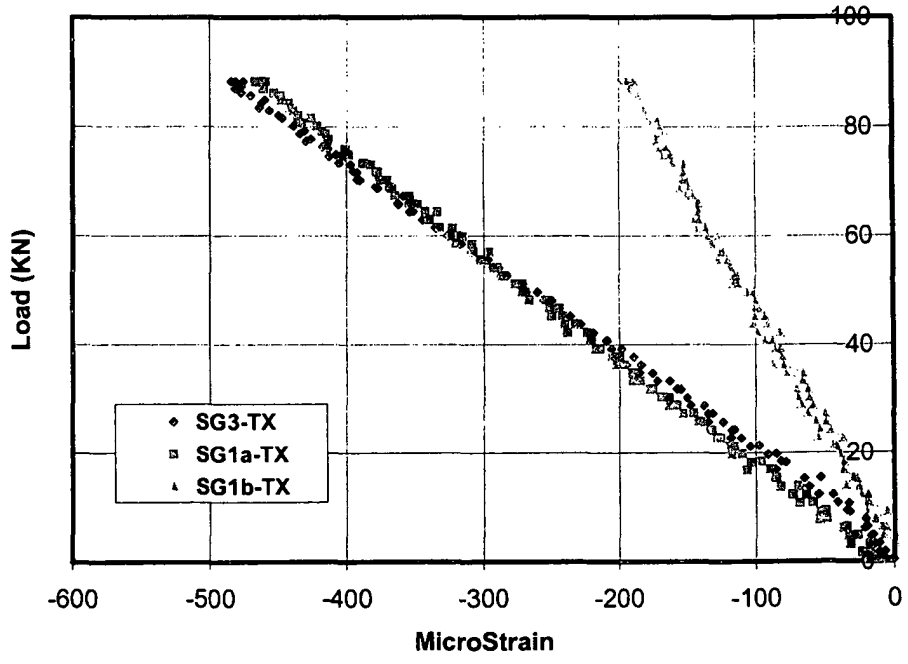

Figure III.4.10 Room-Temperature Strain (x-Direction) Curves Prior to Fatigue Cycling for Top Gauges (Loaded Span): SG1a-TX, SG1b-TX, SG3-TX

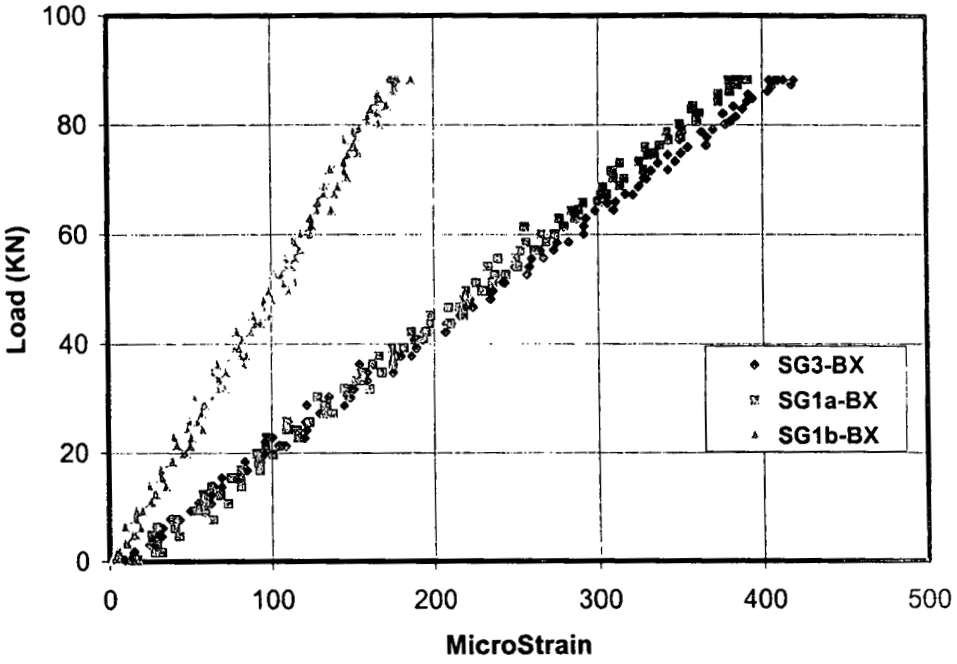

Figure III.4.11 Room-Temperature Strain (x-Direction) Curves Prior to Fatigue Cycling for Bottom Gauges (Loaded Span): SG1a-BX, SG1b-BX, SG3-BX

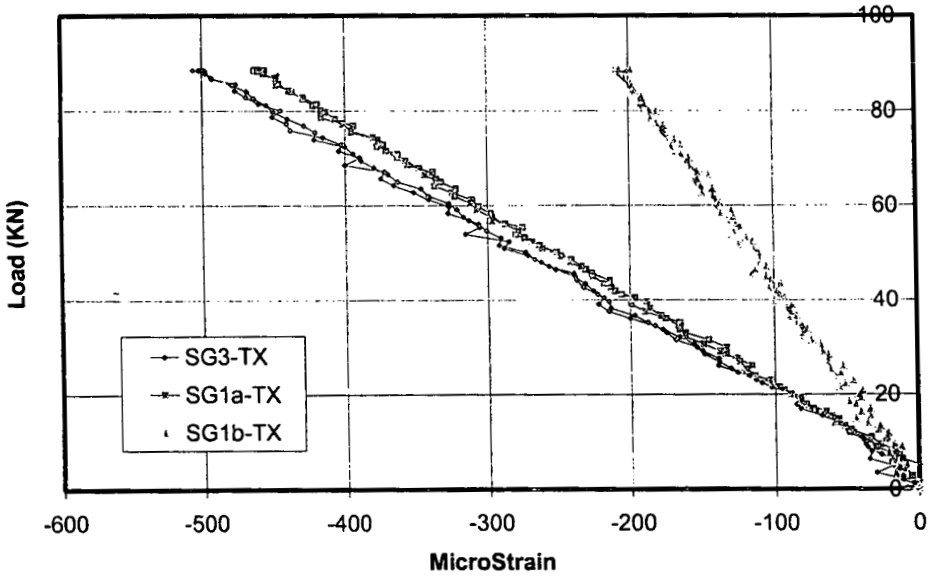

Figure III.4.12 High-Temperature Strain (x-Direction) Curves after One Million Hot Cycles for Top Gauges (Loaded Span): SG1a-TX, SG1b-TX, SG3-TX

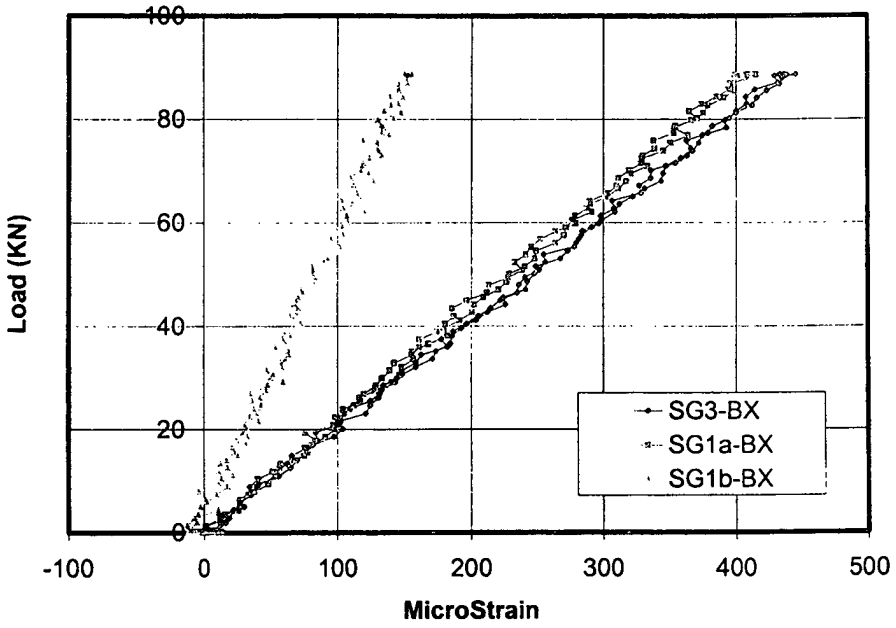

Figure III.4.13 High-Temperature Strain (x-Direction) Curves after One Million Hot Cycles for Bottom Gauges (Loaded Span): SG1a-BX, SG1b-BX, SG3-BX

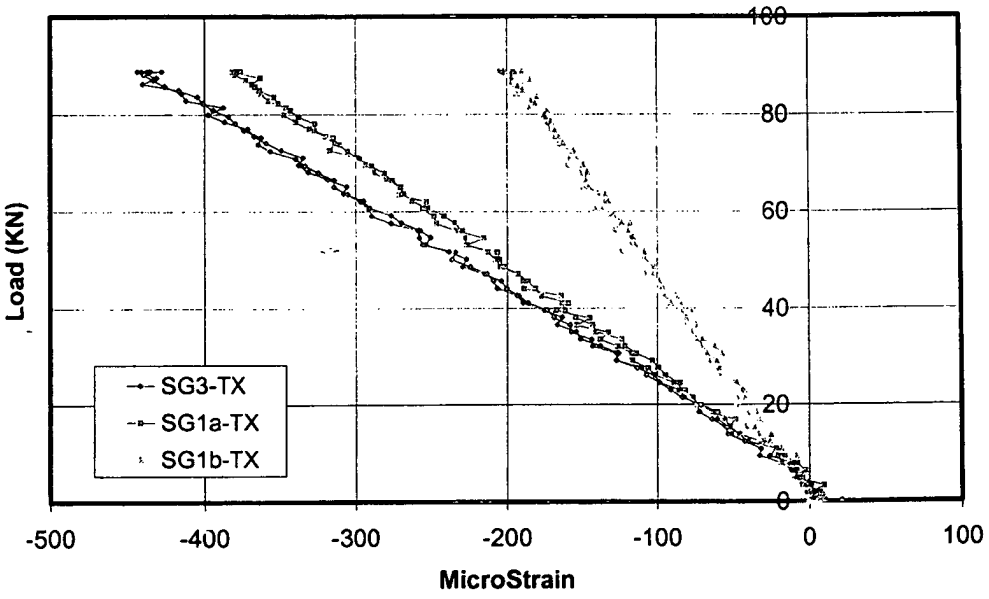

Figure III.4.14 Low-Temperature Strain (x-Direction) Curves after One Million Hot plus One Million Cold Cycles for Top Gauges (Loaded Span): SG1a-TX, SG1b-TX, SG3-TX

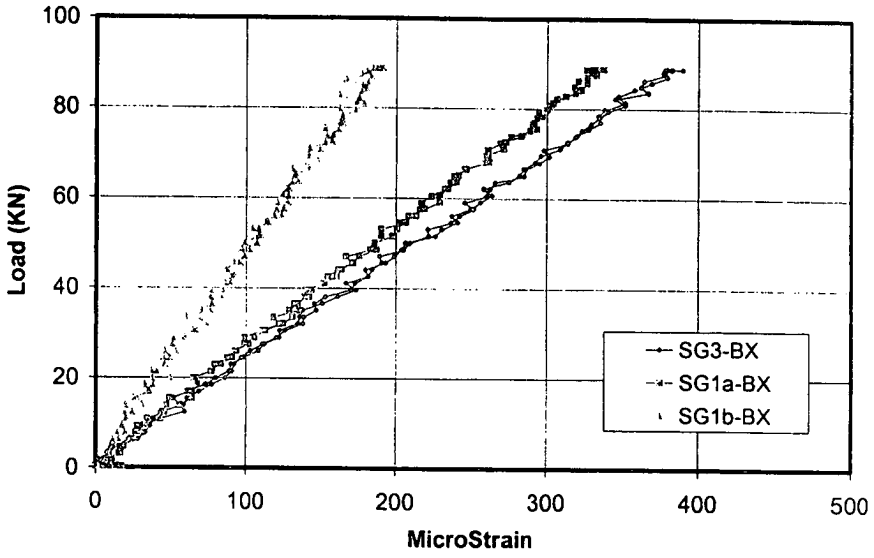

Figure III.4.15 Low-Temperature Strain (x-Direction) Curves after One Million Hot plus One Million Cold Cycles for Bottom Gauges (Loaded Span): SG1a-BX, SG1b-BX, SG3-BX

III.4.7 Data Analysis

To evaluate the FRP deck response with temperature and number of load cycles, two stiffness indicators are defined:

1) Stiffness indicator in the x-direction is computed based on corrected maximum deflections along a longitudinal line (LV1T, LV2T, LV3T); and
2) Stiffness indicator in the y-direction is computed based on maximum deflections across a transverse line (LV2T, LV7T, LV11T).

III.4.7.1 Retained Stiffness in the x-Direction

The maximum deflection, δ_c, was corrected to account for support deflection according to equation III.4.1:

$$\delta_c = (LV2T) - \tfrac{1}{2}(LV1T + LV3T) \qquad \text{(III.4.1)}$$

where LV1T, LV2T, and LV3T are defined as deflection at the points given in Figure III.4.1. For each quasi-static test corresponding to the number of applied load cycles, n, the six segments of the load-deflection curves (see the loading and unloading segments in Figure III.4.3) for varying load intervals were plotted. A linear response was observed in all cases and approximated with a linear least-squares regression line to compute the load-deflection ratio $\left(P/\delta_c\right)_n$. These load-deflection ratios are related to the stiffness of the deck in the x-direction. The resulting load-deflection ratios are given in Table III.4.1.

An indicator of retained stiffness in the x-direction, $R_{x,n}$, is defined as the mean residual load-deflection ratio after n load cycles with controlled temperature with respect to the mean initial load-deflection ratio, as shown in equation III.4.2

$$R_{x,n} = \frac{\left(P/\delta_c\right)_n}{\left(P/\delta_c\right)_o} \tag{III.4.2}$$

Then $R_{x,n} < 1$ implies a reduction in deck stiffness, while $R_{x,n} > 1$ implies an increase in deck stiffness. The resulting retained stiffness indicators are given in Table III.4.2.

Table III.4.1 - FRP Deck x-Direction Load-Deflection Ratio

	Temperature (°C)					
	24		49		–30	
Load Cycles	Mean (kN/mm)	COV (%)	Mean (kN/mm)	COV (%)	Mean (kN/mm)	COV (%)
0	30.9	0.31	29.3	0.56		
100000			29.2	0.30		
500000			29.3	0.15		
1000000			29.6	0.25	34.0	1.10
1000000 + 100000					35.2	0.25
1000000 + 500000					35.2	0.47
1000000 + 1000000					35.1	0.31

Note: 1 kN/mm = 5.71 kip/in.

Table III.4.2 - FRP Deck x-Direction Stiffness Indicator

	Temperature (°C)					
	24		49		–30	
Load Cycles	Statistical Level	$R_{x,n}$	Statistical Level	$R_{x,n}$	Statistical Level	$R_{x,n}$
0	A	1.000	B	0.946		
100000			B	0.945		
500000			B	0.957		
1000000			C	0.958	D	1.098
1000000 + 100000					E	1.138
1000000 + 500000					E	1.138
1000000 + 1000000					E	1.135

*The same letter indicates the same stiffness ratio with 95% confidence

III.4.7.2 Retained Stiffness in the y-Direction

Deflections were measured at three points aligned across the FRP deck (LV2-T, LV7-T, and LV11-T), as shown in Figure III.4.1. Load-deflection curves were plotted for the six load-varying intervals of each quasi-static test. These load-deflection curves followed a linear trend and were fitted using linear least-squares regression analysis. The trend lines were then used to calculate the deflection corresponding to P = 89 kN (20,000 lb) for the six segments of the load-deflection curves. The resulting deflections were used to compute the secant slopes at both sides of the longitudinal FRP joint (i.e., $y > 0$ and $y < 0$), as shown in equation III.4.3:

$$\tan\theta_{Y+} = \frac{LV2T - LV7T}{B/4}$$
$$\tan\theta_{Y-} = \frac{LV7T - LV11T}{B/4} \qquad \text{(III.4.3)}$$

Then, the change in the slope angle at the longitudinal joint location is computed as shown in equation III.4.4:

$$\Delta\theta_n = \theta_{Y+} - \theta_{Y-}. \tag{III.4.4}$$

If $\Delta\theta_n > 0$, then the deck curves transversely concave down, and if $\Delta\theta_n < 0$, it curves concave up. The resulting changes in slope angles are given in Table III.4.3

Table III.4.3 - FRP Deck y-Direction Slope Change

	Temperature (°C)					
	24		49		-30	
Load Cycles	Mean (rad)	COV (%)	Mean (rad)	COV (%)	Mean (rad)	COV (%)
0	2.20E-04	6.53	2.93E-04	9.24		
100000			4.39E-04	4.18		
500000			4.33E-04	1.30		
1000000			4.20E-04	1.31	N.A.	- - -
1000000 + 100000					-1.68E-04	10.92
1000000 + 500000					-1.30E-04	9.62
1000000 + 1000000					-1.54E-04	11.84

An indicator of retained deck and joint stiffness in the y-direction, $R_{y,n}$, is defined as the mean change in slope angle after n load cycles with controlled temperature with respect to the mean initial change in slope angle, as shown in equation III.4.5

$$R_{y,n} = \frac{\Delta\theta_o}{\Delta\theta_n} \tag{III.4.5}$$

If $R_{y,n} > 0$, then the deck does not change the curvature orientation. In particular, if $0 < R_{y,n} < 1$, the change in slope angle is more pronounced, and if $R_{y,n} > 1$, the change in slope angle is less pronounced than the baseline quasi-static test. On the other hand, if $R_{y,n} < 0$, the deck changes the curvature orientation (e.g., from concave up to concave down, or vice versa). The resulting retained stiffness indicators are given in Table III.4.4.

Table III.4.4 - FRP Deck y-Direction Stiffness Indicator

	Temperature (°C)					
	24		49		-30	
Load Cycles	Statistical Level	$R_{y,n}$	Statistical Level	$R_{y,n}$	Statistical Level	$R_{y,n}$
0	A	1.000	B	0.749		
100000			C	0.500		
500000			C	0.508		
1000000			C	0.522	D	-4.011
1000000 + 100000					E	-1.309
1000000 + 500000					F	-1.691
1000000 + 1000000					E, F	-1.428

*The same letter indicates the same curvature with 95% confidence

The longitudinal panel joint, which is located between LV2-T and LV11-T, incorporates additional shear and bending flexibility that affects the change in the slope angle. Therefore, the change in the slope angle not only measures the bending and shear stiffness of the panels, but it also accounts for the discrete bending and shear stiffness of the joint. The reason for adopting the slope angle method of measuring the stiffness response in the transverse direction instead of a more conventional quadratic fit of deflections, which is more applicable to reinforced-concrete decks, is to model the articulated nature of the pultruded panels.

III.4.7.3 Statistical Analysis

Statistical analysis of the load-deflection ratio and the change in slope angle for the FRP deck system was performed using one-way analyses of variance (ANOVA) for each number of cycles and temperature condition. The analysis was conducted using the SYSTAT software package. The ANOVA analysis determined if the response of the

deck system was a function of number of cycles or temperature. The model for a one-way ANOVA is represented symbolically as follows:

$$Y_n = B_o + B_1 \cdot X_n + \varepsilon_n \tag{III.4.6}$$

where Y_n = observed mechanical property (load-deflection ratio or change in slope angle) for the number of cycles n under controlled temperature

B_o, B_1 = coefficients of the model

X_n = code associated with the variable under study (e.g., temperature or cumulative load cycles)

ε_n = random unit variation within the block of data.

The null hypothesis and alternative hypothesis are given in equation III.4.7:

$$\begin{aligned} &H_0 : B_1 = 0 \\ &H_A : B_1 \neq 0 \end{aligned} \tag{III.4.7}$$

Post hoc analysis of type Bonferroni was used for pair-wise comparisons with a confidence level of 95% (α = 0.05). Four one-way ANOVA tests were performed for each mechanical property (i.e., load-deflection slope and change in slope angle) of the FRP deck system. The first two compared the mechanical property as the dependent variable with the temperature as the factor and the number of cycles held constant (0 and 1,000,000 cycles, respectively). The second two used the mechanical property as the dependent variable with the number of cycles as the factor, holding the temperature constant, 49°C (120°F) and –30°C (–22°F), respectively. Additional tests were done only if the stiffness ratio was close between two or more cycles across temperatures and compared only those specific tests. This was equivalent to performing paired t-tests.

III.4.8 Discussion

In the x-direction the load-deflection ratios are lower than those of RCC, as shown in Figure III.4.16. Load-deflection ratios show more variance with temperature than with load cycles. The coefficients of variance are small, with the x-direction ratios indicating a tight spread of data. Statistically there is almost no change in load-deflection with cycles. There is, however, a large difference with temperature changes. For RCC the differences were about 6%, where in CPI the difference is between 6% and 13%. The y-direction stiffness shows an abnormality with the room- and high-temperature data. The change in slope-angle values are positive, indicating a concave-down deck at these temperatures. This indicates that either the deck or the joint is very flexibl,e allowing the load to be non-uniformly transferred from deck section to section. The coefficients of variance are also large compared to those in the x-direction. This indicates a joint that is not very consistent with high temperatures. Most likely the adhesives used caused the joint to behave as a hinge at higher temperatures and as a fixed joint at lower temperatures.

The variation of strains in the x-direction with temperature and number of load cycles is illustrated in Figure III.4.17. Both the top and bottom strain curves have shown a reduction in micro-strains per unit load with the decrease in temperature

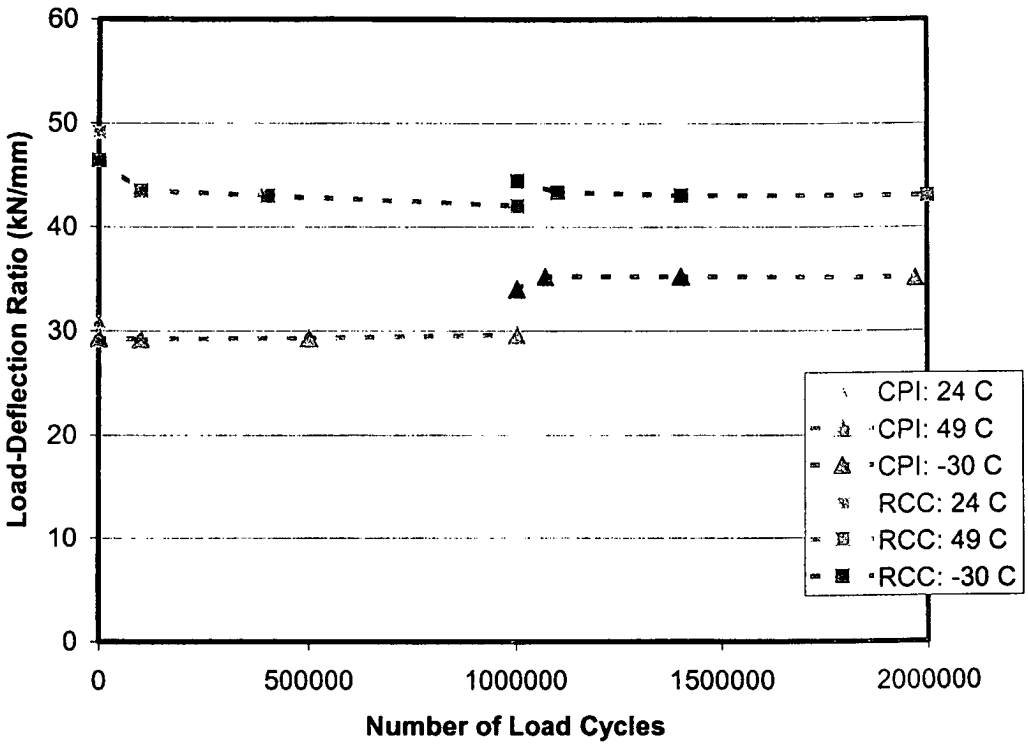

Figure III.4.16 Load-Deflection Ratio History Comparison

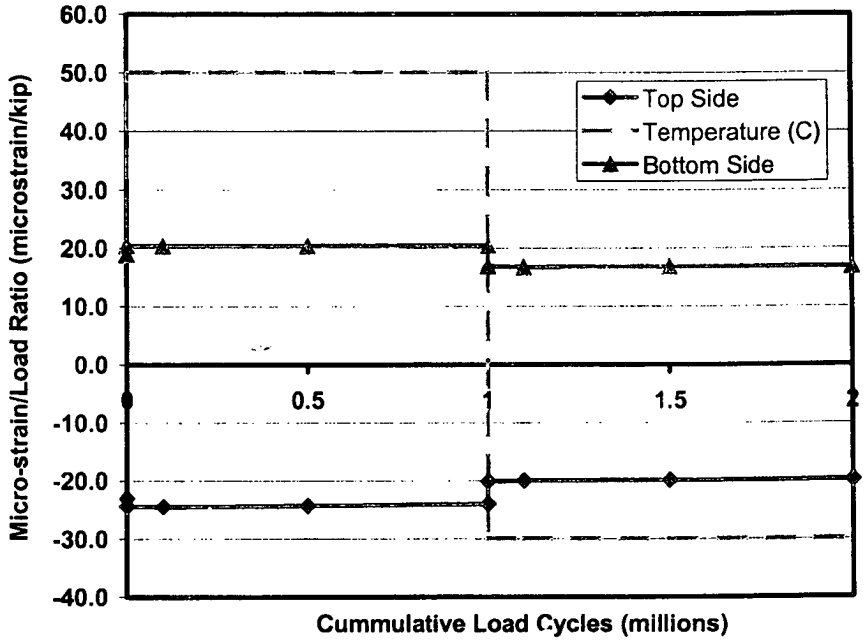

Figure III.4.17 Micro-strain per 4.45 kN (1000 lb) Load during Fatigue Cycling

III.4.9 Conclusions

The analysis done on the deck is a useful measure of stiffness in the x-direction and a useful indicator of stiffness in the y-direction. The x-direction load-deflection analysis takes into account support deflections and is conducted over a continuous span. Both of these factors combine to provide a useful measure for the amount of deflection expected with applied load.

The y-direction analysis is less useful because of the many uncertainties incorporated into one number, the change in slope angle, by the analysis. Unlike the x-direction analysis, the y-direction analysis did not take into account the support deflections and was not conducted over a continuous span.

The statistical analysis performed was adequate for the desired information. The one-way ANOVA was proven to be an efficient analysis tool for determining significant changes in load-deflection ratios and change in slope angle between quasi-static tests.

Overall the FRP pultruded deck is sensitive to temperature changes compared to RCC. In the x-direction this is shown by the change in load-deflection ratios from high temperature to low temperature. In the y-direction the behavior is very different from that of conventional reinforced-concrete decks. The FRP pultruded deck has a different curvature compared to that of RCC at room and high temperature. It also exhibits a drastic degradation with load cycles in the y-direction. This is shown by the large jumps in the residuals in Table III.4.4 in the first 100,000 cycles at both high and low temperatures.

III.5 Fatigue Response of FRP Bridge Deck Fabricated by Contact Molding Hand Lay-up under Extreme Temperature Conditions

III.5.1 Abstract

The fatigue performance evaluation at extreme temperature of a two-span continuous fiber-reinforced polymer (FRP) deck prototype built on three W-section steel girders is presented. The FRP deck panels were fabricated by the contact molding hand lay-up process.

II.5.2 Introduction

The fatigue performance evaluation at extreme temperature of a two-span continuous fiber-reinforced polymer (FRP) deck prototype built on three W-section steel girders is presented. The FRP deck was fabricated by contact molding hand lay-up. The FRP deck was supplied by Infrastructure Composites International (ICI), San Diego, CA, and Mesa Fiberglass Inc., Commerce City, CO.

The deck-girder system was subjected to an eccentric cyclic load that simulates an AASHTO HS20 design truck wheel load with impact. Initially, one million load cycles were applied at a controlled high temperature, 49°C (120°F), and then another million load cycles were applied at a controlled low temperature, –30°C (–22°F). Quasi-static load tests were conducted at specific intervals during fatigue cycling to evaluate the load-deflection and load-strain response at several deck locations. A reinforced-concrete conventional (RCC) deck designed by the Ohio Department of Transportation was

fabricated and tested under the same load and temperature regime (See Chapter III.1). The RCC deck was utilized to establish the "current practice" benchmark response. The contact molding hand lay-up deck performance was compared with the RCC deck. The fatigue tests of the contact molding hand lay-up and RCC decks were conducted at the U.S. Army Cold Regions Research and Engineering Laboratory in Hanover (CRREL), N.H.

The fatigue-temperature performance was assessed based on two damage indicators by

1. Establishing if the contact molding hand lay-up deck apparent bending stiffness in the x-direction degrades with number of load cycles and temperature changes. The apparent bending stiffness in the x-direction is associated with and is measured by the corrected maximum deflections.
2. Establishing if the contact molding hand lay-up deck apparent bending stiffness in the y-direction degrades with number of load cycles and temperature changes. The apparent bending stiffness in the y-direction is associated with and is measured by the change in slope angle in the transverse direction of the deck under maximum loading conditions.

III.5.3 Description of the Deck System

The FRP deck was fabricated by the contact molding hand lay-up process with a honeycomb core and top and bottom face skins. Two panels of 0.914 m (36 in.) in width and 6.10 m (240 in.) in length were connected with a longitudinal joint to form the deck test specimen, as shown in Figure III.5.1.

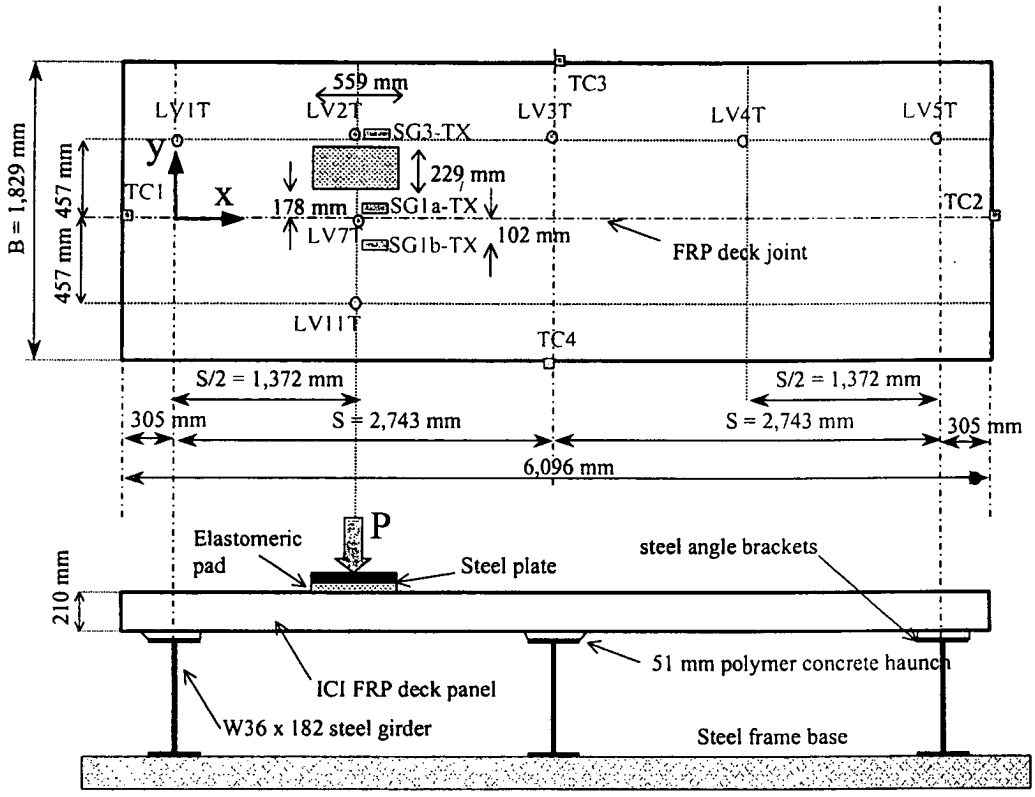

Figure III.5.1 Test Setup

The contact molding hand lay-up deck was attached to the supporting W-beams using steel angle brackets. One angle bracket per panel was bolted through the FRP panel. A 51-mm (2-in.) haunch made of polymer concrete wrapped with a glass fabric was placed on the steel girders. The haunch was bonded to the FRP deck with an adhesive. One steel turnbuckle per span was placed underneath the FRP deck and across the longitudinal joint to hold the panels together.

The tongue-and-groove construction joint between the two panels was not square and tight. It was possible to look into the joint from one end towards the other end of the FRP deck and see daylight. No adhesive was used in the panel longitudinal joint. The outer edges of the FRP panels were actually curled upwards so that the bottom surface was not in contact with the supporting W- beams.

III.5.4 Test Protocol

There are no specifications available for FRP bridge decks on the number of load cycles required for fatigue performance evaluation. A fatigue performance evaluation procedure was initially developed and applied to qualify FRP decks panels fabricated by pultrusion and vacuum-assisted resin transfer molding (VARTM) (Lopez-Anido et al. 1998). The present evaluation procedure consisted of applying two million simulated wheel load cycles at two controlled extreme temperatures, 49°C (120°F) and –30°C (–22°F), on FRP panels attached to steel girders, i.e., one million cycles at 49°C (120°F) and one million cycles at –30°C (–22°F). The two-span continuously supported FRP deck was subjected to a simulated AASHTO HS20-44 design truck wheel load (Figure III.5. Figure III.5.2). A girder spacing of 2.74 m (108 in.) was selected, as shown in Figure III.5.1.

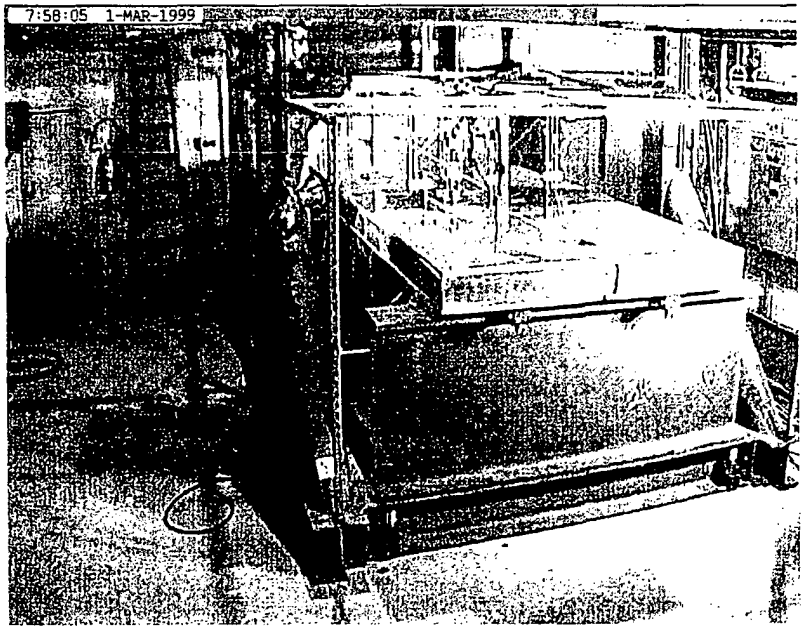

Figure III.5.2 Contact Molding Hand Lay-Up Panel Supported by Steel Beams during Fatigue Testing

The maximum load to be applied was computed based on an AASHTO HS20-44 design truck wheel load with a dynamic load allowance (impact factor). The design truck wheel load is one half of the axle load. The impact factor adopted was 30%. Then, the maximum computed fatigue load resulted in P_{max} = 71.2 kN (16,000 lb) × 1.3 = 92.5 kN (20,800 lb). The applied load frequency ranged between 2.4 and 3 Hz. Based on these applied load frequencies and the flexibility of the FRP deck, the actual maximum applied fatigue load attained was P_{max} = 89.0 kN (20,000 lb). The minimum applied load was P_{min} = 8.9 kN (2,000 lb). Therefore, the fatigue stress ratio was approximately R = 0.1.

The fatigue test specimens were not anticipated to fail during the two-million-cycle duration, so the fatigue analysis was focused on assessing the structural degradation associated with the cyclic loading. Fatigue damage accumulation can induce stiffness degradation of the FRP deck panels and in the panel-to-panel longitudinal joint. Besides, fatigue damage can lead to residual damage in the FRP deck-steel girder haunch connection. To assess fatigue damage, quasi-static tests were conducted prior to the application of load-cycling and at specified increments of fatigue cycling, as shown in Figure III.5.3.

First, at ambient temperature, 24°C (75°F), a set of quasi-static tests was conducted to obtain baseline load-deflection and load-strain values. Then, the test room was warmed to 49°C (120°F). The FRP deck temperature was monitored until it reached the room temperature. Then, a second set of quasi-static test, but now at high temperature, was conducted. After this evaluation, one million load cycles were applied. Quasi-static tests were conducted at 100,000, 500,000, and 1,000,000 load cycles. For the

low-temperature tests, the room was cooled to –30°C (–22°F), and the fatigue test and the corresponding quasi-static tests were repeated for the second million of load cycles.

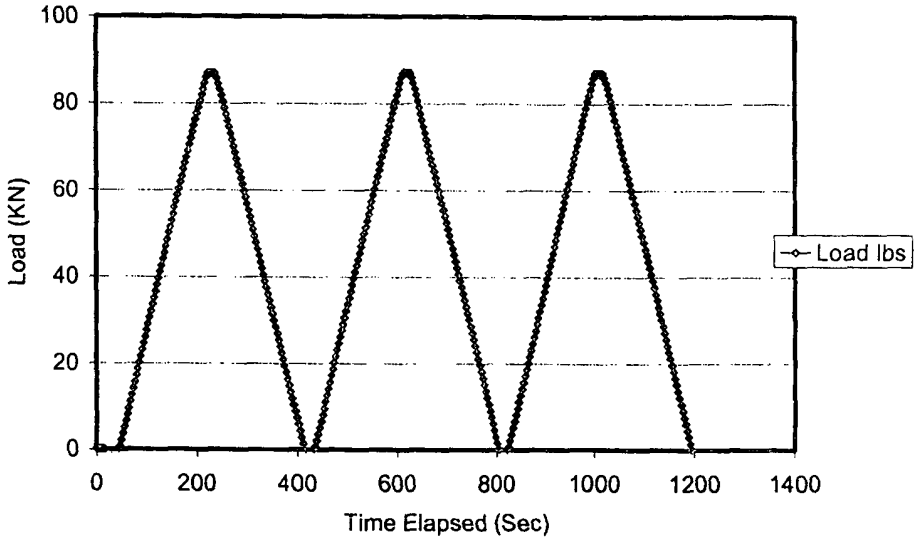

Figure III.5.3 Typical Quasi-Static Load Tests

III.5.5 Test Setup

The FRP deck dimensions were specified to model a typical slab-on-steel girder highway bridge, as shown in Figure III.5.1. A fatigue-testing frame was designed to accommodate the deck system prototype with the three connected steel girders. The deck prototype was instrumented with strain gauges, thermocouples, and Linear Voltage Differential Transducers (LVDTs) to measure vertical deflection (Figure III.5.1). As discussed before, the applied load represents an AASHTO HS20-44 design truck wheel load with a dynamic load allowance (impact factor). The impact factor adopted was 30%. Thus, the maximum applied load resulted in P_{max} = 71.2 kN (16,000 lb) × 1.3 = 92.5 kN (20,800 lb).

The fatigue tests were performed in CRREL's Material Evaluation Facility (MEF). This is a well-insulated room with interior dimensions of approximately 7.92 m (26 ft) wide by 12.80 m (42 ft) long and 3.66 m (12 ft) high. A set of double doors 3.35 m (11 ft) wide by 3.35 m (11 ft) tall allows the large fatigue test frame and the FRP bridge deck prototypes to be moved in and out of the MEF facility. A self-reacting steel test frame was designed and built at CRREL for a maximum load capacity of 266.9 kN (60,000 lb). One 97.9-kN- (22,000-lb-) capacity hydraulic actuator was mounted on the steel reaction frame to apply cyclic loading on the deck. The FRP deck specimen was attached to three steel girders W36x182, resulting in a continuous two-span bridge structure (Figure III.5.2). The actuator applied the load on a rectangular steel plate of 229 × 559 mm (9 × 22 in.) that simulates a wheel load contact area (AASHTO 1996). An elastomeric pad was placed between the steel plate and the FRP deck surface to provide uniform pressure. The load was applied eccentrically with respect to the traffic flow direction to study the load distribution in the y-direction, as shown in Figure III.5.1.

Load, deflection, strain, and temperature were the general parameters of measurement in this test program. The FRP deck specimen was instrumented with strain gauges, LVDTs, and thermocouples. Seven LVDTs supported by an independent frame were used to measure deflections on the top surface of the deck. Four thermocouples were placed on four sides of the top FRP deck surface, and one thermocouple was used for air temperature. The thermocouples were used to verify that the FRP deck panel reached equilibrium with room temperature. The locations of the LVDTs, strain gauges, and thermocouples on the top of the deck are shown in Figure III.5.1. The location of the strain gauges bonded to the bottom deck surface (BX) was symmetrical with respect to

the numerically matching strain gauges bonded to the top surface (TX). However, the actual location of the bottom strain gauges (BX) in the loaded span needed to be shifted 51 mm (2 in.) in the x-direction toward the end support to avoid interference with the turnbuckle that holds the two panels together.

The entire FRP deck prototype was bowed upwards along its 20-ft length so that the bottom of the middle steel W-beam was approximately 0.5–0.75 in. off the middle support beam in the load frame. Shims were placed at a number of locations on this deck to attempt to provide more intimate contact between the various surfaces. Also, because there was a 0.5-in. depression in the surface of the deck right under the loading plate, a leveling layer of "Levelastic" was placed on the surface of the deck at the low point to provide good surface contact between the deck and the loading plate. Levelastic is a cementitious material that comes in dry form. Water is added to it until it becomes a paste consistency, and it is troweled on and smoothed.

The test setup induced a positive bending moment under the applied load ($x = S/2$) and a negative bending moment on the central support ($x = S$) and the adjacent span. An uplifting force resulted on the end girder support ($x = 2 \times S$). This uplifting force was partially counteracted by the weight of the deck and steel beams.

As mentioned before, the FRP deck was evaluated for approximately 2,000,000 load cycles with controlled temperature. The first million load cycles were conducted at 49°C (120°F), while the second million cycles were performed at about –30°C (–22°F). The first quasi-static test was at room temperature, about 24°C (75°F), before the fatigue cycles began and served as the control baseline. In the quasi-static tests, the load was applied at a rate of 1 mm/min (0.04 in/min), and sensor measurements were recorded

every 3 s. Each quasi-static test consisted of a loading and unloading cycle. The quasi-static test was repeated three times, resulting in three peak loads and six varying-load intervals for data analysis (Figure III.5.3).

III.5.6 Experimental Results

The raw data were analyzed to produce load-deflection curves for each deck test. Typical load-deflection curves for room temperature, 24°C (75°F), at five deck locations corresponding to LVDTs mounted on the top of the panel and aligned in the x-direction, are shown in Figure III.5.4. Similarly, high-temperature load-deflection curves at the five locations after one million high-temperature load cycling is shown in Figure III.5.5. Figure III.5.6 shows the low-temperature load-deflection curves for the same locations after one million hot plus one million cold fatigue cycles. Figure III.5.7 compares the maximum deflection data for the room-temperature baseline, after one million cycle at high temperature, and after an additional one million cycles at low temperature. A nonlinearity in the load-deflection response was observed in the LVDTs in the loaded span after one million load cycles, which indicates a slip in the panel to panel joint (Figure III.5.6 and Figure III.5.7).

The maximum total deflections measured with the top LVDTs (LV1T, LV2T, LV3T, LV4T, and LV5T) aligned the x-direction are shown in Figure III.5.8 for room-temperature (RT) baseline, high temperature (HT), and low temperature (LT), the last two after one million cycles at each temperature. These total deflections include both deck deflections and support deflections measured during the quasi-static tests. No deck uplifting was observed over the end girder. These deflection curves confirm the previous

observation that the decrease in temperature increases the panel stiffness, even after higher number of accumulated load cycles.

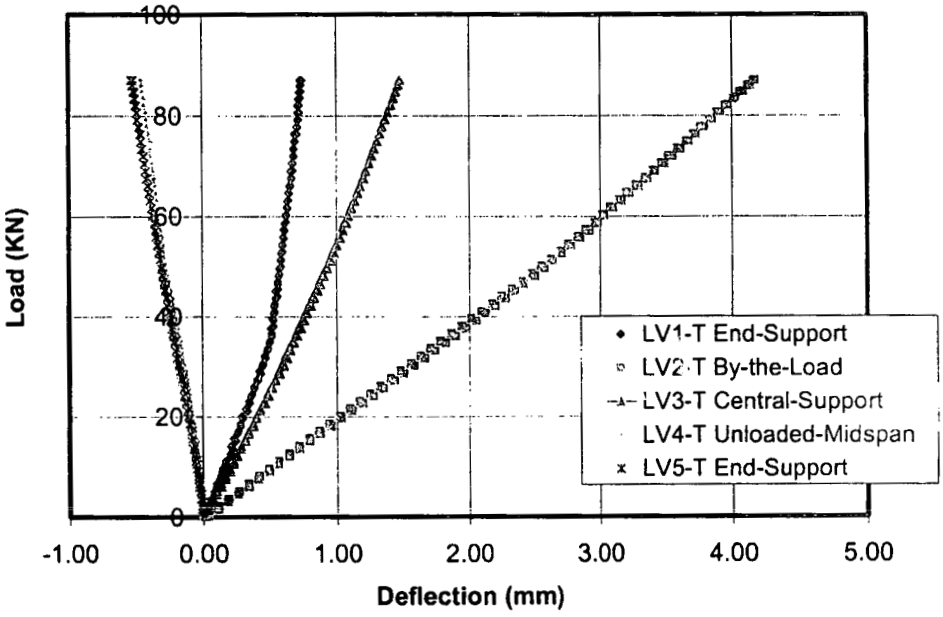

Figure III.5.4 Room-Temperature Load-Deflection Curves for Top LVDTs aligned in x-Direction prior to Fatigue Cycling

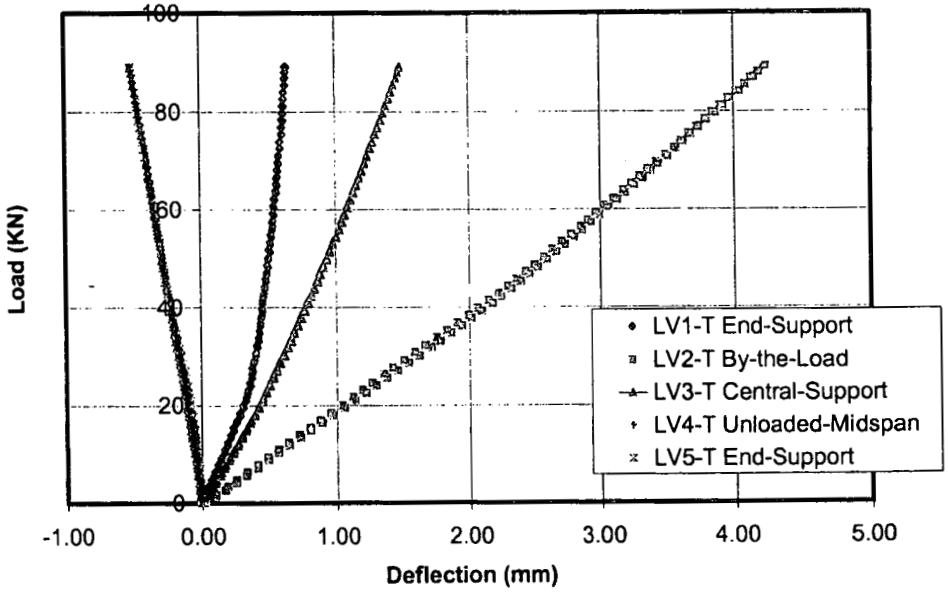

Figure III.5.5 High-Temperature Load-Deflection Curves for Top LVDTs aligned in x-Direction after One Million Hot Fatigue Cycles

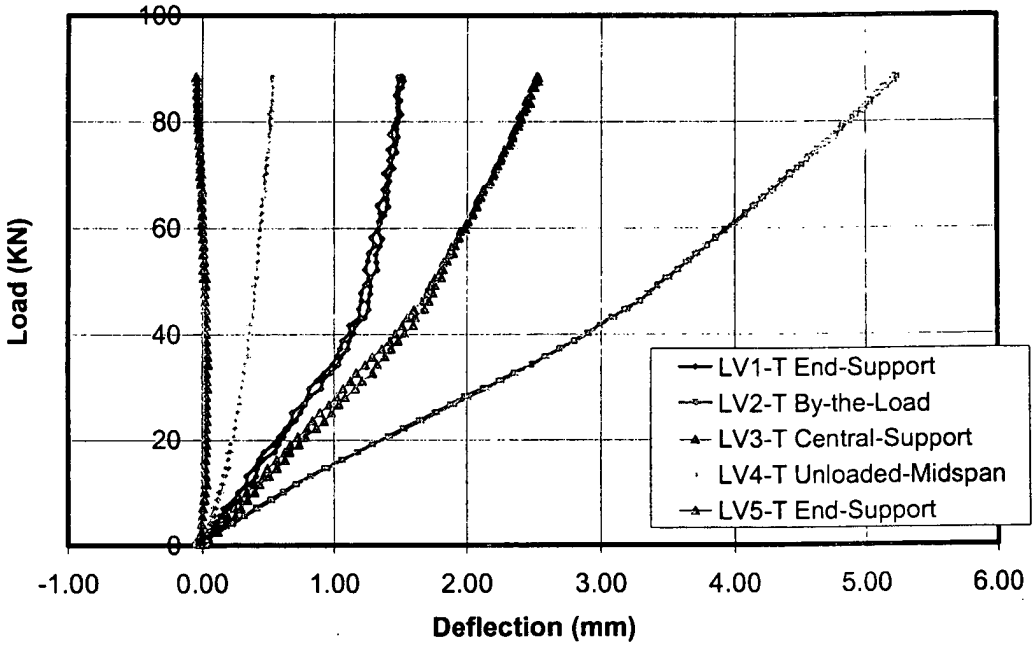

Figure III.5.6 Low-Temperature Load-Deflection Curves for Top LVDTs aligned in x-Direction after One Million Hot plus One Million Cold Fatigue Cycles

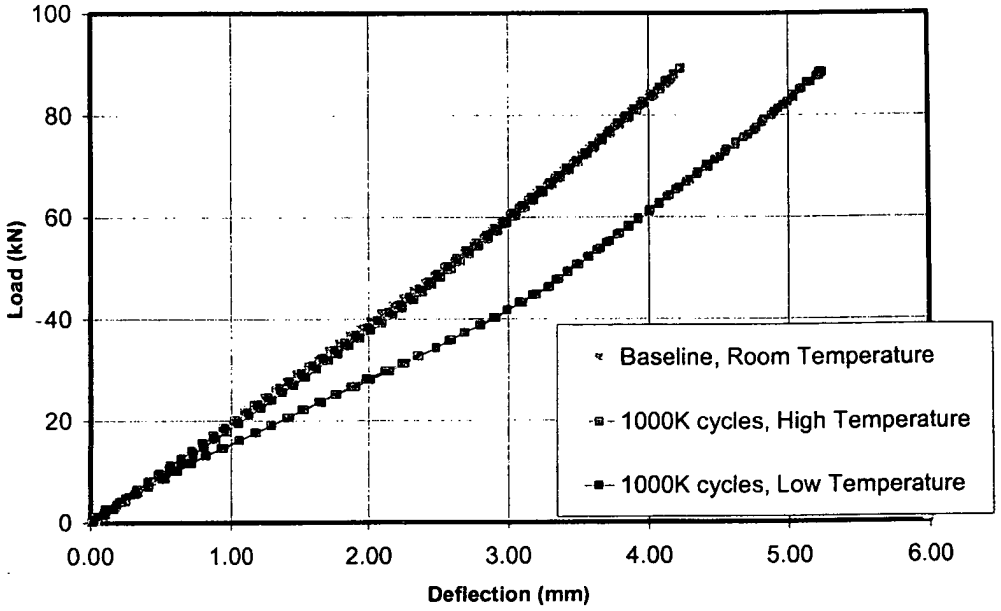

Figure III.5.7 Maximum Deflections for Three Test Conditions (Measured by LV2-T)

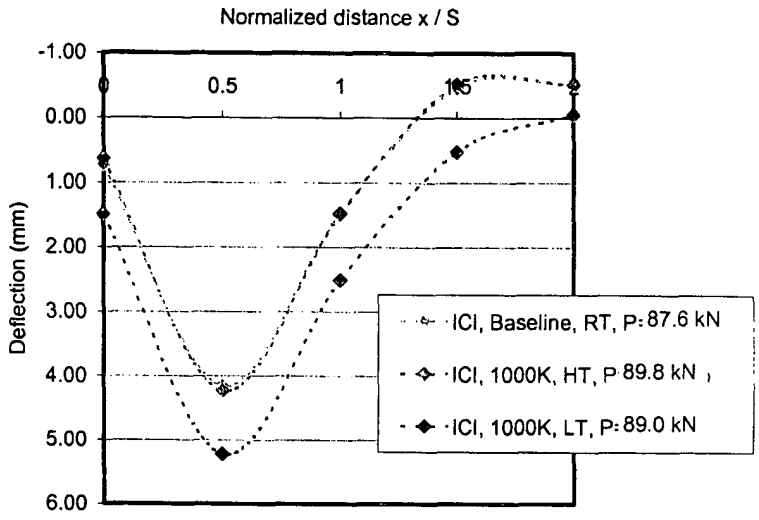

Figure III.5.8 Top Deflection Variation along the x-Direction for Maximum Load: LV1-T, LV2-T, LV3-T, LV4-T, LV5-T

The maximum deflections measured with the top LVDTs (LV2T, LV7T, and LV11T) aligned along the y-direction during the quasi-static tests are shown in Figure III.5.9. From this figure we observe that the panel longitudinal joint is not able to transfer the shear force in the y-direction and a noticeable joint slip has occurred.

Compressive strains on the top of the deck in the x-direction measured at room temperature prior to fatigue cycling are shown in Figure III.5.10. Similarly, tensile strains at symmetric locations on the bottom surface are shown in Figure III.5.11. Two curves, SG3-TX and SG1a-TX, are linear within the loading range, but SG1b-TX is not linear. This is because the shear force in the y-direction was not efficiently transferred across the joint. Compressive strains on the top surface are slightly larger than the corresponding tensile strains on the bottom surface. Again, linear strain curves were obtained for SG1a-TX and SG3-TX at high temperature after one million load cycles (Figure III.5.12 and Figure III.5.13). SG1b-TX always showed a non-linear erratic trend, confirming the

panel-to-panel load transfer problem. In the same way, strain curves were plotted at low temperature after an additional million of load cycles (Figure III.5.14 and Figure III.5.15).

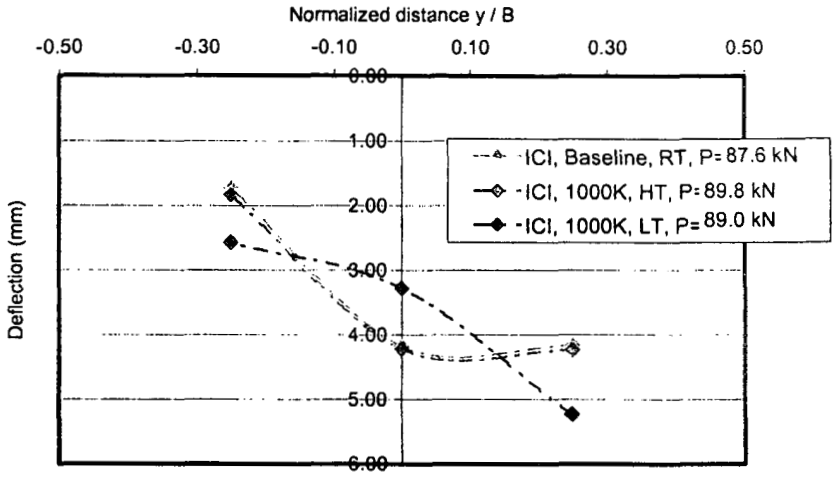

Figure III.5.9 Top Deflection Variation along the y-Direction for Maximum Load: LV2-T, LV7-T, LV11-T

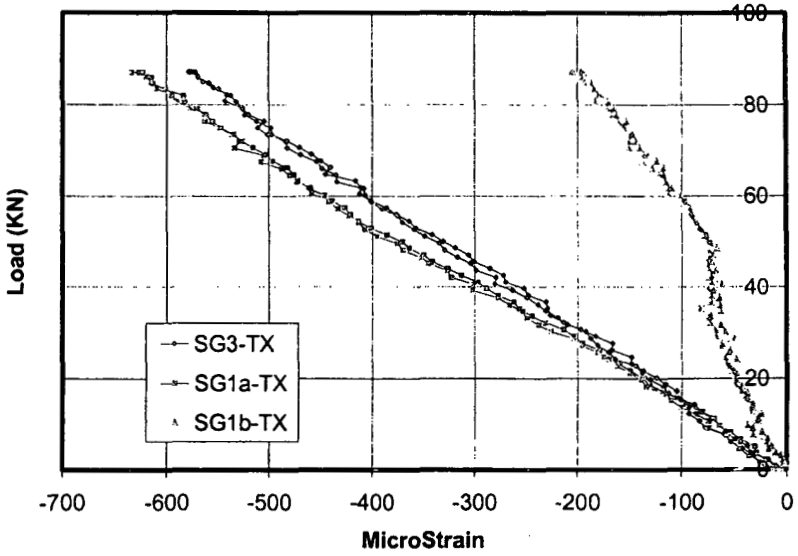

Figure III.5.10 Room-Temperature Strain (x-Direction) Curves Prior to Fatigue Cycling for Top Gauges (Loaded Span): SG1a-TX, SG1b-TX, SG3-TX

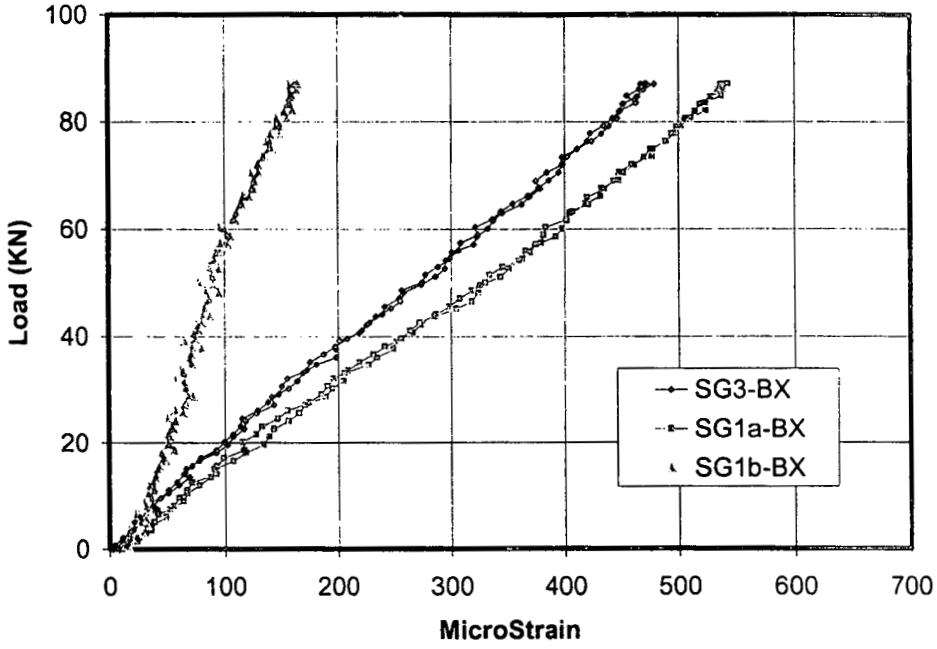

Figure III.5.11 Room-Temperature Strain (x-Direction) Curves Prior to Fatigue Cycling for Bottom Gauges (Loaded Span): SG1a-BX, SG1b-BX, SG3-BX

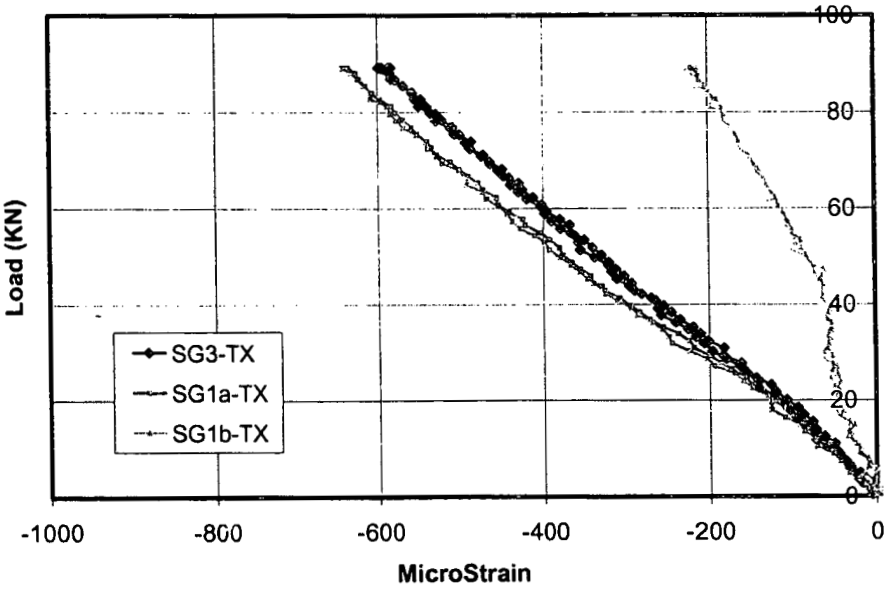

Figure III.5.12 High-Temperature Strain (x-Direction) Curves after One Million Hot Cycles for Top Gauges (Loaded Span): SG1a-TX, SG1b-TX, SG3-TX

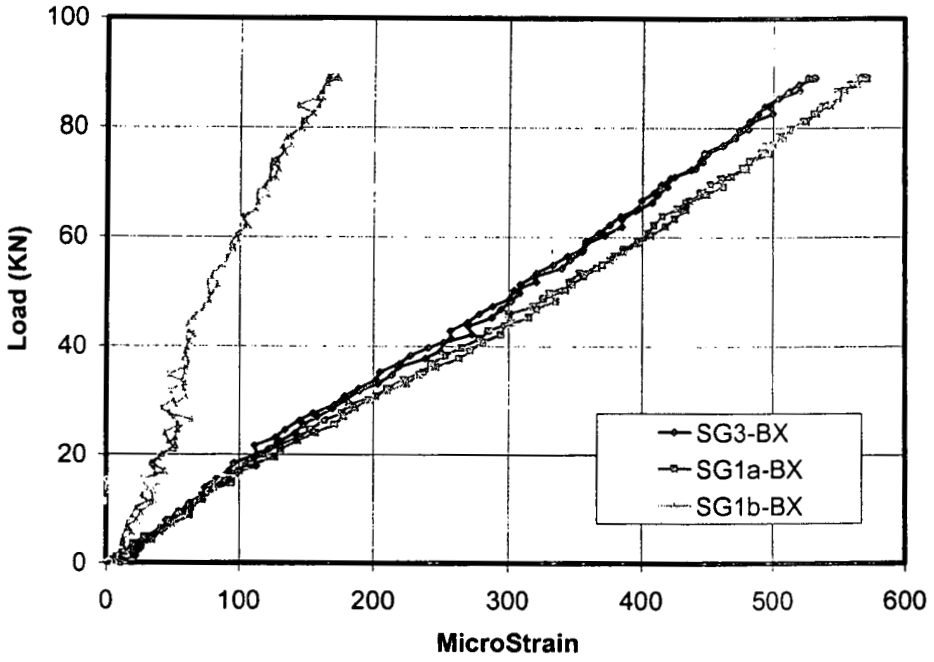

Figure III.5.13 High-Temperature Strain (x-Direction) Curves after One Million Hot Cycles for Bottom Gauges (Loaded Span): SG1a-BX, SG1b-BX, SG3-BX

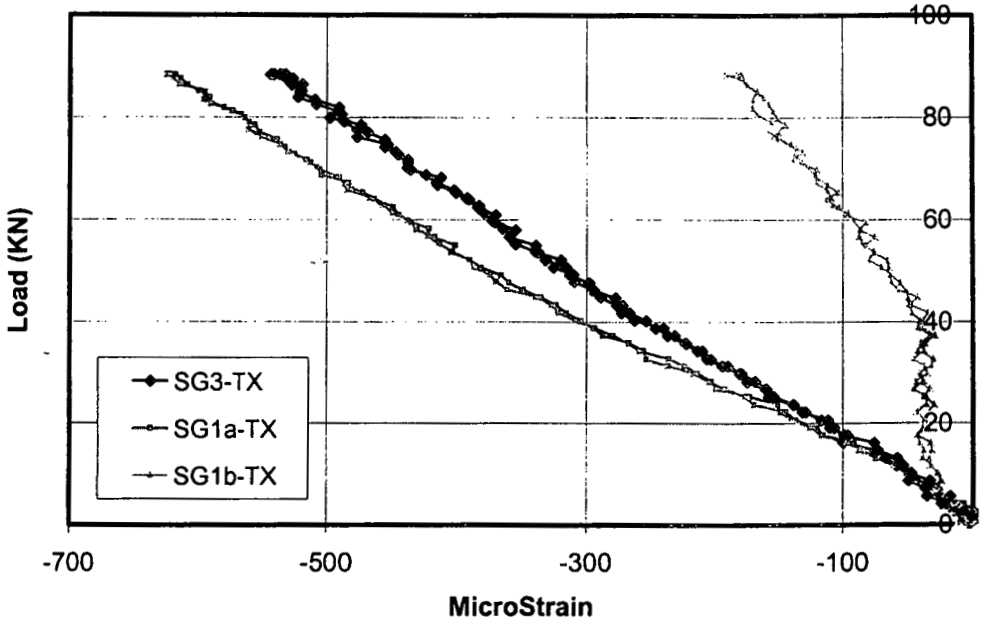

Figure III.5.14 Low-Temperature Strain (x-Direction) Curves after One Million Hot plus One Million Cold Cycles for Top Gauges (Loaded Span): SG1a-TX, SG1b-TX, SG3-TX

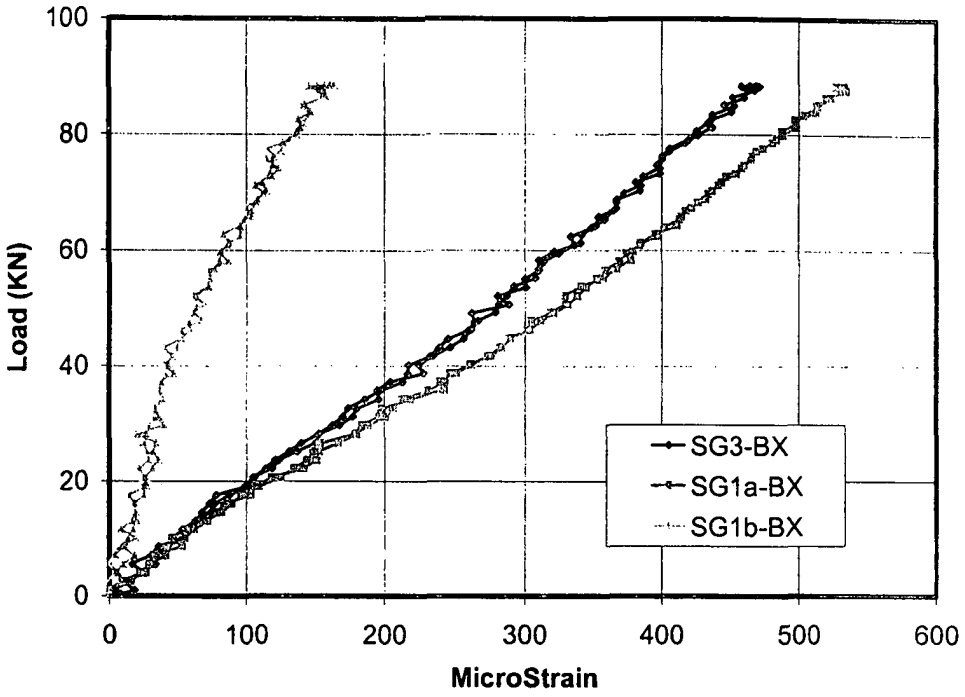

Figure III.5.15 Low-Temperature Strain (x-Direction) Curves after One Million Hot plus One Million Cold Cycles for Bottom Gauges (Loaded Span): SG1a-BX, SG1b-BX, SG3-BX

The FRP deck was inspected visually for signs of distress such as cracks and damage at connections after fatigue cycling. After the low-temperature load cycling (i.e. at the end of the cumulative two million cycles), one of the two-panel joining turnbuckles steel rods came off from the bolted head.

As mentioned before, the longitudinal joint did not perform well and did not allow proper load transfer from one FRP panel to the other. The lack of well-engineered joints would hinder the use of this FRP deck system for bridge deck replacement projects.

III.5.7 Data Analysis

To evaluate the FRP deck response with temperature and number of load cycles, two stiffness indicators are defined:

1) Stiffness indicator in the x-direction is computed based on corrected maximum deflections along a longitudinal line (LV1T, LV2T, LV3T); and
2) Stiffness indicator in the y-direction is computed based on maximum deflections across a transverse line (LV2T, LV7T, LV11T).

III.5.7.1 Retained Stiffness in the x-Direction

The maximum deflection, δ_c, was corrected to account for support deflection according to (III.5.1)

$$\delta_c = (LV2T) - \tfrac{1}{2}(LV1T + LV3T) \qquad \text{(III.5.1)}$$

where LV1T, LV2T, and LV3T are defined as deflection at the points given in Figure III.5.1. For each quasi-static test corresponding to the number of applied load cycles, n, the six segments of the load-deflection curves (see the loading and unloading segments in Figure III.5.3) for varying-load intervals were plotted. A linear response was observed in all cases and approximated with a linear least-squares regression line to compute the load-deflection ratio $\left(P/\delta_c\right)_n$. These load-deflection ratios are related to the stiffness of the deck in the x-direction. The resulting load-deflection ratios are given in Table III.5.1.

An indicator of retained stiffness in the x-direction, $R_{x,n}$, is defined as the mean residual load-deflection ratio after n load cycles with controlled temperature with respect to the mean initial load-deflection ratio, as shown in equation III.5.2:

$$R_{x,n} = \frac{\left(P/\delta_c\right)_n}{\left(P/\delta_c\right)_o}. \qquad \text{(III.5.2)}$$

Then $R_{x,n} < 1$ implies a reduction in deck stiffness, while $R_{x,n} > 1$ implies an increase in deck stiffness. The resulting retained stiffness indicators are given in Table III.5.2.

Table III.5.1 Contact Molding Hand Lay-Up Deck x-Direction Load-Deflection Ratio

	Temperature (°C)					
	24		49		–30	
Load Cycles	Mean (kN/mm)	COV (%)	Mean (kN/mm)	COV (%)	Mean (kN/mm)	COV (%)
0	28.1	0.36	27.6	0.47		
100000			27.7	0.40		
500000			27.7	0.38		
1000000			27.8	0.19	29.5	0.17
1000000 + 100000					28.1	0.50
1000000 + 500000					27.0	0.33
1000000 + 1000000					26.6	0.53

Note: 1 kN/mm = 5.71 kip/in.

Table III.5.2 Contact Molding Hand Lay-Up Deck x-Direction Stiffness Indicator

	Temperature (°C)					
	24		49		–30	
Load Cycles	Statistical Level	$R_{x,n}$	Statistical Level	$R_{x,n}$	Statistical Level	$R_{x,n}$
0	A	1.000	B	0.981		
100000			B, C	0.986		
500000			B, C	0.984		
1000000			C	0.988	D	1.048
1000000 + 100000					A	0.999
1000000 + 500000					E	0.959
1000000 + 1000000					F	0.943

*The same letter indicates the same stiffness ratio with 95% confidence.

III.5.7.2 Retained Stiffness in the y-Direction

Deflections were measured at three points aligned across the FRP deck (LV2-T, LV7-T, and LV11-T), as shown in Figure III.5.1. Load-deflection curves were plotted for the six load-varying intervals of each quasi-static test. These load-deflection curves followed a linear trend and were fitted using linear least-squares regression analysis. The

trend lines were then used to calculate the deflection corresponding to P = 89 kN (20,000 lb) for the six segments of the load-deflection curves. The resulting deflections were used to compute the secant slopes at both sides of the longitudinal FRP joint (i.e., y > 0 and y < 0), as shown in equation III.5.3:

$$\tan\theta_{Y+} = \frac{LV2T - LV7T}{B/4}$$
$$\tan\theta_{Y-} = \frac{LV7T - LV11T}{B/4} \quad \text{(III.5.3)}$$

Then, the change in the slope angle at the longitudinal joint location is computed as shown in equation III.5.4:

$$\Delta\theta_n = \theta_{Y+} - \theta_{Y-} \quad \text{(III.5.4)}$$

If $\Delta\theta_n > 0$, then the deck curves transversely concave down, and if $\Delta\theta_n < 0$, it curves concave up. The resulting changes in slope angles are given in Table III.5.3.

Table III.5.3 - FRP Deck y-Direction Slope Change

	Temperature (°C)					
	24		49		–30	
Load Cycles	Mean (rad)	COV (%)	Mean (rad)	COV (%)	Mean (rad)	COV (%)
0	–5.97E-03	-0.57	–5.87E-03	1.48		
100000			–5.62E-03	0.55		
500000			–5.83E-03	1.39		
1000000			–5.79E-03	0.46	2.15E-03	2.77
1000000 + 100000					2.83E-03	1.11
1000000 + 500000					3.52E-03	1.36
1000000 + 1000000					3.78E-03	3.10

An indicator of retained deck and joint stiffness in the y-direction, $R_{y,n}$, is defined as the mean change in slope angle after n load cycles with controlled temperature with respect to the mean initial change in slope angle, as shown in equation III.5.5:

$$R_{y,n} = \frac{\Delta\theta_o}{\Delta\theta_n} \tag{III.5.5}$$

If $R_{y,n} > 0$, then the deck does not change the curvature orientation. In particular, if $0 < R_{y,n} < 1$, the change in slope angle is more pronounced, and if $R_{y,n} > 1$, the change in slope angle is less pronounced than the baseline quasi-static test. On the other hand, if $R_{y,n} < 0$, the deck changes the curvature orientation (e.g., from concave up to concave down, or vice versa). The resulting retained stiffness indicators are given in Table III.5.4.

Table III.5.4 Contact Molding Hand Lay-Up Deck y-Direction Stiffness Indicator

	Temperature (°C)					
	24		49		−30	
Load Cycles	Statistical Level	$R_{y,n}$	Statistical Level	$R_{y,n}$	Statistical Level	$R_{y,n}$
0	A	1.00	B	1.017		
100000			C	1.061		
500000			B	1.023		
1000000			B	1.031	D	−2.773
1000000 + 100000					E	−2.107
1000000 + 500000					F	−1.697
1000000 + 1000000					G	−1.578

*The same letter indicates the same curvature with 95% confidence

The longitudinal panel joint, which is located between LV2-T and LV11-T, incorporates additional shear and bending flexibility that affects the change in the slope angle. Therefore, the change in the slope angle not only measures the bending and shear stiffness of the panels, but it also accounts for the discrete bending and shear stiffness of the joint. The reason for adopting the slope angle method of measuring the stiffness response in the transverse direction instead of a more conventional quadratic fit of deflections, which is more applicable to reinforced-concrete decks, is to model the articulated nature of the contact molding hand lay-up panels.

III.5.7.3 Statistical Analysis

Statistical analysis of the load-deflection ratio and the change in slope angle for the FRP deck system was performed using one-way analyses of variance (ANOVA) for each number of cycles and temperature condition. The analysis was conducted using the SYSTAT software package. The ANOVA analysis determined if the response of the deck system was a function of number of cycles or temperature. The model for a one-way ANOVA is represented symbolically as follows:

$$Y_n = B_o + B_1 \cdot X_n + \varepsilon_n \tag{III.5.6}$$

where Y_n = observed mechanical property (load-deflection ratio or change in slope angle) for the number of cycles n under controlled temperature

B_o, B_1 = coefficients of the model

X_n = code associated with the variable under study (e.g., temperature or cumulative load cycles)

ε_n = random unit variation within the block of data.

The null hypothesis and alternative hypothesis are given in equation III.5.7:

$$H_0 : B_1 = 0$$
$$H_A : B_1 \neq 0 \tag{III.5.7}$$

Post hoc analysis of type Bonferroni was used for pair-wise comparisons with a confidence level of 95% (α = 0.05). Four one-way ANOVA tests were performed for each mechanical property (i.e., load-deflection slope and change in slope angle) of the FRP deck system. The first two compared the mechanical property as the dependent variable with the temperature as the factor and the number of cycles held constant (0 and 1,000,000 cycles, respectively). The second two used the mechanical property as the

dependent variable with the number of cycles as the factor, holding the temperature constant, 49°C (120°F) and –30°C (–22°F), respectively. Additional tests were done only if the stiffness ratio was close between two or more cycles across temperatures and compared only those specific tests. This was equivalent to performing paired t-tests.

III.5.8 Discussion

In the x-direction the contact molding hand lay-up deck behaves similarly to the benchmark reinforced-concrete deck, except that the magnitude of stiffness reduction due to temperature and accumulated fatigue cycles is smaller (Figure III.5.16). In the x-direction the coefficients of variance are relatively small, and therefore the statistical levels are not the same through the load cycles and temperature changes. However, the actual variance between quasi-static tests is relatively small. The largest variation of the stiffness indicator in the x-direction does not exceed 6% after 2,000,000 load cycles. This variation is less than half than the corresponding one for the benchmark reinforced-concrete deck. The y-direction stiffness shows an abnormality with the low-temperature data. The change in slope angle values is positive, indicating a concave-down deck curvature at this temperature and number of accumulated fatigue cycles. This indicates that either the deck panel or the joint between panels is very flexible, allowing the load to be non-uniformly transferred from panel to panel. Most likely the joint has been damaged due to load cycles or temperature change and is not performing properly. This deviates from the behavior of the reinforced-concrete deck, which has always a concave-up curvature.

The variation of strains in the x-direction with temperature and number of load cycles is illustrated in Figure III.5.17. Both the top and bottom strain curves have shown a slight reduction in micro-strains per unit load with the decrease in temperature.

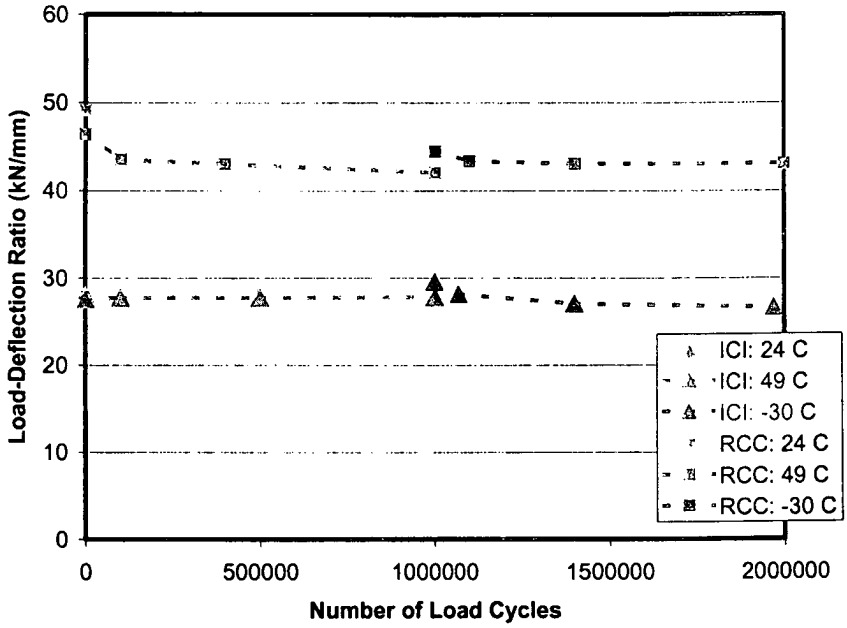

Figure III.5.16 Load-Deflection Ratio History Comparison

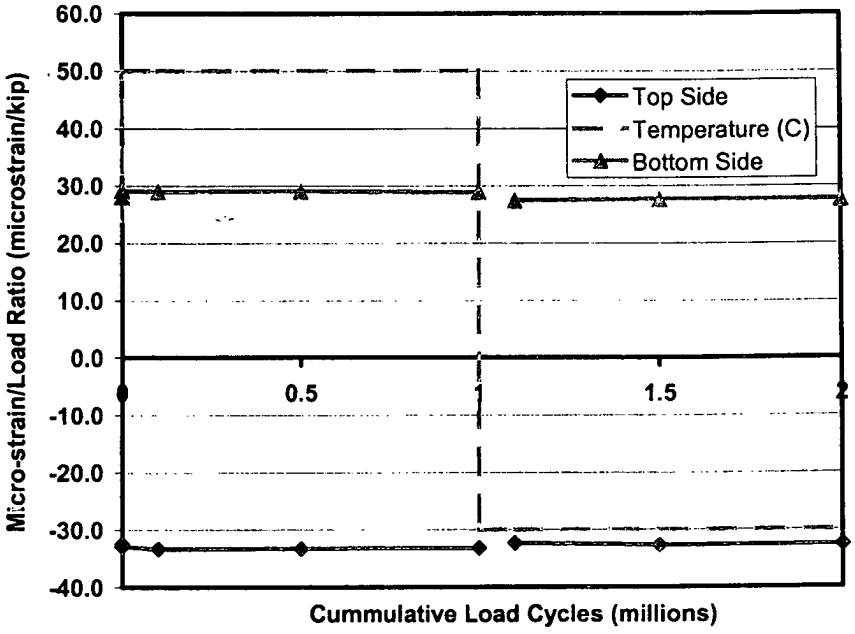

Figure III.5.17 Micro-strain per 4.45 kN (1000 lb) Load during Fatigue Cycling

III.5.9 Conclusions

The analysis done on the deck is a useful measure of stiffness in the x-direction and a useful indicator of stiffness in the y-direction. The x-direction load-deflection analysis takes into account support deflections and is conducted over a continuous span. Both of these factors combine to provide a useful measure for the amount of deflection expected with applied load.

The y-direction analysis has clearly shown the load transfer problem from panel to panel in transverse direction. Unlike the x-direction analysis, the y-direction analysis did not take into account the support deflections and was not conducted over a continuous span.

The statistical analysis performed was adequate for the desired information. The one-way ANOVA was proven to be an efficient analysis tool for determining significant changes in load-deflection ratios and change in slope angle between quasi-static tests.

Overall the contact molding hand lay-up deck stiffness in the x-direction shows a relatively small variance and adequate initial load-deflection ratio compared to the benchmark reinforced-concrete deck. In the y-direction, however, the deck experienced sudden joint damage after one million load cycles.

The tongue-and-groove joint without adhesive resulted in a minimal amount of contact area between the FRP panels. Therefore, the panel that is not directly in contact with the actuator deflected very little compared to what it would have if it were in more intimate contact with the other panel. It is recommended to improve the panel-to-panel joining method.

The lack of tight dimensional tolerances would make it difficult to use this FRP deck system for bridge deck replacement projects. It is recommended to improve the fabrication process quality control.

III.6. References

1. Lopez-Anido, R., L. D. Stephenson and P. Howdyshell, (1998), "Durability of Modular FRP Composite Bridge Decks Under Cyclic Loading," *Durability of FRP Composites for Construction*, Eds. B. Benmokrane and H. Rahman, Sherbrooke, Canada, pp. 611-622.
2. American Association of State Highway and Transportation Officials, (1996), *Standard Specifications for Highway Bridges*, Washington, D.C.

III.7 Acknowledgments

The research work presented was funded by the Ohio Department of Transportation through research contracts with the participating institutions. The financial support is gratefully acknowledged.

The Cold Regions Research and Engineering Lab (CRREL) provided technical support for the fatigue evaluation at extreme temperature. The authors thank John Bouzoun, Thomas Tantillo, Jeffrey Stark, Rosanne Stoops, John Gagnon, and Glenn Durell of CRREL for the design of the fatigue test frame, the instrumentation of the test specimen, the setup of the loading and data acquisition system, and for conducting the tests.

The assistance of Brendan Driscoll (student at the University of Maine), Scott Tomlinson (student at Rose-Hulman Institute of Technology), and Soon-Chul Kwon (student at the University of New Orleans) are gratefully acknowledged.